Group 2 Ring-Opening Polymerisation Catalysts

Junjuda Unruangsri MChem AMRSC

Thesis submitted to the University of Oxford for the degree of
Doctor of Philosophy, October 2014.

The work described in this Thesis was carried out in the Chemistry Research Laboratory, University of Oxford from October 2010 to October 2014 under the supervision of Professor Philip Mountford. All work is my own unless stated to the contrary, and has not previously been submitted for any degree at this or any other university.

Junjuda Unruangsri

October 2014

Abstract

Junjuda Unruangsri
St. Hilda's College

October 2014
D. Phil Thesis

This Thesis describes the synthesis and characterisation of new Group 2 tetrahydroborate, alkoxide and organohydroborate complexes and their uses as catalysts for the living ROP and immortal ring-opening polymerisation (iROP) of ε-caprolactone and *rac*-lactide.

Chapter One introduces cyclic esters and possible mechanistic pathways leading to polyesters by ROP. Living and immortal ROP, including their kinetic characteristics are discussed. An overview of ROP from an industrial perspective is also given.

Chapter Two describes the synthesis and characterisation of a new series of Group 2 tetrahydroborate complexes supported by a 3-methyl, 5-*tert*-butyl tris(pyrazolyl)hydroborate ligand. Their activities towards the ROP of ε-caprolactone are presented. Detailed mechanistic studies using spectroscopic techniques are discussed and a new mechanism is proposed.

Chapter Three describes the ROP of *rac*-lactide using the Group 2 tetrahydroborate complexes introduced in Chapter Two, including their mechanistic studies.

Chapter Four introduces the new immortal ROP using trialkyl borate and organoborane derivatives as chain-transfer agents (CTAs). The immortal ROP of ε-caprolactone and *rac*-lactide using Group 2 initiators with trialkyl borates/organoboranes as CTAs from either *in situ* generation or external addition is discussed. Possible immortal ROP pathways using this new class of CTAs are illustrated.

Chapter Five details the synthesis and characterisation of a new series of Group 2 organohydroborate complexes. The ε-caprolactone and *rac*-lactide ROP activity shown by the complexes presented is discussed and compared with those obtained from the corresponding tetrahydroborate analogues.

Chapter Six contains experimental details and characterising data for the new complexes reported in this Thesis.

CD Appendix contains .CIF files for all the new crystallographically-characterised complexes.

Contents

	Declaration	i
	Abstract	ii
	Contents	iii
	Acknowledgements	vii
	Abbreviations	viii
	Notes	xi
Chapter One – Introduction		1
1.1	Overview	2
1.2	General Introduction	2
1.2.1	Polycaprolactone (PCL)	2
1.2.2	Polylactide (PLA)	2
1.3	Thermodynamic aspects of ROP	3
1.4	ROP mechanisms	4
1.4.1	Ionic and metal-free ROP mechanisms	4
	Anionic ROP	4
	Cationic ROP	6
	Organocatalysis	8
1.4.2	Metal mediated ROP mechanisms	9
	Coordination-insertion mechanism	10
	Activated monomer mechanism	12
1.5	Living and immortal ROP	13
1.6	Stereocontrol and tacticity of PLA	17
1.6.1	Determining stereosequencing of PLA using NMR spectroscopy	18
1.7	Polymer molecular weight: definition	20
1.8	Polymer characterisation	21
1.8.1	MALDI-ToF mass spectrometry	21
1.8.2	Gel permeation chromatography	21
1.8.3	NMR spectroscopy	23
1.9	Industrial ROP catalysts	23
1.10	Aims and outlook	25
1.11	References for Chapter One	25

Chapter Two – Group 2 tetrahydroborate complexes for the ROP of ε-CL and their mechanistic studies 37

2.1 Overview 38
2.2 Introduction 38
2.2.1 Alkaline earth complexes as ROP catalysts 38
2.2.2 Early work on alkaline earth tetrahydroborate initiators in ROP 41
2.2.3 Possible coordination modes of the terminal tetrahydroborate ligand 44
2.2.4 Mechanistic aspects of tetrahydroborate initiated ROP of ε-CL 45
2.3 Alkaline earth tetrahydroborate initiators using $Tp^{tBu,Me}$ supporting ligand 47
2.3.1 Synthesis and solid state structure of $(Tp^{tBu,Me})Ca(BH_4)(THF)$ (**1**) 47
2.3.2 Synthesis and solid state structures of $(Tp^{tBu,Me})Mg(BH_4)$ (**2**) and $(Tp^{tBu,Me})Mg(Cl)$ (**3**) 50
2.3.3 Synthesis and solid state structures of $(Tp^{tBu,Me})Sr(BH_4)(THF)_2$ (**4**) and $(Tp^{tBu,Me})Sr(I)(THF)_2$ (**5**) 54
2.3.4 Synthesis and solid state structure of κ^2,κ^3-$(Tp^{tBu,Me})_2Sr$ (**6**) 59
2.3.5 Further NMR and IR analyses of alkaline earth tetrahydroborate catalysts 63
2.4 Polymerisation studies: ROP of ε-CL 64
2.4.1 ROP of ε-CL using $(Tp^{tBu,Me})Mg(BH_4)$ (**2**) 66
2.4.1.1 Mechanistic studies of ROP of ε-CL using $(Tp^{tBu,Me})Mg(BH_4)$ (**2**) 68
2.4.2 ROP of ε-CL using $(Tp^{tBu,Me})Ca(BH_4)(THF)$ (**1**) 73
2.4.3 ROP of ε-CL using $(Tp^{tBu,Me})Sr(BH_4)(THF)_2$ (**4**) 75
2.5 Summary and conclusions 76
2.6 References for Chapter Two 77

Chapter Three – Group 2 tetrahydroborate complexes for the ROP of *rac*-LA and their mechanistic studies 82

3.1 Overview 83
3.2 Introduction 83

3.3	ROP of *rac*-LA using ($Tp^{tBu,Me}$)Mg(BH_4) (**2**)	83
3.3.1	Kinetic and mechanistic studies of *rac*-LA ROP using complexes of the ($Tp^{tBu,Me}$)Mg(OR) type	86
3.4	ROP of *rac*-LA using ($Tp^{tBu,Me}$)Ca(BH_4)(THF) (**1**)	107
3.4.1	Deuterium labelling ROP using ($Tp^{tBu,Me}$)Ca(BD_4)(THF) (**1-*d*$_4$**)	108
3.5	ROP of *rac*-LA using ($Tp^{tBu,Me}$)Sr(BH_4)$(THF)_2$ (**4**)	110
3.6	Summary and conclusions	113
3.7	References for Chapter Three	114
Chapter Four – Trialkyl borate ester and borane derivatives as a new class of chain-transfer agents in the iROP of ε-CL and *rac*-LA		117
4.1	Overview	118
4.2	Introduction	118
4.3	*In situ* generated catalysts	121
4.3.1	Isolation of ($Tp^{tBu,Me}$)Mg(OBn) (**10**)	123
4.3.2	The dissociation of $B(OBn)_3$ from ($Tp^{tBu,Me}$)Sr{$B(OBn)_4$} (**14**)	127
4.3.3	Intramolecular exchange and its thermodynamic parameters	129
4.3.4	Exchange reaction	136
4.4	Immortal ROP of ε-CL and *rac*-LA using alkaline earth initiators	138
4.4.1	Immortal ROP of ε-CL using magnesium initiators	139
4.4.2	Proposed mechanism for the iROP of ε-CL using magnesium	148
4.4.3	Immortal ROP of *rac*-LA using magnesium initiators	151
4.4.4	Immortal ROP of ε-CL using calcium and strontium initiators	156
4.4.5	Mechanistic consideration of the iROP of ε-CL using ($Tp^{tBu,Me}$)Sr{$B(OBn)_4$} and various additives	160
4.4.6	ROP of *rac*-LA using calcium and strontium initiators	165
4.5	Summary and conclusions	166
4.6	References for Chapter Four	168

Chapter Five – New Group 2 organohydroborate complexes for the ROP of ε-CL and *rac*-LA 173

5.1 Overview 174

5.2 Introduction 174

5.2.1 Alkaline earth organohydroborate complexes 175

5.2.2 Reactivity of metal organohydroborate complexes 177

5.3 Synthesis and characterisation of alkaline earth triethylhydroborate complexes 178

5.4 Synthesis and characterisation of alkaline earth dialkyl 9-borabicycle [3.3.1] nonane dihydridoborate complexes 182

5.5 Polymerisation studies: ROP of *rac*-LA 190

5.5.1 ROP of *rac*-LA using ($Tp^{tBu,Me}$)Ca($HBEt_3$)(THF) (**17**) and ($Tp^{tBu,Me}$)Sr($HBEt_3$)$(THF)_2$ (**18**) 191

5.5.2 ROP of *rac*-LA using ($Tp^{tBu,Me}$)Ca{H(9-BBN)}(THF) (**19**) and ($Tp^{tBu,Me}$)Sr{H(9-BBN)}$(THF)_2$ (**20**) 192

5.6 Polymerisation studies: ROP of ε-CL 199

5.6.1 ROP of ε-CL using ($Tp^{tBu,Me}$)Ca{H(9-BBN)}(THF) (**19**) and ($Tp^{tBu,Me}$)Sr{H(9-BBN)}$(THF)_2$ (**20**) 199

5.7 Summary and conclusions 201

5.8 References for Chapter Five 202

Chapter Six – Experimental details and characterising data 206

6.1 General methods and instrumentation 207

6.2 Literature preparations and reagent purification 208

6.3 Experimental details and characterisation data for Chapter Two 209

6.4 Experimental details and characterisation data for Chapter Three 213

6.5 Experimental details and characterisation data for Chapter Four 216

6.6 Experimental details and characterisation data for Chapter Five 219

6.7 Polymerisation procedures 222

6.8 X-ray data collection and processing parameters 224

6.9 References 230

Appendix xii

Acknowledgements

First and foremost, I would like to thank my supervisor, Prof. Philip Mountford, for his help, support and guidance throughout the course of my part II and DPhil studies. These five years have been tough, but I have learnt a lot from it both chemistry-wise and life-wise. This has provided me with a solid foundation, which I can build on in my future career. I am grateful for all the opportunities that were given.

I would also like to express my sincere thanks to the Mountford group's members, both past and present, whom I have shared my up and down time with, and made the lab an enjoyable place to work in. I truly appreciate being part of them! I would like to thank Dr Michael Cushion (my ancestor in the ROP project), Dr Andrey Protchenko for showing/teaching me his awesome schlenk techniques and walked home with me after midnight from the lab, Dr Insun Yu for many helpful discussions towards the end of my project, Bryony Core for sharing the success and pain in the ROP works, Dr Liban Saleh and Dr Adam Russell for creating an enjoyable and laid-back atmosphere in the lab, Richard Collins for being my lovely and fantastic part II student, Xinning Yin for being my little sister in the lab, making me laugh and cheering me up, and Laura Stevenson for being helpful with all the lab matters. Special mention must go to Dr Matthew Blake and Dr Laura Groom. I owe them endless thanks for being great friends, who often help me out with a lot of things since the early days in the Mountford group. I truly enjoy sharing time and experience with them in all these years. I cannot finish without acknowledging Matt, Laura Groom and Rich for their help to proofread my chapters.

Additionally, I must express my gratitude to Dr. Nick Rees, Collin Sparrow and Dr Amber Thompson for their great helps with NMR spectroscopy, mass spectrometry and X-Ray crystallography. Without them, I would not be able to put all my works together.

Lastly, I reserve the greatest thanks to my mum, grandmother, uncle, aunties, and boyfriend, who are always behind all the success in my life. Their understanding, unconditioned love and endless support have been essential for me. I cannot finish my acknowledgement without mentioning my Thai friends in Oxford, who always look after me and make me feel like having another family here. Without the people mentioned in this acknowledgement, it would be impossible to get this thesis done.

Abbreviations

General

Å	Ångstrom
av.	average
ca.	*circa*, about
calcd	calculated
cal	calories
CTA	chain-transfer agent(s)
d	day(s)
º	degrees
ºC	degrees Celsius
DFT	Density Functional Theory
equiv(s).	equivalent(s)
g	gram(s)
GPC	gel permeation chromatography
h	hour(s)
iROP	immortal ring-opening polymerisation
η	intrinsic viscosity
J	Joule(s)
k	kilo
K	Kelvin
k_{app}	apparent rate constant
k_i	rate constant of initiation
k_p	rate constant of propagation
k_{tr}	rate constant of chain-transfer reaction
L	litre(s)
mg	milligram(s)
min	minute(s)
mL	millilitre(s)
μL	microliter(s)
ROP	ring-opening polymerisation
RT	room temperature
s	second(s)
SEC	Size Exclusion Chromatography

T	temperature
T_g	glass transition temperature
T_m	melting temperature

Chemical

Ar	aryl group
Bn	benzyl
BnOH	benzyl alcohol
BPin	$BO_2(CMe_2)_2$
Cp	C_5H_5
Cp*	C_5Me_5
Cy	cyclohexyl
ε-CL	ε-caprolactone
D-lactide	(*R,R*)-cis-3,6-dimethyl-1,4-dioxane-2,5-dione
DMAP	4-dimethylaminopyridine
^{n}Bu	*n*-butyl
^{t}Bu	*tert*-butyl
^{i}Pr	*iso*-propyl
^{i}PrOH	*iso*-propyl alcohol
L	a supporting ligand (set)
LA	lactide
L-lactide	(*S,S*)-cis-3,6-dimethyl-1,4-dioxane-2,5-dione
Me	methyl
Meso-lactide	(*R,S*)-cis-3,6-dimethyl-1,4-dioxane-2,5-dione
M_n	number average molecular weight
M_p	peak molecular weight
M-OR	metal alkoxide
M_w	weight average molecular weight
PDI	poly dispersity index
Ph	phenyl
PhCHO	benzaldehyde
P_m	probability of *meso*- linkages
PLA	poly(lactic acid)
PCL	poly(ε-caprolactone)
P_r	probability of racemic linkages

py	pyridine
pz	pyrazolyl
R	generic aryl or alkyl
rac-lactide	a racemic mixture of *D*- and *L*-lactide
ROP	ring-opening polymerisation
$Sn(Oct)_2$	Tin octanoate
THF	tetrahydrofuran
$Tp^{(^tBu,Me)}$	3-methyl, 5-*tert*-butyl tris(pyrazolyl)hydroborate

Mass Spectrometry

EI	electron impact
FI	field ionisation
m/z	mass to charge ratio
MS	mass spectrometry
MALDI-ToF MS	matrix-assisted laser desorption/ionization - time of flight mass spectrometry

Nuclear Magnetic Resonance Spectroscopy

$^{11}B-\{^1H\}$	proton-decoupled ^{11}B
$^{13}C-\{^1H\}$	proton-decoupled ^{13}C
app.	apparent
br	broad
COSY	correlation spectroscopy
d	doublet
dq	doublet of quartets
HETCOR	heteronuclear correlation
HMBC	heteronuclear multiple bond correlation
HMQC	heteronuclear single quantum correlation
i	*ipso*
J	coupling constant
m	*meta*
m	multiplet
NMR	nuclear magnetic resonance
nOe	nuclear Overhauser effect
o	*ortho*

p	*para*
ppm	parts per million
q	quartet
ROESY	rotating-frame nuclear Overhauser Effect spectroscopy
s	singlet
sept	septet
t	triplet
VT	variable temperature
δ	chemical shift in ppm

Infrared Spectroscopy

br	broad
FT-IR	fourier transform infrared
IR	infrared
m	medium
s	strong
w	weak
ν	frequency

Note about numbering of compounds described in this Thesis

Literature compounds described in this Thesis are numbered **1.x**, **2.x**, **3.x**, **4.x, 5.x** according to the Chapter in which they first occur. The new compounds described in this Thesis are numbered **1** - **xx**. MALDI-ToF mass spectrometry was performed by Colin Sparrow, and elemental analyses were performed by Stephen Boyer at London Metropolitan University and Elemental Microanalysis Ltd at Devon.

Chapter One

Introduction

1.1 Overview

This Chapter will provide an introduction to the ring-opening polymerisation (ROP) of cyclic esters with a brief account of the main mechanistic pathways. Common polymer characterisation techniques used in this Thesis will be described. The Thesis will focus mainly on metal-mediated ROP, the concept of living and immortal ROP, including their mechanism, will be discussed. Moreover, an overview of industrial ROP catalysis will also be given.

1.2 General Introduction

The awareness of the depletion of petrochemical feedstocks has brought about the use of materials from sustainable sources. Biorenewable and biodegradable polymers have received much attention as alternative materials to the non-renewable oil-based polyolefins. The global production of bio-derived plastics, suggested by the European Bioplastics association, is predicted to grow from 1.4 million tonnes in 2012 to approximately 6.2 million tonnes in 2017.[1] The two prominent examples of biodegradable polymers are the aliphatic polyesters, poly(ε-caprolactone) and polylactide.

1.2.1 Poly(ε-caprolactone) (PCL)

Polycaprolactone (PCL) is a thermoplastic polymer, whereby its monomer is synthesised by chemical conversion of non-renewable starting materials such as crude oil. The Baeyer-Villiger oxidation of cyclohexanone with peroxyacetic acid is used in industrial scale preparation of the monomer.[2] PCL, with a low melting point (58-60 °C) and viscosity, imparts good chemical, water and oil resistance. Commonly, PCL is used in the manufacture of polyurethanes. Furthermore, starch or fibre-blending PCL can be used for household commodities produced at low manufacturing costs.[3]

1.2.2 Polylactide (PLA)

One of the most promising polymers among biodegradable aliphatic polyesters studies so far is polylactide (PLA). The lactide monomer is a dimer of lactic acid, which is derived from the microbial fermentation (usually based on a strain of *lactobacillus*) of ultimate biomass such as corns or sugar beets.[4-9] Notably, this polymer is also intrinsically bioassimilable as their hydrolysed products are lactic acid, which could

be metabolised to yield non-toxic carbon dioxide and water both *in vivo* and in the environment (Figure 1.1).[10-12]

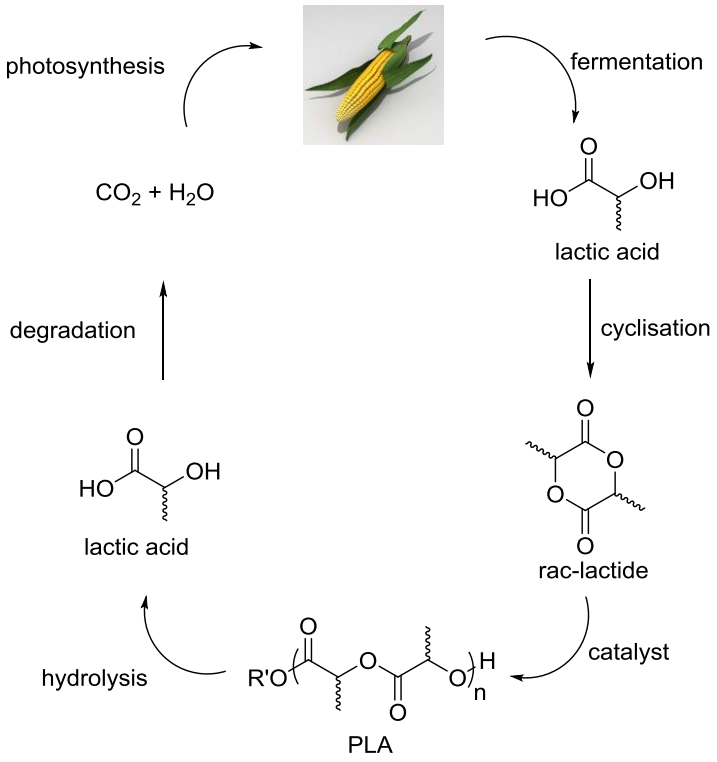

Figure 1.1. Life cycle of polylactide.[10, 11]

The unique properties of PLA enable it to be used in a broad spectrum of applications, ranging from packaging to sophisticated biomedical applications, for example, devices (sutures and stents), drug delivery and tissue engineering.[5, 12-15] The early era of manufacturing PLA and other cyclic esters was reported by Carothers in 1932, when the ring-opening polymerisation technique was employed over the traditional condensation of lactic acid, which gave poorly controlled polymerisation and irregular stereoselectivity of PLA.[16] A further development by Dupont in 1954 resulted in the production of high molecular weight PLA being patented.[3, 17, 18] The market demand for PLA has intensified in recent years. Nature Works LLC, the leading PLA manufacturer, revealed a capacity of PLA production of 140,000 tonnes per year in 2008.[19]

1.3 Thermodynamic aspects of ROP

Ring-opening polymerisation is the most convenient and efficient method to obtain such aliphatic polyester materials from cyclic monomers; it enables polymerisation with well-controlled polymer weight, low polydispersity index (PDI) and desired

stereochemistry.[20, 21] The thermodynamic driving force for ROP of cyclic esters is the relief of ring strain, which is caused by the angular, conformational and transannular strain. In the case where the interaction between monomer, polymer and solvent is negligible, the enthalpy of polymerisation depends solely on the ring strain.[22] In general, the presence of substituents on the same ring-size cyclic esters influences the decrease of the ring strain and hence polymerisability of the cyclic monomers (i.e. glycolide > lactide > tetramethyl glycolide). This is due to the more pronounced interactions between the substituents in the linear *vs*. the cyclic molecules.[23]

ROP is accompanied by an unfavourable decrease in entropy, this is due to the loss in the translational degree of freedom as monomers are polymerised. However, ROP of macrocyclic esters, such as tridecanolide (14-membered ring) and pentadecanolide (16-membered ring), are entropy driven. This is owing to the relatively high flexibility of the long polymer chain being produced from the less strained macrocyclic monomers.[22] The thermodynamic parameters of ROP using simple lactones were investigated and measured by Duda and Penczek.[23-25]

1.4 ROP mechanisms

There are a number of routes to the ring-opening polymerisation (ROP) of heterocycles or cyclic esters, including ionic,[12, 22, 26] organocatalytic[27-29] and metal-mediated pathways.[11, 12, 30] This section will give an overview of the common mechanisms of ROP reported in the literature.

1.4.1 Ionic and metal-free ROP mechanisms

A class of cyclic monomers generally used in ROP are polar heterocycles. Their polar nature allows many suitable nucleophiles and electrophiles to initiate ionic ROP by either anionic or cationic method, respectively. Metal-free mediated pathways to synthesise PCL and PLA are also possible and well documented,[12, 22, 31] these commonly involved simple organic molecules, carbenes or enzymes. The previously mentioned ROP processes are discussed as following.

1.4.1.1 Anionic ROP

Nucleophile initiated ROP could be categorised as anionic ROP. The effective nucleophiles participating in anionic ROP are in a number of different physical forms, for examples, alkyl lithium, alkyl magnesium bromide, metal amides, alkoxides, phosphines, alkaline metal naphthalenide complexes with crown ethers, etc.[22, 32]

Depending on the nucleophilic strength of initiators, polymerisations of β-lactones are initiated by the nucleophilic attack of a negatively charged initiator on either the alkyl-oxygen bond (alkyl-oxygen cleavage) or the carbonyl carbon atom (acyl-oxygen cleavage). These two possible initiating steps (a) and (b), result in the formation of carboxylate and alkoxide group at the propagating chain-ends, respectively (Scheme 1.1).[33] Alkyl-oxygen bond scission is preferred in the ROP of β-lactones using weak bases. On the other hand, the extensive studies of Jedlinski and co-workers illustrated the preference of acyl-oxygen scission in β-lactone ROP using strong bases.[33-37]

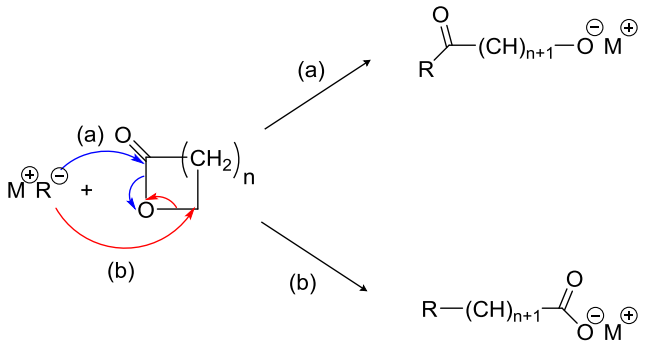

M = metal and R = alkyl, aryl or alkoxide

Scheme 1.1. Initiation of anionic ROP of lactones through (a) acyl-oxygen scission and (b) alkyl-oxygen scission.[33]

With larger ring lactones, such as ε-caprolactone, anionic polymerisation always proceeds through acyl-oxygen cleavage initiation, leading to an alkoxide propagating end-group. The propagation of this linearly growing polycaprolactone chain is often accompanied by a side-reaction, an intramolecular "back-biting" between a terminal alkoxide and ether linkage, forming a macrocyclic oligomer.[22, 26]

Polymerisations of lactide using anionic initiators are commonly highly active but poor controlled owing to the strong nucleophilic/basic nature of initiators. This results in less investigation being carried out on the anionic polymerisation of lactide, in comparison to the coordination-insertion approach (Section 1.4.2.1). From the mechanistic point of view, two possible initiating pathways through acyl-oxygen cleavage were proposed: (a) deprotonation of the monomer and (b) nucleophilic attack (Scheme 1.2).[12, 26] In 2001 Bhaw-Luximon *et al*. introduced an uncommon deprotonation pathway for anionic ROP of lactide using a strong base, lithium

diisopropylamide (LDA), as an initiator. Polylactide obtained from these two pathways can be conveniently differentiated by end-group analysis.[38]

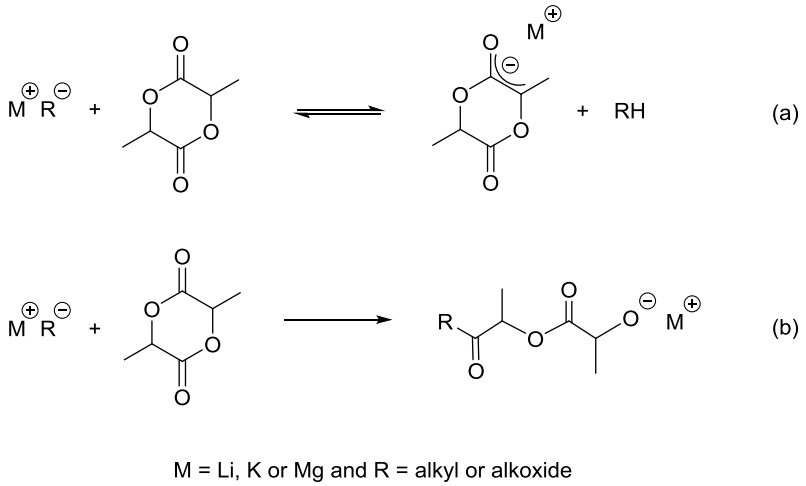

Scheme 1.2. Two possible initiating pathways of anionic ROP of lactide through (a) deprotonation and (b) nucleophilic attack.[12, 26]

1.4.1.2 Cationic ROP

In contrast to anionic ROP, electrophilic initiators including Brønsted acid, Lewis acid and alkyl esters of strong acids participate in cationic ROP. This ROP method is known to be applicable to a range of polymerisations with various monomers, including 3-membered cyclic ethers, lactones and cyclic carbonate.[22, 32, 39, 40] Conventionally, cationic ROP proceeded through an active chain-end (ACE) mechanism.[41, 42] The monomer polarity can be alleviated through the interaction between an electrophile and an electron-rich atom in the monomer, resulting in the creation of a cationic centre. The cationic species could be facile to ring-opening spontaneously giving an acyclic cationic species, which is prone to the attack by other monomer (S_N1 mechanism). Alternatively, the ring-opening step could occur *via* an attack of an electron rich atom of another monomer to the cyclic monomer containing the cationic centre (S_N2 mechanism). The predominance of one mechanism over the other depends on the stability of the cationic species generated in the ring-opening step.[22, 43, 44] Intramolecular back-biting, leading to the formation of a cyclic oligomer, is a significant side-reaction in the ACE mechanism. This side-reaction is a major factor in suppressing polymerisation control.

In 1986, Kircheldorf and co-workers published successful work on polymerisation of LA using trifluoromethanesulfonic acids, triflic acid (HOTf) and methyl triflate

(MeOTf), as initiators. End group analyses by ^{1}H NMR spectroscopy of the PLA obtained showed methyl ester groups when MeOTf was used, indicative of alkyl-oxygen scission in the polymerisation (Scheme 1.3(a)).[42, 45-48] Later, Bourissou *et al*. reported a modified cationic polymerisation system, where primary or secondary alcohol was used, in conjunction with acid.[44] The exogenous alcohol was found to be incorporated into the resultant polymer, indicative of acyl-oxygen scission. This cationic ROP proceeded through an activated monomer mechanism (AM) as described by Penczek, where the acid would activate the monomer, prior to an attack of alcohol as initiator (Scheme 1.3(b)).[39, 41, 49] Polymerisation control was remarkably enhanced through the activated monomer mechanism. The profound discovery led to a number of works published in the field.

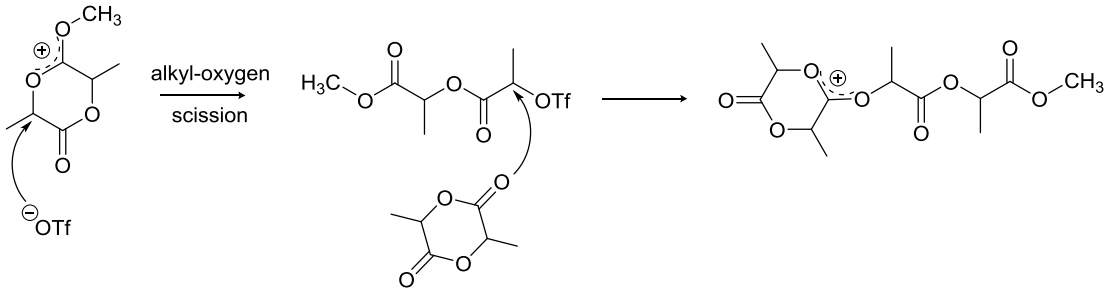

(a) Cationic ROP of LA using Methyl Triflate (MeOTf)

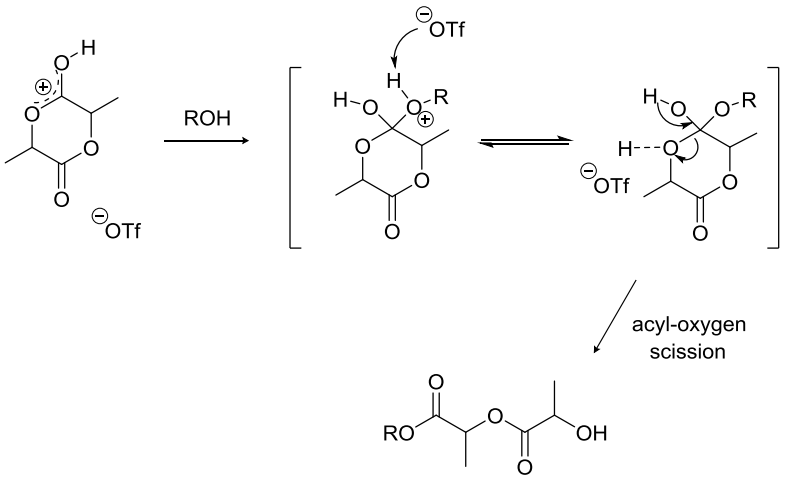

(b) Cationic ROP of LA using trifluoromethanesulfonic acid (HOTf), in conjuction with alcohol (ROH)

Scheme 1.3. Cationic ROP of lactide using (a) methyl triflate and (b) trifluoromethanesulfonic acid in conjunction with alcohol.[31, 41]

1.4.1.3 Organocatalysis

Organocatalysts that mediate ROP of cyclic esters have also received considerable attention, as no requirement is needed to remove toxic metal residues from the resultant polymers prior to their further applications.[27] A certain number of classes of organic molecules are found to be efficient catalysts for ROP of cyclic esters, namely, pyridines,[28] *N*-heterocyclic carbenes (NHCs)[50, 51] and phosphazenes.[29, 52-54] For organocatalysis ROP, most of polymerisations only proceed in the presence of alcohol initiators.[22] Even though the mechanism of the organocatalysis ROP remains ambiguous, well-controlled polymerisations have been established using organocatalysts. Herein, a few key organocatalysts are given as examples.

Lewis basic amines, such as 4-dimethylaminopyridine (DMAP) and 4-pyrrolidinopyridine (PPY), were the first organocatalysts to yield living ROP of LA reported by Hedrick *et al*. in 2001.[28] In the presence of alcohol initiators, the amines polymerised LA in CH_2Cl_2 at 35 °C in a living fashion. The successful polymerisation was predicted to proceed *via* a monomer-activated or a chain-end activated mechanism (Scheme 1.4).[31] The work was later adopted in the ROP of modified lactides and other cyclic ester monomers by Moeller,[55, 56] Bourissou[57] and Pohl *et al*.[58]

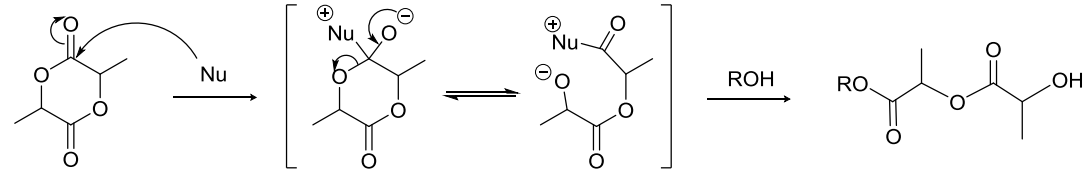

(a) Nucleophilic monomer activated mechanism

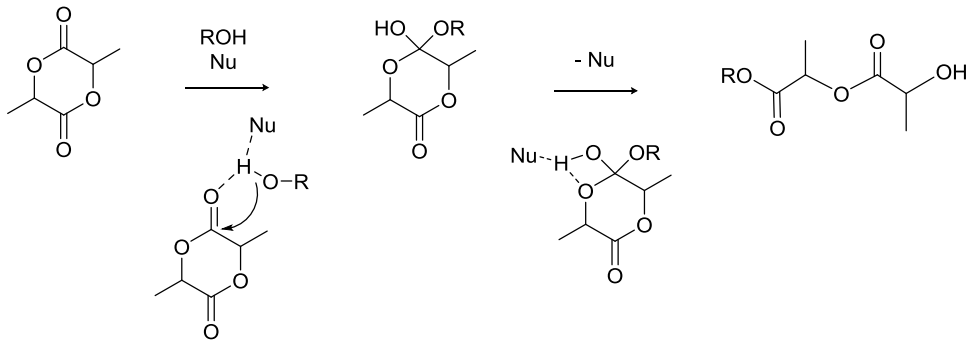

(b) Chain-end activated mechanism

Scheme 1.4. Possible nucleophilic mechanisms of lactide ROP: (a) nucleophilic monomer activated mechanism and (b) chain-end activated mechanism. Nucleophiles are pyridines and NHCs.[22]

In 2001 Hedrick and co-workers demonstrated the ability of *N*-heterocyclic carbene (1,3-bis-(2,4,6-trimethylphenyl)imidazol-2-ylidene), IMes, to polymerise lactides and lactones in living manner.[59] The pioneering work has shed some light on the use of other NHCs with different steric and electronic properties, including imidazolium, imidazolinium, thiazolium and triazolium, in ROP of cyclic esters.[27] All the NHCs were highly active towards a wide range of monomers, such as lactones,[60-62] carbonates[63] and silyl ethers.[64] Similar to the pyridine-type initiation, two possible mechanisms are also envisaged. The formation of zwitterionic propagating species using NHCs possibly leads to the generation of cyclic polyester (Scheme 1.5).[31, 65]

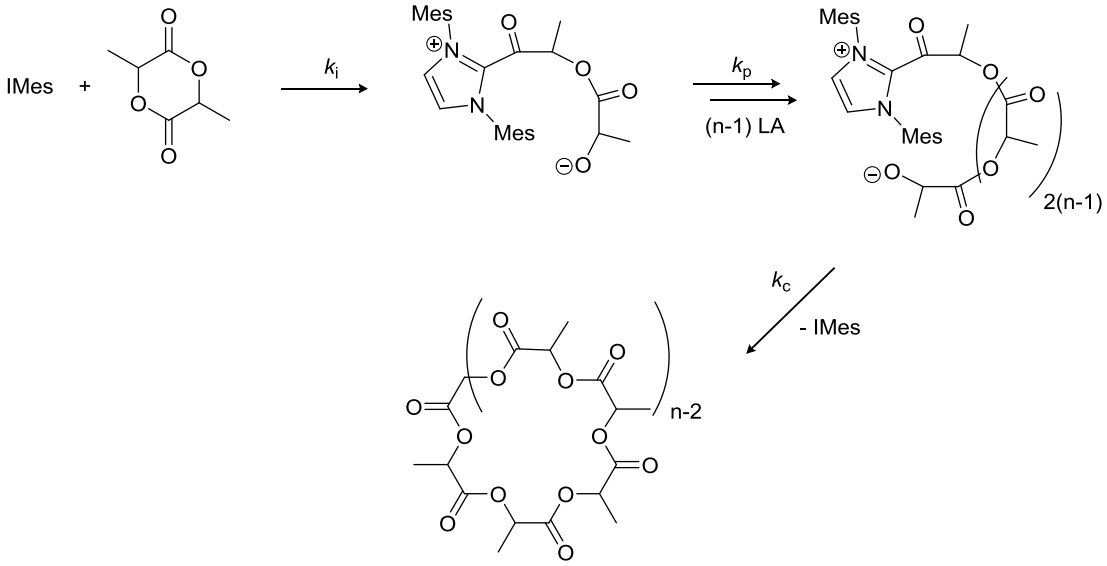

Scheme 1.5. Zwitterionic ring-opening polymerisation of lactide by NHCs.[31, 65]

1.4.2 Metal mediated ROP mechanisms

Metal-based catalysts for the ROP of cyclic esters containing Lewis acidic metal centres featuring one or more nucleophilic initiating groups (e.g. alkoxide, amide or tetrahydroborate) and supporting polydentate ancillary ligands, which exert a significant influence on the metal coordination spheres and eventually polymerisation control. Metal mediated ROP has been an active area in polyester syntheses. The catalytic systems are based on the use of various metals, including alkali metals,[66-74] alkaline earth metals,[75-82] tin,[83-89] zinc,[75, 90-93] alminium,[94-99] yttrium,[100-106] Group 4 metals,[107-113] lanthanides[114-118] and less prevalent metals, such as germanium,[119, 120] indium,[121-123] bismuth[124-126] and iron.[127-129] The metal mediated ROP pathways usually follow either the activated-monomer mechanism or the most widely present coordination-insertion mechanism.

1.4.2.1 Coordination-insertion mechanism

The coordination-insertion is sometimes viewed as a pseudo anionic polymerisation. The three-step coordination-insertion mechanism and its kinetics for the ROP of cyclic esters was firstly elucidated and proposed by Dittrich and Schulz in 1971.[130] The first experimental evidence concerning the coordination-insertion mechanism was obtained in 1988 through the work of Kricheldorf, featuring the cyclic ester ROP using metal alkoxide initiators.[26] Following the pioneering research, further experimental and theoretical studies have been carried out, allowing the mechanism to be established.[30, 131-134]

The coordination-insertion mechanism involves coordination of the cyclic monomer to the Lewis acidic metal centre, increasing the electrophilicity of the carbonyl carbon. This is followed by the insertion of the monomer into the metal-nucleophile bond *via* nucleophilic addition. This results in cleaving of the acyl-oxygen bond and hence ring-opening of the cyclic monomer.[11, 12, 22, 26, 30] The continuous insertion of monomers (propagation) allows chain growth. Hydrolysis of the propagating chain end terminates the polymerisation and the aliphatic polyester can be isolated (Scheme 1.6).[11, 12, 135]

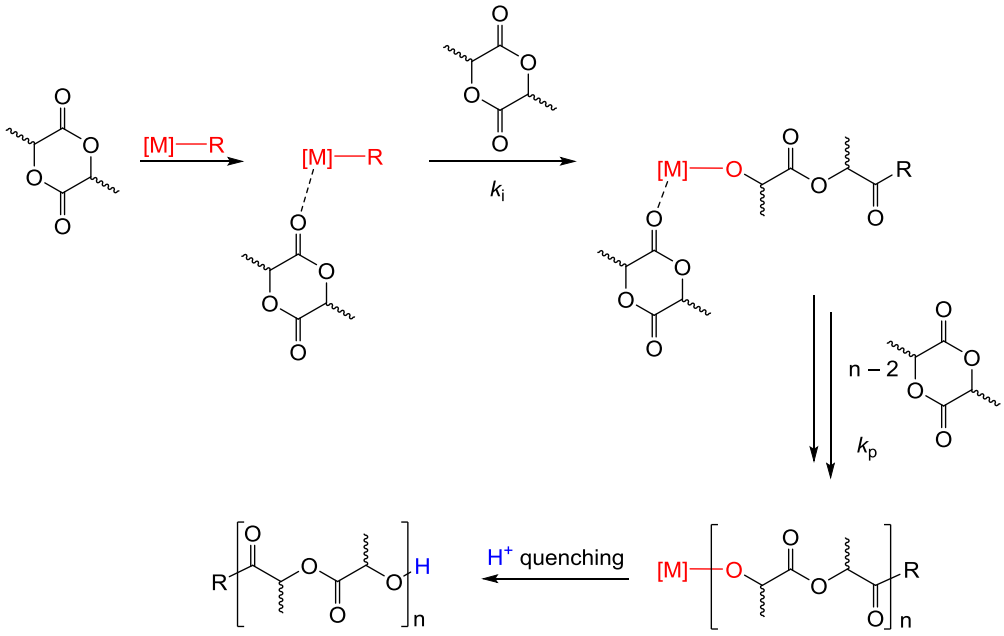

Scheme 1.6. Coordination-insertion mechanism of lactide ROP. R = initiating group, e.g. alkoxide or amide and k_i and k_p are the rate constants for initiation and propagation, respectively.[11, 12, 135]

Transesterification is a deleterious factor affecting the use of metal-based catalysts in ROP, namely intra- and inter-molecular transesterification (Scheme 1.7). Intramolecular transesterification or back-biting involves the insertion of metal alkoxide bond to the internal metal-coordinating ester group, producing an inactive macrocyclic ester and shorter growing polymer chain on the metal centre. As its name suggests, intermolecular transesterification associates with the chain-redistribution between active propagating chains. The active metal alkoxide bond inserts into an ester group of another propagating chain, giving growing polymer chains of different lengths.[12, 26, 136, 137]

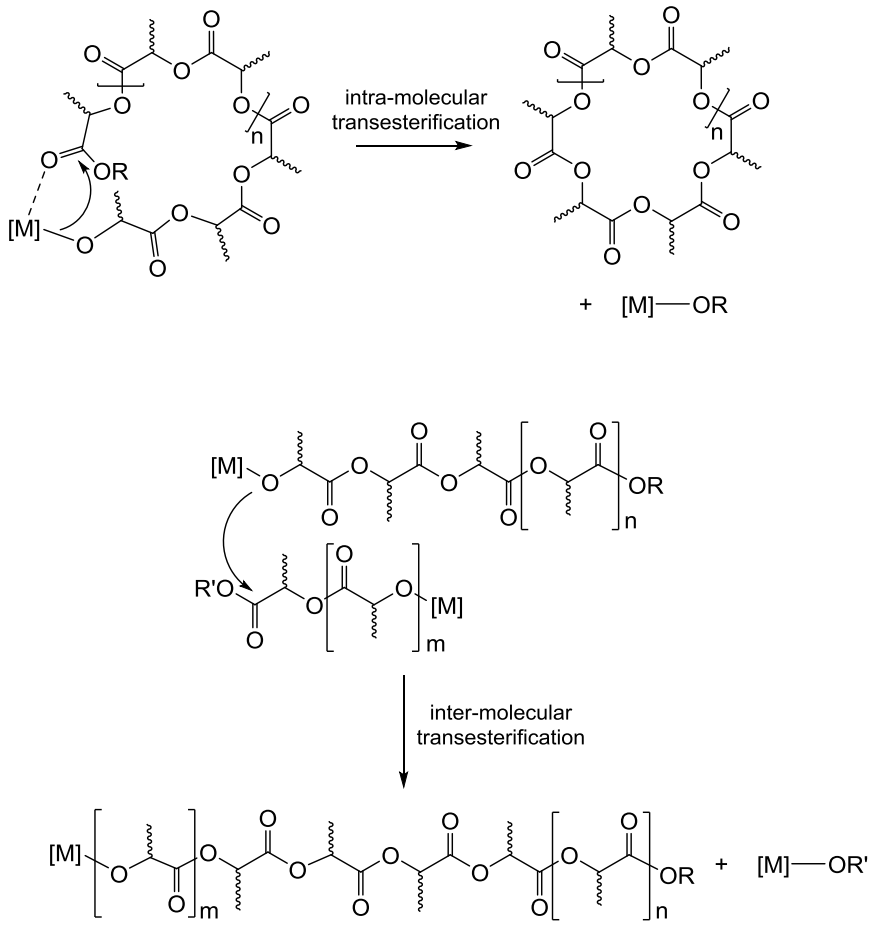

Scheme 1.7. Intra- and inter-molecular transesterification processes in ROP. R and R' represent alkyl group or the PLA chain.[12, 26, 136, 137]

Both inter- and intra-molecular transesterification leads to termination and chain transfer reactions. These processes often result in poor control over chain length and broad molecular weight distribution, which reflect in the following measurements; an increase in PDI in the GPC measurement, the appearance of cyclic PLA with the

separation between the adjacent peak envelops of $\Delta m/z$ = 72 g mol^{-1} (i.e. half of the M_w of a *rac*-LA monomer) in MALDI-ToF MS, as well as an increase in the *isi* resonance and/or the appearance of the *iis* resonance in the $^{13}C\{^1H\}$ NMR analysis at the tetrad level (Section 1.6.1).[11, 137-139] The extent of transesterification depends on a number of possible factors, including the Lewis acidity of the metal centre, ligand and initiating group.[12, 21, 26, 140]

1.4.2.2 Activated monomer mechanism

The activated monomer mechanism provides an alternative metal-mediated ROP pathway to the widely applicable coordination-insertion mechanism. This mechanism is commonly observed when simple Lewis acid metal salts (i.e. triflate salts) are used as ROP catalysts, in conjunction with excess protic agents (i.e. alcohols, water) as nucleophilic initiators. Initiation is accomplished as the external protic agent undergoes nucleophilic addition to the monomer that has been activated by coordination to the metal centre through its carbonyl oxygen atom. The formation of terminal alcohol polymer chains is yielded as a result of the first ring-opening step. Subsequently the hydroxy end-capped polymers act as nucleophile attacking further activated monomers in propagation (Scheme 1.8).[141-145]

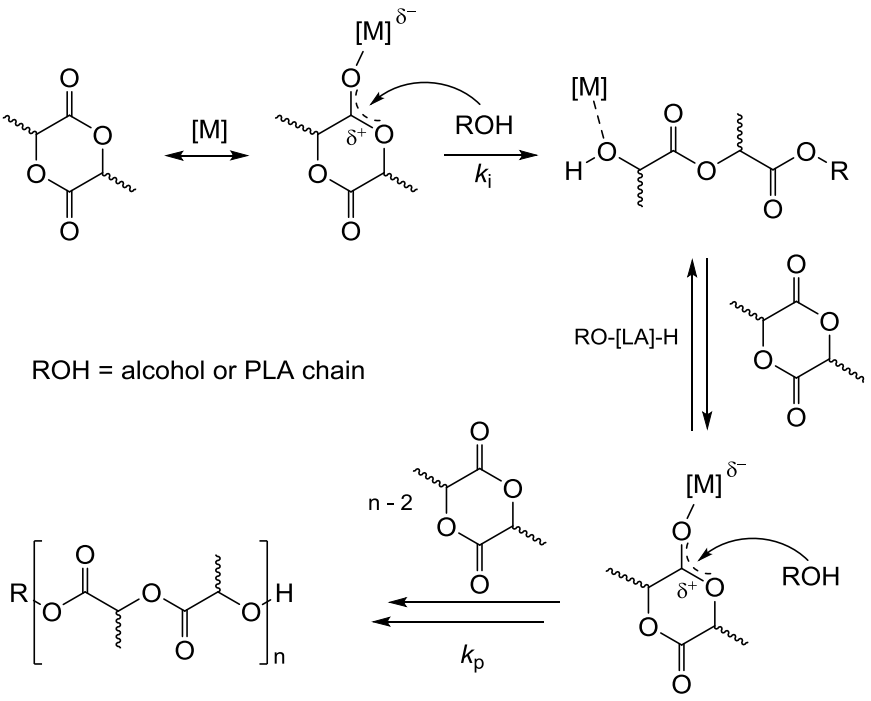

Scheme 1.8. Activated monomer ROP mechanism using metal catalyst. k_i and k_p are the rate constants for initiation and propagation, respectively.[141-145]

A system with efficient initiation allows all of the protic initiators to be consumed at the initial stage of polymerisation. This enables the generation of multiple chains of polymer produced per metal centre. The concept is known as immortal polymerisation, which will be discussed in the following section (Section 1.5).

1.5. Living and immortal ROP

The concept of living polymerisation was first introduced in the work of Szwarc *et al*. in 1956 concerning anionic polymerisation of styrene initiated with sodium napthalenide.[146] Living polymerisation is defined as a polymerisation reaction which proceeds in an absence of chain-transfer or chain termination steps, with a high k_i/k_p (where k_i = rate of initiation and k_p = rate of propagation) and a high k_p/k_{tr} (where k_p = rate of propagation and k_{tr} = rate of transesterification).[11] The characteristic features of living ROP are linear increase in molecular weight with % monomer conversion or $1/[\text{initiator}]_0$, narrow molecular weight distribution, end group control and potential to undergo sequential monomer addition (i.e. potential utility for copolymer and various shaped polymer design). In the ideal system, the molecular weight of the polymer produced is controlled by the stoichiometric ratio of monomer to initiator.[4, 27, 147, 148] The controlled polymerisations enable the physical properties of polymers to be tuned by the quantity and nature of initiators employed.[11] Metal mediated ROP reactions often proceed in a living manner.[4, 12, 23, 149]

For the majority of ROP, the general rate law is $-d[M]/dt = k[I]^a[M]^b$ (where [I] and [M] are initiator and monomer concentration and *a* and *b* are the orders with respect to [I] and [M], respectively). The polymerisation reaction is often overall second order, being first order with respect to both initiator and monomer concentration (i.e. $a = b = 1$).[150] In order to evaluate the rate of polymerisation or the propagating rate, pseudo first order experiments are carried out at various concentrations of the initiators. This enables the k_{app} (sometimes referred as k_{obs}) to be determined at particular initiator concentration.[11] Nevertheless, the reaction orders in $[M]^b$ of greater than one[151, 152] or the non-integer rate order of $[I]^a$ are precedent in literature.[30, 75, 122, 128, 153-156] The possibility of metal initiator or active polymer chain aggregation accounts for the non-unity order in initiator concentration.[156-160] In some cases, initiation processes associating with induction periods in living ROP are also observed, where the rearrangement of ligands of the initiators occur allowing the monomers to access the coordination spheres of metal centres.[161, 162]

Despite yielding well-controlled polymerisation, traditional living ROP is inherently limited by low productivity and potential contamination of metal residues as the number of polymer chains obtained is directly proportional to the number of initiators present in the polymerisation solution.[20] A concept of immortal ring-opening polymerisation (iROP) was introduced to improve the efficiency of the traditional living ROP. The addition of protic agents, known as chain transfer agent (CTA), results in the production of narrow PDI polymers with their number corresponding to the initial amount of CTA introduced in iROP.[27, 163] A pictorial comparison between the classical living ROP and the immortal ROP is illustrated in Figure 1.2.

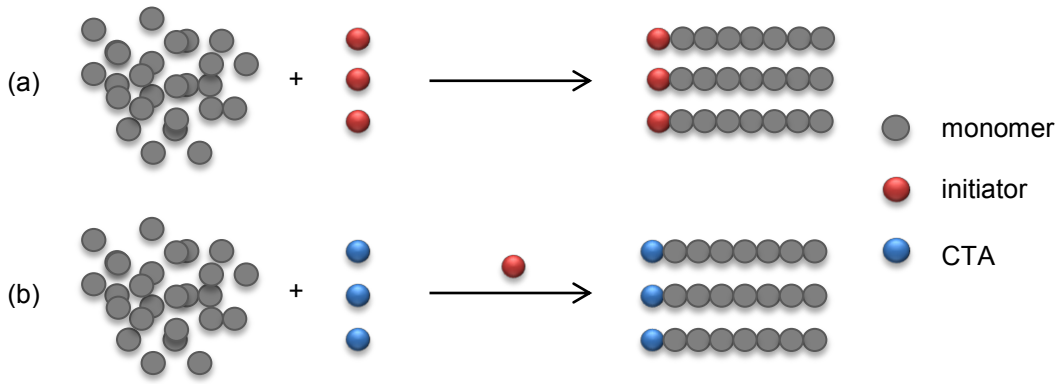

Figure 1.2. Pictorial representation of the distinction between (a) "classical living" and (b) "Immortal" Ring-Opening Polymerisation processes.[20]

Early iROP research was pioneered by Inoue and co-workers in 1980s for iROP of epoxides[164, 165] and some cyclic esters[166-168] using porphyrin supported aluminium alkoxides in the presence of appropriate protic agents. Building upon the early success, other metal (Mg,[72, 169, 170] Ca,[161, 170, 171] Sr, Ba,[170, 171] Al,[163, 167, 172, 173] Zn,[72, 170, 171] Sn[174] and Y[102, 175, 176]) mediated iROPs have been successfully reported.

Similar to living ROP, a much faster rate of initiation to propagation ($k_i >> k_p$) is required. In addition, the crucial feature to achieve the controlled iROP is the faster rate of reversible chain transfer to the propagation ($k_{tr} >> k_p$).[20] Metal mediated iROP could proceed through either coordination-insertion or activated-monomer mechanism. Only coordination-insertion iROP is emphasised in this Thesis and thoroughly explained in this section.

Typically, a preliminary step in the coordination-insertion iROP involves an *in situ* generated initiating species ((L)M-OR) as a result of the protonolysis between a non-

alkoxide (L)M-Nu (Nu = nucleophilic group) and protic CTA. The initiation results in the insertion of a lactide monomer into the M-OR bond leading to the formation of the propagating species (L)M-[pol]-OR, where pol is a growing polymeryl chain. This species then participates in the rapid exchange, driven by the acid-base process, with an excess protic CTA in the reaction medium giving "dormant" H-[pol]-OR and newly active intiator (L)M-OR. In this system, the metal alkoxide species act as active initiators whilst the dormant species serve as comparable CTA. The rapid interconversion between the growing polymer chains on the metal centres and CTAs is maintained over the course of iROP, yielding multiple alkoxy end-capped polymers per metal centre.[20] The coordination-insertion iROP pathway is illustrated in Scheme 1.9.

Owing to the incorporation of protic agents to the polymer chains as their end group functionality, iROP allows the polymer functionality to be tuned in a one-pot process.[23, 177] Furthermore, linear or star block copolymers could also be accessed *via* iROP of comonomer utilising multifunctional CTAs.[178]

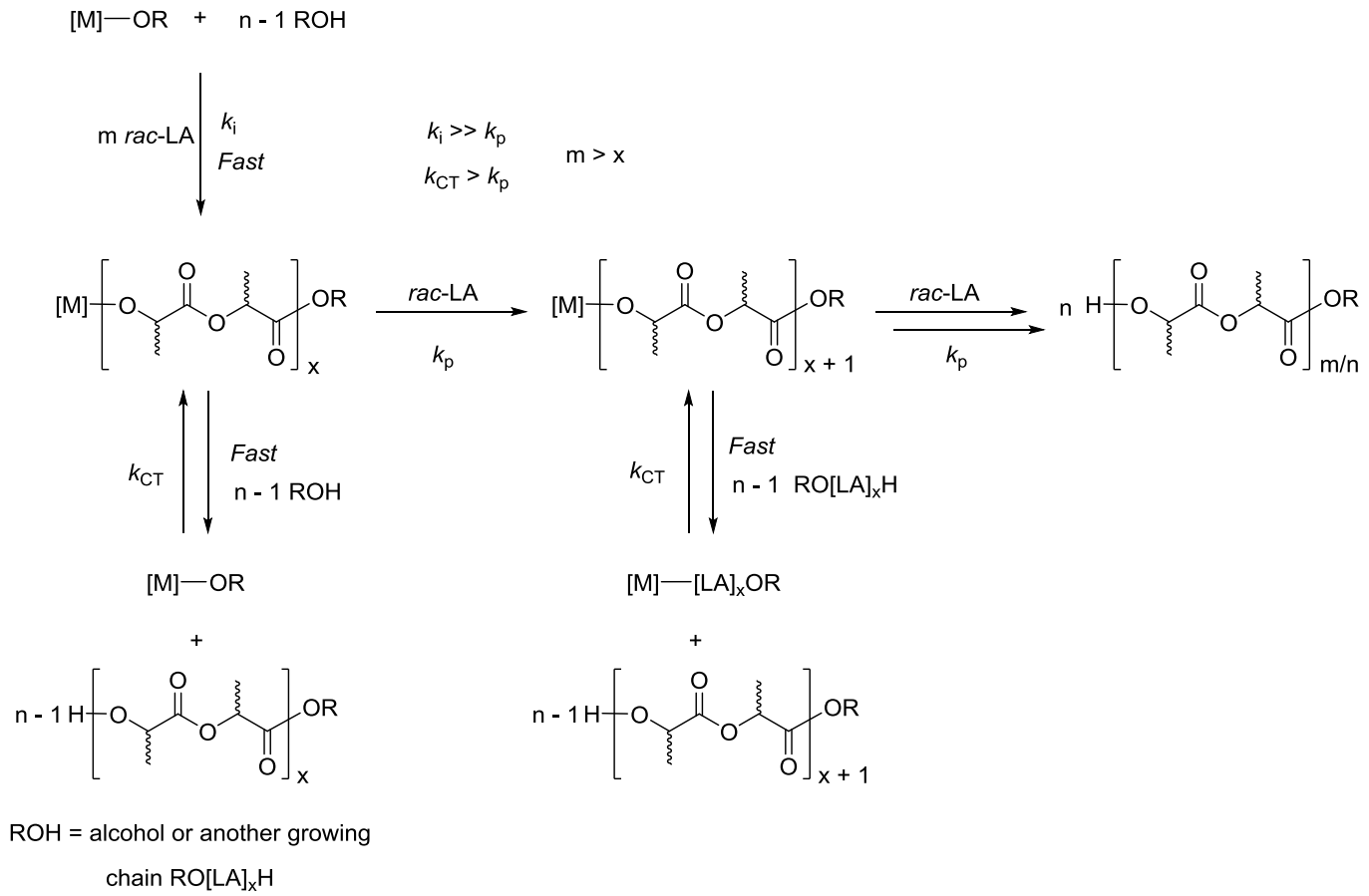

Scheme 1.9. Immortal ROP of *rac*-LA using alcohol chain transfer agents.[175, 179]

1.6. Stereocontrol and tactacity of PLA

Polymer stereochemistry is an important parameter influencing its physical and mechanical properties, as well as the rate of chemical and biological degradation.[98] The stereochemistry of PLA depends on the type of lactide monomers and the initiator selected during the ROP process. The lactide possesses two stereogenic centres and therefore three possible diastereomers: RR-, SS-, and RS- (*meso*-lactide). The commercially available lactides are single enantiomers and racemic mixture (*rac*-lactide). The stereochemistry of PLA depends on both selected initiator and type of lactide monomer. Various microstructures can be envisaged for the PLA obtained from the ROP of these enantiopure (RR-, SS-), *meso*- lactide, and *rac*-lactide (Figure 1.3).[6, 11, 27, 98]

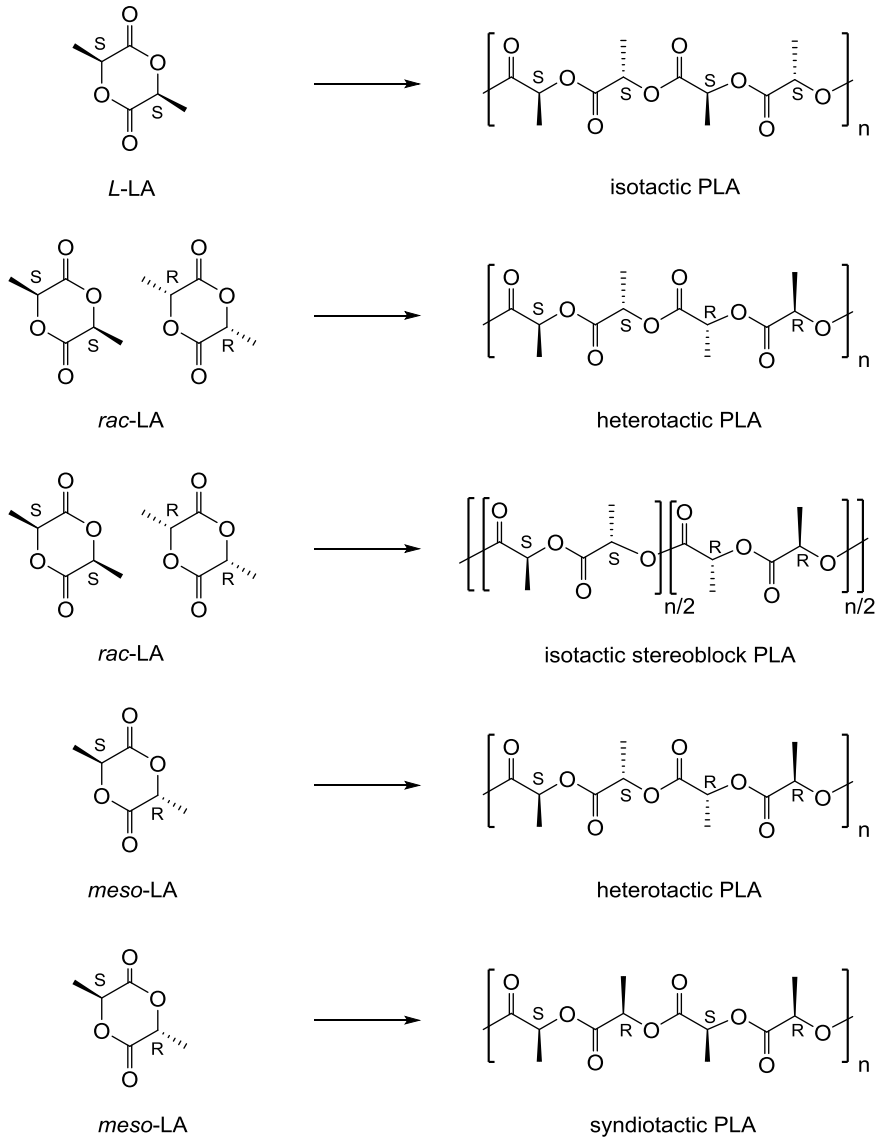

Figure 1.3. Lactide stereoisomers and PLA microstructures.[98]

The tacticity of PLA is expressed in term of the probability of enchainment between two consecutive monomers (stereosequences): P_i is the probability of isotactic enchainment (sometimes referred to as P_m) and P_r for racemic enchainment.[11, 180]

In the absence of epimerisation, ROP of *L*-LA or *D*-LA leads to the formation of isotactic PLLA or PDLA, respectively, with melting temperature (T_m) around 180 °C.[181-184] Stereocomplex PLA produced from the post-modification (blending) between PLLA and PDLA possesses a higher melting temperature of 230 °C, surpassing that of isotactic PLA alone.[185] In 1990, Feijen and co-workers reported the synthesis of stereoblock PLA with its T_m elevated to 205 °C.[186] In contrast, ROP with no control over stereoselectivity of lactide gives atactic PLA, which has a low glass transition temperature (T_g) of 55-60 °C, low tensile strength and short degrading time.[33] The ROP of *rac*-LA and *meso*-LA could lead to the formation of heterotactic (alternating pairs of stereocentres) or isotactic PLA in the case of *rac*-LA and syndiotactic (singly alternating stereocentres) or heterotactic PLA in the case of *meso*-LA.

Due to the difference in physical and mechanical properties of the polymers, the synthesis of stereoregular PLA is crucial. ROP using metal-based catalysts is proposed to proceed through one or a combination of the two mechanisms: chain-end control and enantiomorphic site control. The configuration of the next-inserted *rac*-lactide monomer or the cleavage site of next-inserted *meso*-lactide is determined by the stererogenic centre of the previously enchained monomer in a chain-end control mechanism and determined by the configuration of the ancillary ligand in an enantiomorphic site control mechanism.[85, 135, 187, 188] Both chain-end control and enantiomorphic site control could operate cooperatively in ROP using chiral ligand supporting initiators either in constructive or destructive manner.[187]

1.6.1 Determining stereosequencing of PLA using NMR spectroscopy

Heterodecoupled $^{13}C\{^1H\}$ and homodecoupled $^1H\{^1H\}$ NMR spectroscopy are the most common techniques used to access the tacticity of PLA. The stereosequence distribution in PLA is determined by the assignment of the NMR resonances corresponding to the methine region in $^1H\{^1H\}$ NMR analysis and methine or carbonyl carbon region of $^{13}C\{^1H\}$ NMR analysis.[139, 189-194] This assignment method was first derived using the Bernoullian statistical model of the single and pair-wise

addition of lactide monomers, and introduced by Lillie *et al*. in 1975[195] and Schindler *et al*. in the following year.[196]

Later the assignment of the NMR resonances to specific stereosequences of PLA was revised and established using one- and two-dimentional (HECTOR, HMQC and HMBC) NMR techniques, in combination with selective isotopic labeling by Thakur and co-workers. The widely accepted assignments for PLA synthesised using *rac*-LA and *meso*-LA are shown in Figure 1.4.[197]

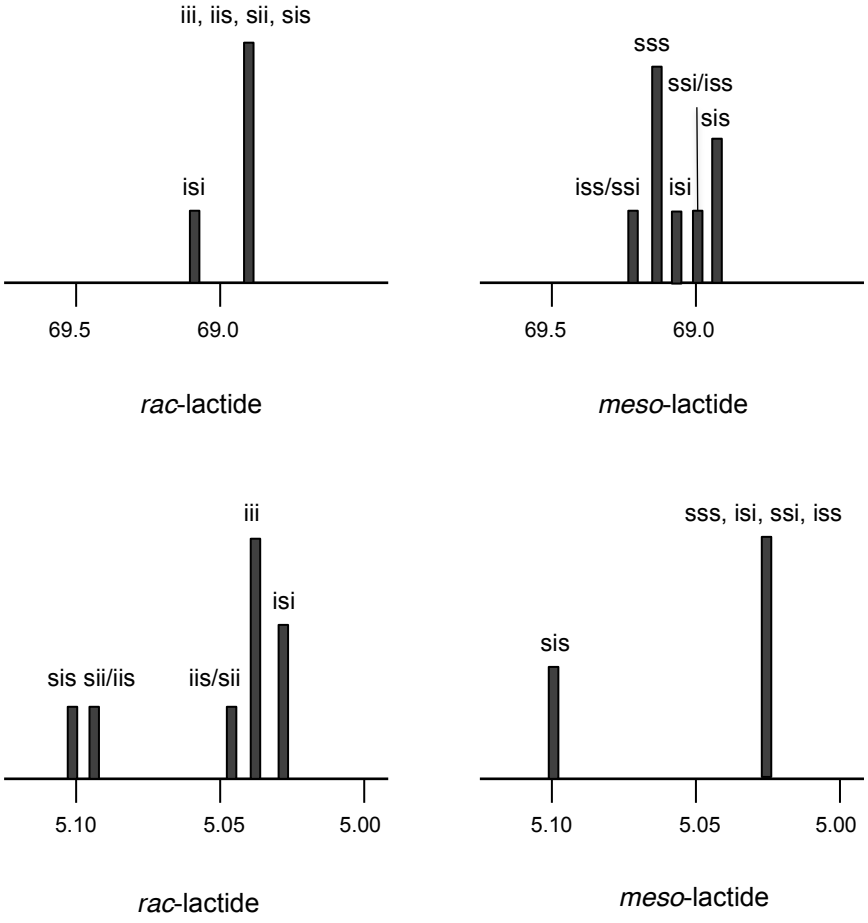

Figure 1.4. Schematic representative of the $^{13}C\{^{1}H\}$ and $^{1}H\{^{1}H\}$ stereosequence assignments for PLA at the tetrad level.[197]

The common notations used to designate the pairwise relationships of two adjacent stereocentres are *i* and *s*, where *i* refers to an isotactic linkage (-*RR*- and -*SS*-) and *s* refers to a syndiotactic linkage (-*SR*- and -*RS*-). Most of the stereosequence determinations of PLA reported in the literature are carried out at the tetrad level (4 stereocentres, 2 LA monomer units) with up to 8 possible combinations of pairwise

relationships observed in the NMR spectra. Moreover, high-resolution hexade assignments can also been made using the same methodology.[192, 194, 197, 198]

1.7. Polymer molecular weight: definitions

Polymers obtained from syntheses are rarely uniform in lengths. The terms commonly used to describe polymer properties are a number average molecular weight, a weight average molecular weight and a polydispersity index.[199]

The number average molecular weight (M_n) can be calculated according to Equation 1.1 (where N_i is a number of molecules having a molecular mass of M_i).

$$M_n = \frac{\sum N_i \times M_i}{\sum N_i}$$

Equation 1.1

The weight average molecular weight (M_w) can be calculated according to Equation 1.2 (where W_i is the total mass of polymer ($N_i \times M_i$) having a molecular mass of M_i).

$$M_w = \frac{\sum W_i \times M_i}{\sum W_i}$$

Equation 1.2

The polydispersity index (PDI) is a measure of molecular mass distribution of a given polymer sample. The PDI value is derived from Equation 1.3.

$$PDI = \frac{M_w}{M_n}$$

Equation 1.3

In living polymerisations, the polymer chains are allowed to grow constantly in the absence of chain termination or chain transfer reaction. These give polymers with invariable chain lengths and the PDI value of unity would be expected. Practically, the weight average molecular weight, M_w, is biased towards polymers chains of higher mass. Polymerisations representing greater M_w than M_n are typically observed with PDIs of greater than one, even in extremely well controlled systems. The deviation of PDI from unity could be due to transesterfication, reversible chain-transfer reaction, chain termination reaction as well as slow initiation with respect to propagation. Regarding ROP of cyclic esters, polymers with PDI < 1.2 are considered

to contain a narrow molecular weight distribution. In this thesis, a PDI of around 1.2 to 1.8 is considered a moderate distribution and a PDI > 1.8 is considered a broad distribution.

1.8 Polymer characterisation

1.8.1 MALDI-ToF mass spectrometry

Matrix Assisted Laser Desorption Ionisation - Time of Flight Mass Spectrometry (MALDI-ToF MS) is one of the crucial techniques used in characterisation of bio-macromolecules and synthetic polymers. MALDI-ToF MS affords structural information such as monomer and polymer masses, as well as functional group identification of the polymers. The selection of an appropriate MALDI matrix and a cationisation salt is essential to attain a reliable mass spectrum.[200]

For analyte preparation, the polymer sample is mixed with selected matrix and embedded into a MALDI target as solvent-free spots. The widely used MALDI matrices can be classified into two classes based on their chemical compounds, namely, cinnamic acid derivatives [e.g. α-cyano-4-hydroxycinnamic acid (α-CHCA)] and aromatic carbonyl derivatives [e.g. 2,5-dihydroxybenzoic acid (2,5-DHB)].[201] The sample is then irradiated with very short pulses of IR or UV laser light inside a vacuum chamber. The matrix absorbs the radiation energy and transfers it to the polymer molecules causing desorption and ionisation, with no thermal degradation. This is the important feature of the technique allowing analyses of macromolecules.[202-204] For relatively polar polymers, sodium or potassium salts are used as cationic dopant forming $[polymer\text{-}M]^+$ adduct ions. These ions are accelerated through a time of flight spectrometer and resolved in mass spectra as peak envelops with units of mass-to-charge ratio. The MALDI-ToF mass spectrometer and sample preparation technique used in this thesis are thoroughly described in Section 6.1.

1.8.2 Gel permeation chromatography

Gel Permeation Chromatography (GPC) or Size Exclusion Chromatography (SEC) is a powerful technique, applicable to determine molecular weights and polydispersity indices of polymer samples based on their hydrodynamic volumes.[205] In this technique polymer samples are dissolved in appropriate organic solvents, THF, aromatic or chlorinated solvents, and eluted through a chromatographic column. Two different materials are used in column packing, silica-based material and polymer beads of

styrene divinyl-benzene copolymer, both of which are of 5-10 μm in diameter. These packing materials contain networks with uniform pores allowing solvent and solute molecules to diffuse through. Separation relies on the relative sizes of polymer molecules in solution to the pore; smaller molecules permeate through the pores with longer retention time and are eluted last in comparison to the larger ones.[206]

Polymer detection is typically performed using either concentration sensitive detectors (e.g. UV, fluorescence, evapourative light scattering and differential refractive index detector) or molecular weight sensitive detectors (e.g. low angle or multi angle light scattering detector), or both in the case of copolymer characterisation. For linear polyesters, a differential refractometer with refractive index (RI method) is widely used.[207] The molecular weights obtained are calculated with reference to the standard polystyrene of known M_n, M_w, M_p (distribution maximum point) and PDI values.

Nevertheless the hydrodynamic volumes of polystyrene and polyesters are different at the same concentration and condition. Therefore a correction is required to relate the observed molecular weights to their true values. It is known that the hydrodynamic volume is proportional to the product [η]M, where [η] is the intrinsic viscosity and M is molecular weight. The universal calibration curve derived from the plot of log[η]M versus elution volume or time holds true for all polymer types, so long as the Mark-Houwink corrections are known for the polymer species. The Mark-Houwink relationship of [η] and M is defined in Equation 1.4.[199, 205, 208]

$$[\eta] = K.M^{\alpha}$$

Equation 1.4

From a linear plot of log[η] against logM, K is determined from the log[η]-axis intercept value and α is obtained directly from the gradient of the plot. The nature of polymer in solution can be evaluated from the α value, which typically ranges between 0.0 and 2.0. An α value of 0.0 refers to a hard sphere, 2.0 referring to an absolute rigid rod and a value of around 1.0 indicates flexible or semi-coils formation. Noteworthily, the Mark-Houwink corrections are solvent- and temperature-specific. The molecular weights and distributions obtained for PCL and PLA in this Thesis were analysed in THF at 30 °C, the previously determined Mark-Houwink corrections are applied.[209, 210] As previously mentioned, only linear polyesters are correctly

measured using the RI method. Cyclic polyesters formed due to the transesterification or other side reactions are taken into account by approximation.

1.8.3 NMR Spectroscopy

^{1}H and ^{13}C NMR spectroscopy are vital tools utilised in characterisation of isolated novel polymers. The resonances of the repeating monomer units are dominant features in the ^{1}H and ^{13}C NMR spectra of polymer products. However, sufficiently low molecular weight polymers allow the end-group or polymer functionality to be observed and hence identified.

Moreover, ^{1}H NMR spectroscopy is also used in the polymerisation kinetic studies. A quantitative conversion to polymer could be calculated at a given time *t* from the integration of the signals corresponding to polymer against unchained monomer. A kinetic profile is an informative overview of catalyst behaviour in polymerisation. Often ^{1}H NMR spectroscopy is a cooperative technique to a GPC/SEC, used in determining the molecular weight of polymer samples. The only drawback is that the NMR spectroscopic method is limited to polymers of low molecular weights.

1.9 Industrial ROP catalysts

Tin(II) bis(2-ethylhexanoate), also known as tin(II) octanoate ($Sn(Oct)_2$), is the most common ROP catalyst used for research purposes and for the technical production of PLA and related copolymers, Figure 1.5.[12, 22, 211] The preferential use of $Sn(Oct)_2$ in the bulk polymerisation of the cyclic esters is owing to its ease of handling, solubility in common organic solvent and in the bulk monomer under melt condition.[33] $Sn(Oct)_2$ exhibits a high catalytic activity, polymerising large-scale lactide monomer in a matter of minutes or hours in the presence of an alcohol as a coinitiator. The ROP affords high molecular weight PLA (10^5-10^6 g mol^{-1}) with less than 1 % racemisation observed.[132, 212] $Sn(Oct)_2$ catalysed ROP is nevertheless not without intra- and intermolecular transesterification, which takes place not only during the solution-phase polymerisation but also under the melt condition.[213] As previously mentioned, protic carrying agents as co-initiators are crucial in the ROP using $Sn(Oct)_2$. Several mechanisms have been proposed, including the activated monomer mechanism whereby the exogenous alcohol molecule attacks the activated LA monomer coordinating to the tin (II) metal centre.[12] Later on, Penczek and coworkers proposed the coordination-insertion mechanism. The alkoxide initiator was generated in the

mixture of $Sn(Oct)_2$ and alcohol, prior to the polymerisation. Evidence supporting this mechanism was obtained through intermediate studies (tin(II) alkoxide and the liberation of octanoic acid), kinetic investigation (the comparable rates of ROP between $Sn(Oct)_2$/butanol and tin(II) butoxide/octanoic acid) and polymer end group characterisation.[12, 211, 214-216]

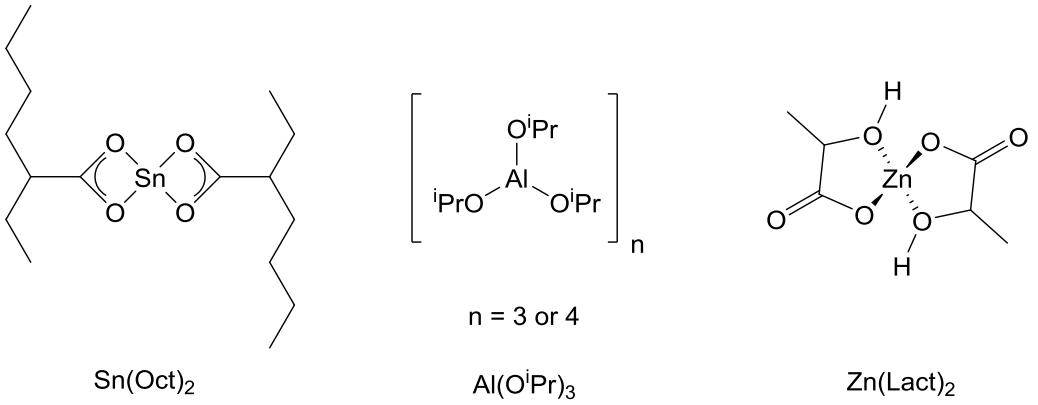

Figure 1.5. Structure of tin (II) octanoate (left), aluminium isopropoxide (middle) and zinc lactate (right).[22]

The major drawback of ROP using $Sn(Oct)_2$ is the amount of the metal residue in the polymer product, especially Sn (IV), and its possible toxicity. This imposes limitations on the use of the polymer in biomedical applications.[217]

In addition to $Sn(Oct)_2$, aluminium alkoxide, namely $Al(O^iPr)_3$, has been of great interest as ROP initiator and used in mechanistic studies.[138, 218, 219] $Al(O^iPr)_3$ polymerises ROP of cyclic esters through the coordination-insertion mechanism, affording isopropyl ester end group polymer. $Al(O^iPr)_3$ is inherently less active than $Sn(Oct)_2$, a bulk polymerisation required several days at 125-180 °C to yield polymer with molecular weight generally lower than 10^5 Da.[132] First order kinetics with respect to the concentration of catalyst and monomer concentration were observed, nevertheless the common induction period was typically found ROP catalysed by aluminium alkoxide initiators. This was attributed to aggregation phenomenon. The type and size of aggregates depend on the nature of substituents, co-ligands and solvent polarity.[160, 217, 220]

Due to the bio-incompatible nature of tin and aluminium, later years have witnessed a renaissance in the research area associating the biocompatible metal initiator catalysed ROP. Zinc powder and various zinc salts including zinc lactate, zinc ethanoate, zinc

stearate and zinc salicylate are found to be improved catalysts and utilised industrially. Comparable catalytic activity between zinc-based catalysts and $Al(O^iPr)_3$ was observed, several days were required to complete bulk polymerisation under the melt condition at 140 °C. Among all the zinc based-catalysts mentioned, a better control of polymer molecular weight was achieved from the ROP catalysed using zinc-lactate.[11, 12, 221, 222]

1.10 Aims and outlook

Owing to a significant increase in the industrial production of biodegradable polymers and their utilities in the past decades, numerous studies have been devoted to enhance catalytic performance of ROP catalysts and reduce other side reactions. Traditional industrial ROP catalysts are mostly homoleptic species as previously described, often these are plagued by aggregation leading to a poorly controlled polymerisation. Later works in both academic and industrial research, influenced by the catalyst development for olefin polymerisation, focus on the development of heteroleptic compounds (L)M-X (L is ancillary ligand, M is Lewis acidic metal centre and X is an initiating group). On this basis, variation in ancillary ligand, metal species and initiator has promoted different polymerisation rate and monomer selectivity. The works described in this Thesis also aim to reflect the development of alkaline earth tetrahydroborates or organohydroborates as ROP initiators for ε-caprolactone and *rac*-lactide. Moreover, the introduction of the immortal ROP using borate and borane derivatives as a new type of CTAs is present.

1.11 References

1. http://bioplasticnews.com, *European Bioplastics 2013*, accessed on 14th August 2014.
2. R. Raja and J. M. Thomas, *Z. Anorg. Allg. Chem.*, 2005, **631**, 2942.
3. R. A. Gross and B. Kalra, *Science*, 2002, **297**, 803.
4. B. J. O'Keefe, M. A. Hillmyer and W. B. Tolman, *J. Chem. Soc., Dalton Trans.*, 2001, 2215.
5. C. A. Wheaton, P. G. Hayes and B. J. Ireland, *Dalton Trans.*, 2009, 4832.
6. C. K. Williams and M. A. Hillmyer, *Polym. Rev.*, 2008, **48**, 1.
7. R. Datta, S.-P. Tsai, P. Bonsignore, S.-H. Moon and J. R. Frank, *FEMS Microbiol. Rev.*, 1995, **16**, 221.

8. K. L. Wasewar, A. A. Yawalkar, J. A. Moulijn and V. G. Pangarkar, *Ind*. *Eng*. *Chem*. *Res*., 2004, **43**, 5969.
9. R. Auras, B. Harte and S. Selke, *Macromol*. *Biosci*., 2004, **4**, 835.
10. S. Mecking, *Angew*. *Chem*. *Int*. *Ed*., 2004, **43**, 1078.
11. R. H. Platel, L. M. Hodgson and C. K. Williams, *Polym*. *Rev*., 2008, **48**, 11.
12. O. Dechy-Cabaret, B. Martin-Vaca and D. Bourissou, *Chem*. *Rev*., 2004, **104**, 6147.
13. R. O. MacRae, C. M. Pask, L. K. Burdsall, R. S. Blackburn, C. M. Rayner and P. C. McGowan, *Angew*. *Chem*. *Int*. *Ed*., 2011, **50**, 291.
14. A. P. Gupta and V. Kumar, *Eur*. *Polym*. *J*., 2007, **43**, 4053.
15. C. M. Thomas, *Chem*. *Soc*. *Rev*., 2010, **39**, 165.
16. W. H. Carothers, G. L. Dorough and F. J. v. Natta, *J*. *Am*. *Chem*. *Soc*., 1932, **54**, 761.
17. K. Madhavan Nampoothiri, N. R. Nair and R. P. John, *Bioresource Technol*., 2010, **101**, 8493.
18. C. E. Lowe, U.S. Patents, 1954.
19. S. Slomkowski, S. Penczek and A. Duda, *Polym*. *Advan*. *Technol*, 2014, **25**, 436.
20. N. Ajellal, J.-F. Carpentier, C. Guillaume, S. M. Guillaume, M. Helou, V. Poirier, Y. Sarazin and A. A. Trifonov, *Dalton Trans*., 2010, **39**, 8363.
21. J. Wu, T.-L. Yu, C.-T. Chen and C.-C. Lin, *Coord*. *Chem*. *Rev*., 2006, **250**, 602.
22. P. Dubois, O. Coulembier and J.-M. Raquez, *Handbook of Ring-Opening Polymerization*, Wiley-VCH, 2009.
23. C. K. Williams, *Chem*. *Soc*. *Rev*., 2007, **36**, 1573.
24. A. Duda and S. Penczek, *Macromolecules*, 1990, **23**, 1636.
25. A. Duda and S. Penczek, *ACS Symp*. *Ser*., 2000, **764**, 160.
26. H. R. Kricheldorf, M. Berl and N. Scharnagl, *Macromolecules*, 1988, **21**, 286.
27. A. P. Dove, *Chem*. *Commun*., 2008, 6446.
28. F. Nederberg, E. F. Connor, M. Möller, T. Glauser and J. L. Hedrick, *Angew*. *Chem*. *Int*. *Ed*., 2001, **40**, 2712.
29. L. Zhang, F. Nederberg, J. M. Messman, R. C. Pratt, J. L. Hedrick and C. G. Wade, *J*. *Am*. *Chem*. *Soc*., 2007, **129**, 12610.

30. P. Dubois, C. Jacobs, R. Jerome and P. Teyssie, *Macromolecules*, 1991, **24**, 2266.
31. M. K. Kiesewetter, E. J. Shin, J. L. Hedrick and R. M. Waymouth, *Macromolecules*, 2010, **43**, 2093.
32. S. Penczek, M. Cypryk, A. Duda, P. Kubisa and S. Slomkowski, *Prog. Polym. Sci.*, 2007, **32**, 247.
33. A.-C. Albertsson and I. K. Varma, *Biomacromolecules*, 2003, **4**, 1466.
34. Z. Jedlinski, P. Kurcok and M. Kowalczuk, *Macromolecules*, 1985, **18**, 2679.
35. Z. Jedlinski, M. Kowalczuk and P. Kurcok, *Macromolecules*, 1991, **24**, 1218.
36. Z. Jedliński, P. Kurcok, W. Walach, H. Janeczek and I. Radecka, *Die Makromol. Chem.*, 1993, **194**, 1681.
37. P. Kurcok, J. Penczek, J. Franek and Z. Jedlinski, *Macromolecules*, 1992, **25**, 2285.
38. A. Bhaw-Luximon, D. Jhurry, N. Spassky, S. Pensec and J. Belleney, *Polymer*, 2001, **42**, 9651.
39. S. Penczek, *J. Polym. Sci., Part A: Polym. Chem.*, 2000, **38**, 1919.
40. M. Baśko and P. Kubisa, *J. Polym. Sci., Part A: Polym. Chem.*, 2006, **44**, 7071.
41. N. E. Kamber, W. Jeong, R. M. Waymouth, R. C. Pratt, B. G. G. Lohmeijer and J. L. Hedrick, *Chem. Rev.*, 2007, **107**, 5813.
42. M. Baśko and P. Kubisa, *J. Polym. Sci., Part A: Polym. Chem.*, 2010, **48**, 2650.
43. J. Matsuo, K. Aoki, F. Sanda and T. Endo, *Macromolecules*, 1998, **31**, 4432.
44. F. Sanda, T. Fueki and T. Endo, *Macromolecules*, 1999, **32**, 4220.
45. H. R. Kricheldorf and I. Kreiser, *Makromol. Chem.*, 1987, **188**, 1861.
46. H. R. Kricheldorf and R. Dunsing, *Makromol. Chem.*, 1986, **187**, 1611.
47. H. R. Kricheldorf, J. M. Jonté and R. Dunsing, *Makromol. Chem.*, 1986, **187**, 771.
48. H. R. Kricheldorf, R. Dunsing and A. Serra, *Macromolecules*, 1987, **20**, 2050.
49. D. Bourissou, B. Martin-Vaca, A. Dumitrescu, M. Graullier and F. Lacombe, *Macromolecules*, 2005, **38**, 9993.
50. A. P. Dove, R. C. Pratt, B. G. G. Lohmeijer, D. A. Culkin, E. C. Hagberg, G. W. Nyce, R. M. Waymouth and J. L. Hedrick, *Polymer*, 2006, **47**, 4018.

51. S. Csihony, D. A. Culkin, A. C. Sentman, A. P. Dove, R. M. Waymouth and J. L. Hedrick, *J. Am. Chem. Soc.*, 2005, **127**, 9079.

52. M. Myers, E. F. Connor, T. Glauser, A. Möck, G. Nyce and J. L. Hedrick, *J. Polym. Sci. Part A: Polym. Chem.*, 2002, **40**, 844.

53. L. Zhang, F. Nederberg, R. C. Pratt, R. M. Waymouth, J. L. Hedrick and C. G. Wade, *Macromolecules*, 2007, **40**, 4154.

54. N. E. Kamber, W. Jeong, S. Gonzalez, J. L. Hedrick and R. M. Waymouth, *Macromolecules*, 2009, **42**, 1634.

55. T. Trimaille, M. Möller and R. Gurny, *J. Polym. Sci. Part A: Polym. Chem.*, 2004, **42**, 4379.

56. T. Trimaille, R. Gurny and M. Moeller, *Chimia*, 2005, **59**, 348.

57. O. Thillaye du Boullay, E. Marchal, B. Martin-Vaca, F. P. Cossío and D. Bourissou, *J. Am. Chem. Soc.*, 2006, **128**, 16442.

58. F. A. Jaipuri, B. D. Bower and N. L. Pohl, *Tetrahedron: Asymmetry*, 2003, **14**, 3249.

59. E. F. Connor, G. W. Nyce, M. Myers, A. Möck and J. L. Hedrick, *J. Am. Chem. Soc.*, 2002, **124**, 914.

60. G. W. Nyce, T. Glauser, E. F. Connor, A. Möck, R. M. Waymouth and J. L. Hedrick, *J. Am. Chem. Soc.*, 2003, **125**, 3046.

61. O. Coulembier, L. Mespouille, J. L. Hedrick, R. M. Waymouth and P. Dubois, *Macromolecules*, 2006, **39**, 4001.

62. O. Coulembier, B. G. G. Lohmeijer, A. P. Dove, R. C. Pratt, L. Mespouille, D. A. Culkin, S. J. Benight, P. Dubois, R. M. Waymouth and J. L. Hedrick, *Macromolecules*, 2006, **39**, 5617.

63. F. Nederberg, B. G. G. Lohmeijer, F. Leibfarth, R. C. Pratt, J. Choi, A. P. Dove, R. M. Waymouth and J. L. Hedrick, *Biomacromolecules*, 2007, **8**, 153.

64. B. G. G. Lohmeijer, G. Dubois, F. Leibfarth, R. C. Pratt, F. Nederberg, A. Nelson, R. M. Waymouth, C. Wade and J. L. Hedrick, *Org. Lett.*, 2006, **8**, 4683.

65. W. Jeong, E. J. Shin, D. A. Culkin, J. L. Hedrick and R. M. Waymouth, *J. Am. Chem. Soc.*, 2009, **131**, 4884.

66. M. H. Chisholm, C.-C. Lin, J. C. Gallucci and B.-T. Ko, *Dalton Trans.*, 2003, 406.

67. B.-T. Ko and C.-C. Lin, *J. Am. Chem. Soc.*, 2001, **123**, 7973.

68. A. K. Sutar, T. Maharana, S. Dutta, C.-T. Chen and C.-C. Lin, *Chem. Soc. Rev.*, 2010, **39**, 1724.
69. W.-Y. Lu, M.-W. Hsiao, S. C. N. Hsu, W.-T. Peng, Y.-J. Chang, Y.-C. Tsou, T.-Y. Wu, Y.-C. Lai, Y. Chen and H.-Y. Chen, *Dalton Trans*, 2012, **41**, 3659.
70. C.-A. Huang and C.-T. Chen, *Dalton Trans.*, 2007, 5561.
71. M.-L. Hsueh, B.-H. Huang, J. Wu and C.-C. Lin, *Macromolecules*, 2005, **38**, 9482.
72. Y. Huang, W. Wang, C.-C. Lin, M. P. Blake, L. Clark, A. D. Schwarz and P. Mountford, *Dalton Trans*, 2013, **42**, 9313.
73. S.-C. Rosca, D.-A. Rosca, V. Dorcet, C. M. Kozak, F. M. Kerton, J.-F. Carpentier and Y. Sarazin, *Dalton Trans*, 2013, **42**, 9361.
74. J. Zhang, C. Jian, Y. Gao, L. Wang, N. Tang and J. Wu, *Inorg. Chem*, 2012, **51**, 13380.
75. B. M. Chamberlain, M. Cheng, D. R. Moore, T. M. Ovitt, E. B. Lobkovsky and G. W. Coates, *J. Am. Chem. Soc.*, 2001, **123**, 3229.
76. M. H. Chisholm and N. W. Eilerts, *Chem. Commun.*, 1996, 853.
77. J. Wu, Y.-Z. Chen, W.-C. Hung and C.-C. Lin, *Organometallics*, 2008, **27**, 4970.
78. V. Poirier, T. Roisnel, J.-F. Carpentier and Y. Sarazin, *Dalton Trans.*, 2009, 9820.
79. B. J. Ireland, C. A. Wheaton and P. G. Hayes, *Organometallics*, 2010, **29**, 1079.
80. R. A. Collins, J. Unruangsri and P. Mountford, *Dalton Trans.*, 2013, **42**, 759.
81. T. J. J. Whitehorne, B. Vabre and F. Schaper, *Dalton Trans.*, 2014, **43**, 6339.
82. M. G. Cushion and P. Mountford, *Chem. Commun.*, 2011, **47**, 2276.
83. H. R. Kricheldorf, K. Bornhorst and H. Hachmann-Thiessen, *Macromolecules*, 2005, **38**, 5017.
84. N. Nimitsiriwat, V. C. Gibson, E. L. Marshall and M. R. J. Elsegood, *Dalton Trans.*, 2009, 3710.
85. A. P. Dove, V. C. Gibson, E. L. Marshall, H. S. Rzepa, A. J. P. White and D. J. Williams, *J. Am. Chem. Soc.*, 2006, **128**, 9834.
86. A. Kowalski, J. Libiszowski, T. Biela, M. Cypryk, A. Duda and S. Penczek, *Macromolecules*, 2005, **38**, 8170.

87. N. Nimitsiriwat, E. L. Marshall, V. C. Gibson, M. R. J. Elsegood and S. H. Dale, *J. Am. Chem. Soc.*, 2004, **126**, 13598.
88. M. Lahcini, P. M. Castro, M. Kalmi, M. Leskelä and T. Repo, *Organometallics*, 2004, **23**, 4547.
89. J. S. Klitzke, T. Roisnel, E. Kirillov, O. d. L. Casagrande and J.-F. Carpentier, *Macromolecules*, 2014, **47**, 2574.
90. C. A. Wheaton, B. J. Ireland and P. G. Hayes, *Organometallics*, 2009, **28**, 1282.
91. H. Sun, J. S. Ritch and P. G. Hayes, *Inorg. Chem.*, 2011, **50**, 8063.
92. Z. Liu, W. Gao, J. Zhang, D. Cui, Q. Wu and Y. Mu, *Organometallics*, 2010, **29**, 5783.
93. S. M. Guillaume and J.-F. Carpentier, *Catal. Sci. Tech.*, 2012, **2**, 898.
94. W. Zhang, Y. Wang, L. Wang, C. Redshaw and W.-H. Sun, *J. Organomet. Chem.*, 2014, **750**, 65.
95. Z. Tang and V. C. Gibson, *Eur. Polym. J.*, 2007, **43**, 150.
96. X. Pang, H. Du, X. Chen, X. Wang and X. Jing, *Chem. Eur. J.*, 2008, **14**, 3126.
97. N. Nomura, R. Ishii, Y. Yamamoto and T. Kondo, *Chem. Eur. J.*, 2007, **13**, 4433.
98. T. M. Ovitt and G. W. Coates, *J. Am. Chem. Soc.*, 2002, **124**, 1316.
99. Z. Zhong, P. J. Dijkstra and J. Feijen, *Angew. Chem. Int. Ed.*, 2002, **41**, 4510.
100. C. Bakewell, T. P. A. Cao, N. Long, X. F. Le Goff, A. Auffrant and C. K. Williams, *J. Am. Chem. Soc.*, 2012, **134**, 20577.
101. C. Bakewell, A. J. P. White, N. J. Long and C. K. Williams, *Angew. Chem. Int. Ed.*, 2014, ASAP.
102. L. Clark, M. G. Cushion, H. D. Dyer, A. D. Schwarz, R. Duchateau and P. Mountford, *Chem.Commun.*, 2010, **46**, 273.
103. C.-X. Cai, A. Amgoune, C. W. Lehmann and J.-F. Carpentier, *Chem. Commun.*, 2004, 330.
104. B. M. Chamberlain, Y. Sun, J. R. Hagadorn, E. W. Hemmesch, V. G. Young, M. Pink, M. A. Hillmyer and W. B. Tolman, *Macromolecules*, 1999, **32**, 2400.
105. S. Yang, Z. Du, Y. Zhang and Q. Shen, *Chem. Commun.*, 2012, **48**, 9780.
106. J. S. Klitzke, T. Roisnel, E. Kirillov, O. d. L. Casagrande and J.-F. Carpentier, *Organometallics*, 2014, **33**, 309.

107. Z. R. Turner, J.-C. Buffet and D. O'Hare, *Organometallics*, 2014, **33**, 3891.
108. A. D. Schwarz, A. L. Thompson and P. Mountford, *Inorg*. *Chem*., 2009, **48**, 10442.
109. A. D. Schwarz, K. R. Herbert, C. Paniagua and P. Mountford, *Organometallics*, 2010, **29**, 4171.
110. M. Jeong Go, J. Min Lee, K. Mun Lee, C. Hwa Oh, K. H. Park, S. H. Kim, M. Kim, H.-R. Park, M. H. Park, Y. Kim and J. Lee, *Polyhedron*, 2014, **67**, 286.
111. R. L. Webster, N. Noroozi, S. G. Hatzikiriakos, J. A. Thomson and L. L. Schafer, *Chem*. *Commun*., 2013, **49**, 57.
112. A. Sauer, A. Kapelski, C. Fliedel, S. Dagorne, M. Kol and J. Okuda, *Dalton Trans*., 2013, **42**, 9007.
113. Y. Kim, G. K. Jnaneshwara and J. G. Verkade, *Inorg*. *Chem*., 2003, **42**, 1437.
114. M. Visseaux and F. Bonnet, *Coord*. *Chem*. *Rev*., 2011, **255**, 374.
115. A. Otero, J. Fernández-Baeza, A. Lara-Sánchez, C. Alonso-Moreno, I. Márquez-Segovia, L. F. Sánchez-Barba and A. M. Rodríguez, *Angew*. *Chem*. *Int*. *Ed*., 2009, **48**, 2176.
116. A. Buchard, R. H. Platel, A. Auffrant, X. F. Le Goff, P. Le Floch and C. K. Williams, *Organometallics*, 2010, **29**, 2892.
117. H. Ma, T. P. Spaniol and J. Okuda, *Angew*. *Chem*. *Int*. *Ed*., 2006, **45**, 7818.
118. J. Kratsch, M. Kuzdrowska, M. Schmid, N. Kazeminejad, C. Kaub, P. Oña-Burgos, S. M. Guillaume and P. W. Roesky, *Organometallics*, 2013, **32**, 1230.
119. A. J. Chmura, C. J. Chuck, M. G. Davidson, M. D. Jones, M. D. Lunn, S. D. Bull and M. F. Mahon, *Angew*. *Chem*. *Int*. *Ed*., 2007, **46**, 2280.
120. J. Guo, P. Haquette, J. Martin, K. Salim and C. M. Thomas, *Angew*. *Chem*., *Int*. *Ed*., 2013, **52**, 13584.
121. M. P. Blake, A. D. Schwarz and P. Mountford, *Organometallics*, 2011, **30**, 1202.
122. I. Yu, A. Acosta-Ramírez and P. Mehrkhodavandi, *J*. *Am*. *Chem*. *Soc*., 2012, **134**, 12758.
123. A. Pietrangelo, S. C. Knight, A. K. Gupta, L. J. Yao, M. A. Hillmyer and W. B. Tolman, *J*. *Am*. *Chem*. *Soc*., 2010, **132**, 11649.
124. V. Balasanthiran, M. H. Chisholm, C. B. Durr and J. C. Gallucci, *Dalton Trans*, 2013, **42**, 11234.

125. H. R. Kricheldorf, G. Behnken, G. Schwarz and J. Kopf, *Macromolecules*, 2008, **41**, 4102.
126. H. R. Kricheldorf, H. Hachmann-Thiessen and G. Schwarz, *Biomacromolecules*, 2004, **5**, 492.
127. A. B. Biernesser, B. Li and J. A. Byers, *J. Am. Chem. Soc*, 2013, **135**, 16553.
128. B. J. O'Keefe, L. E. Breyfogle, M. A. Hillmyer and W. B. Tolman, *J. Am. Chem. Soc*., 2002, **124**, 4384.
129. J. L. Gorczynski, J. Chen and C. L. Fraser, *J. Am. Chem. Soc*., 2005, **127**, 14956.
130. V. W. Dittrich and R. C. Schulz, *Angew. Makromol. Chem*., 1971, **15**, 109.
131. P. Degée, P. Dubois and R. Jérôme, *Macromol. Chem. Phys*., 1997, **198**, 1973.
132. P. Degée, P. Dubois, R. Jérŏme, S. Jacobsen and H.-G. Fritz, *Macromol. Symp*., 1999, **144**, 289.
133. H. D. Dyer, S. Huijser, N. Susperregui, F. Bonnet, A. D. Schwarz, R. Duchateau, L. Maron and P. Mountford, *Organometallics*, 2010, **29**, 3602.
134. H. von Schenck, M. Ryner, A.-C. Albertsson and M. Svensson, *Macromolecules*, 2002, **35**, 1556.
135. P. J. Dijkstra, H. Du and J. Feijen, *Polym. Chem*., 2011, **2**, 520.
136. J. Baran, A. Duda, A. Kowalski, R. Szymanski and S. Penczek, *Macromol. Rapid Commun*., 1997, **18**, 325.
137. N. Spassky, V. Simic, M. S. Montaudo and L. Hubert-Pfalzgraf, *Macromol. Chem. Phys*., 2000, **201**, 2432.
138. M. Bero, J. Kasperczyk and Z. J. Jedlinski, *Makromol. Chem*., 1990, **191**, 2287.
139. J. Coudane, C. Ustariz-Peyret, G. Schwach and M. Vert, *J. Polym. Sci. Part A: Polym. Chem*., 1997, **35**, 1651.
140. G. Montaudo, M. S. Montaudo, C. Puglisi, F. Samperi, N. Spassky, A. LeBorgne and M. Wisniewski, *Macromolecules*, 1996, **29**, 6461.
141. N. Nomura, A. Taira, A. Nakase, T. Tomioka and M. Okada, *Tetrahedron*, 2007, **63**, 8478.
142. N. Nomura, A. Taira, T. Tomioka and M. Okada, *Macromolecules*, 2000, **33**, 1497.
143. M. Möller, R. Kånge and J. L. Hedrick, *J. Polym. Sci., Part A: Polym. Chem*., 2000, **38**, 2067.

144. M. Labet and W. Thielemans, *Chem. Soc. Rev.*, 2009, **38**, 3484.
145. S. M. Weidner, F. Scheliga and H. R. Kricheldorf, *Macromol. Chem. Phys.*, 2013, **214**, 2043.
146. M. Szwarc, M. Levy and R. Milkovich, *J. Am. Chem. Soc.*, 1956, **78**, 2656.
147. T. Aida, *Prog. Polym. Sci.*, 1994, **19**, 469.
148. R. P. Quirk and B. Lee, *Polym. Int.*, 1992, **27**, 359.
149. M. Okada, *Prog. Polym. Sci.*, 2002, **27**, 87.
150. L. Wang, M. Bochmann, R. D. Cannon, J.-F. Carpentier, T. Roisnel and Y. Sarazin, *Eur. J. Inorg. Chem.*, 2013, **2013**, 5896.
151. F. Bonnet, A. R. Cowley and P. Mountford, *Inorg. Chem.*, 2005, **44**, 9046.
152. H.-Y. Chen, B.-H. Huang and C.-C. Lin, *Macromolecules*, 2005, **38**, 5400.
153. H.-Y. Chen, J. Zhang, C.-C. Lin, J. H. Reibenspies and S. A. Miller, *Green Chem.*, 2007, **9**, 1038.
154. A. Duda and S. Penczek, *Macromol. Rapid Commun.*, 1994, **15**, 559.
155. A. Duda and S. Penczek, *Polym. Prepr. (Am. Chem. Soc., Div. Polym. Chem.)*, 1990, **31**, 12.
156. T. Ouhadi, A. Hamitou, R. Jerome and P. Teyssie, *Macromolecules*, 1976, **9**, 927.
157. S. Penczek, A. Duda and T. Biela, *Polym. Prepr. (Am. Chem. Soc., Div. Polym. Chem.)*, 1994, **35**, 508.
158. C. K. Williams, L. E. Breyfogle, S. K. Choi, W. Nam, V. G. Young, M. A. Hillmyer and W. B. Tolman, *J. Am. Chem. Soc.*, 2003, **125**, 11350.
159. A. Kowalski, J. Libiszowski, A. Duda and S. Penczek, *Macromolecules*, 2000, **33**, 1964.
160. A. Duda and S. Penczek, *Makromol. Chem-M. Symp.*, 1991, **47**, 127.
161. Z. Zhong, P. J. Dijkastra, C. Birg, M. Westerhausen and J. Feijen, *Macromolecules*, 2001, **34**, 3863.
162. Z. Zhong, S. Schneiderbauer, P. J. Dijkstra, M. Westerhausen and J. Feijen, *J. Polym. Environ.*, 2002, **9**, 31.
163. Y.-C. Liu, B.-T. Ko and C.-C. Lin, *Macromolecules*, 2001, **34**, 6196.
164. S. Asano, T. Aida and S. Inoue, *J. Chem. Soc., Chem. Commun.*, 1985, 1148.
165. S. Inoue, *Makromol. Chem-M. Symp.*, 1986, **3**, 295.
166. K. Shimasaki, T. Aida and S. Inoue, *Macromolecules*, 1987, **20**, 3076.

167. T. Aida, Y. Maekawa, S. Asano and S. Inoue, *Macromolecules*, 1988, **21**, 1195.
168. S. Inoue, *J. Macromol. Sci., Pure Appl. Chem.*, 1988, **25**, 571.
169. Y. Wang, W. Zhao, X. Liu, D. Cui and E. Y. X. Chen, *Macromolecules*, 2012, **45**, 6957.
170. Y. Sarazin, B. Liu, T. Roisnel, L. Maron and J.-F. Carpentier, *J. Am. Chem. Soc.*, 2011, **133**, 9069.
171. Y. Sarazin, V. Poirier, T. Roisnel and J.-F. Carpentier, *Eur. J. Inorg. Chem.*, 2010, 3423.
172. M. Lamberti, I. D'Auria, M. Mazzeo, S. Milione, V. Bertolasi and D. Pappalardo, *Organometallics*, 2012, **31**, 5551.
173. M.-L. Hsueh, B.-H. Huang and C.-C. Lin, *Macromolecules*, 2002, **35**, 5763.
174. L. Wang, V. Poirier, F. Ghiotto, M. Bochmann, R. D. Cannon, J.-F. Carpentier and Y. Sarazin, *Macromolecules*, 2014, **47**, 2574.
175. A. Amgoune, C. M. Thomas and J.-F. Carpentier, *Pure Appl. Chem.*, 2007, **79**, 2013.
176. W. Zhao, D. Cui, X. Liu and X. Chen, *Macromolecules*, 2010, **43**, 6678.
177. I. Barakat, P. Dubois, R. Jérôme and P. Teyssié, *J. Polym. Sci., Part A: Polym. Chem.*, 1993, **31**, 505.
178. M. Helou, J.-F. Carpentier and S. M. Guillaume, *Green Chem.*, 2011, **13**, 266.
179. A. Amgoune, C. M. Thomas and J.-F. Carpentier, *Macromol. Rapid Commun.*, 2007, **28**, 693.
180. J.-F. Carpentier and Y. Sarazin, *Alkaline-Earth Metal Compounds*, Springer Berlin Heidelberg, 2013, vol. 45, pp. 141.
181. W. Amass, A. Amass and B. Tighe, *Polym. Int.*, 1998, **47**, 89.
182. A. Södergård and M. Stolt, *Prog. Polym. Sci.*, 2002, **27**, 1123.
183. J. Lunt, *Polym. Degrad. Stab.*, 1998, **59**, 145.
184. N. Nomura, J. Hasegawa and R. Ishii, *Macromolecules*, 2009, **42**, 4907.
185. Y. Ikada, K. Jamshidi, H. Tsuji and S. H. Hyon, *Macromolecules*, 1987, **20**, 904.
186. N. Yui, P. J. Dijkstra and J. Feijen, *Makromol. Chem.*, 1990, **191**, 481.
187. M. H. Chisholm, N. J. Patmore and Z. Zhou, *Chem. Comm.*, 2005, 127.
188. A. J. Chmura, M. G. Davidson, M. D. Jones and A. A. D. Tulloch, *Polym. Prepr. (Am. Chem. Soc., Div. Polym. Chem.)*, 2007, **48**, 881.

189. J. E. Kasperczyk, *Macromolecules*, 1995, **28**, 3937.
190. M. H. Chisholm, S. S. Iyer, M. E. Matison, D. G. McCollum and M. Pagel, *Chem. Commun.*, 1997, 1999.
191. M. H. Chisholm, S. S. Iyer, D. G. McCollum, M. Pagel and U. Werner-Zwanziger, *Macromolecules*, 1999, **32**, 963.
192. K. A. M. Thakur, R. T. Kean, K. A. M. Thakur, M. T. Zell, B. E. Padden and E. J. Munson, *Chem. Commun.*, 1998, 1913.
193. M. Wei, D. T. Ivey and A. E. Tonelli, *Macromolecules*, 2002, **35**, 1976.
194. H. R. Kricheldorf, C. Boettcher and K. U. Toennes, *Polymer*, 1992, **33**, 2817.
195. E. Lillie and R. C. Schulz, *Makromol. Chem.*, 1975, **176**, 1901.
196. A. Schindler and D. Harper, *J. Polym. Sci.: Polym. Lett. Ed.*, 1976, **14**, 729.
197. M. T. Zell, B. E. Padden, A. J. Paterick, K. A. M. Thakur, R. T. Kean, M. A. Hillmyer and E. J. Munson, *Macromolecules*, 2002, **35**, 7700.
198. J. L. Espartero, I. Rashkov, S. M. Li, N. Manolova and M. Vert, *Macromolecules*, 1996, **29**, 3535.
199. D. Walton and P. Lorimer, *Polymers, Oxford Chemistry Primers*, Oxford University Press, 2000.
200. M. W. F. Nielen, *Mass Spectrom. Rev.*, 1999, **18**, 309.
201. T. Kinumi, T. Saisu, M. Takayama and H. Niwa, *J. Mass Spectrom.*, 2000, **35**, 417.
202. I. K. D. Dimzon and T. P. Knepper, *Comprehensive Analytical Chemistry*, Elsevier, 2012, vol. 58, pp. 307.
203. J. H. Gross, *Mass Spectrometry: a textbook*, Spinger, Heidelberg, 2004.
204. S. Trimpin, A. Rouhanipour, R. Az, H. J. Rader and K. Mullen, *Rapid Commun. Mass Spectrom.*, 2001, **15**, 1364.
205. A. Rudin and H. L. W. Hoegy, *J. Polym. Sci., Part A: Polym. Chem.*, 1972, **10**, 217.
206. D. A. Skoog, Thompson Brooks/Cole: Belmont, California, 6th Edition, 2006.
207. B. Trathnigg, *Prog. Polym. Sci.*, 1995, **20**, 615.
208. P. C. Hiemenz and T. P. Lodge, *Polymer Chemistry*, 2nd Edition., CRC Press, New York, USA, 2007.
209. M. Save, M. Schappacher and A. Soum, *Macromol. Chem. Phys.*, 2002, **203**, 889.

210. J. R. Dorgan, J. Janzen, D. M. Knauss, S. B. Hait, B. R. Limoges and M. H. Hutchinson, *J. Polym. Sci. Part B: Polym. Phys.*, 2005, **43**, 3100.

211. H. R. Kricheldorf, I. Kreiser-Saunders and A. Stricker, *Macromolecules*, 2000, **33**, 702.

212. R. E. Drumright, P. R. Gruber and D. E. Henton, *Adv. Mater.*, 2000, **12**, 1841.

213. S. Gogolewski, M. Jovanovic, S. M. Perren, J. G. Dillon and M. K. Hughes, *Polym. Degrad. Stab.*, 1993, **40**, 313.

214. A. Duda, S. Penczek, A. Kowalski and J. Libiszowski, *Macromol. Symp.*, 2000, **153**, 41.

215. A. Kowalski, A. Duda and S. Penczek, *Macromolecules*, 2000, **33**, 7359.

216. J. Libiszowski, A. Kowalski, A. Duda and S. Penczek, *Macromol. Chem. Phys.*, 2002, **203**, 1694.

217. A. Stjerndahl, A. F. Wistrand and A.-C. Albertsson, *Biomacromolecules*, 2007, **8**, 937.

218. C. Miola-Delaite, T. Hamaide and R. Spitz, *Macromol. Chem. Phys.*, 1999, **200**, 1771.

219. A. Kowalski, A. Duda and S. Penczek, *Macromolecules*, 1998, **31**, 2114.

220. A. Duda, *Macromolecules*, 1996, **29**, 1399.

221. G. Schwach and M. Vert, *Int. J. Biol. Macromol.*, 1999, **25**, 283.

222. G. Schwach, J. Coudane, R. Engel and M. Vert, *Polym. Bull.*, 1996, **37**, 771.

Chapter Two

Group 2 tetrahydroborate complexes for the ROP of ε-CL and their mechanistic studies

2.1 Overview

This Chapter will introduce ROP of ε-CL and *rac*-LA catalysed by alkaline earth complexes. Detailed investigations into a series of alkaline earth tetrahydroborate complexes as ROP catalysts will be described, whereby an overview of the synthesis and characterisation of alkaline earth tetrahydroborate complexes supported by 3-methyl, 5-*tert*-butyl tris(pyrazolyl)hydroborate ligands ($Tp^{tBu,Me}$) will be presented. Their solid state structures and solution behaviours will be discussed, in conjuction with their activities towards the ROP of ε-CL. Comparative studies with appropriate literature examples will be drawn. Moreover, in-depth mechanistic studies of the tetrahydroborate initiating group in ε-CL using spectroscopic techniques will be present and discussed. Comparisons of the newly proposed mechanistic studies and the previously reported ones will be made. Complementary studies on the ROP of *rac*-LA using the same series of alkaline earth tetrahydroborate catalysts will be presented in the following Chapter, along with the corresponding mechanistic studies. In this Chapter, seven new Group 2 complexes are presented, as well as six X-ray crystal structures.

2.2 Introduction

2.2.1 Alkaline earth complexes as ROP catalysts

Transition metal complexes have dominated catalysis due to their available d-orbitals, allowing fast reversibility and switching of oxidation states. This is a prerequisite in many catalytic cycles. However, the success of d^0-transition metal (i.e. Ti(+4), Sc(+3)) complexes in metal-based catalysis demonstrates that the role of these d-orbitals may not always be important.[1-4] As a result, the past decade has seen a tremendous development of organoalkaline earth metal chemistry as a new emerging field. Significant potential of alkaline earth compounds has been recognised to cover a broad range of applications including organic transformations,[5-9] polymerisation catalysis[10-15] and materials.[16, 17]

The alkaline earth metals are among the most abundant elements in the Earth's crust, and therefore they provide cheaper alternatives to the transition metals or lanthanides in the syntheses of metal catalysts. The variations in size to charge ratios enable coordination and reactivity tuning.[4, 18] From a ROP perspective, most alkaline earth metals are suitable for the production of biodegradable and biocompatible PLA or

PCL, owing to their low toxicity. Moreover, the polarity of M–X bond aids initiation and subsequent propagation in polymerisation operating through a coordination-insertion mechanism.[19, 20]

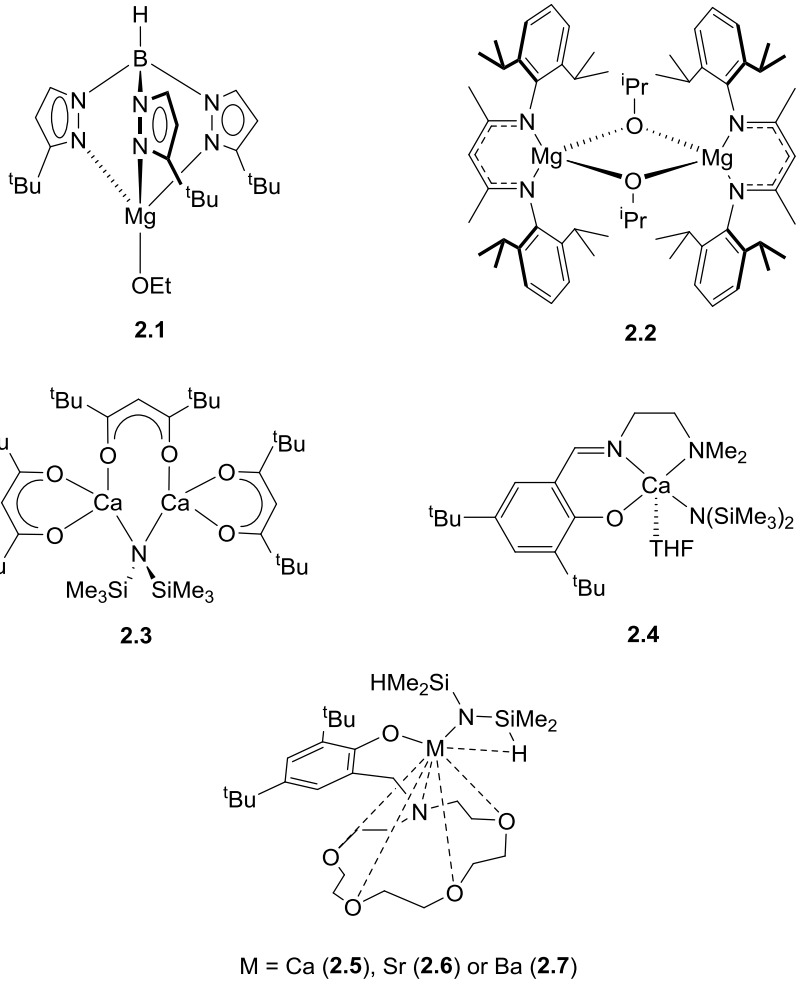

Figure 2.1. Examples of alkaline earth initiators for the ROP of ε-CL and *rac*-LA.[21-25]

The early developments in this particular area involved the use of simple salts such as hydride, oxide, alkoxide and amide. Often, a co-initiator was used in conjunction with those salts.[26-32] The initial breakthroughs in this regard came from the elegant works of Chisholm *et al*. and Coates *et al*. Their well-defined magnesium and calcium complexes with either tris(pyrazolyl)hydroborate or β-diketiminate supporting ligands were reported.[33] {HB(3-^{t}Bupz)$_3$}Mg(OEt) (**2.1**, Figure 2.1) was reported in 1996 as an efficient ROP catalyst for L-LA, by Chisholm *et al*. The ROP using **2.1** revealed a linear relationship between the observed polymer molecular weights and the predicted ones, assuming one chain per metal centre. Moreover, the catalyst polymerised up to 1000 equivs. of L-LA in CH_2Cl_2 at room temperature, yielding isotactic PLA with a PDI of 1.2. Around the time of this publication, the rate of polymerisation using **2.1**

was notably better than the tin and zinc octanoate catalyst systems where heating was often required in melt polymerisations.[21, 34] From this successful implementation of the work by Chisholm *et al*., Coates *et al*. reported [{HC(C(Me)N(2,6-$C_6H_3{}^iPr_2)_2$}Mg(O^{i}Pr)]$_2$ (**2.2**, Figure 2.1) as a single site catalyst for ROP of lactones in 2001. Compound **2.2** is highly active for ROP of *rac*-LA, and complete conversion of 200 equivs. of *rac*-LA was obtained in 2 mins at room temperature in CH_2Cl_2. Atactic polymer with high molecular weight and PDI was obtained. However, addition of ^{i}PrOH to the polymerisation led to the formation of PLA with narrower PDI and well controlled molecular weight. Regardless of the mechanism of polymerisation, **2.2** was claimed to exhibit a rate of polymerisation among the highest around that time.[22]

In 2003 the heteroleptic β-diketone {(TMHD)Ca(THF)}$_2${μ-N(SiMe$_3$)$_2$}(μ-TMHD) (**2.3**, Figure 2.1), was synthesised by Westerhausen and Feijen by the reaction between H-TMHD (2,2,6,6-tetramethylheptane-3,5-dione) and Ca{N(SiMe$_3$)$_2$}$_2$(THF)$_2$ in a stoichiometric ratio of 3:2. Compound **2.3** was reported as an efficient catalyst for ε-CL and *rac*-LA ROP, giving higher than expected molecular weight polymers with broad PDIs.[23] In the presence of ^{i}PrOH, the ROP of ε-CL and *rac*-LA using **2.3** were living, and gave polymers of controlled molecular weights with isopropyl ester and hydroxy end-groups.[15] Darensbourg *et al*. introduced Schiff base (salen) calcium complex **2.4** for *rac*-LA ROP in 2008. For *rac*-LA ROP, up to 700 equivs. of the monomer could be polymerised in 30 mins at room temperature, giving atactic PLA with a narrow PDI. However, heterotactic enrichment was only observed when polymerisation was performed at -33 °C.[24]

The main challenge impeding syntheses of discrete heteroleptic heavier alkaline earth metal catalysts is the Schlenk equilibrium, resulting in ligand exchange and eventually leading to undesired homoleptic species.[4] However, in the last four years, a series of these heavier alkaline earth compounds as ROP catalysts were made through the work of Capentier, Sarazin and co-workers. In 2010 a series of heavier alkaline earth amide complexes, {LO^3}MN(SiMe$_2$H)$_2$, were prepared through a protonolysis reaction of the protio ligand HLO^3 and corresponding alkaline earth metal amide M{N[(SiMe$_2$H)$_2$}$_2$(THF)$_2$ ({LO^3}$^-$ = 2-{(1,4,7,10-tetraoxa-13-azacyclopentadecan-13-yl)-methyl-4,6-di-*tert*-butylphenolate; M = Ca (**2.5**), Sr (**2.6**) and Ba (**2.7**), Figure 2.1). These complexes were stable in solution due to the presence of an internal β-agostic Ae···H-Si interaction. Evidence for this interaction in the solid state and

solution was supported by X-ray crystallography, NMR spectroscopy and DFT calculations. These complexes showed good promise as catalysts in immortal ROP (iROP) in the presence of an alcohol (2-propanol, benzyl or propargyl alcohol) as a chain-transfer agent. For example, in polymerising L-LA in toluene, polymerisations reached completion in a matter of minutes. All complexes showed very high ROP activities, increasing in order of Ca (**2.5**) < Sr (**2.6**) < Ba (**2.7**). Good control over polymer molecular weights and PDI values were also exhibited.[25] Following this success, further work on neutral and cationic alkaline earth metal complexes bearing similar supporting ligands were published by the same group.[35-37]

2.2.2 Early work on alkaline earth tetrahydroborate initiators in ROP

Over the past decade, Lanthanide tetrahydroborate either as simple salts, $Ln(BH_4)_3(THF)_x$, or heteroleptic complexes, $\{L\}Ln(BH_4)_x$, have been thoroughly studied and well-established as efficient ROP catalysts for cyclic esters.[38] Certain studies showed that the initiating efficiency and polymer molecular weight control of tetrahydroborate initiators are superior to amides, and comparable to alkoxides.[39, 40] Drawing upon the potential parallels to lanthanides, alkaline earth tetrahydroborate complexes,[41] containing comparable ionic radii, should be considered as good candidates for ROP catalysts.

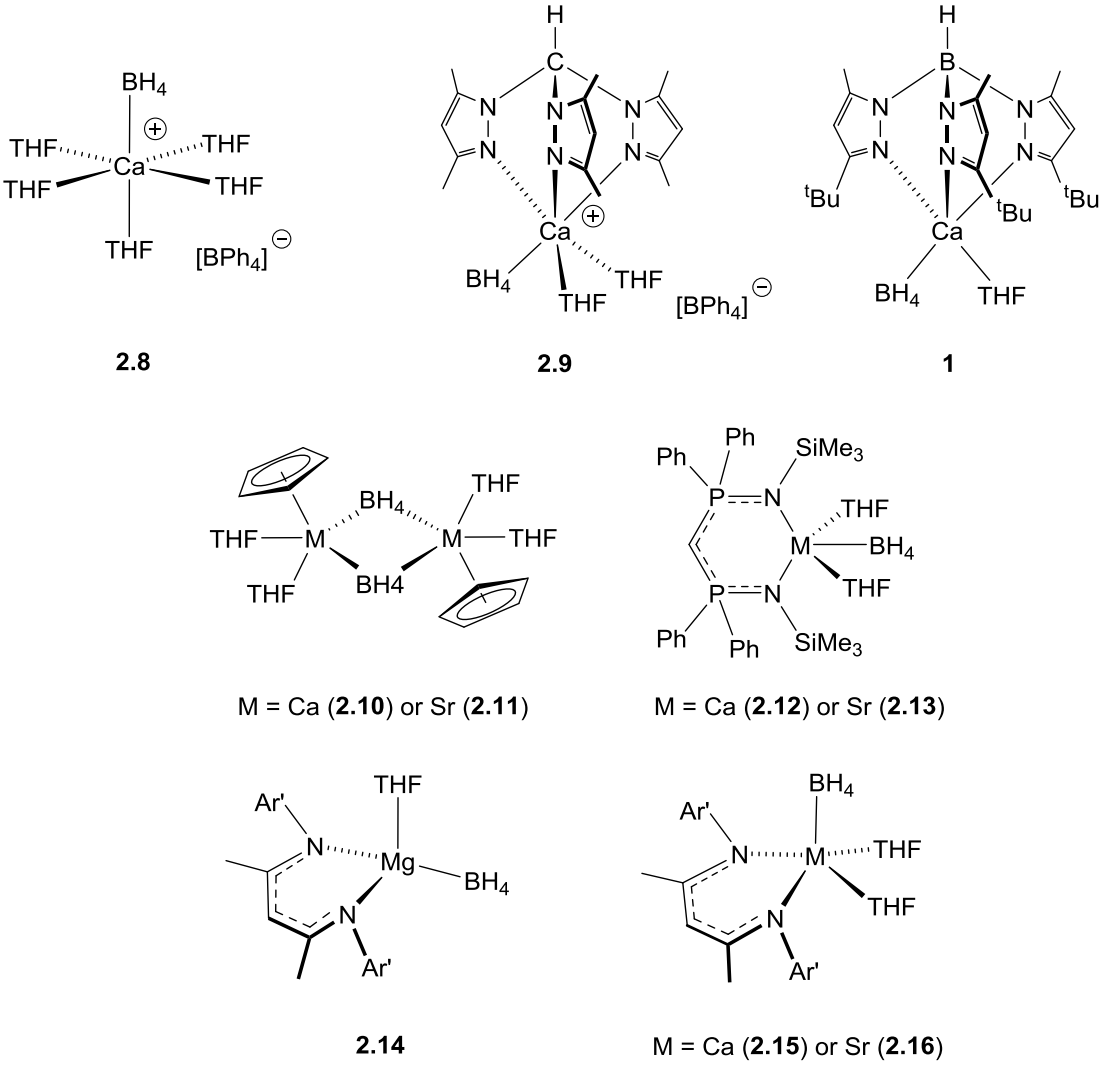

Figure 2.2. Examples of alkaline earth tetrahydroborate initiators for ROP of ε-CL and *rac*-LA.[20, 41-43] Ar' = 2,6-$C_6H_3{}^iPr_2$.

In 2011, Mountford *et al*. reported the first cationic calcium tetrahydroborate complexes and a charge-neutral calcium tetrahydroborate initiator for the ROP of ε-CL and *rac*-LA.[41] $[Ca(BH_4)(THF)_5][BPh_4]$ (**2.8**, Figure 2.2) was synthesised *via* protonolysis of $Ca(BH_4)_2(THF)_2$ with $[NEt_3H][BPh_4]$. The same methodology was adapted from those of lanthanide analogues. The further treatment of **2.8** with $HC(3,5\text{-}Me_2pz)_3$ (Tpm) in dichloromethane produced $[(Tpm)Ca(BH_4)(THF)_2][BPh_4]$ (**2.9**, Figure 2.2) in a high yield. Both **2.8** and **2.9** were spectroscopically and crystallographically characterised and found to possess κ^3-borohydride groups. Compound **2.8** is active as an ε-CL and *rac*-LA ROP initiator. Complete conversion of ε-CL was achieved within 2 mins at room temperature. Whilst in the case of *rac*-LA, polymerisation was slow even when performed at 70 °C (>80 % conversion

within 5 h at 70 °C). Faster rate of polymerisation was observed when using **2.9**, where the Tpm ligand could prevent formation of a LA chain chelated resting state during the propagation. Up to 250 equivs. of *rac*-LA were converted at room temperature within 2 h, yielding good agreement of M_n to the expected value and moderate PDIs. However, neither catalyst gave any stererochemical control, thus atactic polymers were obtained. Bulkier ligands are believed to induce better tacticity through the chain-end control mechanism. Therefore ($Tp^{tBu,Me}$)$Ca(BH_4)(THF)$ (**1**) was synthesised *via* the salt metathesis reaction between $KTp^{tBu,Me}$ and $Ca(BH_4)_2(THF)_2$. Compound **1** effectively polymerised both ε-CL and *rac*-LA, giving good control over molecular weight at both room temperature and 20 °C. High heterotactic enrichment was achieved with a P_r value of 0.80 at room temperature and 0.88-0.90 at -20 °C.[41]

In the two successive years, the half sandwich $[Cp^*M(BH_4)(THF)_2]_2$ ($Cp^* = C_5Me_5$, M = Ca (**2.10**) and Sr (**2.11**)) and bis(phosphinimino)methanide $\{(Me_3SiNPPh_2)_2CH\}M(BH_4)(THF)_2$ (M = Ca (**2.12**) and Sr (**2.13**)) complexes were synthesised by Roesky, Guillaume, Maron and their co-workers and employed in the ROP of ε-CL and *L*-LA, Figure 2.2.[42, 43] Compound **2.10** and **2.11** exhibited high activities towards the ROP of ε-CL and *L*-LA, giving corresponding polymers with molecular weights matched with the calculated values, assuming one polymer chain per metal centre. The recovered PCL and PLA were monodispersed with narrow to broad PDIs. The ROP activities of **2.10** were shown to be relatively higher than that of **2.11**. Relatively lower activities were observed in the ROP of ε-CL and *L*-LA using compound **2.12** and **2.13**. All ROP experiments gave higher than expected molecular weight polymers with moderate PDI. For example, compound **2.11** polymerised 300 equivs. of ε-CL at room temperature within *c.a.* 80 mins, whilst an increased temperature of 50 °C was required to raise the activity of **2.13** in polymerising 300 equivs. of ε-CL. Moreover, the decrease in catalytic efficiency of **2.12** and **2.13** was observed in the ROP of ε-CL and *L*-LA at high loadings. The experimental observation agreed well with the DFT calculations. ^1H NMR analyses of the recovered polymers after precipitation indicated α,ω-dihydroxy telechelic end groups in all cases.

Also in 2013, Mountford and co-workers reported a family of alkaline earth tetrahydroborates with bulky NacNac supporting ligands, namely $\{HC(C(Me)NAr')_2\}Mg(BH_4)(THF)$ (**2.14**) and $\{HC(C(Me)NAr')_2\}M(BH_4)(THF)_2$

(M = Ca (**2.15**) or Sr (**2.16**); Ar' = 2,6-$C_6H_3{}^iPr_2$, Figure 2.2). All complexes in this family were accessed through the salt metathesis reactions between K[HC(C(Me)NAr')$_2$] and corresponding metal bis(borohydride) in THF. Only **2.14** and **2.15** were made in good yields and used in ROP. Both were highly active towards ROP of ε-CL, polymerising 200 equivs. of ε-CL within 30 and 90 seconds, respectively. α,ω-dihydroxy telechelic PCL with five-fold higher molecular weight than expected was obtained using **2.14**, whilst PCL with good agreement between calculated and expected molecular weight was obtained using **2.15**. Compound **2.14** was also extremely active towards ROP of *rac*-LA forming PLA with appreciable levels of heterotacticity (P_r = 0.74-0.86) and good agreement for the molecular weights. These observations are comparable to those for the previously studied magnesium and zinc alkoxide and amide initiators with the same ligand class.[44, 45] On the other hand, *rac*-LA ROP using compound **2.15** showed deterioration in polymerisation rate, molecular weight control and heterotactic enrichment.[20] The MALDI-ToF analyses showed a mixture of dihydroxy end-capped PLA, as well as, HOCH(Me)-/aldehyde (-CH(Me)CHO) terminated PLA.

2.2.3 Possible coordination modes of the terminal tetrahydroborate ligand

To date, several reports have reviewed the well-established main group, transition metal and lanthanide tetrahydroborate complexes both structurally and chemically.[46-48] From a structural point of view, the tetrahydroborate group can exhibit a number of coordination modes to the metal centre; these include terminal (κ^1, κ^2, and κ^3 – see Figure 2.3) and bridging. The tetrahydroborate moiety can undergo dynamic intramolecular bridge-terminal hydrogen exchange. Moreover, it has shown that the rapid hydrogen exchange of tetrahydroborate and other ligands coordinated to the metal centre is also viable.[48-50]

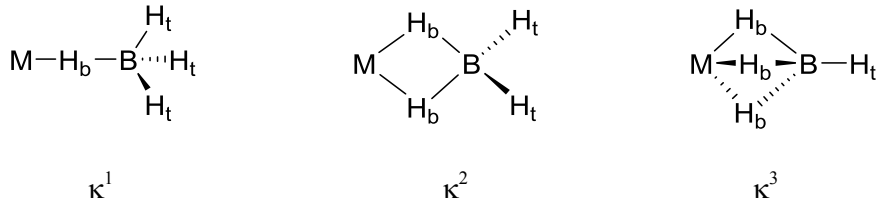

Figure 2.3. Possible coordination modes of the tetrahydroborate ligand. H_b and H_t denote bridging and terminal hydride.

The vital tools for structural characterisation of tetrahydroborate complexes are X-ray diffraction, neutron diffraction, and NMR and IR spectroscopy. IR spectroscopy is extensively employed, together with X-ray diffraction to determine the hapticity of the tetrahydroborate in both the solution and solid state. IR spectroscopy gives diagnostic bands between 2500 and 1000 cm^{-1}. The number and position of these bands found for the B-H stretches can be used to distinguish between κ^1, κ^2, and κ^3 coordination modes (Table 2.1).[48]

Table 2.1. IR active fundamental vibrational modes commonly observed for mononuclear MBH_4 configurations.[48] H_b and H_t denote bridging and terminal hydride.

Structure	Freq, cm^{-1}	Normal Mode	Symmetry	Comments
Monodentate	2450-2300	B-H_t stretching	A_1, E	Strong doublet
	~ 2000	B-H_b stretching	A_1	Strong
	~ 2000-1700	M-H_b stretching	A_1	Often broad
	1150-1000	BH_3 deformation	A_1, E	Strong band
Bidentate	2600-2400	B-H_t stretching	A_1, B_1	Strong doublet ($50-80\ cm^{-1}$)
	2150-1650	B-H_b stretching	A_1, B_2	Strong band possible shoulder
	1500-1300	M-H_b stretching	A_1	Strong band
	1200-1100	BH_2 deformation	B_2	Strong
Tridentate	2600-2450	B-H_t stretching	A_1	Strong singlet
	2200-2100	B-H_b stretching	A_1, E	Doublet ($50-80\ cm^{-1}$)
	1250-1150	Bridge deformation	E	Strong

2.2.4 Mechanistic aspects of tetrahydroborate initiated ROP of ε-CL

α,ω-Dihydroxy functionalised PCL is industrially valuable as a building block for further AB_2 triblock copolymerization, for instance poly(caprolactone)-*b*-[poly(benzylglutamate)]$_2$ and poly(caprolactone)-*b*-[poly(methyl methacrylate)]$_2$.[51, 52] The desirable dihydroxy end-capped PCL can be readily prepared through the

tetrahydroborate initiated ROP of ε-CL without any inherent constraints associated with the post-polymerisation chemical modification.[53, 54] In the past decade, Maron, Guillaume, Roesky, Mountford and their coworkers have made a significant contribution in the mechanistic studies of the ε-CL ROP using lanthanide and alkaline earth tetrahydroborate initiators through DFT calculations and experimental work.[53, 55-59] The proposed mechanism is shown in Scheme 2.1.[56]

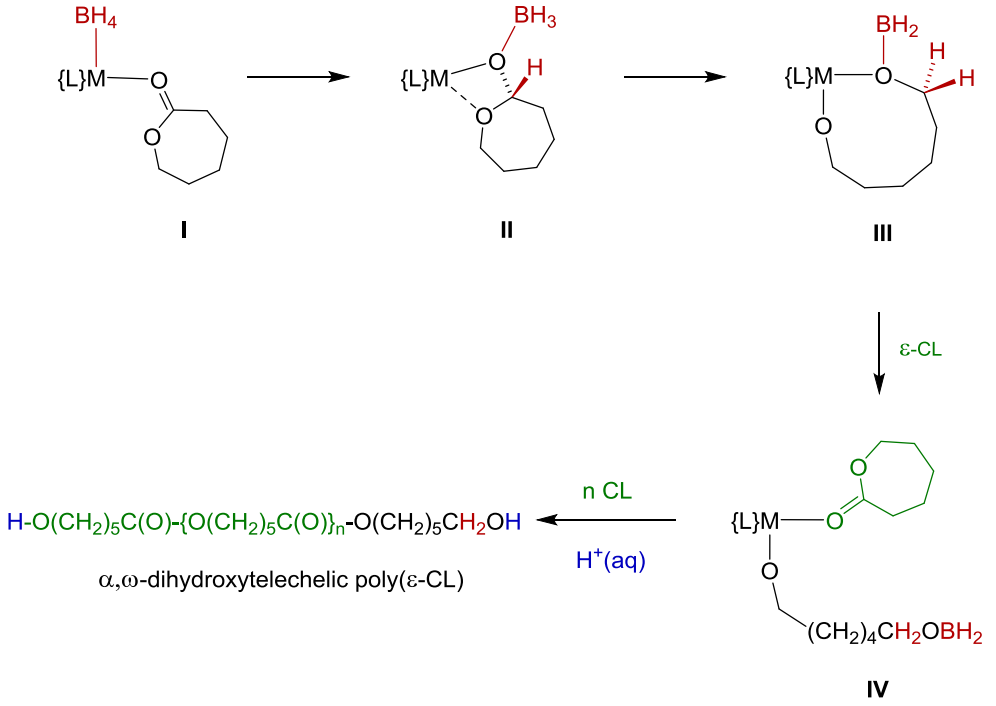

Scheme 2.1. Mechanism of tetrahydroborate initiating group in ROP of ε-CL.[56]

The initial step involves the adduct formation of ε-CL and catalyst (**I**). Subsequently, hydride transfer to the carbonyl carbon and BH_3 transfer to the formally anionic oxygen takes place (**II**). The crucial ring-opening step happens after a further hydride transfer, this forms **III**, with its carbonyl moiety fully reduced to an active alkoxy chain-end. Later on the propagation step occurs which involves a coordination of a further ε-CL to the reactive species. Finally the termination by hydrolysis leads to α,ω-dihydroxytelechelic polymer.

The experimental work supporting the proposed mechanism was reported by Guillaume *et al*., whereby the reaction between $Nd(BH_4)_3(THF)_3$ and 3 equivs. of ε-CL followed by hydrolysis and purification gave 1,6-hexanediol, identified by ^{1}H and $^{13}C\{^{1}H\}$ NMR, gas chromatography and mass spectrometry. The 1,6-hexanediol showed indirect evidence of **III** as a propagating species in the ε-CL ROP.[57]

Following on from the pioneer work, a further investigation into this area was carried out by the same authors using $Cp^*_2Sm(BH_4)(THF)$. The $Cp^*_2Sm(BH_4)(\varepsilon\text{-CL})$ (an analogue of **I**) produced during the equimolar reaction between $Cp^*_2Sm(BH_4)(THF)$ and ε-CL in CD_2Cl_2, was observed and identified by ^1H NMR analysis. The reaction finally led to the formation of an insoluble product, which was characterised by IR spectroscopy and elemental analysis as $[Cp^*_2Sm\{O(CH_2)_2O(BH_2)\}]$ (an analogue of **III**). Propagation occurred when further equivalents of ε-CL were added into the CH_2Cl_2 suspension of the insoluble product.[55, 58]

2.3 Alkaline earth tetrahydroborate initiators using $Tp^{tBu,Me}$ supporting ligand

2.3.1 Synthesis and solid state structure of $(Tp^{tBu,Me})Ca(BH_4)(THF)$ (1)

$(Tp^{tBu,Me})Ca(BH_4)(THF)$ (**1**) was first introduced by Mountford *et al*. in 2011 as an efficient initiator for ROP.[41] Compound **1** was synthesised by reaction of $KTp^{tBu,Me}$ and $Ca(BH_4)_2(THF)_2$ in THF. An alternative synthetic route was successfully achieved using the analogous iodide, $(Tp^{tBu,Me})Ca(I)(THF)$ (**2.17**), and KBH_4 in acetonitrile, giving **1** in 58 % yield (Scheme 2.2).[60] In this Thesis, the synthesis of **1** from the reaction of $KTp^{tBu,Me}$ and $Ca(BH_4)_2(THF)_2$ was refined to obtain an improved yield of 84 %. A displacement ellipsoid plot of **1** is shown in Figure 2.4, and its selected bond lengths and angles are shown in Table 2.2. The NMR and IR data for **1** are identical to those reported previously.[41]

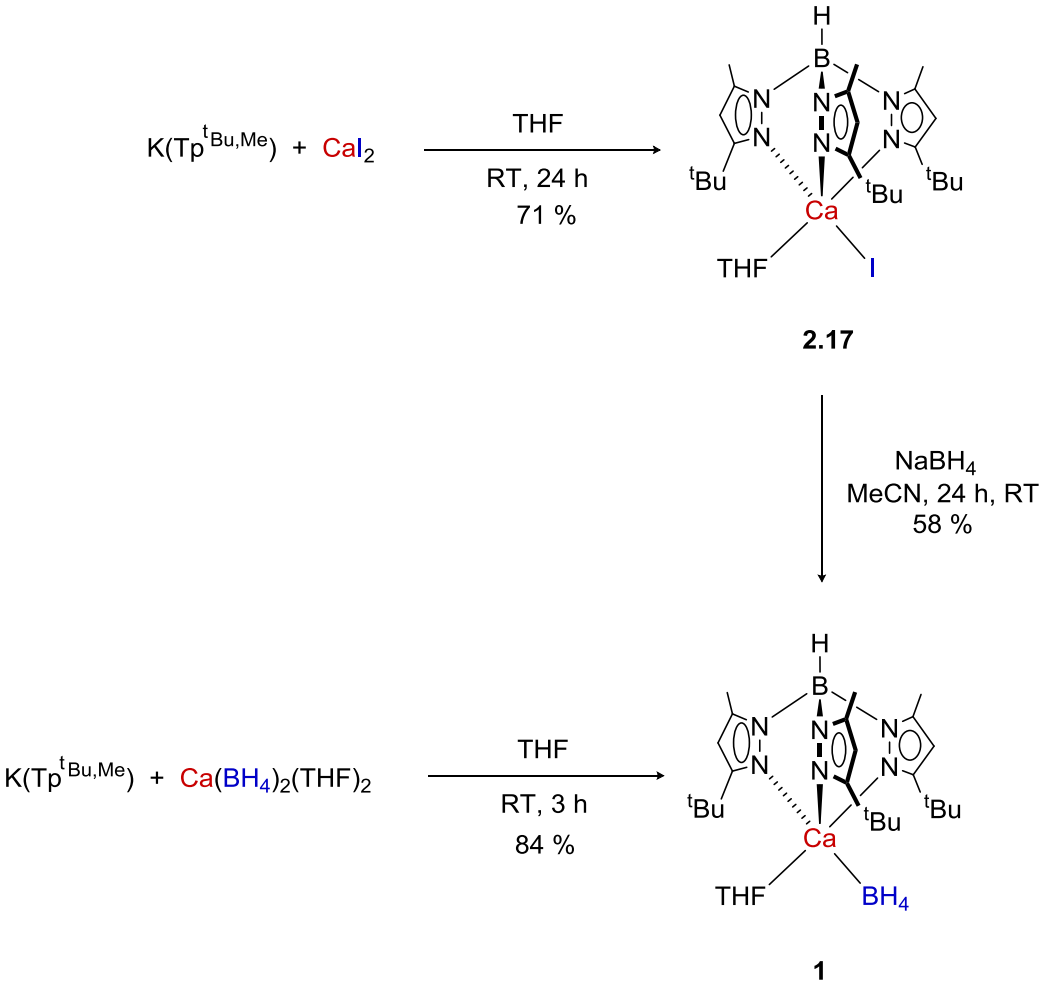

Scheme 2.2. Synthesis of ($Tp^{tBu,Me}$)Ca(BH_4)(THF) (**1**) *via* salt metathesis routes.

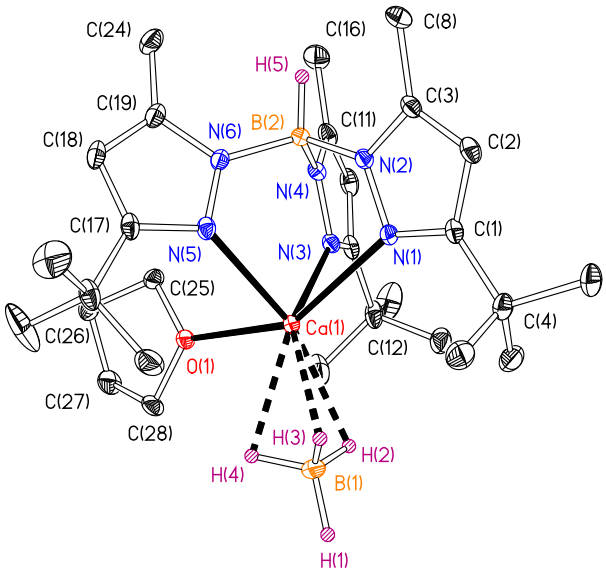

Figure 2.4. Displacement ellipsoid plot (20% probability level) of ($Tp^{tBu,Me}$)Ca(BH_4)(THF) (**1**). C-bound H atoms are omitted for clarity.

Table 2.2. Selected bond lengths (Å) and angles (°) for ($Tp^{tBu,Me}$)Ca(BH_4)(THF) (**1**).

Ca(1)-N(1)	2.5053(16)	Ca(1)-H(2)	2.44(4)
Ca(1)-N(3)	2.4256(17)	Ca(1)-H(3)	2.40(3)
Ca(1)-N(5)	2.4307(16)	Ca(1)-H(4)	2.41(3)
Ca(1)-O(1)	2.4291(14)	B(1)-H(2)	1.09(4)
Ca(1)···B(1)	2.567(3)	B(1)-H(3)	1.17(4)
B(1)-H(1)	1.19(4)	B(1)-H(4)	1.13(3)
N(1)-Ca(1)-N(3)	74.54(5)	N(3)-Ca(1)-N(5)	94.81(6)
N(1)-Ca(1)-N(5)	78.46(5)	N(1)-Ca(1)-O(1)	148.97(5)

Compound **1** is *pseudo* five-coordinate with Ca(1) coordinated to the three N donors of a κ^3-$Tp^{tBu,Me}$ ligand, O(1) of the THF ligand and a κ^3-bound BH_4 ligand. The hydrogen atoms of the latter were located in a Fourier difference map and positionally and isotropically refined. The coordination mode found by X-ray crystallography agrees with the solid state IR data.

The coordination geometry at Ca(1) is distorted pseudo trigonal bipyramidal with N(1) and O(1) occupying the formal axial sites of the trigonal bipyramidal. The Ca-H distances (av. 2.42(3) Å) and Ca···B distance (2.567(3) Å – *cf.* κ^3-BH_4) are similar within error to those of the calcium compounds shown in Figure 2.2.[20, 41, 43] The Ca-N_{pz} bond distances (av. 2.4541(16) Å) lie within the usual ranges.[44, 61-63] Ca(1)-N(3) and Ca(1)-N(5) bond lengths are equivalent within error ($\Delta_{Ca\text{-}N}$ = 0.005(2) Å), whereas Ca(1)-N(1) bond length is significantly longer than the others by *ca*. 0.07 Å.

Interestingly, compound **1** is both isostructural and isomorphous with the analogous Yb complex, ($Tp^{tBu,Me}$)Yb(BH_4)(THF), reported by Sella, Takats and their coworkers.[61] The geometries, bond lengths and angles associated with these two compounds are very similar, although the bond distances for Yb are systematically longer. The very similar ionic radii of Ca^{2+} and Yb^{2+} (1.14 and 1.16 Å, respectively) explain this phenomenon.[62]

2.3.2 Synthesis and solid state structures of ($Tp^{tBu,Me}$)Mg(BH_4) (2) and ($Tp^{tBu,Me}$)Mg(Cl) (3)

Building on successful work in the Mountford group, other alkaline earth tetrahydroborate complexes were targeted. ($Tp^{tBu,Me}$)Mg(BH_4) was previously synthesised *via* a salt metathesis reaction between K($Tp^{tBu,Me}$) and Mg(BH_4)$_2$. A moderate yield of 57 % was obtained in the preliminary study.[60] In this Thesis, a better yield of 72 % was achieved by extending the reaction time and improving the crystallisation conditions.

An alternative salt metathesis reaction between ($Tp^{tBu,Me}$)Mg(Cl) (**3**) and $NaBH_4$ was attempted. The new compound **3** was prepared by a salt metathesis reaction between Tl($Tp^{tBu,Me}$) and $MgCl_2$, giving a yield of 64 % following crystallisation. The synthetic preparation was adopted over another known method using Tl($Tp^{tBu,Me}$) and a Grignard chloride, which could lead to the mixture of the desired product and ($Tp^{tBu,Me}$)MgR (R = alkyl).[63-66] Unfortunately, reaction of **3** with $NaBH_4$ in either THF or MeCN at room temperature or 60 °C did not lead to the formation of **2** over the course of days.

The possible synthetic pathways to **2** are illustrated in Scheme 2.3. Compounds **2** and **3** were crystallographically characterised. Their displacement ellipsoid plots are shown in Figure 2.5 and the selected bond lengths and angles are presented in Table 2.3 and 2.4, respectively. The NMR and IR data for **2** are identical to those reported previously. Compound **3** was fully characterised by ^{1}H, ^{13}C, ^{11}B NMR spectroscopy, IR spectroscopy, mass spectrometry and elemental analysis.

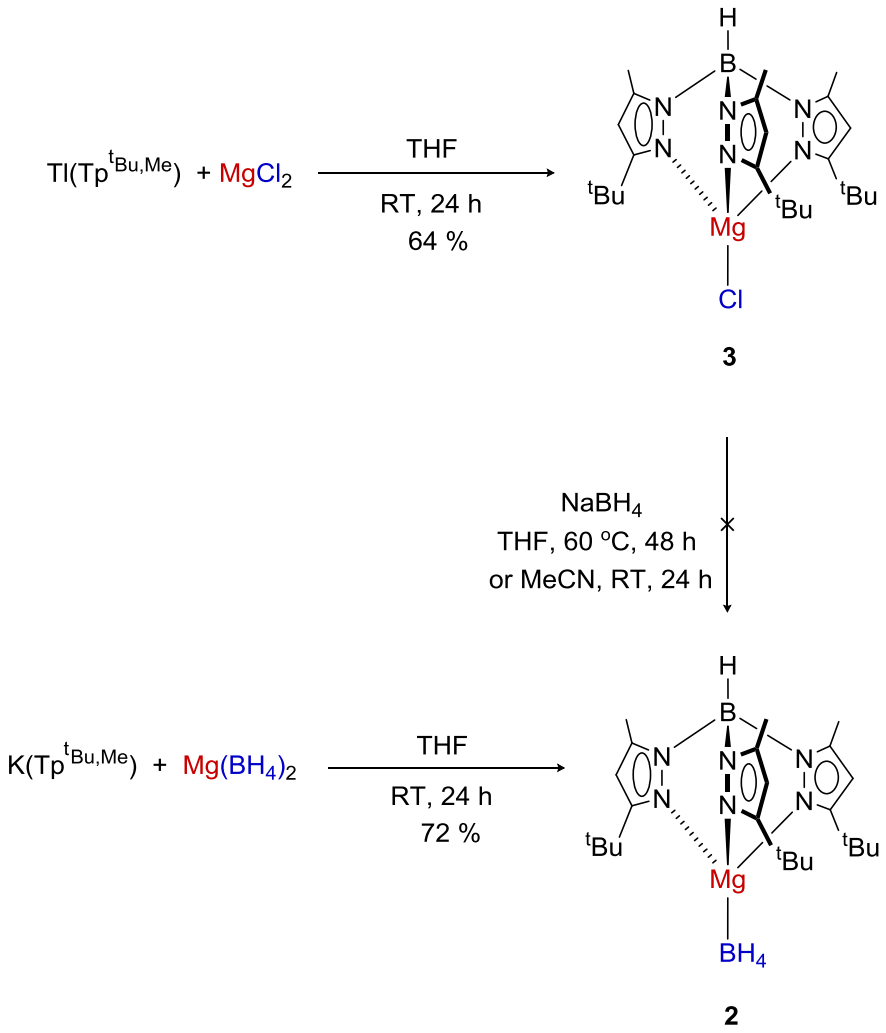

Scheme 2.3. Synthesis of ($Tp^{tBu,Me}$)Mg(BH_4) (**2**) and ($Tp^{tBu,Me}$)Mg(Cl) (**3**).

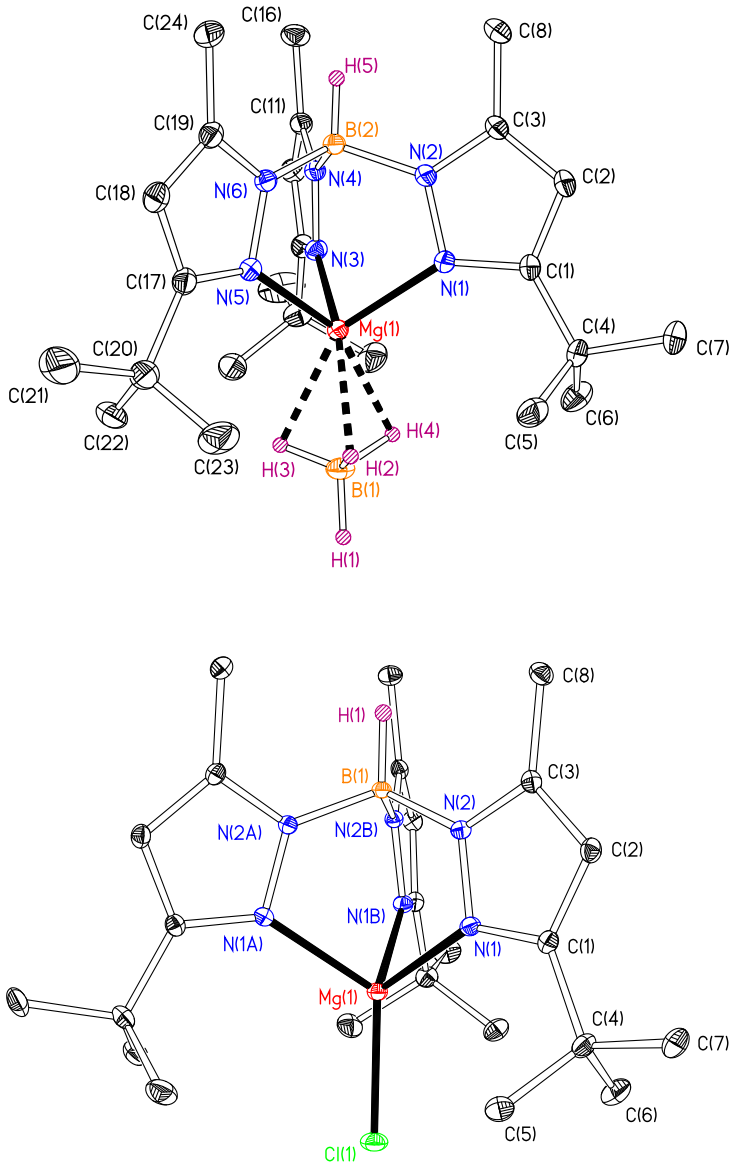

Figure 2.5. Displacement ellipsoid plots (20% probability level) of ($Tp^{tBu,Me}$)Mg(BH_4) (top) (**2**) and ($Tp^{tBu,Me}$)Mg(Cl) (bottom) (**3**). C-bound H atoms are omitted for clarity. For **3**, atoms carrying the suffix 'A' and 'B' are related to their counterparts by the symmetry operations [*z*, *x*, *y*] and [*y*, *z*, *x*], respectively).

Table 2.3. Selected bond lengths (Å) and angles (°) for ($Tp^{tBu,Me}$)Mg(BH_4) (**2**).

Mg(1)-N(1)	2.1077(14)	Mg(1)-H(3)	2.18(2)
Mg(1)-N(3)	2.1199(16)	Mg(1)-H(4)	2.18(2)
Mg(1)-N(5)	2.1087(16)	B(1)-H(2)	1.12(3)
Mg(1)···B(1)	2.263(2)	B(1)-H(3)	1.08(3)
Mg(1)-H(2)	2.11(2)	B(1)-H(4)	1.19(3)
N(1)-Mg(1)-N(3)	94.94(6)	N(3)-Mg(1)-N(5)	95.75(6)
N(1)-Mg(1)-N(5)	92.31(6)	B(2)-Mg(1)B(1)	178.95(8)

Table 2.4. Selected bond lengths (Å) and angles (°) for ($Tp^{tBu,Me}$)Mg(Cl) (**3**).

Mg(1)-N(1)	2.0992(11)	Mg(1)-Cl(1)	2.2587(9)
N(1)-Mg(1)-N(1A/1B)	93.58(5)	N(1)-Mg(1)-Cl(1)	122.69(3)
B(1)···Mg(1)-Cl(1)	180		

Compound **2** is *pseudo* four-coordinate with Mg coordinated to the three N donors of the $Tp^{tBu,Me}$ ligand and a κ^3-bound BH_4 ligand with a Mg(1)···B(1) distance of 2.263(2) Å. Examples of other κ^3-BH_4 compounds present in the literature are $Mg(BH_4)_2(Me_2NC_2H_4NMe_2)$,[67] **2.14**[20] and {HC(C(Me)NAr')$_2$}Mg(BH_4)(Et_2O)[68] with similar Mg···B bond distances of 2.277(3), 2.223(3) and 2.241 Å, respectively. The hydrogen atoms of the BH_4 ligand were located in a Fourier difference map and positionally and isotropically refined, giving the Mg···H distances in the usual range.[69] The mean Mg-N_{pz} bond length of **2** (2.1121(15) Å) is reasonably close to those observed in the sterically similar structures, for example ($Tp^{tBu,Me}$)Mg(Cl) (**3**) (2.0992(11) Å) and (Tp^{tBu})Mg(Cl) (2.097(5) and 2.100(3) Å).[66]

It is noteworthy that the molecular structure of the starting material, $Mg(BH_4)_2$, has been largely characterised using powder X-ray diffraction, the single crystal X-ray diffraction was only achieved using a synchrotron beam.[70, 71] Some crystal structures of solvated $Mg(BH_4)_2$ have been obtained, including $Mg(BH_4)_2$(diglyme),[67] $Mg(BH_4)_2(H_2N^tBu)_3$, $Mg(BH_4)_2(py)_6$ and $Mg(BH_4)_2(HNC_5H_{10})_3$.[72] All of these compounds possess κ^2-BH_4 groups.

Molecules of **3** have crystallographically imposed C_3 symmetry, crystallising in the cubic space group $I\bar{4}3d$. The metric parameters and geometry at Mg(1) are identical within error to those for (Tp^{tBu})Mg(Cl) reported previously by Perkin *et al*.,[66] and will not be further discussed here.

2.3.3 Synthesis and solid state structures of ($Tp^{tBu,Me}$)Sr(BH_4)(THF)$_2$ (4) and ($Tp^{tBu,Me}$)Sr(I)(THF)$_2$ (5).

Owing to the commercial unavailability of $Sr(BH_4)_2(THF)_2$, the initial synthesis of $Sr(BH_4)_2(THF)_2$ was required. The preparation used in this Thesis was adapted from the publication of Nöth *et al*. in 1994.[73] $Sr(BH_4)_2(THF)_2$ was synthesised by refluxing a suspension of $Sr(O^iPr)_2$ in THF with an excess of $BH_3{\cdot}THF$ for 5 h (Equation 2.1). The product was isolated as a white powder in 64 % yield.

$$3\ Sr(O^iPr)_2 + 8\ BH_3{\cdot}THF \xrightarrow[\text{reflux, 5 h}]{\text{THF}} 3\ Sr(BH_4)_2(THF)_2 + 2\ THF + 2\ B(O^iPr)_3$$

64 %

Equation 2.1

A pivotal issue impeding synthesis of heavier alkaline earth metal complexes is the previously mentioned Schlenk equilibrium, resulting in ligand exchange between heteroleptic compounds which can lead to the undesired homoleptic species.[4] The synthesis of ($Tp^{tBu,Me}$)Sr(BH_4)(THF)$_2$ (**4**) was carried out at low temperature (-78 °C) *via* the salt metathesis reaction of K($Tp^{tBu,Me}$) and $Sr(BH_4)_2(THF)_2$ in THF. Low temperature, a donor solvent and the bulky $Tp^{tBu,Me}$ ligand were employed in the synthesis to suppress the Schlenk equilibrium. Crystallisation was carried out from THF/hexanes solution at -30 °C to afford diffraction-quality crystals of **4** in 65 % yield. It is noteworthy that the formation of the homoleptic product, (κ^2,κ^3-$Tp^{tBu,Me}$)$_2$Sr (**6**), was observed in the synthesis of **4** prior to purification (*vide infra*).

The commercially available SrI_2 allows easy access to ($Tp^{tBu,Me}$)Sr(I)(THF)$_2$ (**5**) by reacting K($Tp^{tBu,Me}$) and SrI_2 in THF at -78 °C. Suitable crystals for X-ray diffraction were also grown from THF/hexane solution at -30 °C. This also allowed the product to be isolated as a crystalline solid in 74 % yield.

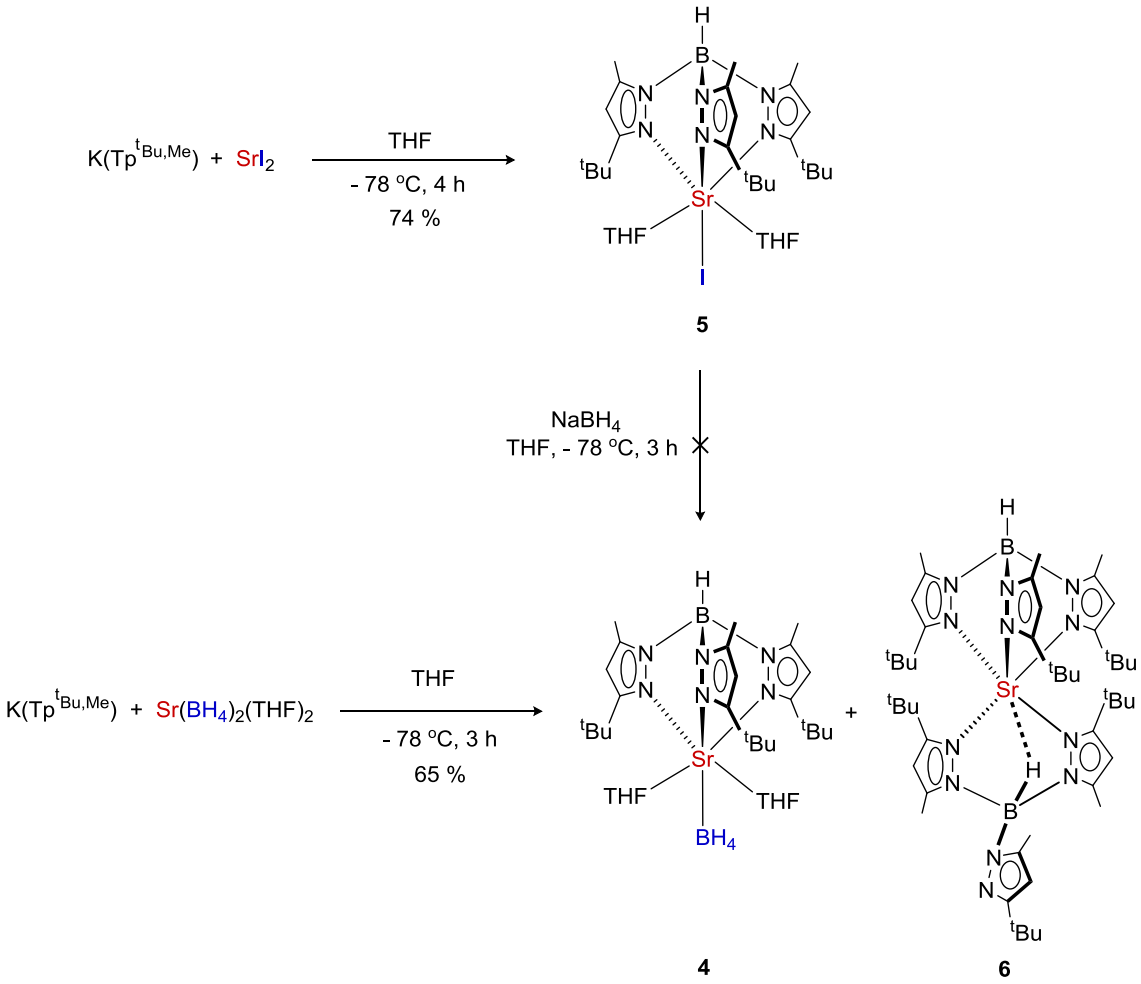

Scheme 2.4. Synthesis of $(Tp^{tBu,Me})Sr(BH_4)(THF)_2$ (**4**), $(Tp^{tBu,Me})Sr(I)(THF)_2$ (**5**) and $(\kappa^2,\kappa^3\text{-}Tp^{tBu,Me})_2Sr$ (**6**).

Compounds **4** and **5** were fully characterised by ^1H, $^{13}C\{^1H\}$, ^{11}B NMR spectroscopy, IR spectroscopy, mass spectrometry and elemental analysis. The ^1H NMR (C_6D_6) spectra of **4** and **5** showed expected signals for the $Tp^{tBu,Me}$ and THF ligands at very similar chemical shifts: three singlets (δ = 5.69, 2.21 and 1.36 ppm for **4**, as well as 5.65, 2.20 and 1.36 ppm for **5**) corresponding to the Pz-H, methyl and *tert*-butyl substituent of the $Tp^{tBu,Me}$, and two multiplets (δ = 3.33 and 1.24 ppm for **4**, as well as 3.40 and 1.22 ppm for **5**) corresponding to the THF ligands. The BH_4 ligand of **4** and the B-H of the $Tp^{tBu,Me}$ ligands of **4** and **5** were not observed in the ^1H NMR analyses due to quadrupolar broadening. Despite being unobserved in the ^1H NMR spectra, ^{11}B NMR spectra showed the BH_4 resonance of **4** at δ = -31.6 ppm ($^1J_{B\text{-}H}$ = 84.5 Hz) and the B-H of $Tp^{tBu,Me}$ ligands of **4** and **5** appeared as broad singlets at δ = -7.5 and -7.9 ppm, respectively. The $^1J_{B\text{-}H}$ coupling of 84.5 Hz is within the expected range (*ca.* 75-

85 Hz) of terminal BH_4 compounds.[20, 42, 43, 74] The IR spectra of **4** and **5** exhibited common bands at a wavenumber of *ca*. 2550 cm^{-1}, assigned as the B-H stretching of the $Tp^{tBu,Me}$ ligands. Moreover, the IR data of **4** showed characteristic υ(B-H) patterns of κ^3-BH_4 in both solid state and THF solution, these are υ(B-H) stretching frequencies of 2398 (A_1), 2245 and 2202 (A_1 and E) cm^{-1} in the solid state, and υ(B-H) stretching frequencies of 2364 (A_1), 2246 and 2203 (A_1 and E) cm^{-1} in the solution state.

An alternative route to **4** *via* a salt metathesis reaction of **5** and $NaBH_4$ in THF was unsuccessful, giving a mixture of **4** and unreacted **5** which co-crystallised and could not be separated from each other. The possible synthetic pathways to **4** are illustrated in Scheme 2.4. Compounds **4** and **5** were crystallographically characterised. Their displacement ellipsoid plots are shown in Figure 2.6 and the selected bond lengths and angles are presented in Table 2.5 and 2.6, respectively.

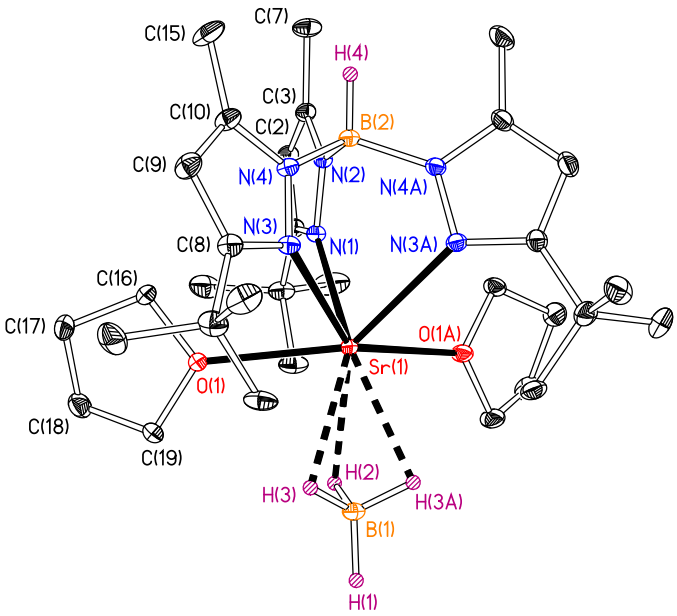

Figure 2.6. Displacement ellipsoid plots (20% probability level) of $(Tp^{tBu,Me})Sr(BH_4)(THF)_2$ (**4**, top) and $(Tp^{tBu,Me})Sr(I)(THF)_2$ (**5**, bottom). C-bound H atoms are omitted for clarity. The atoms carrying the suffix 'A' are related to their counterparts by the symmetry operator *x*, 1-*y*, *z*.

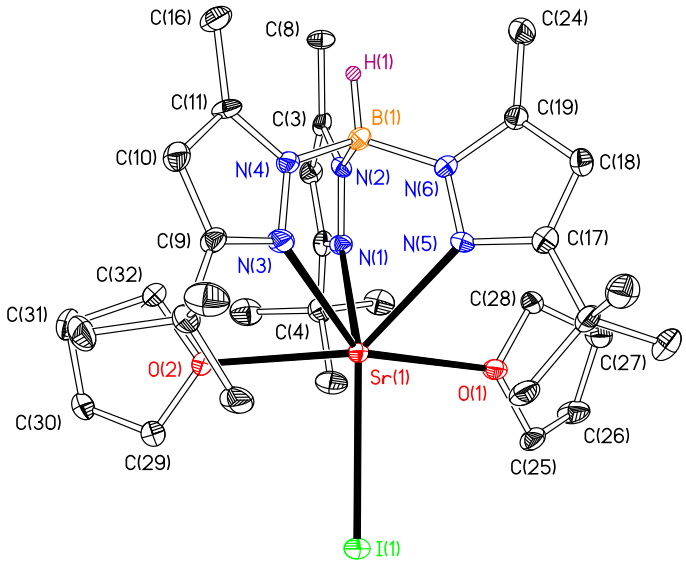

Figure 2.6 (continued). Displacement ellipsoid plots (20% probability level) of ($Tp^{tBu,Me}$)Sr(BH_4)(THF)$_2$ (**4**, top) and ($Tp^{tBu,Me}$)Sr(I)(THF)$_2$ (**5**, bottom). C-bound H atoms are omitted for clarity. The atoms carrying the suffix 'A' are related to their counterparts by the symmetry operator *x*, 1-*y*, *z*.

Table 2.5. Selected bond lengths (Å) and angles (°) for ($Tp^{tBu,Me}$)Sr(BH_4)(THF)$_2$ (**4**).

Sr(1)-N(1)	2.677(2)	Sr(1)-H(2)	2.60(4)
Sr(1)-N(3)	2.6604(15)	Sr(1)-H(3)	2.52(3)
Sr(1)-O(1)	2.6076(13)	B(1)-H(1)	1.16(4)
Sr(1)···B(1)	2.786(3)	B(1)-H(2)	1.14(4)
		B(1)-H(3)	1.14(3)
N(1)-Sr(1)-N(3)	83.63(5)	O(1)-Sr(1)-O(1A)	134.58
N(1)-Sr(1)-N(3A)	65.51	N(1)-Sr(1)···B(1)	138.18(9)
		N(3)-Sr(1)···B(1)	129.68(6)

Table 2.6. Selected bond lengths (Å) and angles (°) for ($Tp^{tBu,Me}$)Sr(I)$(THF)_2$ (**5**).

Sr(1)-N(1)	2.637(5)	Sr(1)-O(1)	2.627(4)
Sr(1)-N(3)	2.648(6)	Sr(1)-O(2)	2.637(4)
Sr(1)-N(5)	2.629(6)	Sr(1)-I(1)	3.2181(7)
N(1)-Sr(1)-N(3)	83.35(18)	N(3)-Sr(1)-N(5)	66.0(2)
N(1)-Sr(1)-N(5)	82.52(18)	O(1)-Sr(1)-O(2)	136.62(16)
N(1)-Sr(1)-I(1)	138.41(11)	N(3)-Sr(1)-I(1)	129.21(13)
N(5)-Sr(1)-I(1)	130.76(13)		

Compounds **4** and **5** are *pseudo* 6-coordinate with Sr(1) coordinated to the three N donors of a $Tp^{tBu,Me}$ ligand, two oxygen atoms of the two THF ligands and a κ^3-bound BH_4 ligand for **4** or iodide ligand for **5**. It is worth noting that compound **4** has crystallographic symmetry. The coordination geometry at Sr(1) for **4** and **5** is best described as *pseudo* octahedral with Sr(1) 0.45 or 0.44 Å below the least square plane defined by N(3), N(3A), O(1) and O(1A) in **4** or N(3), N(5), O(1) and O(2) in **5**. Atoms N(1) and B(1) occupy the axial positions in **4** with the N(1)-Sr(1)···B(1) angle (138.18(9) °) deviating significantly from linearity. Similarly for **5**, the N(1) and I(1) at axial positions formed N(1)-Sr(1)-I(1) angle of 138.41(11) °. The Sr(1)-I(1) bond length (3.2181(7) Å) of **5** is considerably longer than the Sr(1)···B(1) distance (2.786(3) Å) in **4**.

All the bond lengths in **4** and **5** are significantly longer than those in their calcium (i.e. compound **1** and **2.17**, respectively) and magnesium counterparts (i.e. compound **2**) as a result of the increased size and coordination number of the strontium centres. The additional THF ligands in **4** and **5** reflect the relative larger atomic radius of Sr. Considering the bond angles of N_{pz}-M-N_{pz}, these could be seen to become more acute descending the group (*ca*. 65.5-83.8 for **4** and 66.6-83.9 ° for **5**). The effect is pronounced in **4** and **5** which have the longest Sr-N_{pz} distances (*ca*. 2.66-2.68 Å for **4** and 2.61-2.67 Å for **5**) within the corresponding series.

($Tp^{tBu,Me}$)Sr(BH_4)$(THF)_2$ (**4**) also possesses a κ^3-BH_4 group in both the solid state and THF solution, these are consistent with the results obtained from the solid state and the THF solution IR data described previously. The hydrogen atoms of the BH_4 ligand

were located in the Fourier difference map and positionally and isotropically refined. Compound **4** is among a small number of κ^3-BH_4 containing strontium compounds reported in the literature to date. The Sr···B distance (2.786(3) Å) is somewhat shorter than those of the polymeric $Sr(BH_4)_2(THF)_2$ (2.906(6) Å),[73] the monomeric $Sr(BH_4)_2$(18-crown-6) (2.833(6) Å)[73] and $[\{(Me_3Si)_2C(Me_2P)\}BH_3]_2Sr(THF)_5$ (2.893(4) Å),[75] however, comparable to $\{(Me_3SiNNPh_2)_2CH\}Sr(BH_4)(THF)_2$ (**2.13**, 2.777(4) Å)[42, 43] and $\{HC(C(Me)NAr')_2\}Sr(BH_4)(THF)_2$ (**2.16**; Ar' = 2,6-$C_6H_3{}^iPr_2$, 2.7906(17) Å)[20] within error.

2.3.4. Synthesis and solid state structure of $(\kappa^2,\kappa^3\text{-}Tp^{tBu,Me})_2Sr$ (6)

The synthesis of **4**, from $K(Tp^{tBu,Me})$ and $Sr(BH_4)_2(THF)_2$, is accompanied by a Schlenk equilibrium by-product **6** (Scheme 2.4), which can be observed in ^1H and ^{11}B NMR spectra of the crude material. The by-product, $(\kappa^2,\kappa^3\text{-}Tp^{tBu,Me})_2Sr$ (**6**), was independently synthesised by reacting 2 equivs. of $K(Tp^{tBu,Me})$ with an equivalent of SrI_2 in THF at room temperature for 24 h. The pure product was isolated by crystallisation from a saturated benzene or pentane solution at 4 °C. Due to the high solubility of the product in hydrocarbon solvents, the isolated yield is moderate (53 %). A displacement ellipsoid plot of **6** is illustrated in Figure 2.7 and its selected bond lengths and angles are reported in Table 2.7.

The molecular structure obtained from X-ray diffraction was consistent with the homoleptic sandwich species as expected. The solid state structure of **6** exhibits an intriguing molecule containing two different coordinating $Tp^{tBu,Me}$ ligands; one is coordinated *via* the common κ^3-bonding mode and other is bonded *via* a κ^2-bonding mode through two pyrazolyl nitrogen atoms and an agostic B-H···Sr interaction (H(1)···Sr(1) = 2.49(2) Å). The solid state IR spectrum of **6** demonstrated a shift of B-H stretch to lower frequency from 2520 cm^{-1} (terminal B-H stretches) to 2361 cm^{-1} (B-H stretch associated with the agostic B-H···Sr interaction). The trend observed is consistent with those obtained from other compounds containing agostic B-H···M interactions.[76]

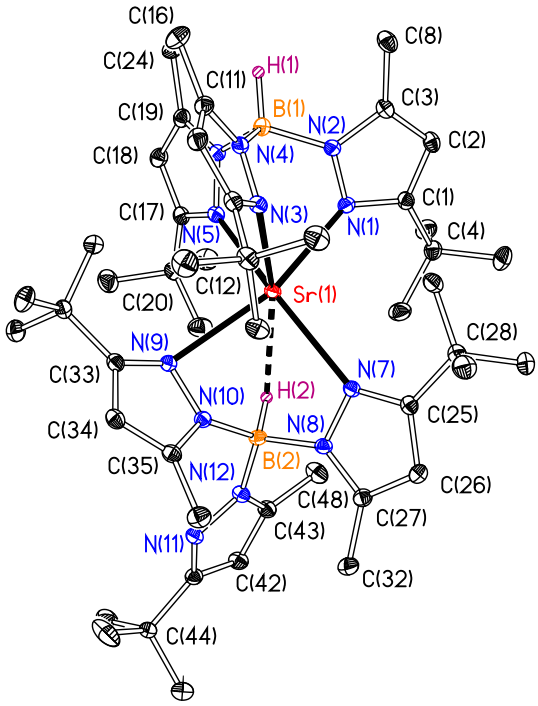

Figure 2.7. Displacement ellipsoid plot (20% probability level) of $(\kappa^2,\kappa^3\text{-Tp}^{t\text{Bu,Me}})_2\text{Sr}$ (**6**). C-bound H atoms omitted.

Table 2.7. Selected bond lengths (Å) and angles (°) for $(\kappa^2,\kappa^3\text{-Tp}^{t\text{Bu,Me}})_2\text{Sr}$ (**6**).

Sr(1)-N(1)	2.622(2)	Sr(1)-N(7)	2.715(2)
Sr(1)-N(3)	2.593(2)	Sr(1)-N(9)	2.650(2)
Sr(1)-N(5)	2.640(2)	Sr(1)···H(2)	2.49(2)
N(1)-Sr(1)-N(3)	83.97(7)	N(3)-Sr(1)-N(7)	108.80(7)
N(1)-Sr(1)-N(5)	65.76(7)	N(3)-Sr(1)-N(9)	99.94(6)
N(3)-Sr(1)-N(5)	89.71(7)	N(3)-Sr(1)-H(2)	154.5(6)
N(7)-Sr(1)-N(9)	91.13(6)		

The coordination geometry of **6** is distorted octahedral with the least-square plane defined by the four equatorial nitrogen atoms (N(1), N(5), N(7) and N(9)) and the axial position occupied by N(3) and H(2). With this arrangement, the Sr metal centre lies 0.305 Å above the least-square plane. The distortion of the molecule is reflected by large deviation from linearity of the N(3)-Sr(1)-H(2) angle (154.5(6) Å). Homoleptic compounds, $(\text{Tp}^{t\text{Bu,Me}})_2\text{M}$ or $(\text{Tp}^{3\text{-}t\text{Bu}})_2\text{M}$, featuring alkaline earth metals

and the lanthanides with similar ionic radii to Sr^{2+}, also exhibit the κ^2,κ^3-ligand bonding modes; these are $(\kappa^2,\kappa^3\text{-}Tp^{3\text{-}tBu})_2Ca$,[77] $(\kappa^2,\kappa^3\text{-}Tp^{tBu,Me})_2Sm$ and $(\kappa^2,\kappa^3\text{-}Tp^{tBu,Me})_2Yb$.[78] On the other hand, the series of heavier alkaline earth compounds supported by the less sterically crowded Tp derivatives ($(Tp^{R2})_2M$ or $(Tp^{R'2})_2M'$, when R = Me, M = Ca or Sr and R' = Et or ^{i}Pr, M' = Ca, Sr or Ba) demonstrated symmetric κ^3-ligand bonding modes.[79-81]

Compound **6** was found to be fluxional in solution at room temperature, the fast exchange of the pyrazolyl rings within the individual $Tp^{tBu,Me}$ ligands without the change in bonding modes was observed, suggesting the B-H···Sr agostic interaction was retained. This resulted in two sets of signals with equal integrations corresponding to each set of the $Tp^{tBu,Me}$ ligands in the ^{1}H NMR spectrum, moreover, the two different environments of boron atoms were identified with two signals (-2.3 and -6.6 ppm) in the $^{11}B\{^1H\}$ NMR spectrum. The ^{1}H NMR analysis in toluene-d_8 at 80 °C demonstrated high fluxionality of **6**, where both sets of $Tp^{tBu,Me}$ ligands exchanged, giving averaged signals. At -90 °C, the ^{1}H NMR spectrum showed 4 sets of signals with a ratio of 1:2:2:1 consistent with different pyrazolyl environments as labeled in Figure 2.8. Due to the peak broadening in the ^{1}H NMR spectrum at -90 °C, complete NMR characterisation at this temperature was not possible.

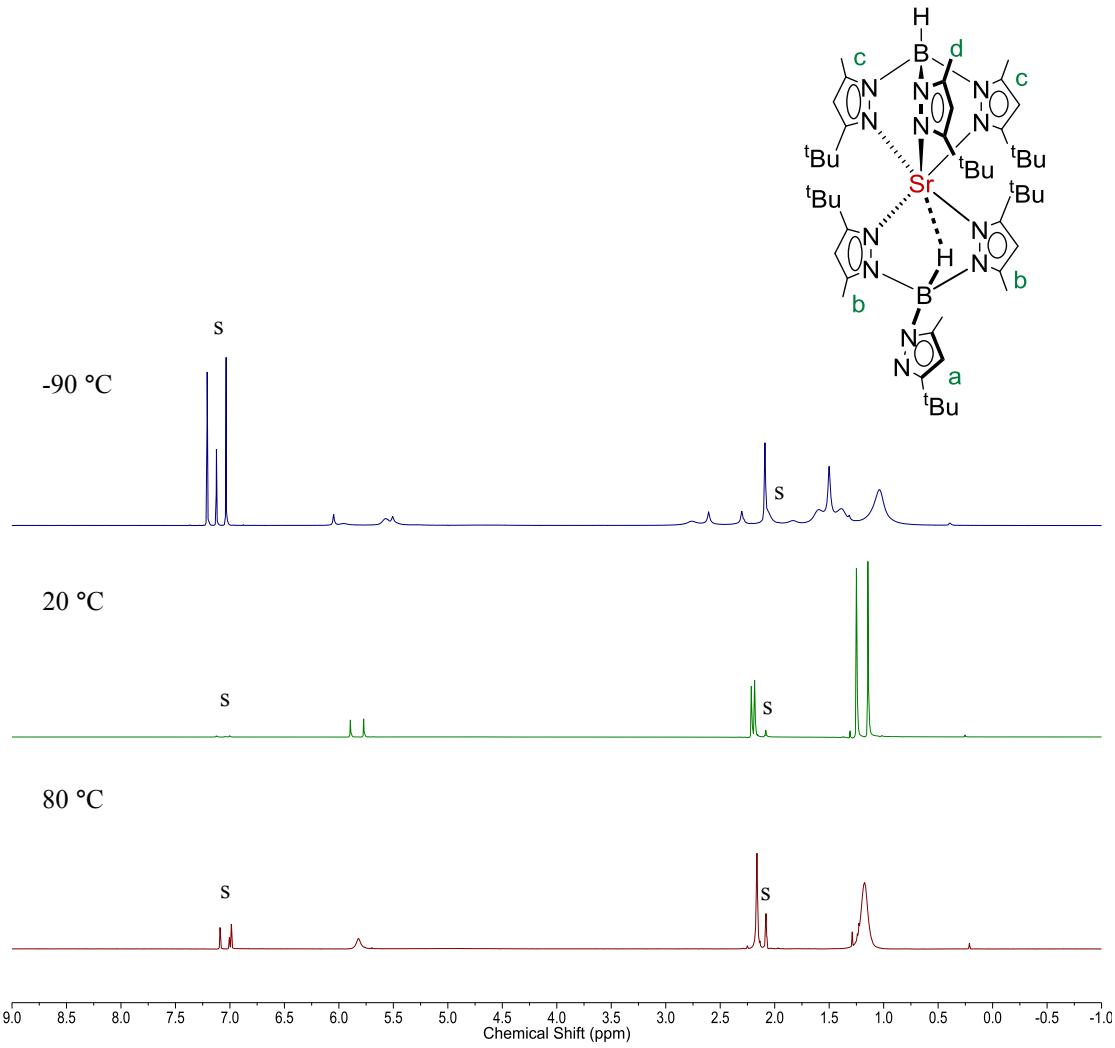

Figure 2.8. ^{1}H NMR spectra (299.9 MHz, toluene-d_8) of (κ^2,κ^3-Tp^{tBu,Me})$_2$Sr (**6**) at -90 °C, 20 °C and 80 °C ('s' denotes residual protio solvent).

Additional kinetic studies of the exchange between the two bonding modes of κ^2-Tp^{tBu,Me} and κ^3-Tp^{tBu,Me} ligands were carried out. Variable temperature ^{1}H NMR spectra of **6** were recorded between the temperatures 31-55 °C. The line broadening of the resonances corresponding to the *tert*-butyl substituent was measured at appropriate temperature increments. The exchange rate constants can be derived from the relationship with the line broadening: $k = (\Delta\nu_{1/2} - \Delta\nu_{1/2\ ref})\pi$. An Eyring plot of ln($k$/T) *vs*. 1/T (Figure 2.9) was constructed leading to the evaluation of thermodynamic parameters of the activation barrier associated with the exchange process.

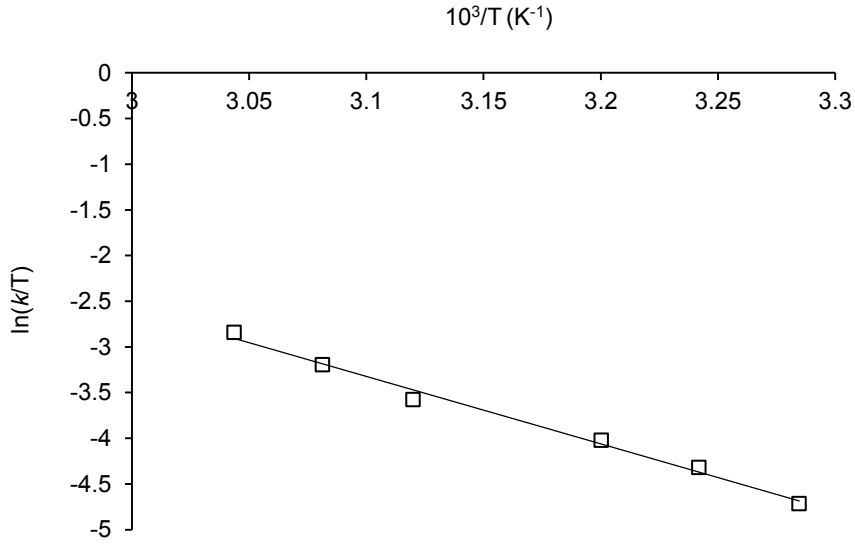

Figure 2.9. Eyring Plot for compound **6** ($R^2 = 0.9916$): $\Delta H^{\ddagger} = 14.7(7)$ kcal mol^{-1}, $\Delta S^{\ddagger} = -8.3(2)$ cal K^{-1} mol^{-1} and $\Delta G^{\ddagger}(298\ K) = 17.2(7)$ kcal mol^{-1}.

The activation Gibbs free energy of the exchange between the two bonding modes of the ligands of (κ^2,κ^3-Tp^{tBu,Me})$_2$Sr (**6**) at room temperature is 17.2(7) kcal mol^{-1}. These values obtained fit extremely well with those observed in the same process of the analogous lanthanide complexes (κ^2,κ^3-Tp^{tBu,Me})$_2$Sm (17.2(1.1) kcal mol^{-1}) and (κ^2,κ^3-Tp^{tBu,Me})$_2$Yb (16.0(3) kcal mol^{-1}).[78] The experimental findings reinforce a strong relationship between heavier alkaline earth and lanthanide complexes containing metal centres of similar ionic radii.

2.3.5 Further NMR and IR analyses of alkaline earth tetrahydroborate catalysts

The degree of ionicity of alkaline earth tetrahydroborate complexes can be evaluated from their physical measurements utilising various techniques, for instance, IR and NMR spectroscopy. The ionicity trend of compounds **1**, **2** and **4** is summarised in Table 2.8.

Table 2.8. Solid state (Nujol mull), solution (THF) υ(B-H) values (cm^{-1}) and ^{11}B chemical shifts including $^{1}J_{B\text{-}H}$ coupling constant for the tetrahydroborate ligands of ($Tp^{tBu,Me}$)Mg(BH_4) (**2**), ($Tp^{tBu,Me}$)Ca(BH_4)(THF) (**1**) and ($Tp^{tBu,Me}$)Sr(BH_4)$(THF)_2$ (**4**). H_b and H_t refer to M-H-B bridging or terminal hydrogens, respectively.

	2	**1**	**4**
Solid state			
υ(B-H_t) (cm^{-1})	2445	2396	2398
υ(B-H_b) (cm^{-1})	2227, 2166	2255, 2214	2245, 2202
Solution state			
υ(B-H_t) (cm^{-1})	2439	2416	2364
υ(B-H_b) (cm^{-1})	2229, 2174	2223, 2174	2246, 2203
δ ^{11}B (ppm)	-37.6	-32.1	-31.6
$^{1}J_{B\text{-}H}$ (Hz)	68.7	84.2	84.5

A general decrease in frequency for υ(B-H_t) and increase for υ(B-H_b) was recognised from Mg to Sr in both the solid state and solution. This convergence of the terminal A_1 to bridging A_1 and E band frequencies towards the T_2 band frequency for an anionic $[BH_4]^-$ species is a result of an increasing in ionicity of the M-BH_4 bonds from Mg to Sr. Non-coordinated, ionic $[BH_4]^-$ only demonstrates one IR symmetry-allowed band (T_2 in T_d symmetry) in the region of 2260-2300 cm^{-1}.[48] Furthermore, the increase in average $^{1}J_{B\text{-}H}$ coupling constants from 68.7 Hz in **2** to 84.2 Hz in **1** and 84.5 Hz in **4** due to the decreasing Ae···H bonding (Ae···H-B, 3-centre-2-electron bond) and, accordingly, a greater emphasis in the B-H bonding ($M^+[H\text{-}BH_3]^-$, 2-centre-2-electron bond). A similar trend was observed for compounds **2.14**, **2.15** and **2.16**.[20]

2.4. Polymerisation studies: ROP of ε-CL

A principal aim of this work was to evaluate the catalytic potential of the tetrahydroborate initiators ($Tp^{tBu,Me}$)Mg(BH_4) (**2**), ($Tp^{tBu,Me}$)Ca(BH_4)(THF) (**1**) and ($Tp^{tBu,Me}$)Sr(BH_4)$(THF)_2$ (**4**) towards the ROP of ε-CL and *rac*-LA. The very large amount of literature for the ROP of ε-CL shows it to be one of the most attractive monomers used for desirable biodegradable polymers. ROP of ε-CL was performed in both THF and toluene at room temperature, and under these conditions all the

complexes were active. The polymerisation was followed by regular aliquots taken and the polymer samples were characterised by ^{1}H NMR spectroscopy, MALDI-ToF mass spectrometry and gel permeation chromatography (GPC). The results of ROP of ε-CL in THF and toluene are summarised in Table 2.9 and Table 2.10, respectively. It is worth noting that the given times are those at which the stated conversions were reached.

Table 2.9. Selected data for the polymerisation of ε-CL using ($Tp^{tBu,Me}$)Mg(BH_4) (**2**), ($Tp^{tBu,Me}$)Ca(BH_4)(THF) (**1**) and ($Tp^{tBu,Me}$)Sr(BH_4)(THF)$_2$ (**4**) in THF.[a]

Entry	Initiator	Time (min)	Conversion (%)[b]	M_n (GPC)[c]	M_n (Calcd)[d]	PDI[e]	Yield (%)[f]
1	**2**	60	56	12,160	12,780	1.17	-
2	**2**	120	84	13,440	19,180	1.33	79
3	**1**	2	100	62,250	22,830	1.27	87
4	**4**	85	97	30,910	22,140	1.46	97

[a] Conditions: $[\varepsilon\text{-CL}]_0$: $[\text{initiator}]_0$ = 200 : 1, 3.4 mL THF at 23 °C. $[\varepsilon\text{-CL}]_0$ = 1.0 M. [b] Measured by ^{1}H NMR ($CDCl_3$) analyses. [c] Molecular weights (g mol^{-1}) determined from GPC using the appropriate Mark-Houwink corrections. [d] Expected M_n (g mol^{-1}) for 1 polymer chain growing per metal centre; M_n = converstion (%) × 200 × 114.1 + 4. [e] PDI = M_w/M_n. [f] PDI = M_w/M_n. [f] Isolated yield at 100% conversion.

Table 2.10. Selected data for the polymerisation of ε-CL using ($Tp^{tBu,Me}$)Mg(BH_4) (**2**), ($Tp^{tBu,Me}$)Ca(BH_4)(THF) (**1**) and ($Tp^{tBu,Me}$)Sr(BH_4)(THF)$_2$ (**4**) in toluene.[a]

Entry	Initiator	Time (min)	Conversion (%)[b]	M_n (GPC)[c]	M_n (Calcd)[d]	PDI[e]	Yield (%)[f]
1	**2**	80	95	20,690	21,690	1.18	83
2	**1**	1	100	55,440	22,830	1.30	89
3	**4**	7	80	106,190	18,260	1.20	79

[a] Conditions: $[\varepsilon\text{-CL}]_0$: $[\text{initiator}]_0$ = 200 : 1, 3.4 mL toluene at 23 °C. $[\varepsilon\text{-CL}]_0$ = 1.0 M. [b] Measured by ^{1}H NMR ($CDCl_3$) analyses. [c] Molecular weights (g mol^{-1}) determined from GPC using the appropriate Mark-Houwink corrections. [d] Expected M_n (g mol^{-1}) for 1 polymer chain growing per metal centre; M_n = converstion (%) × 200 × 114.1 + 4. [e] PDI = M_w/M_n. [f] PDI = M_w/M_n. [f] Isolated yield at 100% conversion.

2.4.1 Solution ROP of ε-CL using ($Tp^{tBu,Me}$)Mg(BH_4) (2)

In contrast to the catalytic activity of {HC(C(Me)N(2,6-$C_6H_3{}^iPr_2$))$_2$}Mg(BH_4)(THF) (**2.12**) towards the ROP of ε-CL (79 % conversion at [ε-CL] : [**2.14**] = 200 : 1 at 30 s.), ($Tp^{tBu,Me}$)Mg(BH_4) (**2**) polymerised the lactone at a noticeably slower rate. Well-controlled polymerisations were obtained in both THF and toluene solution as shown by a linear evolution in the M_n (GPC) with % conversion and narrow PDIs (1.11-1.20). Expected M_n for one PCL chain produced per metal centre was achieved in both solvents. However, extensive transesterification suppressed the living behaviour of ε-CL polymerisation in THF since a decrease in M_n was observed towards the end of polymerisation together with a notable increase in PDI values from 1.11 to 1.33 (Figure 2.10). First order polymerisation kinetics were observed and the apparent rate constants, k_{app} = 0.0170(6) min^{-1} (R^2 = 0.991) and k_{app} = 0.0446(14) min^{-1} (R^2 = 0.992) were obtained in THF and toluene solution, respectively (Figure 2.11). In the presence of donor solvent, competition occurs between the lactone monomers and solvent molecules in binding to the metal centre. Therefore, the slower rate of polymerisation in THF than in toluene is expected.

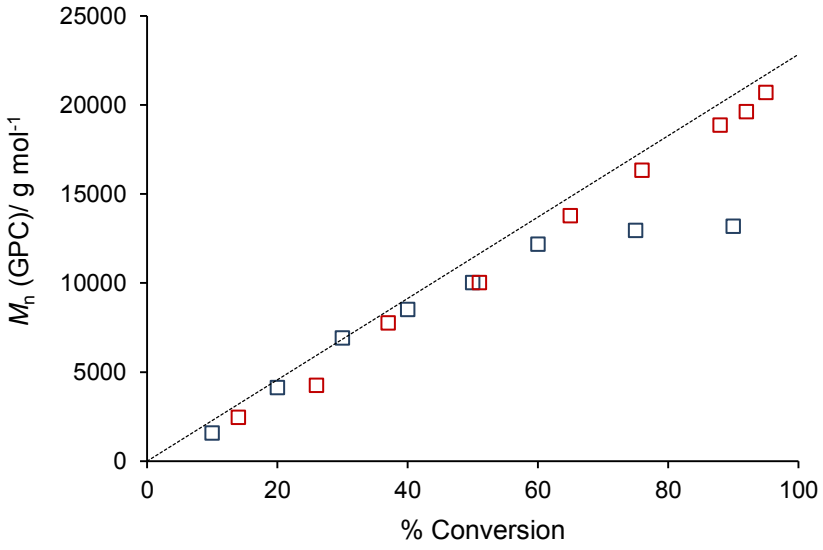

Figure 2.10. Data for ROP of ε-CL using ($Tp^{tBu,Me}$)Mg(BH_4) (**2**). M_n (GPC) vs. % conversion plot. The dotted line is that expected for one PLA chain per metal centre. Conditions: 3.4 mL THF (blue squares) or toluene (red squares), 23 °C, $[\varepsilon\text{-CL}]_0$:$[\mathbf{2}]_0$ = 200:1 and $[\varepsilon\text{-CL}]_0$ = 1.0 M. PDIs = 1.12-1.33 (THF) and 1.11-1.20 (toluene).

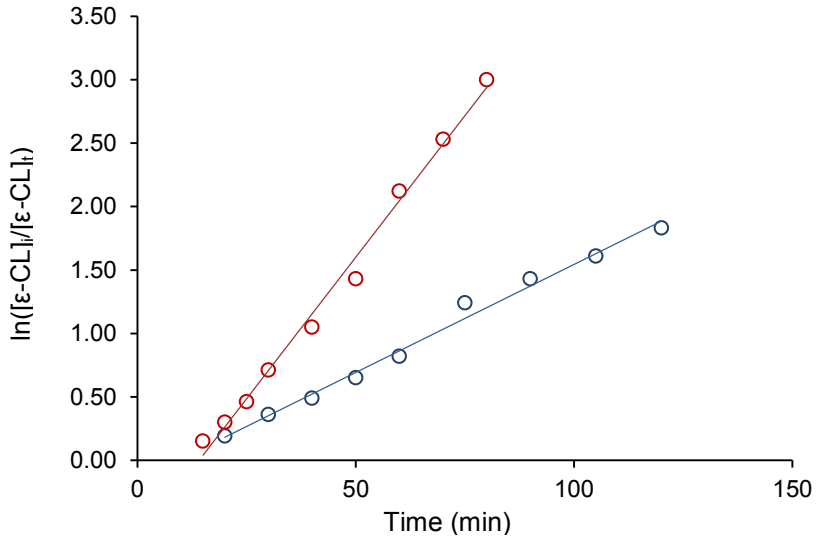

Figure 2.11. First order plot of $\ln([\varepsilon\text{-CL}]_i/[\varepsilon\text{-CL}]_t)$ *vs*. time. Apparent rate constants, k_{app} = 0.0170(6) min^{-1} (R^2 = 0.991, THF, blue circles), k_{app} = 0.0446(14) min^{-1} (R^2 = 0.992, toluene, red circles). Conditions: 3.4 mL THF or toluene, 23 °C, $[\varepsilon\text{-CL}]_0$:[**2**]$_0$ = 200:1 and $[\varepsilon\text{-CL}]_0$ = 1.0 M.

^{1}H NMR and MALDI-ToF MS analysis showed α,ω-dihydroxytelechelic polymers obtained from ε-CL ROP using **2** (Figure 2.12). This is consistent with the product derived from the coordination-insertion mechanism outlined in Scheme 2.1, and prevalent ROP literature of main group and lanthanide tetrahydroborate catalysts.

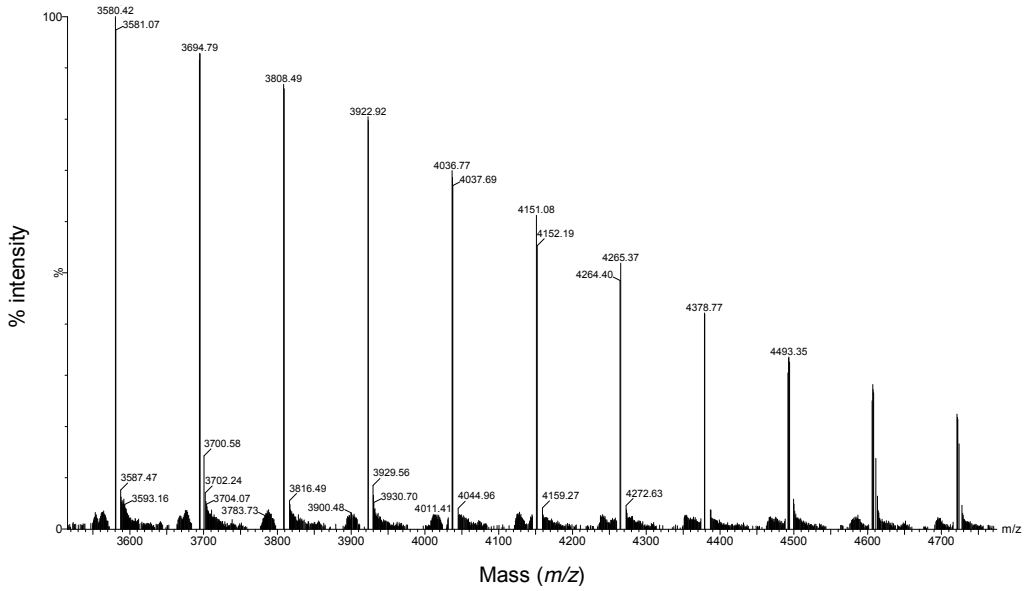

Figure 2.12. MALDI-ToF MS of PCL synthesised using ($Tp^{tBu,Me}$)Mg(BH_4) (**2**). M_n by GPC analysis was 2,460 g mol^{-1} (from a [ε-CL]:[**2**]$_0$ = 200:1 polymerisation in toluene at 23 °C). K^+ dopant, Δ(*m*/*z*) = 114.1 g mol^{-1}.

2.4.1.1 Mechanistic studies of ROP of ε-CL using ($Tp^{tBu,Me}$)Mg(BH_4) (2)

Although a mechanistic pathway of ε-CL ROP using tetrahydroborate initiators was established through experiments and DFT calculations (Section 2.2.4), little NMR spectroscopic information was reported in literature accounting the existence of intermediate species in the pathway. In order to detect the species formed in ROP of ε-CL, an NMR tube scale polymerisation between **2** and 15 equivs of ε-CL was conducted in THF-d_8 between 238 and 298 K, and monitored using ^{1}H and ^{11}B NMR spectroscopy. The sample preparation was carried out at 238 K in a dry-box under an inert atmosphere of dinitrogen. The sample was preserved at the preparative temperature in a dry ice/acetone bath before insertion into a pre-cooled NMR probe at 238 K.

The first ^{11}B NMR spectrum recorded at 238 K showed a diminished resonance for the tetrahydroborate ligand of **2**, which appeared as a quintet at -37.6 ppm. Concurrently, BH_3·THF and new tetra-coordinated boron[82] signals were observed as a quartet at -1.0 ppm and a small broad singlet at 5.1 ppm, repectively (Figure 2.13 (a)). The observation implies that the first hydride transfer reaction of the tetrahydroborate initiator to ε-CL is accompanied by the liberation of BH_3, which is trapped by a large concentration of donor solvent as BH_3·THF. The intensity of BH_3·THF resonance diminished as the tetra-coordinated boron resonance became dominant at 253 K (Figure 2.13 (b)). Interestingly the complementary ^{1}H NMR spectrum showed multiple sets of signals corresponding to $Tp^{tBu,Me}$ ligand, suggesting multiple species with different ligand environments present in solution. However, no PCL was produced at this stage (Figure 2.14 (a)). Similar observation was made at 5 mins after the sample was equilibrated to an NMR probe temperature at 273 K in the ^{1}H NMR analysis. However, the ^{11}B NMR spectrum at 273 K contained a new resonance growing in at 18.3 ppm as the 5.1 ppm resonance decreased in intensity (Figure 2.13 (c)). The large number of literature reports concerning boron-containing compounds suggest that the singlet at 18.3 ppm corresponds to a $B(OR)_3$ species, where R is an alkyl group.[82] Finally, the NMR probe temperature was elevated to 298 K allowing polymerisation to proceed. The propagation was monitored using ^{1}H NMR spectroscopy and spectra were recorded at appropriate time intervals (Figure 2.14 (b), (c) and (d)). Complete monomer conversion was achieved within 1 h, at which point

the ^{11}B NMR spectrum showed only the chracteristic resononances of the Tp^{tBu,Me} ligand and that of a trialkyl borate ester B(OR)$_3$ (Figure 2.13 (d)).

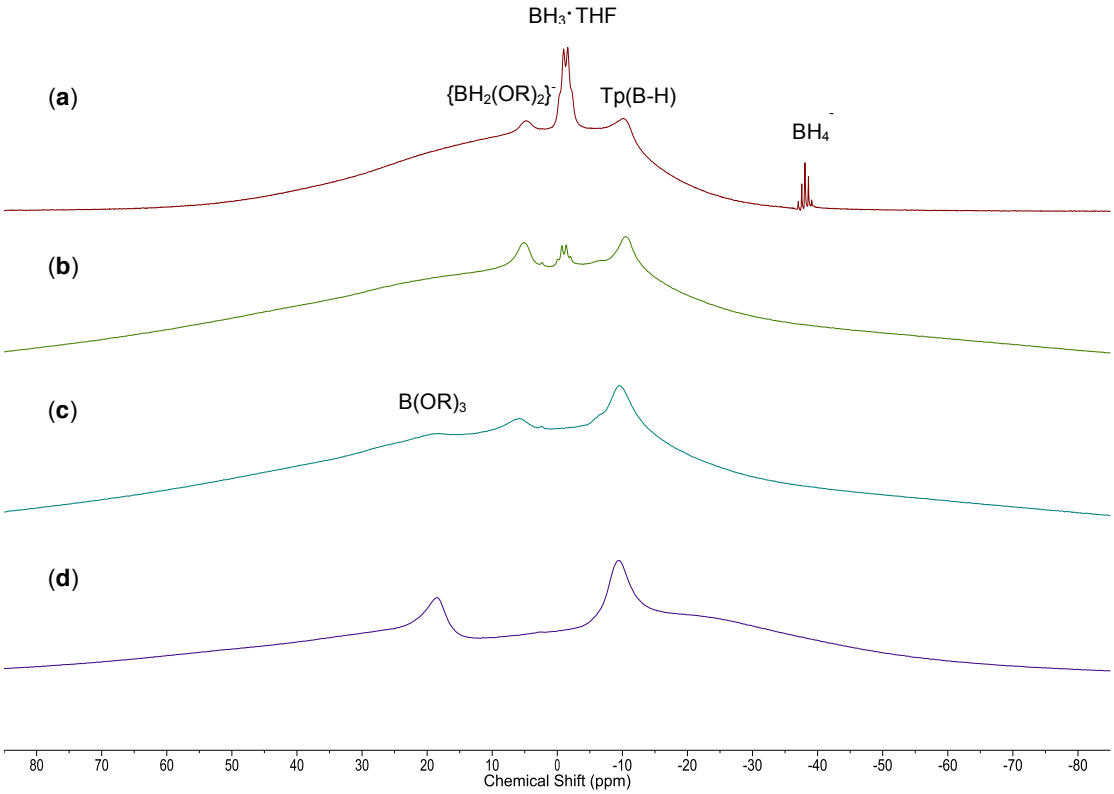

Figure 2.13. ^{11}B NMR spectra (THF-d_8, 160.4 MHz, 238-298 K) for the NMR tube scale polymerisation between (Tp^{tBu,Me})Mg(BH$_4$) (**2**) and 15 equivs. of ε-CL. (a) immediately at 238 K, (b) at 253 K (0 % PCL observed), (c) after 5 mins at 273 K (0 % PCL observed) and (d) after 1 h at 298 K (100 % PCL observed).

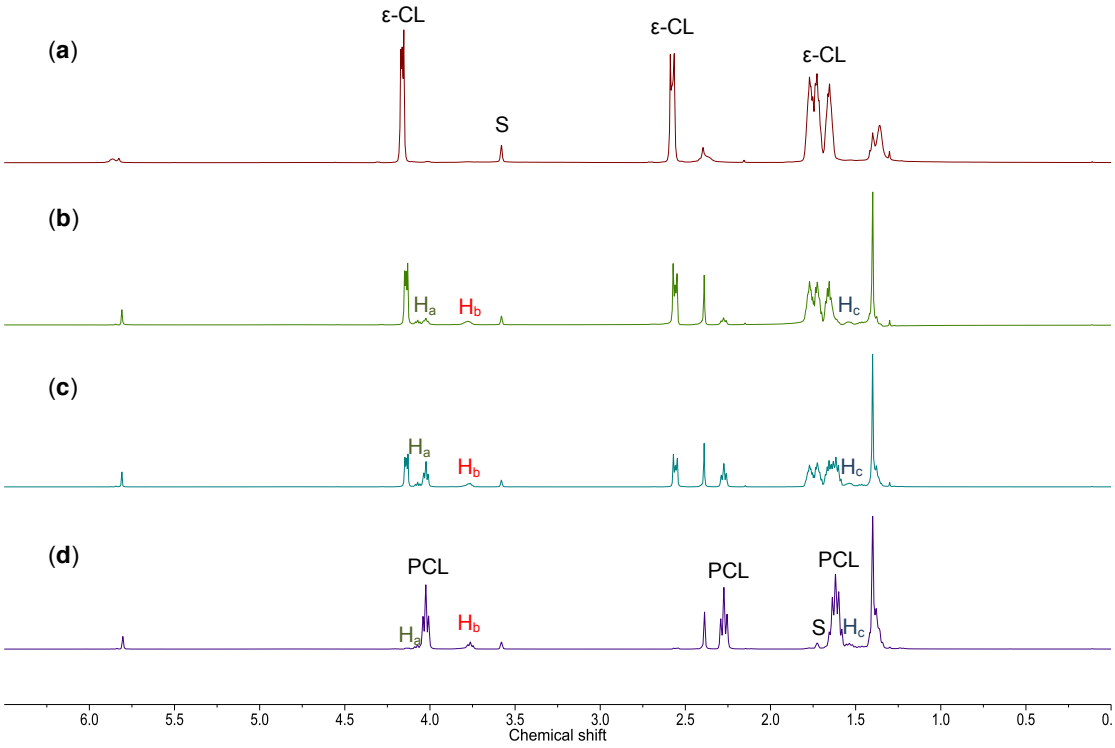

Figure 2.14. ^{1}H NMR spectra (THF-d_8, 499.9 MHz, 253-298 K) for the NMR scale polymerisation reaction between ($Tp^{tBu,Me}$)Mg(BH_4) (**2**) and 15 equiv. of ε-CL. (a) immediate products formed at 253 K (0 % PCL observed), (b) immediate products formed at 298 K (*ca*. 25 % PCL observed), (c) products formed after 20 mins at 298 K (*ca*. 50 % PCL observed) and (d) products formed after 1 h at 298 K (100 % PCL observed). "s" denotes residual protio-solvent. H_a, H_b and H_c denote the methylene proton resonances of the *in situ* product of the ε-CL ROP using **2** (Figure 2.15).

^{1}H and ^{13}C{^{1}H} one- and two-dimensional NMR spectroscopy were used to characterise the *in situ* product of ε-CL ROP using **2**, the product is established and illustrated as ($Tp^{tBu,Me}$)Mg{$(O(CH_2)_5C(O))_{13}O(CH_2)_6O)B(O_2C_6H_{12})$} (**7**, Figure 2.15). The ^{1}H NMR resonances marked with H_a, H_b and H_c (Figure 2.14 (b), (c) and (d)) are corresponding to the methylene protons of the *in situ* product **7** (Figure 2.15) with integral values of 2 H, 6 H and 6 H, respectively, relative to the $Tp^{tBu,Me}$ resonances. It is noteworthy that these resonances appeared as the propagation started and remained throughout the process with constant relative integral values. The same observations were made with different monomer concentrations and solvent (i.e. benzene).

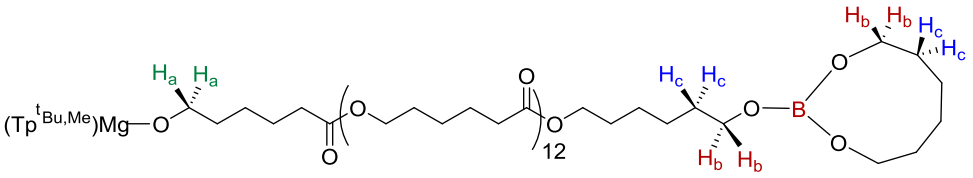

Figure 2.15. The *in situ* product **7** obtained from the NMR tube scale polymerisation experiment of ε-CL using **2** ([ε-CL] : [**2**] = 15 : 1).

Furthermore, a solution IR (NaCl cell, THF-d_8) spectrum of the product was performed. The IR spectrum obtained featured C-H (2984-2697 cm^{-1}), C=O (1717 cm^{-1}), B-O (1455 cm^{-1}) stretches.[83, 84] More importantly, there were no other B-H stretches observed, apart from the apical B-H of $Tp^{tBu,Me}$ ligand at 2552 cm^{-1}. All the experimental results point towards the trialkyl borate ester derivative as a propagating species in the ε-CL ROP using **2**.

An inverse-gated $^{11}B\{^1H\}$ NMR spectroscopic experiment[85] was undertaken to accurately quantify the integration of the boron resonances in the *in situ* product **7**. The investigation showed an integral ratio of $\underline{B}(OR)_3$ to $\underline{B}$-H of $Tp^{tBu,Me}$ of unity. This confirmed no borane loss during the polymerisation. The finding contradicts the mechanism previously proposed by Maron, Guillaume, Roesky, Mountford, and coworkers, of which the propagating intermediate is a derivative of $H_2B(OR)$ (R = alkyl group) species. Arguably, an extensive literature search shows no such species existing in solution. Only the smallest congener, $H_2B(OMe)$ was documented and its existence was identified using microwave spectroscopic techniques.[86] In these studies, a known possibility of redistribution of substituted alkoxy borane to $B(OR)_3$ accompanied by the loss of BH_3 was considered.[87, 88] The revised mechanistic pathway of ε-CL ROP using $(Tp^{tBu,Me})Mg(BH_4)$ (**2**) is shown in Scheme 2.5.

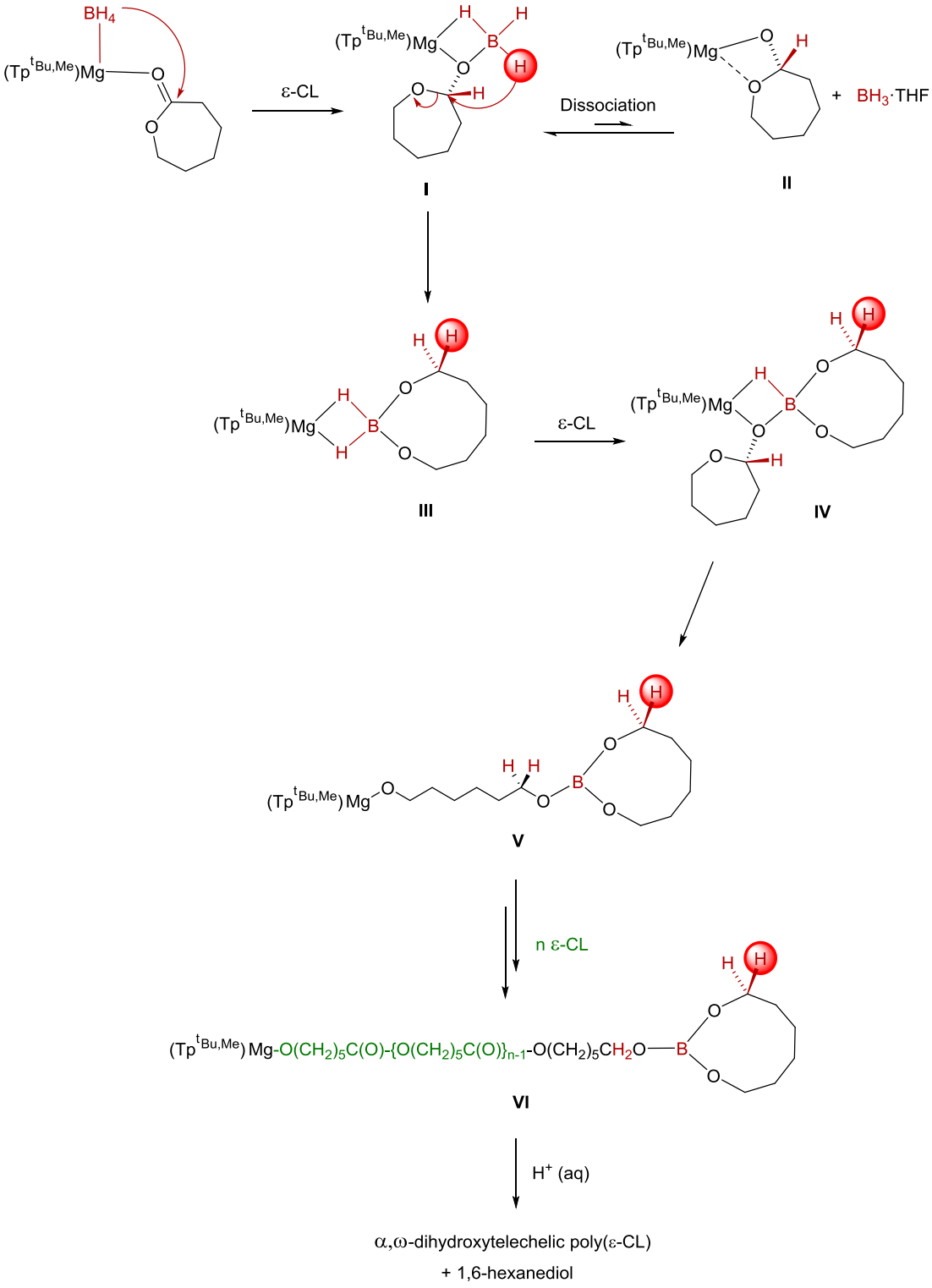

Scheme 2.5. The new proposed mechanism of the ROP of ε-CL using ($Tp^{tBu,Me}$)Mg(BH_4) (**2**).

The first carbonyl reduction takes place immediately in the ROP of ε-CL using tetrahydroborate initiator, possibly through a concerted pathway. A hydride transfer from the boron to carbon atom is expected to happen synchronously to the formation

of an oxygen-boron bond, producing a transient monoalkoxy substituted trihydroborate intermediate (**I**). In THF, the transient intermediate is in a dissociative equilibrium with the first hydride transferred ε-CL product (**II**) along with $BH_3 \cdot THF$, which is the first species observed by ^{11}B NMR analysis. It is worth noting that no aldehyde proton was observed in the expected range (δ = 9-12 ppm) in the ^{1}H NMR spectrum. The second hydride transfer is apparently very facile leading to the formation of intermediate **III**, even before all of **2** has been consumed. The only two structurally related alkaline earth compounds in the literature to date are $[(HC\{(Me)CN(2,6\text{-}^{i}Pr_2C_6H_3)\}_2Mg)_2\text{-}\mu\text{-}H\text{-}\mu\text{-}\{H_2Bpin\}]$ and $[(HC\{(Me)CN(2,6\text{-}^{i}Pr_2C_6H_3)\}_2Ca(H_2BPin)]_3$ reported by Hill *et al*.[89] and Harder *et al*.,[90] respectively (Pin = $O_2C_2Me_2$). The latter was isolated with a corresponding ^{11}B NMR resonance at δ = 2.1 ppm. This strongly supports the formation of intermediate **III** and its appearance as an apparently broad singlet at δ = 5.1 ppm in ^{11}B NMR spectrum.

The intermediate possessing bridging hydrides can act as a reductant, reducing further ε-CL monomers giving a metal complex intermediate **V** *via* **IV**. The intermediate **V** is the first species anticipated in propagation. Once propagating, further ring-opening ε-CL inserts into the metal-oxygen bond forming a propagating species **VI**. This step is comparable to the established mechanism of ε-CL ROP using an alkoxide initiator (Scheme 1.6). Both intermediate **V** and **VI** possess trialkyl borate functional group, and their corresponding ^{11}B NMR resonances are observed at 18.3 ppm. After quenching, α,ω-dihydroxy telechelic PCL is formed, along with 1,6-hexanediol. The products were confirmed by ^{1}H NMR ($CDCl_3$) analysis and mass spectrometry (Appendix, Figure A1.1 and A1.2).

Prior to the formation of $(Tp^{tBu,Me})Mg\{(O(CH_2)_5C(O))_nO(CH_2)_6O)B(O_2C_6H_{12})\}$ ($n \geq 1$, **VI**), compound **2** and species **II**, then **II** and **III**, are simultaneously present in the NMR mixtures at low temperature (238-273 K). This complication impedes the attempts to isolate or fully characterise these intermediate species.

2.4.2 ROP of ε-CL using $(Tp^{tBu,Me})Ca(BH_4)(THF)$ (1)

Similar to catalytic activities of other calcium tetrahydroborate complexes in ROP of ε-CL, $(Tp^{tBu,Me})Ca(BH_4)(THF)$ (**1**) is an extremely active catalyst in both THF and toluene at room temperature, producing α,ω-dihydroxy telechelic PCL in a matter of minutes, after hydrolytic work-up. However catalyst **1** exhibits a poor molecular

weight control, giving PCL with molecular weight of approximately two to three-times the expected values. The PDIs (1.27-1.30) obtained were moderate (Entry 3, Table 2.9 and Entry 2, Table 2.10). The detailed kinetic studies using **1** could not be carried out due to a rapid rate of the polymerisation. A very viscous polymerisation mixture was developed during the ε-CL ROP in both solvents.

The physical gel formation is recognised as a common feature of tetrahydroborate catalysed ε-CL ROP containing high molecular weight PCL. The previous studies described that the phenomenon is caused by the various inter and intramolecular Van der Waals interaction between the polymer active end-groups (–OBH_2) and metal centres or the carbonyl groups on the polymer chains.[40, 55, 57, 58] According to the new mechanism proposed in Scheme 2.5, the gel formation could possibly be attributed to the scrambling of $(Tp^{tBu,Me})M\{(O(CH_2)_5C(O))_nO(CH_2)_6O)B(O_2C_6H_{12})\}$ species as shown in Figure 2.16. The concept concerning the exchange or scrambling of trialkyl borate substituents is introduced in Chapter Four.

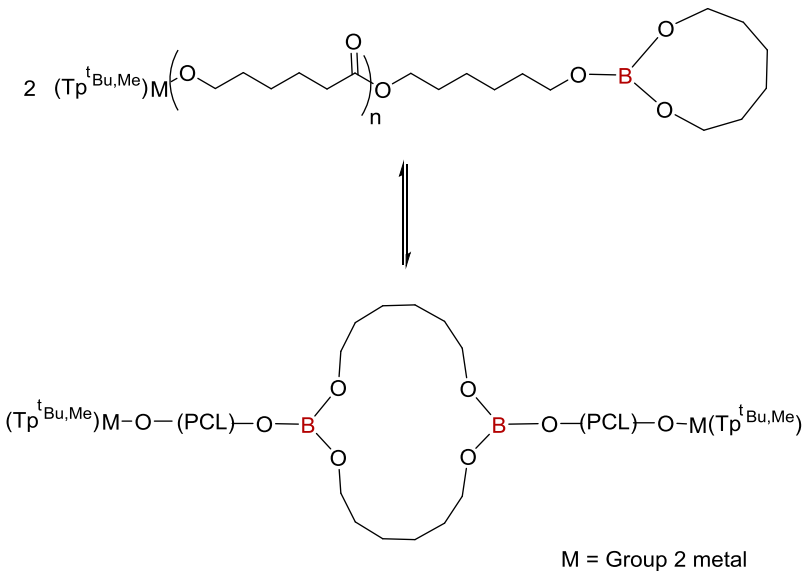

Figure 2.16. Possible interactions account for the gel formation of PCL from the ROP catalysed by $Tp^{tBu,Me}$ supported alkaline earth complexes.

In order to gain some insight into the behaviour of **1** in ε-CL ROP, an NMR tube scale polymerisation between **1** and 5 equivs. of ε-CL in C_6D_6 was carried out and monitored using ^1H and ^{11}B NMR spectroscopy. The ^1H NMR spectrum recorded within 5 mins after addition, revealed a full conversion of monomers to PCL, the dissociation of THF and a relatively small change in the chemical shifts of the

$Tp^{tBu,Me}$ ligand. However, the ^{11}B NMR spectrum showed neither a noticeable decrease in intensity of the ^{11}B resonance of BH_4^- nor the formation of new ^{11}B resonances, when compared to those of the catalyst **1**. This suggests only a small fraction of catalyst was active in the polymerisation. The faster rate of propagation to initiation, as well as a small fraction of active catalyst in the initiating and propagating steps could account for the production of high molecular weight PCL as observed.

The preparative concentration of the NMR spectroscopic studies ([**1**] = 0.05 M, 0.6 mL of C_6D_6) resulted in a remarkably viscous solution. A much diluted polymerisation was attempted on a larger scale by the addition of 5 equivs of ε-CL into a vigorously stirred solution of **1** in benzene ([**1**] = 0.025 M, 2 mL of C_6H_6). An aliquot was taken within 5 mins of polymerisation for ^{11}B NMR analysis. However, no change was observed relative to the NMR tube scale polymerisation discussed previously. Moreover, the same observation was also made in THF.

2.4.3 ROP of ε-CL using $(Tp^{tBu,Me})Sr(BH_4)(THF)_2$ (4)

$(Tp^{tBu,Me})Sr(BH_4)(THF)_2$ (**4**) is among a few characterised heteroleptic strontium tetrahydroborate compounds, successfully used as ROP catalysts. Compound **4** is also active towards ROP of ε-CL in both toluene and THF, producing α,ω-dihydroxy telechelic PCL according to MALDI-ToF MS and NMR spectroscopy. Low activity was observed for the ε-CL ROP in THF. This is similar to some previously reported studies.[42, 43] The polymerisation gave a higher than expected molecular weight PCL with moderate PDIs of 1.2-1.5 (Entry 4, Table 2.9). An increasing viscosity of the polymerisation solution was observed as higher conversion of monomer to PCL was achieved. The rate of polymerisation obtained from the kinetic analysis was neither first nor second order with respect to the concentration of ε-CL. Nevertheless, the accuracy in the polymerisation rate measurement is somewhat hindered by the diffusing capabilities of species in the viscous polymerisation solution.

As expected, rapid ε-CL polymerisation was observed in toluene. A very tough gel formation was obtained in 7 mins with 80 % monomer conversion. A significantly higher than expected molecular weight PCL was obtained (Entry 3, Table 2.10). A kinetic study was not feasible due to the difficulty in maintaining ideal polymerisation conditions.

Both ^{1}H and ^{11}B NMR spectroscopy were also used to monitor the change of **4** in NMR tube scale polymerisations in both THF-d_8 and C_6D_6. Only the experiment in THF gave a ^{11}B NMR spectrum with any detectable change. In this case, a low intensity broad singlet was observed at δ = 18.6 ppm alongside the resonances corresponding to catalyst **4**. Therefore, as for compound **1**, the production of high molecular weight PCL with **4** is caused by the faster rate of propagation compared to initiation, in conjunction with a small portion of active catalyst in the initiating and propagating steps.

2.5 Summary and Conclusions

This Chapter has developed a series of $Tp^{tBu,Me}$ ligand supported alkaline earth tetrahydroborate complexes, compound **1**, **2** and **4**, as ε-CL and *rac*-LA ROP initiators. The complexes were conveniently prepared in good yields *via* salt metathesis reactions between $K(Tp^{tBu,Me})$ and corresponding metal bis(tetrahydroborate) in THF. Alternative syntheses using the analogous halide derivatives (compound **2.17**, **3**, **5**) are also presented. The Schlenk equilibrium product **6** found in the synthesis of **4** was independently prepared. The compound exhibits an intriguing κ^2, κ^3- $Tp^{tBu,Me}$ ligand bonding modes. Detailed kinetic studies were carried out to evaluate the activation energy for the exchange between the two ligand bonding modes, and the value is found to be in accordance with those obtained from the analogous homoleptic lanthanide compounds (i.e. Yb and Sm).

Compound **1**, **2** and **4** are active towards ε-CL ROP in both THF or toluene at RT, giving α,ω-dihydroxytelechelic polymers. The type of solvent used in ε-CL ROP has a marked effect only on the rate of polymerisation and the molecular weight control of the ε-CL ROP using **4**. Overall an increase in reactivity of the catalysts is observed in the order of Mg (**2**) < Sr (**4**) < Ca (**1**). A well-control living ROP of ε-CL ROP using **2** allowed a mechanistic investigation utilising variable temperature ^{1}H, $^{13}C\{^{1}H\}$, ^{11}B and two-dimensional correlation NMR spectroscopic techniques. The studies showed a trialkyl borate ester derivative as a propagating species, leading to the newly proposed mechanism of ε-CL ROP using **2**. The mechanistic studies for the ε-CL ROP using **1** and **4** yielded less obvious results due to the partially active catalysts in initiation/propagation and the faster rate of propagation to initiation.

However, the mechanism is expected as a common pathway in all three catalytic systems.

2.6 References for Chapter Two

1. H. H. Brintzinger, D. Fischer, R. Mülhaupt, B. Rieger and R. M. Waymouth, *Angew. Chem. Int. Ed.*, 1995, **34**, 1143.
2. P. Margl, L. Deng and T. Ziegler, *Top. Catal.*, 1999, **7**, 187.
3. W. Kaminsky, *Advances in Catalysis*, Academic Press, 2001, vol. 46, pp. 89.
4. S. Harder, *Chem. Rev.*, 2010, **110**, 3852.
5. M. R. Crimmin, A. G. M. Barrett, M. S. Hill, P. B. Hitchcock and P. A. Procopiou, *Organometallics*, 2008, **27**, 497.
6. M. R. Crimmin, I. J. Casely and M. S. Hill, *J. Am. Chem. Soc.*, 2005, **127**, 2042.
7. X. He, E. Hurley, B. C. Noll and K. W. Henderson, *Organometallics*, 2008, **27**, 3094.
8. S. Datta, M. T. Gamer and P. W. Roesky, *Organometallics*, 2008, **27**, 1207.
9. F. Buch, J. Brettar and S. Harder, *Angew. Chem. Int. Ed.*, 2006, **45**, 2741.
10. S. Harder, F. Feil and A. Weeber, *Organometallics*, 2001, **20**, 1044.
11. W. E. Lindsell, F. C. Robertson and I. Soutar, *Eur. Polym. J.*, 1983, **19**, 115.
12. Y. Sarazin, R. H. Howard, D. L. Hughes, S. M. Humphrey and M. Bochmann, *Dalton Trans.*, 2006, 340.
13. F. Feil and S. Harder, *Eur. J. Inorg. Chem.*, 2005, **2005**, 4438.
14. L. Piao, M. Deng, X. Chen, L. Jiang and X. Jing, *Polymer*, 2003, **44**, 2331.
15. Z. Zhong, S. Schneiderbauer, P. J. Dijkastra, M. Westerhausen and J. Feijen, *Polym. Bull.*, 2003, **51**, 175.
16. A. C. Jones, *J. Mater. Chem.*, 2002, **12**, 2576.
17. A. Torvisco and K. Ruhlandt-Senge, *Alkaline-Earth Metal Compounds*, Springer Berlin Heidelberg, 2013, vol. 45, pp. 1.
18. S. Kobayashi and Y. Yamashita, *Acc. Chem. Res.*, 2011, **44**, 58.
19. C. A. Wheaton, P. G. Hayes and B. J. Ireland, *Dalton Trans.*, 2009, 4832.
20. R. A. Collins, J. Unruangsri and P. Mountford, *Dalton Trans.*, 2013, **42**, 759.
21. M. H. Chisholm and N. W. Eilerts, *Chem. Commun.*, 1996, 853.
22. B. M. Chamberlain, M. Cheng, D. R. Moore, T. M. Ovitt, E. Lobkovsky and G. W. Coates, *J. Am. Chem. Soc.*, 2001, **123**, 3229.

23. M. Westerhausen, S. Schneiderbauer, A. N. Kneifel, Y. Söltl, P. Mayer, H. Nöth, Z. Zhong, P. J. Dijkastra and J. Feijen, *Eur. J. Inorg. Chem.*, 2003, 3432.
24. D. J. Darensbourg, W. Choi, O. Karroonnirun and N. Bhuvanesh, *Macromolecules*, 2008, **41**, 3493.
25. Y. Sarazin, D. Rosca, V. Poirier, T. Roisnel, A. Silvestru, L. Maron and J.-F. Carpentier, *Organometallics*, 2010, **29**, 6569.
26. R. Dunsing and H. R. Kricheldorf, *Polym. Bull.*, 1985, **14**, 491.
27. H. R. Kricheldorf and A. Serra, *Polym. Bull.*, 1985, **14**, 497.
28. I. Rashkov, J. L. Espartero, N. Manolova and M. Vert, *Macromolecules*, 1996, **29**, 57.
29. I. Rashkov, N. Manolova, S. M. Li, J. L. Espartero and M. Vert, *Macromolecules*, 1996, **29**, 50.
30. Z. Zhong, M. J. K. Ankoné, P. J. Dijkastra, C. Birg, M. Westerhausen and J. Feijen, *Polym. Bull.*, 2001, **46**, 51.
31. Z. Zhong, P. J. Dijkastra, C. Birg, M. Westerhausen and J. Feijen, *Macromolecules*, 2001, **34**, 3863.
32. H. Guan, Z. Xie, Z. Tang, X. Xu, X. Chen and X. Jing, *Polymer*, 2005, **46**, 2817.
33. J.-F. Carpentier and Y. Sarazin, *Alkaline-Earth Metal Compounds*, Springer Berlin Heidelberg, 2013, vol. 45, pp. 141.
34. M. H. Chisholm, N. W. Eilerts, J. C. Huffman, S. S. Iyer, M. Pacold and K. Phomphrai, *J. Am. Chem. Soc.*, 2000, **122**, 11845.
35. Y. Sarazin, V. Poirier, T. Roisnel and J.-F. Carpentier, *Eur. J. Inorg. Chem.*, 2010, 3423.
36. Y. Sarazin, B. Liu, T. Roisnel, L. Maron and J.-F. Carpentier, *J. Am. Chem. Soc.*, 2011, **133**, 9069.
37. B. Liu, T. Roisnel, J. P. Guegan, J.-F. Carpentier and Y. Sarazin, *Chem. Eur. J.*, 2012, **18**, 6289.
38. M. Visseaux and F. Bonnet, *Coord. Chem. Rev.*, 2011, **255**, 374.
39. Y. Nakayama, S. Okuda, H. Yasuda and T. Shiono, *React. Func. Polym.*, 2007, **67**, 798.
40. H. D. Dyer, S. Huijser, N. Susperregui, F. Bonnet, A. D. Schwarz, R. Duchateau, L. Maron and P. Mountford, *Organometallics*, 2010, **29**, 3602.

41. M. G. Cushion and P. Mountford, *Chem. Commun.*, 2011, **47**, 2276.
42. S. Marks, M. Kuzdrowska, P. W. Roesky, L. Annunziata, S. M. Guillaume and L. Maron, *ChemPlusChem* 2012, **77**, 350.
43. M. Kuzdrowska, L. Annunziata, S. Marks, M. Schmid, C. G. Jaffredo, P. W. Roesky, S. M. Guillaume and L. Maron, *Dalton Trans.*, 2013, **42**, 9352
44. M. H. Chisholm, J. C. Gallucci and K. Phomphrai, *Inorg. Chem.*, 2004, **43**, 6717.
45. M. H. Chisholm, J. C. Gallucci and K. Phomphrai, *Inorg. Chem.*, 2005, **44**, 8004.
46. M. Besora and A. Lledós, *Contemporary Metal Boron Chemistry I*, Springer Berlin Heidelberg, 2008, vol. 130, pp. 149.
47. M. Visseaux and F. Bonnet, *Coord. Chem. Rev.*, 2011, **255**, 374.
48. T. J. Marks and J. R. Kolb, *Chem. Rev.*, 1977, **77**, 263.
49. Z. Xu and Z. Lin, *Coord. Chem. Rev.*, 1996, **156**, 139.
50. M. Ephritikhine, *Chem. Rev.*, 1997, **97**, 2193.
51. M. Schappacher, N. Fur and S. M. Guillaume, *Macromolecules*, 2007, **40**, 8887.
52. M. Schappacher, A. Soum and S. M. Guillaume, *Biomacromolecules*, 2006, **7**, 1373.
53. J. Jenter, P. W. Roesky, N. Ajellal, S. M. Guillaume, N. Susperregui and L. Maron, *Chem. Eur. J.*, 2010, **16**, 4629.
54. S. M. Guillaume, *Eur. Polym. J.*, 2013, **49**, 768.
55. I. Palard, A. Soum and S. M. Guillaume, *Macromolecules*, 2005, **38**, 6888.
56. N. Barros, P. Mountford, S. M. Guillaume and L. Maron, *Chem. Eur. J.*, 2008, **14**, 5507.
57. S. M. Guillaume, M. Schappacher and A. Soum, *Macromolecules*, 2003, **36**, 54.
58. I. Palard, A. Soum and S. M. Guillaume, *Chem. Eur. J.*, 2004, **10**, 4054.
59. I. Palard, M. Schappacher, A. Soum and S. M. Guillaume, *Polym. Int.*, 2006, **55**, 1132.
60. M. G. Cushion, D.Phil Thesis, University of Oxford, 2011.
61. K. O. Saliu, G. H. Maunder, M. J. Ferguson, A. Sella and J. Takats, *Inorg. Chim. Acta*, 2009, **362**, 4616.
62. R. D. Shannon, *Acta Crystallogr. A*, 1976, **32**, 751.

63. F. Marchetti, C. Pettinari, R. Pettinari, B. W. Skelton and A. H. White, *Inorg. Chim. Acta*, 2009, **362**, 4480.
64. R. Han and G. Parkin, *Organometallics*, 1991, **10**, 1010.
65. R. Han and G. Parkin, *J. Am. Chem. Soc.*, 1990, **112**, 3662.
66. R. Han, M. Bachrach and G. Parkin, *Polyhedron*, 1990, **9**, 1775.
67. É. B. Lobkovskii, L. V. Titov, M. D. Levicheva and A. N. Chekhlov, *J Struct Chem*, 1990, **31**, 506.
68. J. Prust, K. Most, I. Müller, E. Alexopoulos, A. Stasch, I. Usón and H. W. Roesky, *Z. anorg. allg. Chem.*, 2001, **627**, 2032.
69. F. Allen, *Acta Crystallogr. B*, 2002, **58**, 380.
70. G. L. Soloveichik, M. Andrus and E. B. Lobkovsky, *Inorg. Chem.*, 2007, **46**, 3790.
71. Y. Filinchuk, R. Černý and H. Hagemann, *Chem. Mater.*, 2009, **21**, 925.
72. M. Bremer, H. Nöth and M. Warchhold, *Eur. J. Inorg. Chem.*, 2003, **2003**, 111.
73. M. Bremer, H. Nöth, M. Thomann and M. Schmidt, *Chem. Ber.*, 1995, **128**, 455.
74. B. Wrackmeyer, *Z. Naturforsch., B: Chem. Sci.*, 2004, **59**, 1192.
75. K. Izod, C. Wills, W. Clegg and R. W. Harrington, *Inorg. Chem.*, 2007, **46**, 4320.
76. D. L. Reger, R. Mahtab, J. C. Baxter and L. Lebioda, *Inorg. Chem.*, 1986, **25**, 2046.
77. S. Harder and J. Brettar, *Angew. Chem. Int. Ed.*, 2006, **45**, 3474.
78. X. Zhang, R. McDonald and J. Takats, *New J. Chem.*, 1995, **19**, 573.
79. Y. Sohrin, M. Matsui, Y. Hata, H. Hasegawa and H. Kokusen, *Inorg. Chem.*, 1994, **33**, 4376.
80. M. J. Saly, M. J. Heeg and C. H. Winter, *Inorg. Chem.*, 2009, **48**, 5303.
81. T. R. Belderraín, L. Contreras, M. Paneque, E. Carmona, A. Monge and C. Ruiz, *Polyhedron*, 1996, **15**, 3453.
82. H. Nöth and B. Wrackmeyer, *Nuclear Magnetic Resonance Spectroscopy of Boron Compounds*, 1st edn., Springer-Verlag, Berlin, Heidelberg Germany, 1978.

83. Dudley H Williams and I. Fleming, *Spectroscopic Methods in Organic Chemistry*, 5th edn., McGraw-Hill Higher Education, Berkshire England, 1995.

84. K. Nakamoto, *Infrared and Raman Spectra of Inorganic and Coordination Compounds*, 6th edn., John Wiley & Sons, Inc., Hoboken, New Jersey, 2009.

85. P. Giraudeau and E. Baguet, *J*. *Magn*. *Reson*., 2006, **180**, 110.

86. Y. Kawashima, H. Takeo and C. Matsumura, *J*. *Mol*. *Spectrosc*., 1986, **116**, 23.

87. D. J. Pasto, V. Balasubramaniyan and P. W. Wojtkowski, *Inorg*. *Chem*., 1969, **8**, 594.

88. A. Lang, H. Nöth and M. Thomann-Albach, *Chem*. *Ber*., 1997, **130**, 363.

89. M. Arrowsmith, M. S. Hill, T. Hadlington, G. Kociok-Kohn and C. Weetman, *Organometallics*, 2011, **30**, 5556.

90. S. Harder and J. Spielmann, *J*. *Organomet*. *Chem*., 2012, **698**, 7.

Chapter Three

Group 2 tetrahydroborate complexes for the ROP of *rac*-LA and their mechanistic studies

3.1 Overview

This Chapter will describe detailed investigations into the ROP of *rac*-LA using alkaline earth tetrahydroborate complexes introduced in Chapter Two, namely ($Tp^{tBu,Me}$)Mg(BH_4) (**2**), ($Tp^{tBu,Me}$)Ca(BH_4)(THF) (**1**) and ($Tp^{tBu,Me}$)Sr(BH_4)$(THF)_2$ (**4**). Kinetic and mechanistic studies of the ($Tp^{tBu,Me}$)Mg(BH_4) catalysed *rac*-LA ROP carried out using spectroscopic techniques through the alkoxy-type analogues, will be presented and discussed. Comparison of the newly proposed mechanistic studies and the previously reported ones will be made. Five new Group 2 complexes will be presented, as well as three X-ray crystallographic structures.

3.2 Introduction

Up to now, a relatively small number of literature reports on the tetrahydroborate-catalysed ROP of *rac*-LA and their mechanisms have been disclosed. The end group analyses using ^{1}H and $^{13}C\{^{1}H\}$ NMR spectroscopy and MALDI-ToF MS of the PLA formed from the lanthanide or alkaline earth tetrahydroborate catalysed ROP apparently show the mixture of -CH(Me)CHO and -CH(Me)CH_2OH functional groups.[1-6] DFT calculations on Eu(O_2'N^{NMe_2})(BH_4) (O_2'N^{NMe_2} = $Me_2NCH_2CH_2N(CH_2$-2-O-$C_6H_4)_2$) with *L*-LA were carried out by Maron and co-workers, giving two possible initiation pathways leading to alcohol and aldehyde-terminated PLA.[1] The pathway leading to the production of aldehyde end-capped PLA involves the loss of BH_3 after the first hydride transfer from the tetrahydroborate initiator to a lactide monomer. The following ring-opening step gives the growing polymer chain with an aldehyde functional group prior to propagation. Nevertheless, a similar pathway to that in Scheme 2.1 (i.e. two hydride-transfer steps) was calculated to be more thermodynamically favourable and led to the formation of the -OBH_2 active end group. This pathway led to the formation of α,ω-dihydroxy telechelic PLA after the hydrolytic work-up.

3.3. ROP of *rac*-LA using ($Tp^{tBu,Me}$)Mg(BH_4) (2)

Unexpectedly, ($Tp^{tBu,Me}$)Mg(BH_4) (**2**) was inactive towards the ROP of *rac*-LA at room temperature with no polymer observed after 12 h. An increased temperature of 70 °C was required for the polymeristion to proceed. The preliminary studies revealed resultant polymer with much lower than expected molecular weight, moderate PDI

and no monomer-stereoselectivity (P_r = 0.52). However, a further effort to carry out kinetic studies was undertaken. A *rac*-LA ROP experiment was performed in THF at 70 °C ([*rac*-LA]:[**2**] = 100:1). The progress was monitored by regular sampling, the results are shown in Figure 3.1. The general procedure for polymer characterisation can be found in Chapter 6.

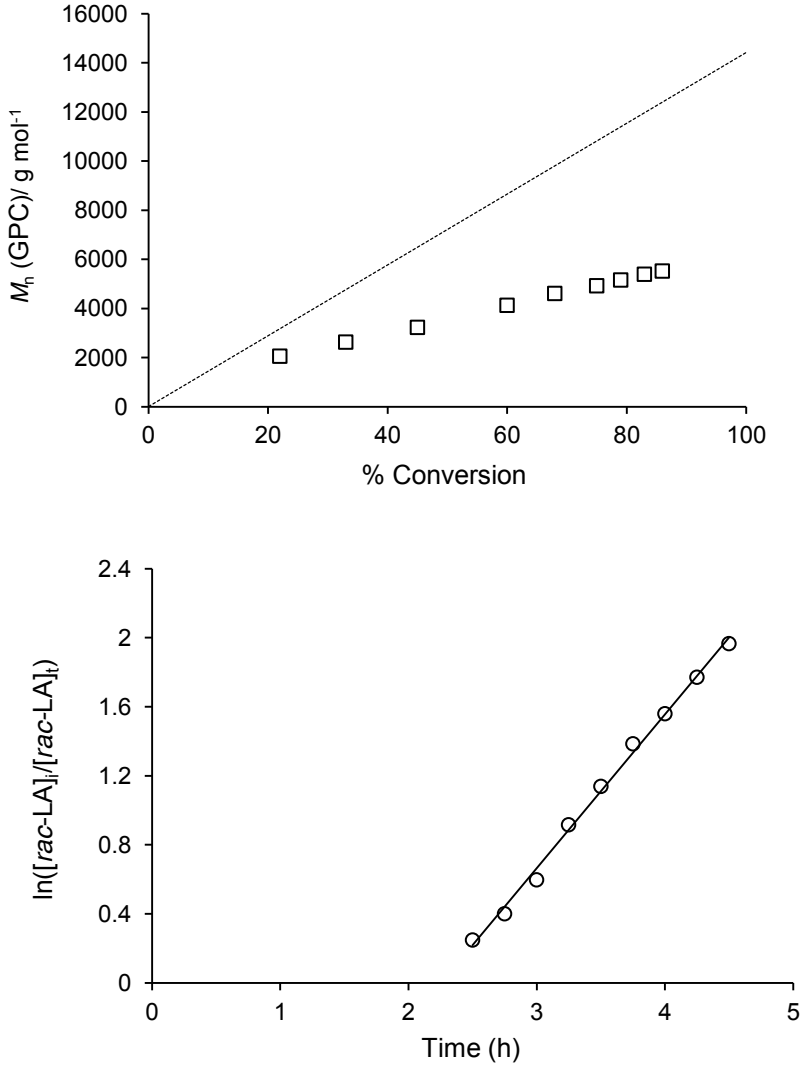

Figure 3.1. Data for ROP of *rac*-LA using ($Tp^{tBu,Me}$)Mg(BH_4) (**2**). Top: M_n (GPC) *vs*. % conversion plot. The dotted line is that expected for one PLA chain per metal centre. Condition: 6 mL THF, 70 °C, [*rac*-LA]$_0$:[**2**]$_0$ = 100:1, [*rac*-LA] = 0.5 M. PDIs = 1.25-1.35. Bottom: First order plot of ln([*rac*-LA]$_i$/[*rac*-LA]$_t$) *vs*. time. Apparent rate constant, k_{app} = 0.89(2) h^{-1} (R^2 = 0.996).

Catalyst **2** gave a linear M_n (GPC) *vs*. % conversion plot with lower than expected molecular weight PLA obtained throughout the polymerisation. The gradient of M_n

(GPC) *vs*. % conversion is 54.9(6) g mol^{-1} (% conversion)$^{-1}$ (R^2 = 0.999), which is almost a third of that expected (144.1 g mol^{-1} (% conversion)$^{-1}$) for one growing PLA chain per metal centre. This is perhaps indicative of multiple PLA chains being produced per metal centre, or transesterfication (back-biting) that have often been invoked as typical causes of lower than expected M_n values in *rac*-LA ROP.

The rate of polymerisation is first order with respect to *rac*-LA concentration and the apparent rate constant k_{app} is 0.89(2) h^{-1} (R^2 = 0.996). A significantly long induction period was observed even though the polymerisation took place at 70 °C. As for tetrahydroborate initiators previously reported,[5-7] MALDI-ToF MS analysis of the PLA formed using **2** apparently showed a mixture of both –CH(Me)CHO and –CH(Me)CH_2OH termini (Figure 3.2) according to end group mass. The predominant distribution consists of peak envelopes with Δ*m*/*z* of 72, indicating the tranesterification in the polymerisation.

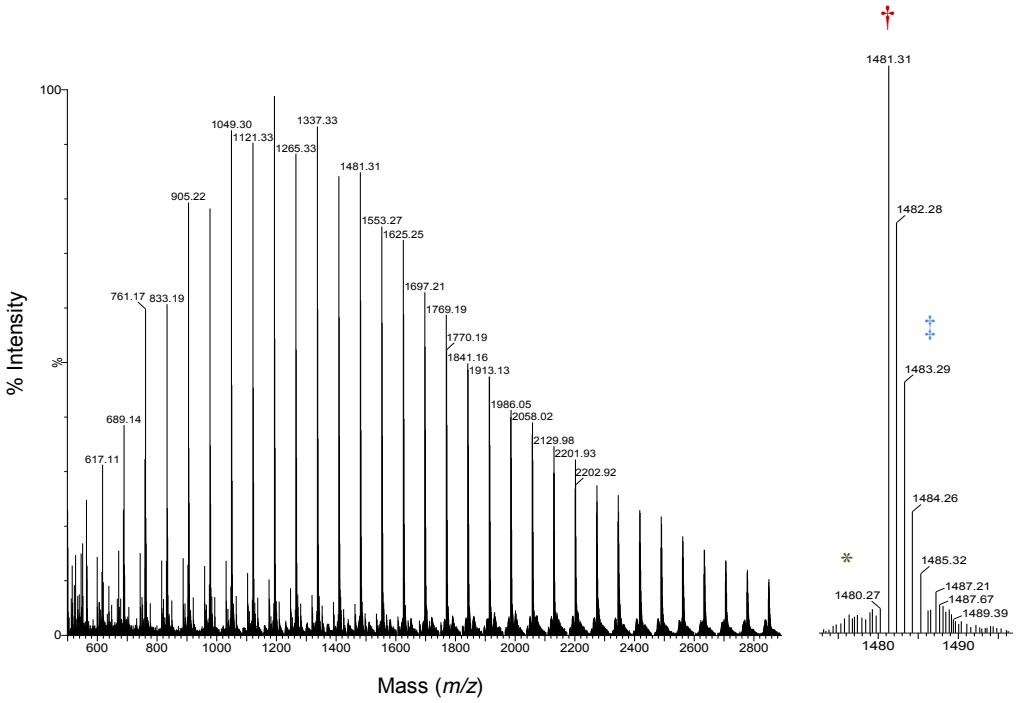

Figure 3.2. MALDI-ToF MS of PLA synthesised using (Tp^{tBu,Me})Mg(BH$_4$) (**2**)**.** M_n by GPC analysis was 2,630 g mol^{-1} (from a [*rac*-LA]:[**2**]$_0$ = 100:1 polymerisation at 70 °C) (left). A MALDI-ToF peak envelope of PLA with a length of 10 lactide monomer units (right). Maxima in the isotopic distributions shown are corresponding to cyclic PLA (green asterisk), apparent -CH(Me)CHO termini (red dagger) and -CH(Me)CH_2OH termini (blue double dagger).

Overall, there are two main issues evaluated from the poor performance of the ROP of *rac*-LA using **2**, namely the polymerisation rate and the molecular weight control. To understand the origin of the factor causing no polymerisation at room temperature and a long induction period observed at high temperature ROP using **2**, a series of experiments using both **2** and closely related compounds were undertaken.

3.3.1. Kinetic and mechanistic studies of *rac*-LA ROP using complexes of the ($Tp^{tBu,Me}$)Mg(OR) type

To begin with, an investigation into the propagating step of *rac*-LA ROP using **2** was attempted. Representative models utilized in this study are the alkoxide derivatives, ($Tp^{tBu,Me}$)Mg(OR) (R = alkyl), as they better imitate the propagating species in the tetrahydroborate catalysed ROP. ($Tp^{tBu,Me}$)Mg(OR) species could be conveniently prepared either from the protonolysis reaction of an analogous amide or from an alkyl derivative.

The precursor ($Tp^{tBu,Me}$)Mg(^{n}Bu) (**8**) was synthesised *via* a metathesis reaction between $KTp^{tBu,Me}$ and Mg(^{n}Bu)$_2$ in a 61 % yield (Equation 3.1). Diffraction-quality crystals were grown from a saturated hexanes solution at -20 °C. The solid state structure and its selected bond lengths and angles are illustrated in Figure 3.3 and Table 3.2, respectively. Related compounds (Tp^{tBu})Mg(R) or ($Tp^{3,5\text{-}Me}$)Mg(R) (R = primary alkyl, secondary alkyl, tertiary alkyl, vinyl or phenyl group) were previously prepared by the reactions between salt forms of the ligand M($Tp^{R'}$) (M = K or Tl and R' = alkyl) and corresponding MgR_2 or Grignard reagents RMgX (X = Cl, Br or I).[8-10]

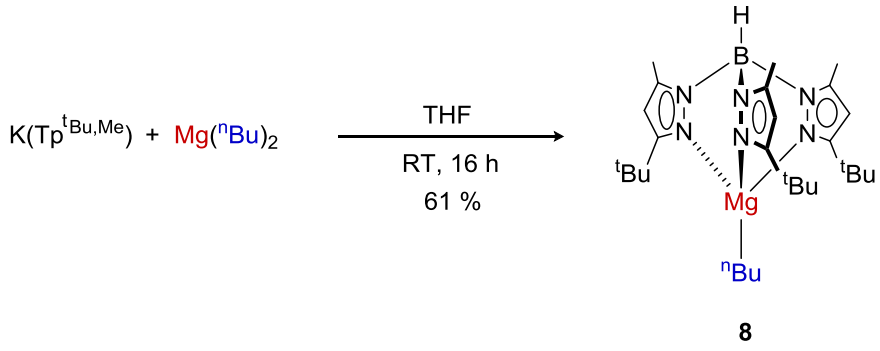

8

Equation 3.1

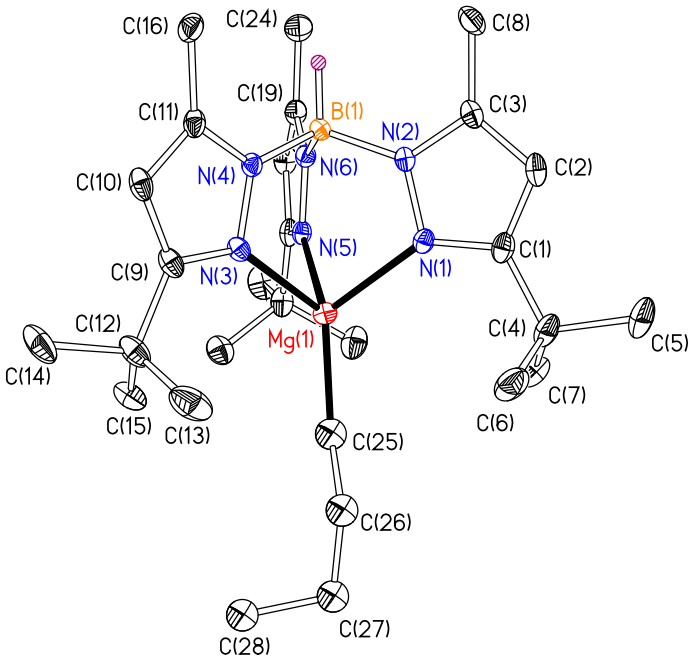

Figure 3.3. Displacement ellipsoid plot (20% probability level) of (Tp^{tBu,Me})Mg(^{n}Bu) (**8**). H atoms omitted for clarity.

Table 3.2. Selected bond lengths (Å) and angles (°) for (Tp^{tBu,Me})Mg(^{n}Bu) (**8**).

Mg(1)-N(1)	2.1365(15)	Mg(1)-N(5)	2.1309(15)
Mg(1)-N(3)	2.1259(15)	Mg(1)-C(25)	2.070(4)
N(1)-Mg(1)-N(3)	91.42(6)	N(1)-Mg(1)-C(25)	124.59(15)
N(1)-Mg(1)-N(5)	91.40(6)	N(3)-Mg(1)-C(25)	127.62(15)
N(3)-Mg(1)-N(5)	88.55(5)	N(5)-Mg(1)-C(25)	122.51(14)
Mg(1)-C(25)-C(26)	131.5(3)		

Compound **8** is four-coordinate with Mg coordinated to the three N atoms of the Tp^{tBu,Me} ligand and a C atom of the ^{n}Bu ligand. The coordination geometry at Mg(1) is best described as approximately tetrahedral with N-Mg-N and N-Mg-C angles of 88.55(5)-91.42(6)° and 122.51(14)-127.62(15)°, respectively. The Mg-C bond distance of 2.070(4) Å is consistent with those of analogous (Tp^{tBu})Mg(R) or (Tp$^{3,5\text{-}Me}$)Mg(R) (*ca.* 2.07-2.15 Å, R = primary alkyl, secondary alkyl, tertiary alkyl, vinyl or phenyl group).[8-10] However, the average Mg-N_{pz} bond distance of 2.1311(15) Å is

slightly longer than those of ($Tp^{tBu,Me}$)Mg(BH_4) (**2**, av. Mg-N_{pz} bond distance = 2.1121(15) Å) and ($Tp^{tBu,Me}$)Mg(Cl) (**3**, av. Mg-N_{pz} bond distance = 2.0992(11) Å).

The first model, ($Tp^{tBu,Me}$)Mg(S-lactate) (**9**), was synthesised through a protonolysis reaction between ($Tp^{tBu,Me}$)Mg(^{n}Bu) (**8**) and (S)-methyl-lactate alcohol in diethyl ether at -78 °C. A crystalline product was obtained in a 47 % yield (Equation 3.2). Diffraction-quality crystals were grown from a saturated pentane solution at 4 °C. The solid state structure and its selected bond lengths and angles are shown in Figure 3.4 and Table 3.3, respectively.

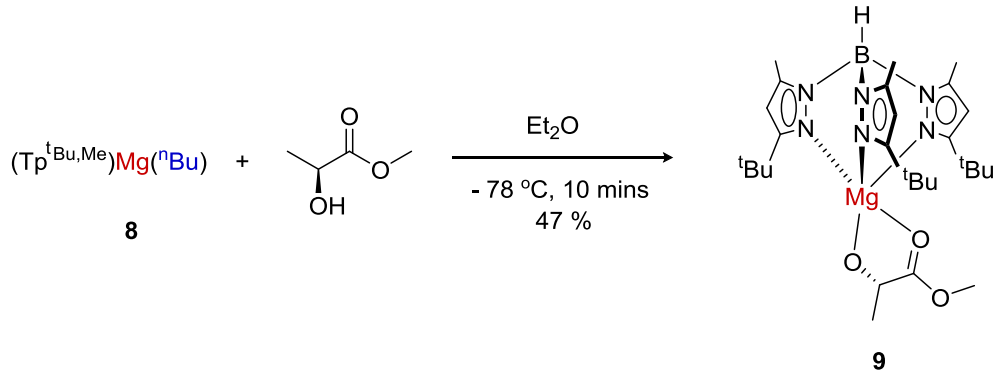

Equation 3.2

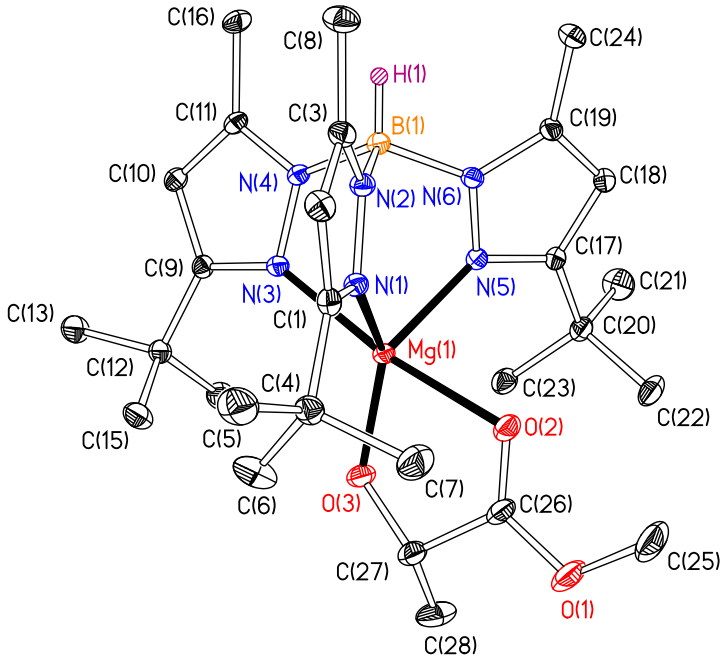

Figure 3.4. Displacement ellipsoid plot (20% probability level) of ($Tp^{tBu,Me}$)Mg(S-lactate) (**9**). H atoms omitted for clarity.

Table 3.3. Selected bond lengths (Å) and angles (°) for ($Tp^{tBu,Me}$)Mg(S-lactate) (**9**).

Mg(1)-N(1)	2.191(3)	Mg(1)-O(2)	2.177(3)
Mg(1)-N(3)	2.169(3)	Mg(1)-O(3)	1.910(3)
Mg(1)-N(5)	2.159(3)		
N(1)-Mg(1)-N(3)	85.78(12)	N(2)-B(1)-N(4)	107.7(3)
N(1)-Mg(1)-N(5)	102.63(12)	N(2)-B(1)-N(6)	111.0(3)
N(3)-Mg(1)-N(5)	85.29(12)	N(4)-B(1)-N(6)	110.0(3)
N(3)-Mg(1)-O(2)	170.94(13)	N(3)-Mg(1)-O(3)	109.65(13)
Mg(1)-N(1)-N(2)-B(1)	4.5	Mg(1)-N(3)-N(4)-B(1)	9.8
Mg(1)-N(5)-N(6)-B(1)	36.0		

N.B. two independent chiral molecules in P1 unit cell but with no significant difference in trends between them.

A large number of well-defined *O*-lactate and *O*-lactyllactate complexes of transition metals (ie. Sc,[11] Y[12, 13] and Zn[14, 15]) and main group metals (ie. Ga,[16, 17] Sn[18, 19] and Al[13, 20-23]) have been reported in the literature, some of which have been used as catalysts for ROP. Compound **9** is the first example of a crystallographically characterised alkaline earth lactate complex.

Compound **9** is five-coordinate with Mg(1) bound to the three N donors of the κ^3-$Tp^{tBu,Me}$ ligand and two O atoms of the lactate ligand. The latter is coordinated to the metal centre as a five-membered ring through an alkoxy oxygen (O(3)) and a carbonyl oxygen (O(2)), with Mg-O bond distances of 2.177(3) and 1.910(3) Å, respectively. The coordination geometry around Mg(1) is best described as distorted trigonal bipyramidal with N(3) and O(2) occupying the axial positions with the N(3)-Mg(1)-O(2) angle of 170.94(13) °. Mg(1) lies 0.17 Å above the trigonal plane defined by N(1), N(5) and O(3). The coordinating lactate moiety imposes a large steric hindrance around the metal centre. As a result, a distortion of the N(5)-pyrazolyl ring from a regular position of pyrazolyl ring in the otherwise C_3-symmetric ligand was observed with a significantly larger Mg(1)-N(5)-N(6)-B(1) torsion angle (36.0 º) than the counterparts (4.5 and 9.8 °) and those of **2** (2.3-7.9 °), **3** (9.5 °) and **8** (1.1-3.8 °).

($Tp^{tBu,Me}$)Mg(S-lactate) (**9**) can be viewed as a mimic of the first ring-opened lactide monomer coordinating to the metal centre after the initiating step. The ROP of *rac*-LA using **9** is comparable to the propagating step in the *rac*-LA ROP using ($Tp^{tBu,Me}$)Mg(BH_4) (**2**). Compound **9** polymerised 100 equivs. of *rac*-LA in THF at RT within 21 h; the polymerisation was very well controlled and progressed in a living manner. A linear plot of M_n (GPC) *vs*. % conversion was achieved with narrow PDI (1.08-1.17) values obtained throughout the polymerisation. The gradient of M_n (GPC) *vs*. % conversion plot was 139(4) g mol^{-1} (% conversion)$^{-1}$, which is equivalent within error to the expected value of 144.1 g mol^{-1} (% conversion)$^{-1}$ (Figure 3.5). This establishes that one PLA chain is produced per metal centre as expected for a single site catalyst. The rate of polymerisation was monitored, showing first order dependence on *rac*-LA concentration with a short induction period observed. The apparent rate constant k_{app}, evaluated from the plot of ln([*rac*-LA]$_i$/[*rac*-LA]$_t$) *vs*. time, is 0.108(4) h^{-1} (R^2 = 0.992, Figure 3.5).

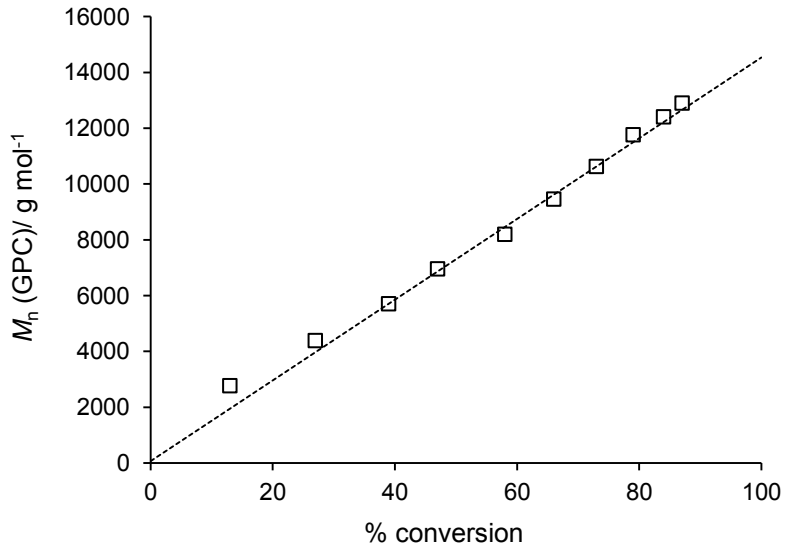

Figure 3.5. Data for ROP of *rac*-LA using ($Tp^{tBu,Me}$)Mg(S-lactate) (**9**). M_n (GPC) *vs*. % conversion plot. The dotted line is that expected for one PLA chain per metal centre. Condition: 6 mL THF, 23 °C, [*rac*-LA]$_0$:[**9**]$_0$ = 100:1, [*rac*-LA]$_0$ = 0.5 M. PDIs = 1.08-1.17.

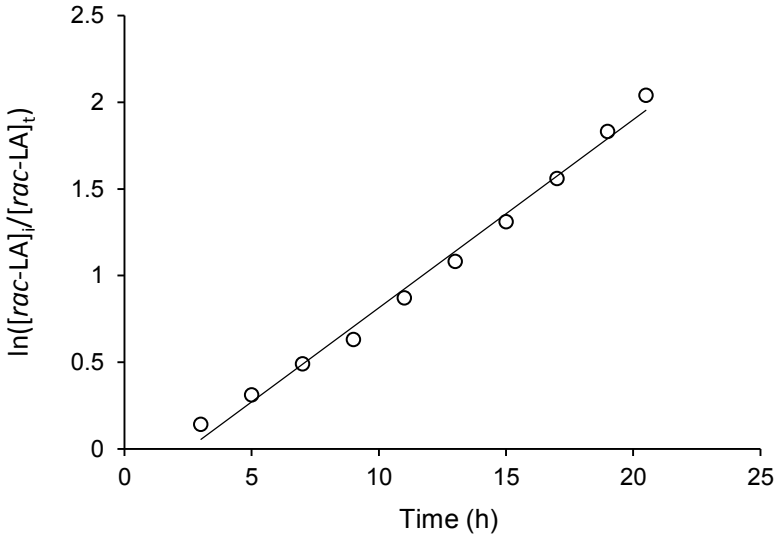

Figure 3.5 (continued). First order plot of ln([*rac*-LA]$_i$/[*rac*-LA]$_t$) *vs*. time. Apparent rate constant, k_{app} = 0.108(4) h^{-1} (R^2 = 0.992).

Heterotactically enriched PLA was produced with P_r of 0.60-0.62. MALDI-ToF MS of the PLA produced using **9** showed lactate end-group incorporation (Figure 3.6). The major distribution showed $\Delta m/z$ of 144 g mol^{-1} between the adjacent peak envelopes. This was consistent with a low degree of transesterification, reflected by the narrow PDI values and good control of M_n with % conversion.

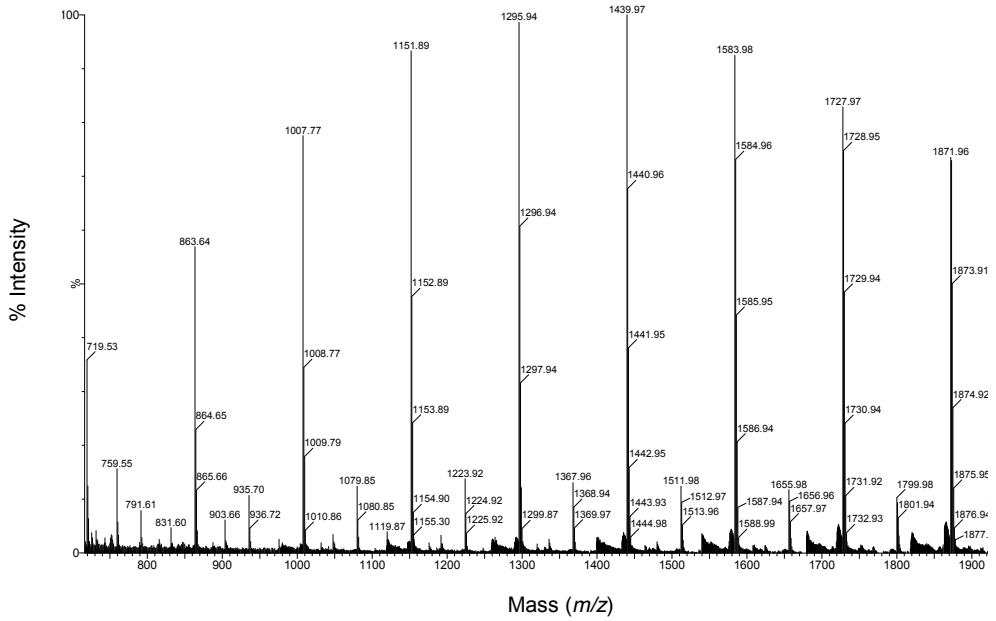

Figure 3.6. MALDI-ToF MS of PLA synthesised using (Tp^{tBu,Me})Mg(S-lactate) (**9**). M_n by GPC analysis was 2,770 g mol^{-1} (from a [*rac*-LA]$_0$:[**9**]$_0$ = 100:1 polymerisation at 23 °C).

Having obtained PLA with much lower than expected M_n from the ROP of *rac*-LA using ($Tp^{tBu,Me}$)Mg(BH_4) (**2**) at 70 °C, the phenomenon was initially considered to be due to the heating effect, which, according to the MALDI-ToF MS data certainly gave transesterification enhancement. To determine the heating effect on polymer results, a control experiment was performed using **9** to catalyse the ROP of *rac*-LA at 70 °C.

The M_n (GPC) *vs*. % conversion plot illustrated that the living ROP behaviour was maintained in the early stage of ROP using **9** at 70 °C, one chain of PLA was produced per metal centre (Figure 3.7, red squares). However, M_n values droped off towards the end of the polymerisation along with an increase in PDI values from 1.11 to 1.21. This observation can be attributed to the more pronouced transesterification effect upon heating. The heating also affected the stereocontrol *via* a chain-end control mechanism, resulting in slightly less heterotactic enriched PLA (P_r = 0.57-0.58) compared to that obtained at 23°C. Overall, the PLA yielded using **9** had significantly higher molecular weights than that obtained using **2** under the same polymerisation condition.

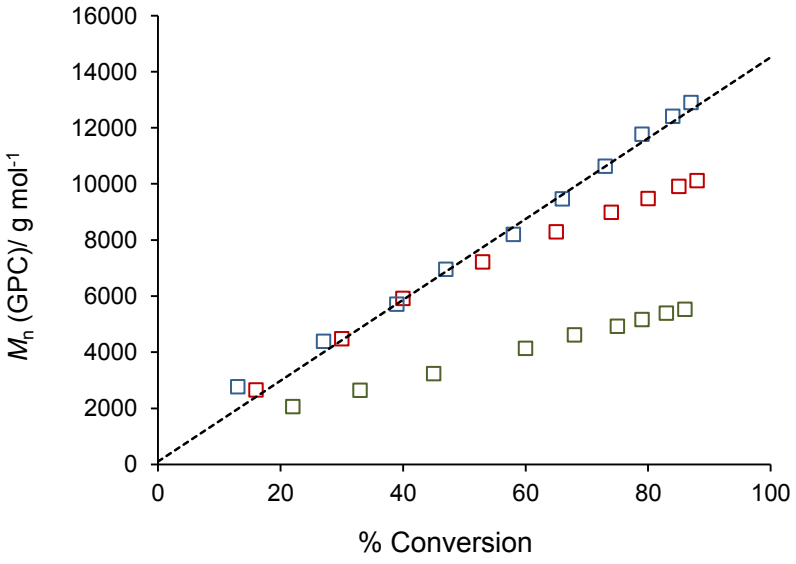

Figure 3.7. M_n (GPC) vs.Conversion plot, (a) ROP using **2** at 70 °C (green squares), (b) ROP using **9** at 23 °C (blue squares) and (c) ROP using **9** at 70 °C (red squares). The dotted line is that expected for one PLA chain per metal centre. Conditions: 6 mL THF, [*rac*-LA]$_0$:[**2** or **9**]$_0$ = 100:1, [*rac*-LA]$_0$ = 0.5 M.

The kinetic profile of *rac*-LA ROP using **9** at 70 °C was evaluated. The rate of polymerisation is first order with respect to the concentration of *rac*-LA. The apparent

rate constant k_{app}, evaluated from the plot of $\ln([rac\text{-LA}]_i/[rac\text{-LA}]_t)$ *vs*. time, is 0.76(2) h^{-1} (R^2 = 0.994, Figure 3.8). No significant induction period was observed in the *rac*-LA ROP using **9** at 70 °C. By neglecting the induction period for **2** at 70 °C, the rates of polymerisations using **2** and **9** under the same conditions are comparable. This suggests a different initiation process in the ROP experiments using **2** and **9**.

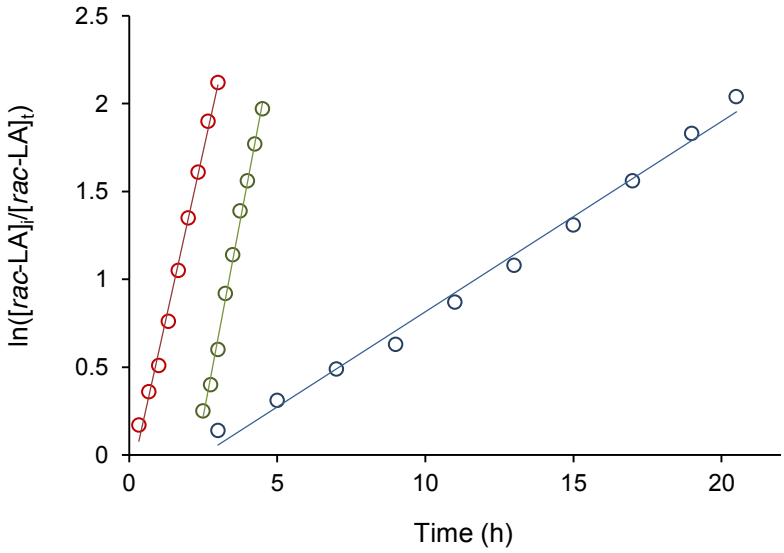

Figure 3.8. First order plot of $\ln([rac\text{-LA}]_i/[rac\text{-LA}]_t)$ *vs*. time. (a) ROP using **2** at 70 °C (green circles); rate constant, k_{app} = 0.89(2) h^{-1} (R^2 = 0.996). (b) ROP using **9** at 23 °C (blue circles); rate constant, k_{app} = 0.108(4) h^{-1} (R^2 = 0.992). (c) ROP using **9** at 70 °C (red circles); rate constant, k_{app} = 0.76(2) h^{-1} (R^2 = 0.994). Conditions: 6 mL THF, $[rac\text{-LA}]_0$:[**2** or **9**]$_0$ = 100:1, $[rac\text{-LA}]_0$ = 0.5 M.

To conclude, compound **9** catalysed the ROP of *rac*-LA in a well-controlled fashion at room temperature. Upon heating, a marginal effect on M_n was observed at high conversion. Nevertheless, a comparable rate of polymerisation to that of ROP using **2** was attained. By inference, the propagation of ROP using **2** at room temperature is feasible. From the control experiment, a significant energy barrier in the initiating step of *rac*-LA ROP using **2** can be proposed.

In an attempt to undertake further investigation into the initiation step of *rac*-LA ROP catalysed by **2** using spectroscopic techniques, some modification was applied to the studied model in order to obtain a better "NMR handle". ($Tp^{tBu,Me}$)Mg(OBn) (**10**) was introduced as a new model, and synthesised either *via* a protonolysis pathway

(Scheme 3.1(a)) or a β-hydride transfer using (Tp^{tBu,Me})Mg(^{n}Bu) (**8**) and benzaldehyde (Scheme 3.1(b)).

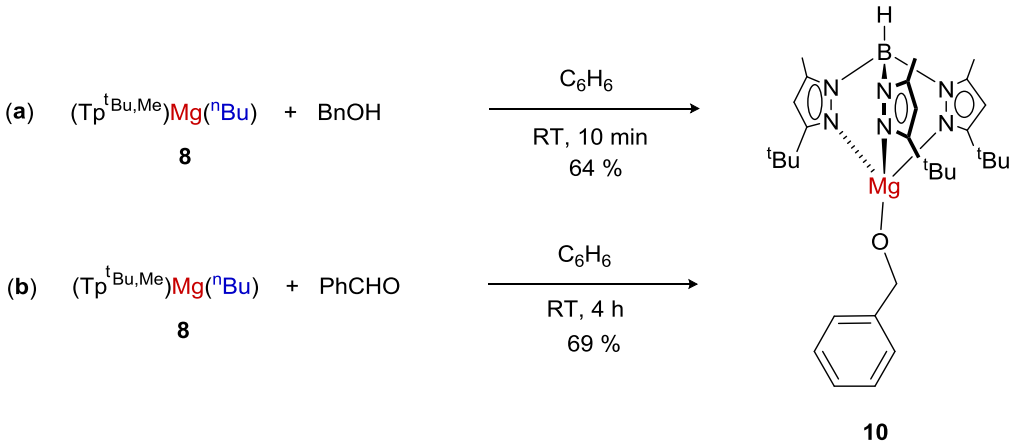

Scheme 3.1. Synthesis of (Tp^{tBu,Me})Mg(OBn) (**10**) *via* (a) a protonolysis reaction or (b) β-hydride transfer reaction.

The protonolysis reaction (Scheme 3.1(a)) of **8** with benzyl alcohol in benzene gave **10** as a pure product in a crystallised yield of 64 %. Compound **10** can also be prepared by a β-hydride transfer reaction (Scheme 3.1(b)) using the same metal starting material. The β-hydrogen of the *n*-butyl moiety in **8** was transferred to the carbonyl carbon of benzaldehyde producing **10** in a yield of 69 %, in conjunction with 1-butene. The reaction proceeds through a 6-membered ring transition state depicted in Figure 3.9. The transition state is equivalent to that found in the Meerwein-Ponndorf-Verley reduction, whereby an aluminium alkoxide catalyses a hydride shift from the α-carbon of a sacrificial alcohol to the carbonyl carbon of an aldehyde or ketone to yield a corresponding alcohol.[24] β-hydride transfer reactions between *n*-butyl Grignard reagents and Ph_2CO are also known in the literature. This methodology was also recently exploited by Chisholm *et al*. in the synthesis of metal alkoxides.[25]

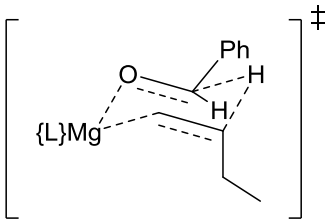

Figure 3.9. Proposed transition state in the β-hydride transfer reaction of **8** and PhCHO.

Diffraction-quality crystals were grown from a saturated hexanes solution at -30 °C. The solid state structure is shown in Figure 3.10 and its selected bond lengths and angles are shown in Table 3.4.

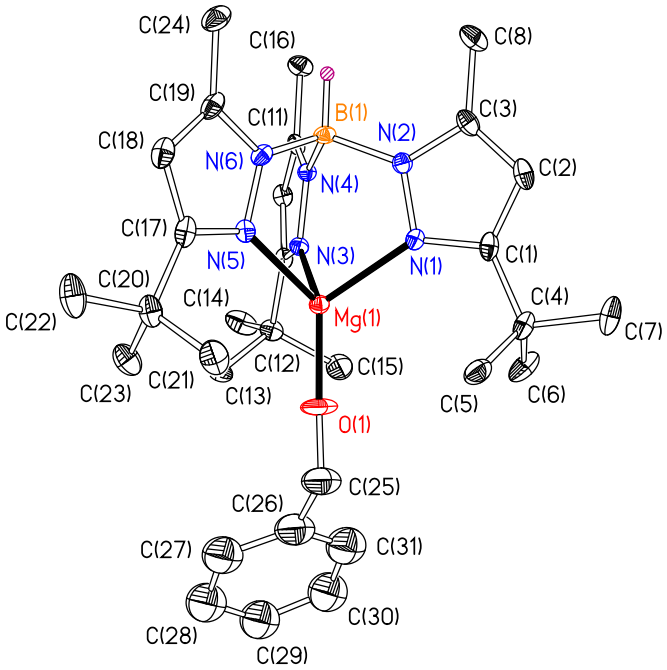

Figure 3.10. Displacement ellipsoid plot (20% probability level) of ($Tp^{tBu,Me}$)Mg(OBn) (**10**). H atoms omitted for clarity.

Table 3.4. Selected bond lengths (Å) and angles (°) for ($Tp^{tBu,Me}$)Mg(OBn) (**10**).

Mg(1)-N(1)	2.094(4)	Mg(1)-O(1)	1.820(4)
Mg(1)-N(3)	2.093(4)	O(1)-C(25)	1.330(9)
Mg(1)-N(5)	2.097(4)	C(25)-C(26)	1.374(13)
N(1)-Mg(1)-N(3)	92.99(16)	N(1)-Mg(1)-O(1)	122.3(2)
N(1)-Mg(1)-N(5)	92.60(16)	N(3)-Mg(1)-O(1)	124.1(2)
N(3)-Mg(1)-N(5)	90.54(16)	N(5)-Mg(1)-O(1)	125.0(2)
O(1)-C(25)-C(26)	122.1(8)		

Overall, compound **10** is four-coordinate with Mg coordinated to the three N atoms of the $Tp^{tBu,Me}$ ligand and an O atom of the benzyloxy ligand. The coordination geometry at Mg(1) is best described as distorted tetrahedral with N-Mg-O angles of 122-126 and N-Mg-N angles of 90-93 °. The average Mg-N_{pz} bond length (2.095(4) Å) is

similar, within error, to those of ($Tp^{tBu,Me}$)Mg(BH_4) (**2**, 2.1121(15) Å) and ($Tp^{tBu,Me}$)Mg(Cl) (**3**, 2.0992(11) Å). However, both of the average Mg-N_{pz} and the Mg-O (1.820(4) Å) bond distances are shorter than those of ($Tp^{tBu,Me}$)Mg(S-lactate) (**9**) (2.173(3) and 1.910 Å, respectively) containing the bidentate lactate ligand. Surprisingly, ($Tp^{tBu,Me}$)Mg(OBn) (**10**) is the only crystallographically characterised example among the analogous series of (Tp^{tBu})Mg(OR) (R = Et, ^{i}Pr, ^{t}Bu, Ph or $SiMe_3$) compounds reported in the literature.[9, 26-28]

The *rac*-LA polymerisation using **10** was well controlled, as shown by the linear evolution in the M_n (GPC) with % conversion. The gradient of M_n (GPC) *vs*. % conversion plot was 153(4) g mol^{-1} (% conversion)$^{-1}$, which is remarkably close to the expected value of 144.1 g mol^{-1} (% conversion)$^{-1}$ (Figure 3.11). This suggests one PLA chain was produced per metal centre. Narrow PDI values (1.07-1.13) were achieved throughout the polymerisation. Similar to the PLA obtained using **9** at room temperature, heterotactic enrichment was observed with P_r values of 0.57-0.61. A first-order dependence on *rac*-LA concentration was determined from ln([*rac*-LA]$_i$/[*rac*-LA]$_t$) *vs*. time plot with the apparent rate constant k_{app}, of 0.124(3) h^{-1} (R^2 = 0.9960, and a short induction period (Figure 3.11). The distinctively comparable catalytic activity of the two alkoxide initiators **9** and **10** is recognised through the equal k_{app} within error (k_{app} of the ROP using **9** is 0.108(4) h^{-1} at 23 °C). Therefore catalysts **9** and **10** could equally serve as representative models for a further mechanistic study.

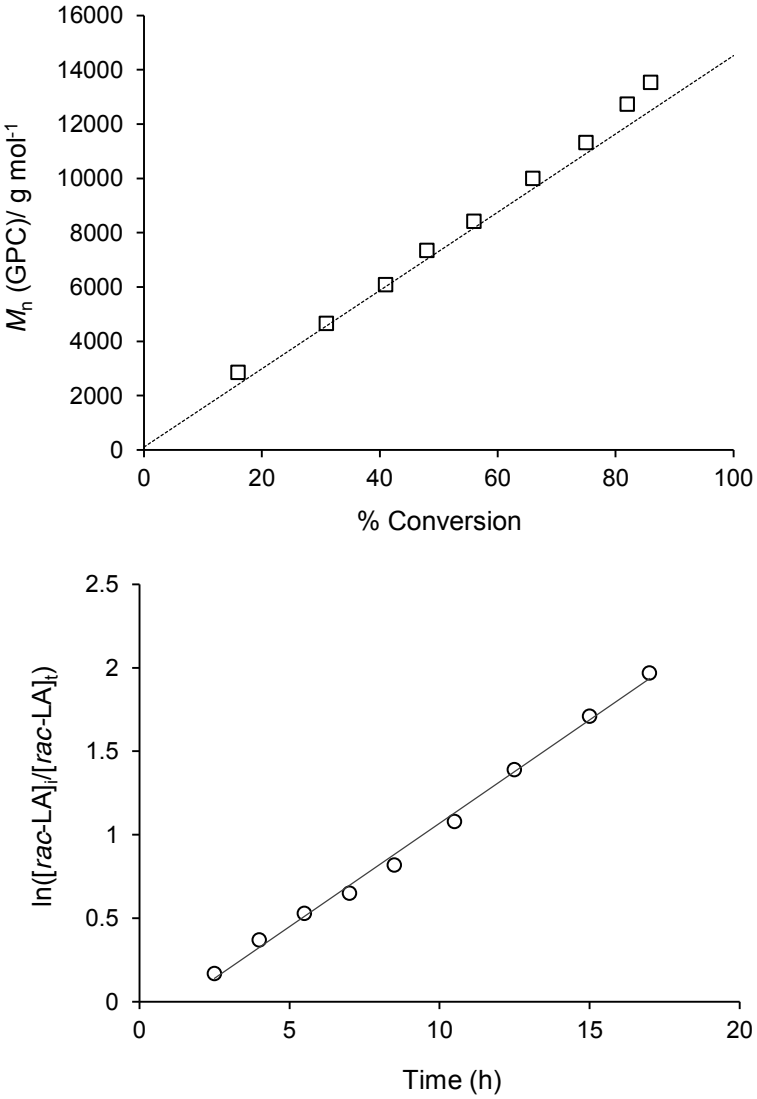

Figure 3.11. (Top) Data for ROP of *rac*-LA using (Tp^{tBu,Me})Mg(OBn) (**10**). M_n (GPC) vs. Conversion plot. The dotted line is that expected for one PLA chain per metal centre. Condition: 6 mL THF, 23 °C, [*rac*-LA]$_0$:[**10**]$_0$ = 100:1. PDIs = 1.07-1.13, [*rac*-LA]$_0$ = 0.5 M. (Bottom) First order plot of ln([*rac*-LA]$_i$/[*rac*-LA]$_t$) *vs*. time. The apparent rate constant, k_{app} = 0.124(3) h^{-1} (R^2 = 0.996).

The MALDI-ToF mass spectrum of the PLA obtained illustrated a predominant distribution corresponding to PLA with benzyloxy ester termini as expected. A $\Delta m/z$ of 144 g mol^{-1} between the adjacent peak envelopes signifies the system with a low degree of transesterification, accounting for narrow PDI values (Figure 3.12).

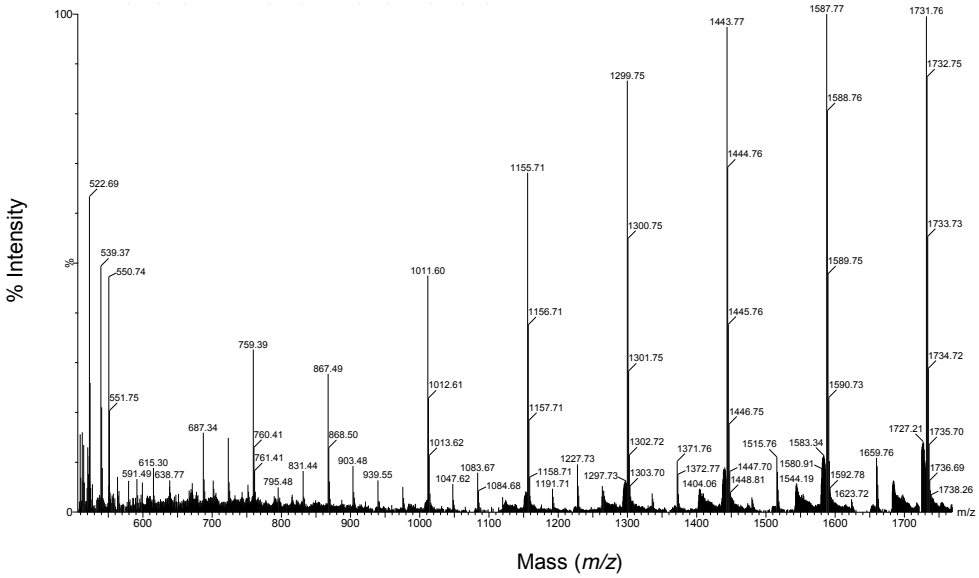

Figure 3.12. MALDI-ToF MS of PLA synthesised using ($Tp^{tBu,Me}$)Mg(OBn) (**10**). M_n by GPC analysis was 2,860 g mol^{-1} (from a [*rac*-LA]:[**10**]$_0$ = 100:1 polymerisation at 23 °C).

A ^{1}H NMR experiment of an NMR scale polymerisation between **10** and 5 equivs. of *rac*-LA was carried out in THF-d_8 at room temperature, and a spectrum was recorded every 2 mins. The NMR scale polymerisation reached completion within 4 h. Close inspection showed a species containing the first ring-opened lactide monomer was produced within the first four mins of polymerisation before the propagating step. An attempt to trap and characterise the species was undertaken in a separate experiment by mixing **10** and *rac*-LA in 1:1 ratio at room temperature. Within 0.5 h after mixing, the first ring-opened lactide monomer inserting into metal-alkoxide bond of the catalyst was obtained as ($Tp^{tBu,Me}$)Mg(LA-OBn) (**11**). The species was stable in THF-d_8 for 3 h before decomposing. This allowed the *in situ* synthesised species to be fully chacterised by NMR spectroscopic techniques (Figure 3.13).

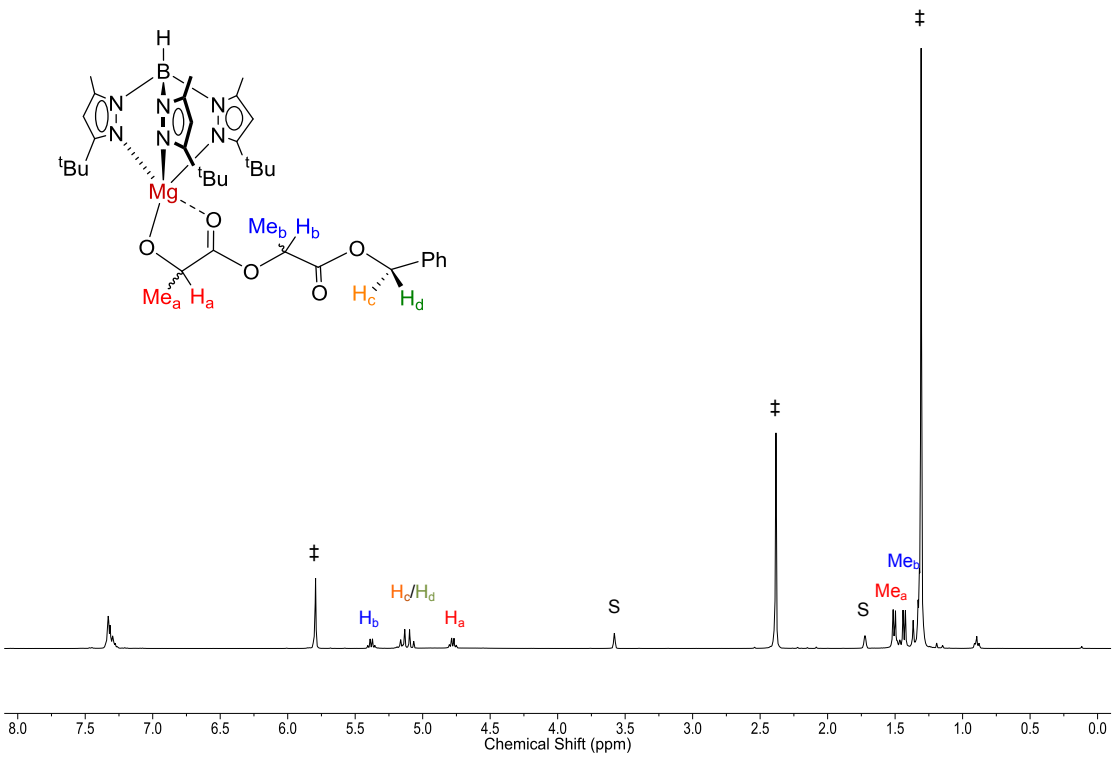

Figure 3.13. ^{1}H NMR spectrum (THF-d_8, 400.0 MHz, 298 K) of (Tp^{tBu,Me})Mg(LA*-OBn) (**11**). "s" denotes residual protio-solvent. H_a, H_b, H_c, H_d, Me_a and Me_b denote the key LA*-OBn resonances in **11**; the Tp^{tBu,Me} resonances are indicated by the black double daggers.

The ^{1}H NMR spectrum (THF-d_8, 298K) shows a diagnostic region with chemical shifts between 4.5 and 5.5 ppm. Two quartet signals at δ = 4.78 (H_a) and 5.38 (H_b) ppm with ^{3}J = 7.1 Hz, correspond to the hydrogen atoms next to the metal centre and half a lactide unit away from the metal centre, respectively. These two protons are coupling to the two methyl groups at δ = 1.51 and 1.43 ppm, respectively. The most informative signals, confirming the successful first ring-opened lactide insertion, are two mutually coupled doublet signals at δ = 5.08-5.15 ppm (H_c and H_d) with ^{2}J = 12.0 Hz. These two doublets correspond to the methylene protons of the benzyloxide moiety, which after the lactide insertion became chemically inequivalent (ie. diastereotropic protons). The doublets are 14.5 Hz apart, a "roofing" effect applies to the overall shape of the signals. This is one of a few examples of characterised species derived from the first ring-opened lactide inserted into a metal-alkoxide bond *via* a coordination-insertion mechanism.[23]

In order to gain some comparative mechanistic studies of *rac*-LA using ($Tp^{tBu,Me}$)Mg(BH_4) (**2**), an identical NMR scale polymerisation experiment was performed between **2** and 5 equivs. of *rac*-LA at room temperature. In contrast to the previous observation made using **10**, the ^{1}H NMR spectrum displayed resonances signifying a different intermediate species being produced (Figure 3.14).

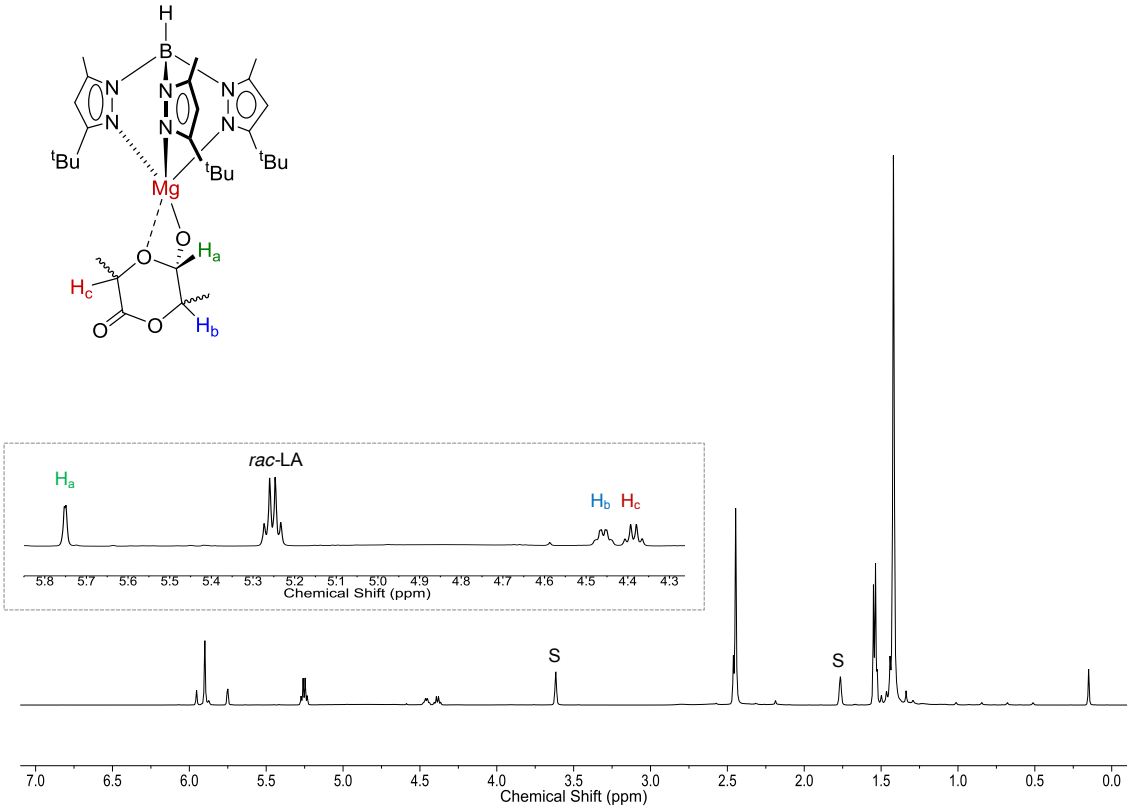

Figure 3.14. ^{1}H NMR spectrum (THF-d_8, 499.9 MHz, 298 K) of ($Tp^{tBu,Me}$)Mg(LA-H) (**12**). An inset shows a region of δ = 4.25-5.85 ppm. "s" denotes residual protio-solvent. H_a, H_b and H_c denote the key resonances corresponding to protons in **12**.

The active metal catalyst species containing an intact (non-opened) lactide ring (LA-H) formed after the first hydride transfer step of tetrahydroborate initiator, ($Tp^{tBu,Me}$)Mg(LA-H) (**12**), was elucidated from the ^{1}H NMR spectrum. An informative region between δ = 4.40-5.80 ppm is shown in the ^{1}H NMR analysis. A doublet at δ = 5.71 ppm (integral 1H, H_a) corresponds to an acetal proton with ^3J = 2.3 Hz. The resonance of a carbon bound proton next to the acetal group appears as a double of quartets at δ = 4.41 ppm (integral 1H, H_b) with ^3J coupling constants of 2.3 and 6.6 Hz to the acetal proton and methyl group (δ = 1.50 ppm), respectively. From the Karplus relationship, a small vicinal H-H coupling of 2.3 Hz suggests a dihedral

angle about 60-90° between the two protons.[29-31] The non-opened reduced lactide ring (LA-H) could therefore adopt either a chair or twisted boat conformation in solution. Another methine proton on the lactide ring has its resonance appearing at δ = 4.32 ppm (integral 1H, H_c) and coupling to the methyl group (δ = 1.40 ppm) with ^3J = 6.9 Hz. The intermediate **12**, elucidated from the ^{1}H NMR spectrum in Figure 3.14, is somewhat reminiscent to the intermediate **II** proposed in the mechanism of tetrahydroborate catalysed of ROP (Scheme 2.1). After 20 mins, the ^{1}H NMR spectrum became more complicated due to the formation of new species (*vide infra*).

The behaviour of ($Tp^{tBu,Me}$)Mg(BH_4) (**2**) towards polymerisation of *rac*-LA was thoroughly monitored using variable temperature ^{1}H, $^{13}C\{^1H\}$ and ^{11}B NMR spectroscopic techniques in the range 228-298 K. The NMR tube-scale polymerisation between **2** and 5 equivs. of *rac*-LA was prepared in a glove-box under an inert atmosphere of dinitrogen at 238 K. The sample was maintained at the preparative temperature in a dry ice/acetone bath before inserting into a pre-cooled NMR probe at 228 K. The NMR probe temperature was increased at the appropriate temperature interval to allow the polymerisation to proceed. The ^{11}B NMR spectra proved to be informative and explicitly revealed the species formed sequentially in the polymerisation (Figure 3.15).

The first ^{11}B NMR spectrum recorded at 228 K after mixing (Figure 3.15(a)) illustrates a quartet resonance at -1.0 ppm corresponding to BH_3·THF. This is evidence of borane being evolved during the polymerisation, in conjunction with a first hydride transferred product **12**. A diminishing borohydride resonance was observed as the resonance of BH_3·THF became more intense at higher temperature. Eventually ($Tp^{tBu,Me}$)Mg(BH_4) (**2**) fully converted into ($Tp^{tBu,Me}$)Mg(LA-H) (**12**). Once produced, compound **12** was stabilised at 228 K and fully characterised by NMR spectroscopic techniques.

On gradually increasing the NMR probe temperature to 273 K, two new resonances appeared in the ^{11}B NMR spectrum (Figure 3.15(b)) as a doublet and a singlet at δ = 28.5 and 23.1 ppm, respectively. As 10 mins elapsed at 273 K (Figure 3.15(c)), a disappearance of the doublet resonance and a decrease in intensity of the quartet resonance of BH_3·THF were observed, whilst a singlet resonance at δ = 23.1 ppm became dominant. Ultimately, only a broad singlet resonance was observed once the

temperature was elevated to 288 K (Figure 3.15(d)). The literature of boron-containing compounds suggest that the doublet and the singlet at 28.5 and 23.1 ppm correspond to $BH(OR)_2$ and $B(OR)_3$ type species, respectively (R = alkyl).[32]

^{1}H and $^{13}C\{^{1}H\}$ and two-dimensional correlation NMR spectroscopy were used to characterise the *in situ* generated trialkyl borate ester $B(LA\text{-}H)_3$ produced along with compound **12**. The ^{1}H NMR spectrum showed highly complicated resonances around the characteristic region of the proton resonances of LA-H (*ca*. δ = 4.0-6.0 ppm). The corresponding $^{13}C\{^{1}H\}$ NMR spectrum showed a new set of resonances containing characteristic signals at δ = 96.4 and 169.3 ppm corresponding to acetal carbon and ester carbonyl carbon of the new LA-H moiety, aside from the resonances of **12** (Appendix, Figure A3.1). This observation suggests that a mixture of **12** and $B(LA\text{-}H)_3$ are present in the polymerisation solution after the initiation.

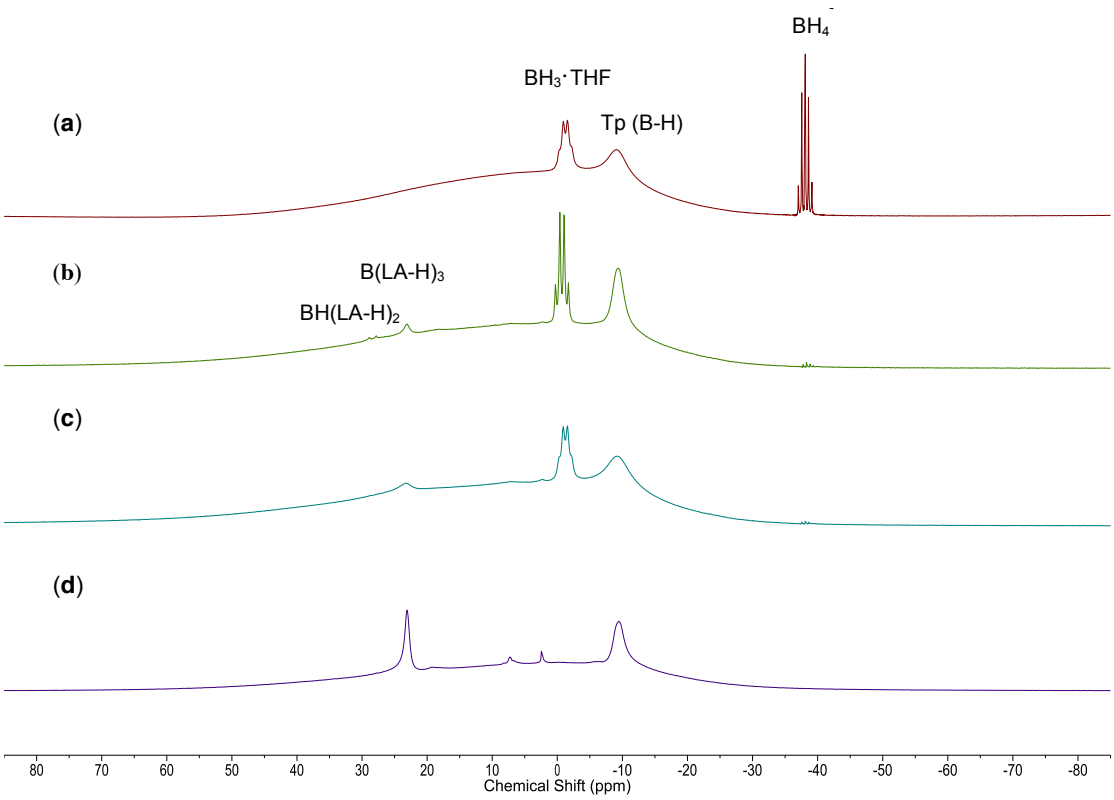

Figure 3.14. ^{11}B NMR spectra (THF-d_8, 160.4 MHz, 228-298 K) of products formed in the NMR tube-scale polymerisation between $(Tp^{tBu,Me})Mg(BH_4)$ (**2**) and 5 equivs. of *rac*-LA. (a) products formed immediately at 228 K, (b) products formed immediately at 273 K, (c) products formed after 10 mins at 273 K and (d) products formed at 288 K.

The *in-situ* generated $BH(LA\text{-}H)_2$ and $B(LA\text{-}H)_3$ most probably result from the exchange reaction between $BH_3{\cdot}THF$ and the bulky alkoxide-type ligand, LA-H, of **12**. The redistribution equilibrium of dialkoxyboranes to trialkyl borate esters and boranes is established with several literature examples.[33, 34] Unfortunately, attempts to independently synthesise $B(LA\text{-}H)_3$ or a representative model *via* a reaction between, for example, $BH_3{\cdot}THF$ or HBPin and 3 equivs. of *rac*-LA were unsuccessful.

A control experiment was carried out between $(Tp^{tBu,Me})Mg(OBn)$ (**10**) and an equivalent of $BH_3{\cdot}THF$. The ^{11}B NMR spectra showed instantaneous formation of $(Tp^{tBu,Me})Mg(BH_4)$ (**2**), $BH(OBn)_2$ (a ^{11}B NMR doublet ($^1J_{B\text{-}H}$ = 165 Hz) at δ = 27.7 ppm) and $B(OBn)_3$ (a ^{11}B NMR singlet at δ = 18.3 ppm, Figure 3.16(a)). The corresponding ^1H NMR spectrum confirmed the formation of the new species along with the unreacted **10**. The redistribution of $BH(OBn)_2$ to $B(OBn)_3$ was observed within 20 mins of the reaction. This is confirmed by the disappearance of the $BH(OBn)_2$ resonance and a concurrent increase in intensity of the $B(OBn)_3$ in the ^{11}B NMR spectrum (Figure 3.16(b)). The corresponding ^1H NMR spectrum showed the presence of **2** and unreacted **10** in the ratio of 3:1, along with $B(OBn)_3$. The observation is consistent with Equation 3.3.

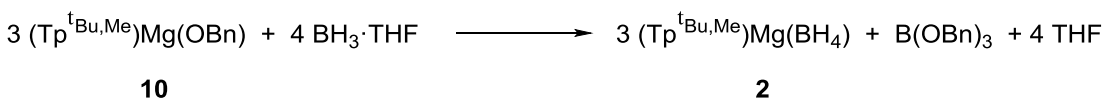

Equation 3.3

A further addition of 5 equivs. of *rac*-LA to the solution mixture resulted in the immediate formation of **12**, $BH_3{\cdot}THF$, $BH(LA\text{-}H)_2$ and $B(LA\text{-}H)_3$, whilst the tetrahydroborate resonance of **2** was no longer observed (Figure 3.16(c)). Although the corresponding ^1H NMR spectrum was complicated, the resonances of **12** and *rac*-LA monomer could be clearly identified. It is worth nothing at this stage that the small amount of the unreacted **10** carried forward from the previous reactions was no longer observed and expected to react with the excess amount of *rac*-LA to form **11**. Within 20 mins at room temperature, the ^{11}B NMR spectrum predominantly showed the trialkyl borate ester resonances (δ = 18.5 and 23.0 ppm) and the $B\text{-}H(Tp^{tBu,Me})$ of **12** (Figure 3.16(d)). It is worth mentioning that the remaining *rac*-LA monomer was observed in the corresponding ^1H NMR spectrum. The production of tetrahydroborate compound (**2**) from the exchange reaction between $BH_3{\cdot}THF$ and benzyloxy complex

10 is consistent with the known preparation for $Sr(BH_4)_2(THF)_2$ (Equation 2.1)[35] and $Ln(BH_4)_3(THF)_3$.[36]

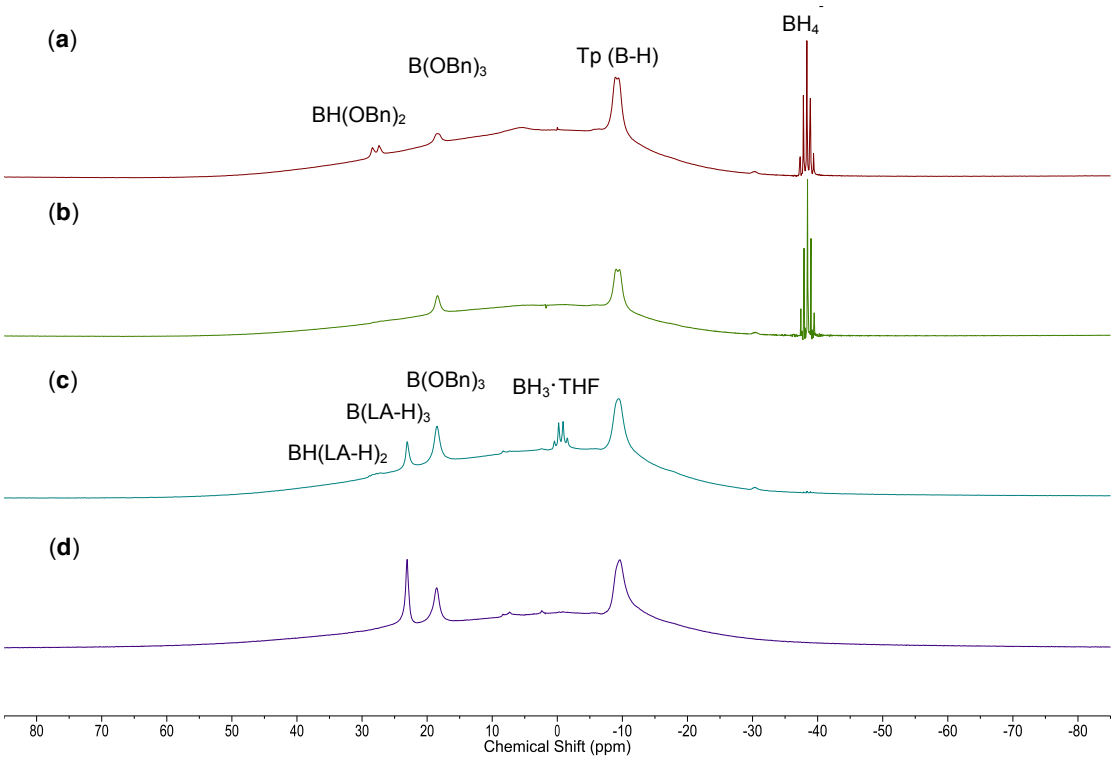

Figure 3.16. ^{11}B NMR spectra (THF-d_8, 160.4 MHz, 298 K) of the reaction between ($Tp^{tBu,Me}$)Mg(OBn) (**10**) and BH_3·THF. (a) products formed immediately, (b) products formed within 20 mins, (c) products formed immediately after the addition of 5 equivs. of *rac*-LA and (d) products formed within 20 mins after the addition of 5 equivs. of *rac*-LA.

The intermediate, $B(LA\text{-}H)_3$, produced in the ROP of *rac*-LA using **2** acts as a chain-transfer agent, hence altering the expected living ROP into an immortal ring-opening polymerisation (iROP). This explains the observation in *rac*-LA ROP at 70 °C using **2**, where multiple chains of PLA were produced per one metal centre. The concept of iROP including literature examples is thoroughly discussed in Chaper One. Furthermore, detailed studies describing borate and borane derivatives as chain transfer agents in iROP will be presented in Chapter Four.

No change was observed in the ^{11}B and $^{13}C\{^1H\}$ NMR spectra upon heating a solution of the *in situ* generated **12** and $B(LA\text{-}H)_3$ at 70 °C for 3 h. The stability of non-opened LA (LA-H) in solution at the polymerisation temperature gives rise to the possibility of it being a bulky alkoxide-initiating group and eventually forming an end group of

PLA. A few literature examples of cyclic end-capped polymers are homo- or co-poly-β-peptides and nylon produced by anionic ring-opening polymerisation of substituted β-lactams.[37-39]

The possible LA-H and aldehyde end-capped PLA give the identical isotopic distribution in MALDI-ToF MS, hence they cannot be distinguished from each other using this technique. A further NMR tube-scale experiment between **2** and 15 equivs. of *rac*-LA was performed in THF-d_8 at 70 °C for 4 h. The ^{1}H NMR spectrum showed broad resonances around the expected region for the resonances of LA-H (δ = 4.0-6.0 ppm) and no resonance corresponding to an aldehyde group (*ca*. δ = 9.0-10.5 ppm). More informative $^{13}C\{^{1}H\}$ NMR analysis showed resonances close to those of LA-H and again no resonance appeared in the diagnostic region of aldehyde R<u>C</u>(O)H (*ca*. δ = 190-200 ppm). In addition, ^{11}B NMR analysis showed two singlets at -9.3 and 23.1 ppm, which is similar to that shown in Figure 3.15(d). The sample was quenched with wet THF resulting in short PLA chains. While the ^{1}H NMR analysis of the resulting PLA was complex due to the possible formation of different conformations and diastereomers of LA-H, the $^{13}C\{^{1}H\}$ NMR spectrum showed very similar resonances as that of the unquenched sample. Although the analysis of PLA end group is still slightly ambiguous at this stage, it is very likely that the alkoxy (LA-H) ester and alcohol terminated PLA were obtained from the *rac*-LA ROP using **2**. Future work using borodeuteride analogue of **2**, $(Tp^{tBu,Me})Mg(BD_4)$, is underway to further characterise and clarify this novel PLA end group.

From the studies, a new mechanistic pathway of *rac*-LA ROP using **2** could potentially be postulated (Scheme 3.2). The proposed pathway is expected to compete with another leading to α,ω-dihydroxy telechelic PLA.

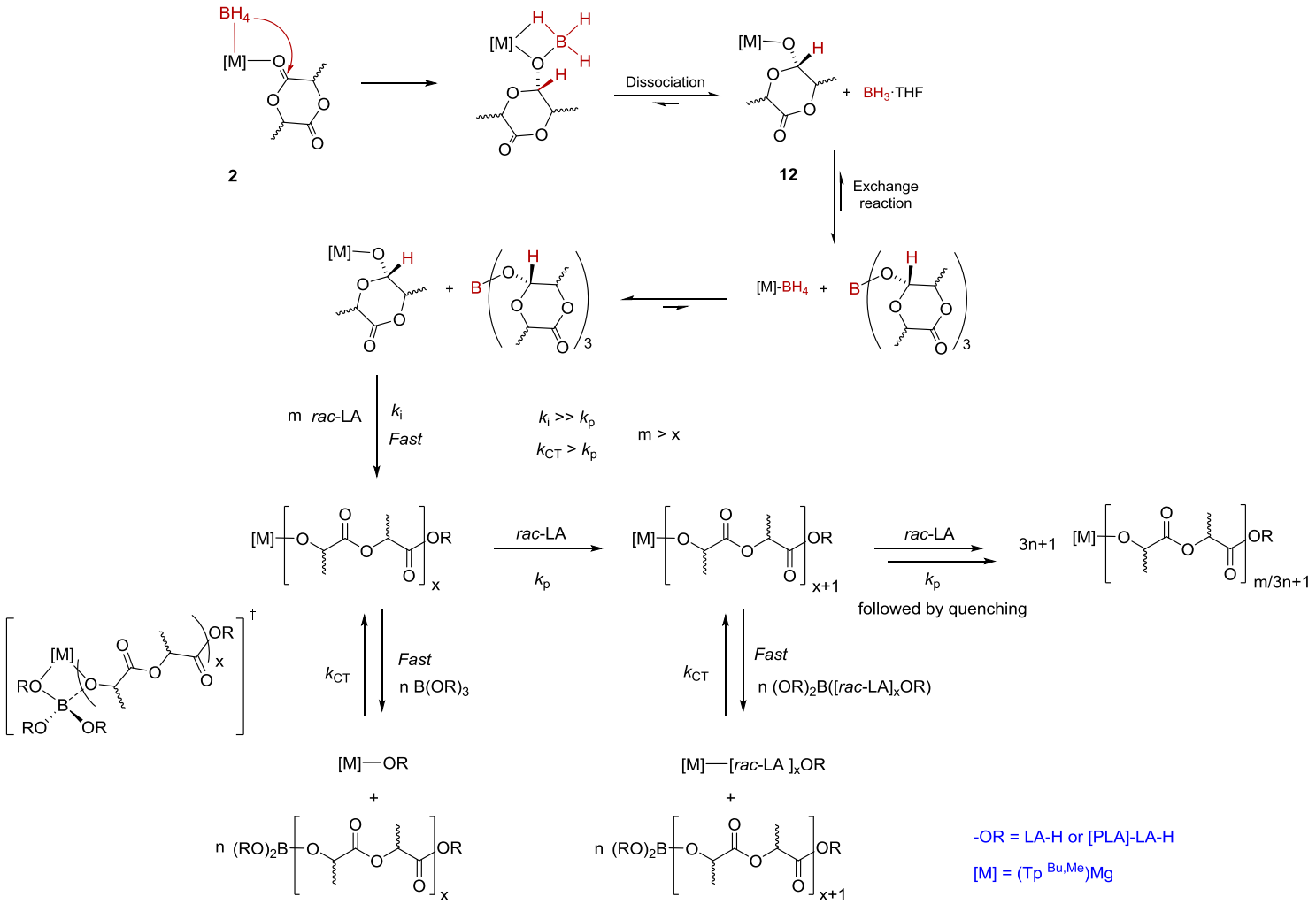

Scheme 3.2. A proposed mechanism of *rac*-LA ROP using (Tp^{tBu,Me})Mg(BH$_4$) (**2**), [M] = (Tp^{tBu,Me})Mg.

3.4 ROP of *rac*-LA using ($Tp^{tBu,Me}$)Ca(BH_4)(THF) (1)

As mentioned previously, the pioneering work of *rac*-LA ROP using ($Tp^{tBu,Me}$)Ca(BH_4)(THF) (**1**) was carried out by Mountford *et al*., and published in 2011.[6] Compound **1** is a very efficient ROP initiator towards *rac*-LA at both room temperature and -20 °C (Section 2.2.2), over 90 % monomer conversion was accomplished at both temperatures. A better agreement between the experimental and calculated M_n (162(4) g mol^{-1} (equivalent converted)$^{-1}$), as well as an improvement in heterotacticity (P_r = 0.88-0.90) were achieved in the polymerisation conducted at -20 °C due to the more optimal control of the relative rate of propagation to initiation. The MALDI-ToF mass spectrum of the resultant PLA is similar to that obtained in *rac*-LA ROP using ($Tp^{tBu,Me}$)Mg(BH_4) (**2**), and consistent with the formation of PLA with alkoxy (LA-H) ester and alcohol termini. Moreover isotopic distributions with $\Delta m/z$ separation of 72.0 g mol^{-1} corresponding to cyclic PLA were also observed, implying inter- and intra-molecular transesterification during the polymerisation.

Analogous NMR spectroscopic studies to those for *rac*-LA ROP using **2** were employed for the calcium catalyst **1**. ^{1}H and ^{13}C{^{1}H} NMR analyses of an NMR tube-scale polymerisation in THF-d_8 between **1** and 15 equivs. of *rac*-LA demonstrated the same results as those obtained using **2**. Quenching with wet THF failed to resolve the broad resonances of the diagnostic end-group (LA-H) region (*ca*. δ = 4.0-6.0 ppm) in ^{1}H NMR analysis. However, PLA obtained from the sample quenched with 1 M HCl in diethyl ether gave a well-resolved but complex ^{1}H NMR spectrum, with no resonance corresponding to aldehyde observed. It is worth noting that the complication in the ^{1}H NMR analysis could be caused by the presence of different diastereomers or conformations of the alkoxy (LA-H) ester end-group.

^{1}H and ^{13}C{^{1}H} NMR spectra of the PLA obtained using **1** agree with those obtained using **2**. An attempt to isolate short chains of PLA from the polymerisation using cold pentane or methanol met with limited success due to the metal residue and organic ligand contaminants. Nonetheless all experimental results also point towards the presence of alcohol and alkoxy (LA-H) ester terminated PLA.

3.4.1 ROP of *rac*-LA using ($Tp^{tBu,Me}$)Ca(BD_4)(THF) (**1-*d*$_4$**)

To achieve a more in-depth end group analysis, deuterium-labelling experiments were pursued. ($Tp^{tBu,Me}$)Ca(BD_4)(THF) (**1-*d*$_4$**) used in this experiment was introduced in the previous work in the Mountford group. Compound **1-*d*$_4$** was synthesised *via* a salt metathesis reaction between ($Tp^{tBu,Me}$)Ca(I)(THF) (**2.17**) and $NaBD_4$ in 58 % yield.[40] The NMR tube-scale polymerisation between **1-*d*$_4$** and 15 equivs. of *rac*-LA was examined under the same polymerisation conditions. The ^{2}H NMR analysis revealed several broad resonances between δ = 3.0 and δ = 6.0 ppm. Based on the success in the preceding experiment, the polymer sample was quenched with 1 M HCl in diethyl ether. The resulting deuterated polymer gave resolved resonances in the ^{2}H NMR spectrum as shown in Figure 3.17.

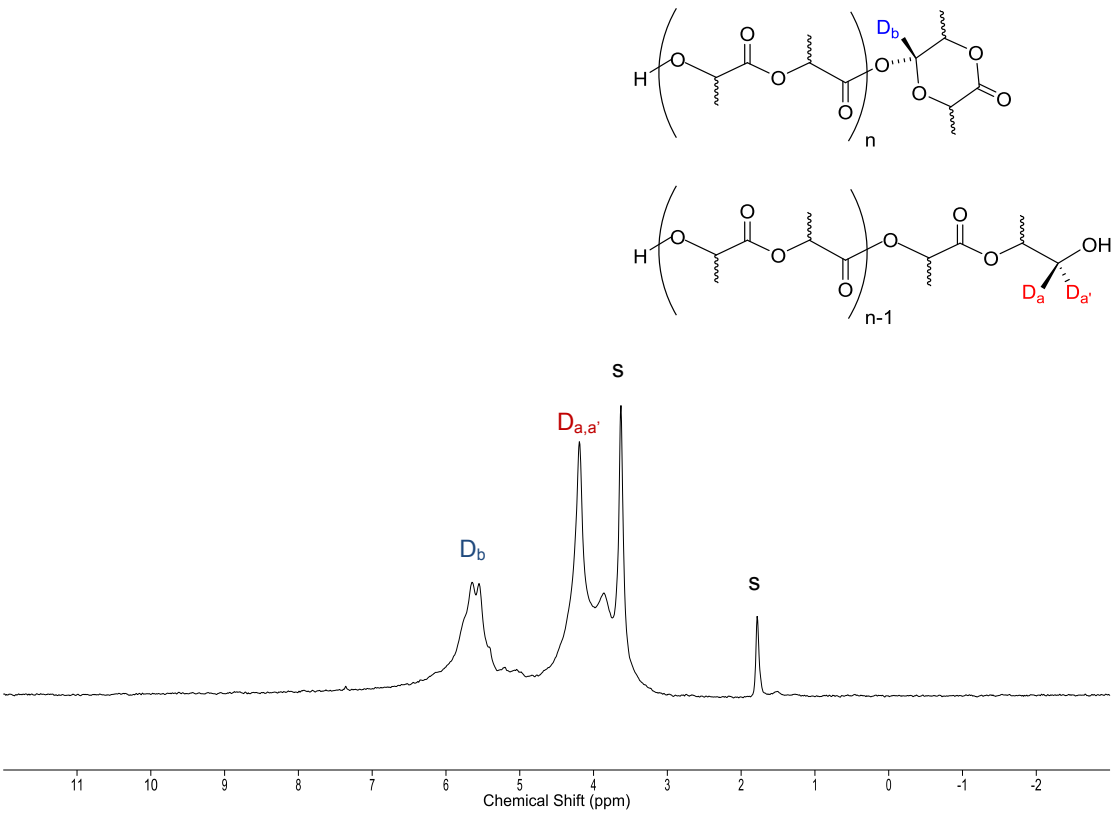
H
O
O
O

LA-*D* ester, respectively. Moreover, no aldehyde –C(O)*D* resonance was observed in the expected region between δ = 9 and δ = 12 ppm. These findings underpin and confirm the existence of the non-opened LA end group in the *rac*-LA ROP using tetrahydroborate catalysts. It is worth noting at this stage that the chemical shifts corresponding to the alkoxy (LA-H) ester end group are similar to those of PLA with the unidentified end group previously observed in the ROP of *L*-LA using $\{(Me_3Si)_2NC(N\text{-}Cy)_2\}_2Nd(\mu\text{-}BH_4)_2Li(THF)_2$ reported by Carpentier, Trifonov and co-workers.[3]

The MALDI-ToF mass spectrum of the deuterated PLA demonstrated the expected isotopic distribution, corresponding to both aforestated end groups; cyclic PLA (green asterisk), -LA-D termini (red dagger) and $-CH(Me)CD_2OH$ termini (blue double dagger, Figure 3.18).

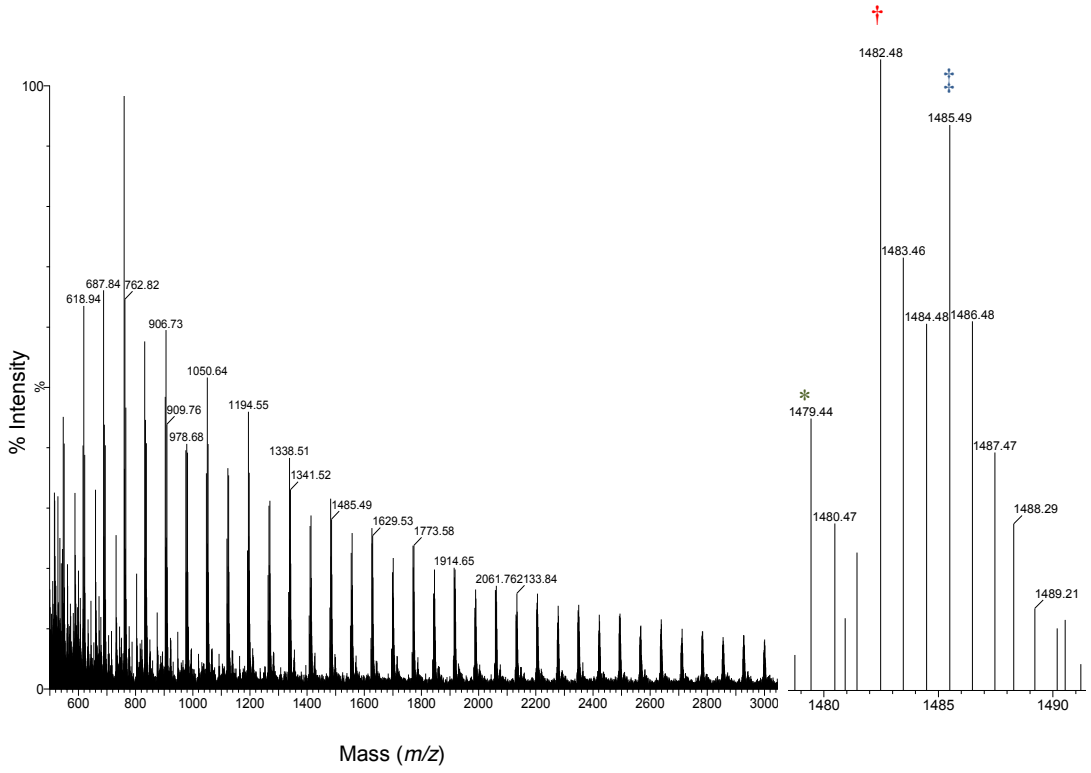

Figure 3.18. MALDI-ToF MS of deuterated PLA synthesised using $(Tp^{tBu,Me})Ca(BD_4)(THF)$ (**1-*d*$_4$**), [*rac*-LA]:[**1-*d*$_4$**]$_0$ = 15 : 1 polymerisation at 23 °C (left). A MALDI-ToF peak envelope of PLA with the length of 10 lactide monomer units (right). Maxima in the isotopic distributions shown are corresponding to cyclic PLA (green asterisk), -alkoxy LA-*D* ester termini (red dagger) and $-CH(Me)CD_2OH$ termini (blue double dagger).

Mechanistically speaking, the ROP of *rac*-LA in THF using **1** might proceed in a different fashion to that using **2**. The larger radius of calcium is responsible for the different observations made in the ^{11}B NMR analysis of the NMR tube-scale ROP of *rac*-LA. The ^{11}B NMR spectra, representing the products of the complete polymerisations between **1** or **1-*d*$_4$** and 15 equivs. of *rac*-LA, showed key resonanances at δ = 7.7 and 3.0 ppm, alongside the resonance of the Tp^{tBu,Me}(B-H) at δ = -6.7 ppm. According to the literature for boron-containing compounds, these resonances may correspond to the alkoxyborates M{B(OR)$_4$} and M{HB(OR)$_3$} (R = alkyl and M = alkali metals), repsctively.[32, 41, 42] The possibility of intermolecular substituent redistribution among a series of M{BH$_{4-n}$(OR)$_n$} compounds (n = 0 - 4) through dissociation has been established in the literature for alkali metal complexes.[42, 43] The exact mechanism is complicated by the rapid nature of propagtion in ROP using **1** at room temperature or even low temperature, uninformative ^{1}H NMR analysis and intermolecular substituent redistribution. Therefore the mechanism cannot be elucidated using these method for this system.

3.5 ROP of *rac*-LA using (Tp^{tBu,Me})Sr(BH$_4$)(THF)$_2$ (4).

Gratifyingly, (Tp^{tBu,Me})Sr(BH$_4$)(THF)$_2$ (**4**) is also an efficient initiator for the ROP of *rac*-LA at room temperature in THF achieving over 95 % conversion within 5 mins with [*rac*-LA]$_0$:[**4**]$_0$ = 100:1. Kinetic studies could not be achieved in such a rapid polymerisation. Therefore the *rac*-LA polymerisations using **4** were carried out for [*rac*-LA]$_0$:[**4**]$_0$ ratios between 50 and 300 at room temperature with aliquots being taken at 5 mins of the polymerisations, Figure 3.19.

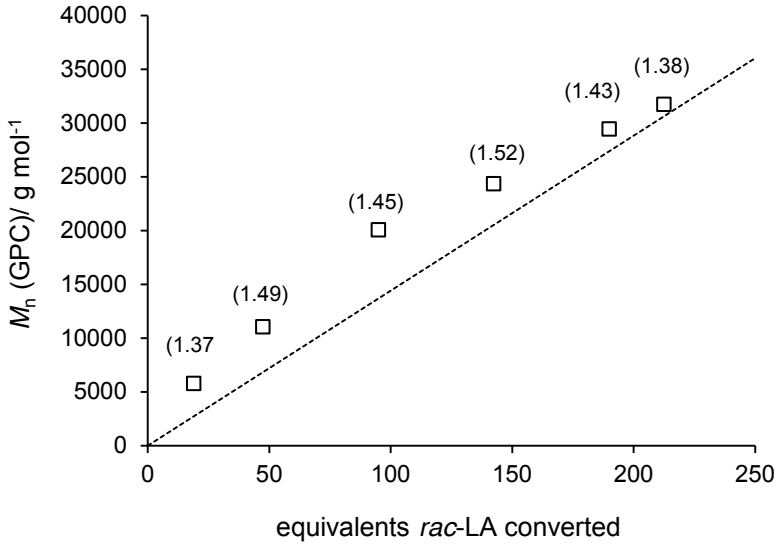

Figure 3.19. M_n (as measured by GPC) *vs*. equivalents *rac*-LA converted using ($Tp^{tBu,Me}$)Sr(BH_4)($THF)_2$ (**4**). The dotted line is that expected for one PLA chain per metal centre. Conditions: 6 mL THF, 23 °C. [*rac*-LA]$_0$:[**4**]$_0$ = 20, 50, 100, 150, 200, and 250, [*rac*-LA]$_0$ = 0.5 M. PDI values are given in parentheses.

Better agreement of the measured and calculated M_n values was observed at high equivalents of *rac*-LA conversion. The higher than expected M_n values obtained at low *rac*-LA concentration could be a consequence of partial catalyst activity in initiation or a greater rate of propagation to initiation. Overall the polymerisations gave moderate molecular weight distributions of 1.4-1.5.

The selectively homonuclear decoupled ^{1}H NMR spectra for the tetrad analysis of the C<u>H</u>(Me)O region of the PLA samples revealed heterotactically enriched polymers with the P_r values of 0.60-0.70. Interestingly, a decrease in steroselectivity in this system was observed in comparison with the results obtained from the ROP using **1**. It is known that the steroselectivity in ROP of *rac*-LA using a series of catalysts containing $Tp^{tBu,Me}$ ligands operate through the chain-end control mechanism. As compound **4** possesses a relatively larger coordination sphere, the bulky *tert*-butyl substituents on the ligand would have less influence on directing the arrangement of the enchained or incoming monomers, resulting in a reduction in the stereoselectivity of the resultant PLA.

By analogy to the observation made using **1**, the MALDI-ToF mass spectrum of PLA produced using **4** predominantly showed cyclic PLA along with alkoxy (LA-H) ester

and –CH(Me)CH_2OH end-capped PLA (Figure 3.20). The major distribution illustrated Δ(*m*/*z*) of 72 g mol^{-1} between peak envelopes. Unlike the ROP using **2** and **1**, the ROP using **4** was extensively affected by both intra- and inter-molecular transesterification. The higher possibility of an intramolecular back-biting could be facilitated by using a larger coordination sphere around the metal centre.

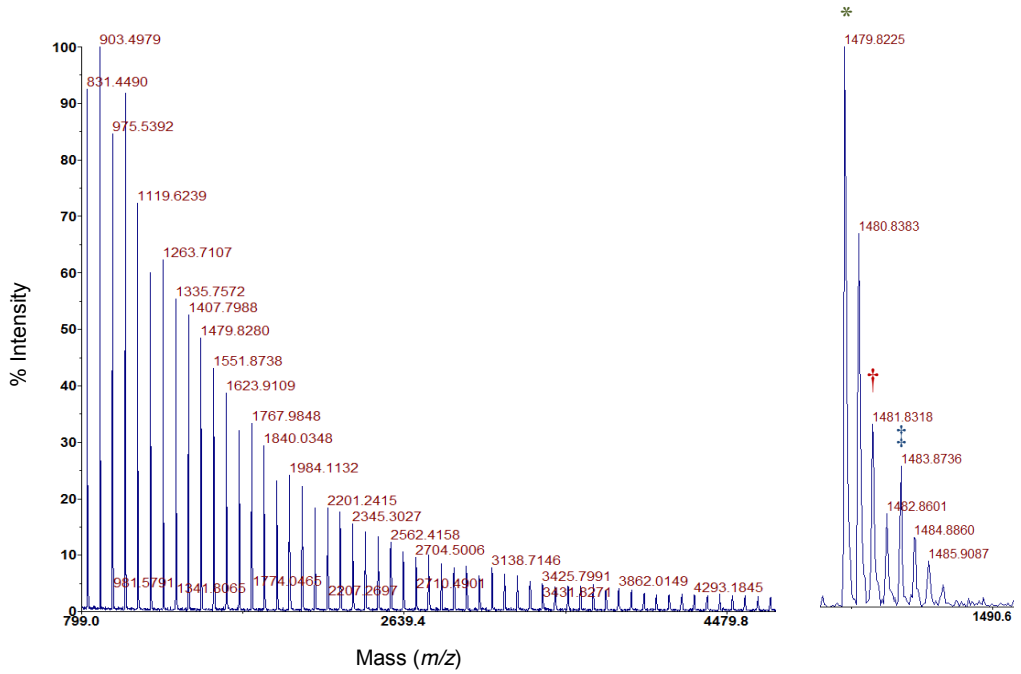

Figure 3.20. MALDI-ToF MS of PLA synthesised using ($Tp^{tBu,Me}$)$Sr(BH_4)(THF)_2$ (**4**). M_n by GPC analysis was 2,740 g mol^{-1} (from a [*rac*-LA]:[**4**]$_0$ = 15:1 polymerisation at 23 °C) (left). A MALDI-ToF peak envelope of PLA with the length of 10 lactide monomer units (right). Maxima in the isotopic distributions shown are corresponding to cyclic PLA (green asterisk), -alkoxy LA-H ester termini (red dagger) and –CH(Me)CH_2OH termini (blue double dagger).

A tentative ^{11}B NMR analysis was carried out for an NMR scale tube polymerisation between **4** and 15 equivs. of *rac*-LA, showing the remaining tetrahydroborate resonance of **4** (δ = -31.6 ppm) after completion and a new set of resonances in the region corresponding to the tetra-coordinate boron species[32] (δ = 9.5, 4.9 and 0.4 ppm), aside from the $Tp^{tBu,Me}$(B-H) resonance (δ = -7.0 ppm). A further detailed NMR study was not carried out for the ROP using **4** as the catalyst has limited initiating potential and the ROP was influenced by extensive transesterification effects.

3.6 Summary and Conclusions

This Chapter has described the ROP of *rac*-LA using alkaline earth tetrahydroborate complexes (**1**, **2** and **4**) introduced in Chapter Two. ($Tp^{tBu,Me}$)Mg(BH_4) (**2**) is inactive towards ROP of *rac*-LA in THF at room temperature. The *rac*-LA ROP using **2** at 70 °C showed a significantly long induction period and a production of atactic PLA with lower than expected molecular weight. The kinetic and mechanistic studies of *rac*-LA ROP using **2** were performed through the representative alkoxide analogues ($Tp^{tBu,Me}$)Mg(S-lactate) (**9**) and ($Tp^{tBu,Me}$)Mg(OBn) (**10**) as mimics of the first ring-opening lactide monomer coordinating to the metal centre of the *rac*-LA ROP of **2**. Compound **9** and **10** were synthesised from the protonolysis reactions between ($Tp^{tBu,Me}$)Mg(^{n}Bu) (**8**) and corresponding alcohols, alternatively, **10** could also be obtained from the β-H transfer reaction between **8** and PhCHO.

Well-controlled ROP experiments were obtained at room temperature using catalysts **9** and **10**. Heterotactic enriched polylactides with expected molecular weights of one chain per metal centre were obtained in both cases. The ROP of *rac*-LA using **9** performed at 70 °C also showed a linear evolution of M_n with % conversion and the expected M_n of one PLA chain per metal centre. However a decrease in M_n was observed towards the end of the polymerisation due to the transesterification caused by the heating effect. It was found that the apparent rate constant obtained in the ROP of *rac*-LA using **9** is comparable to that of **2**, within error, under the same polymerisation conditions (i.e. 70 °C). This implies that the deviation from expected kinetics and molecular weight control of the ROP of *rac*-LA using **2** is influenced by the initiation.

NMR tube-scale polymerisation experiments between 5 equivs. of *rac*-LA and **10** or **2** were performed in THF-d_8 at room temperature. The intermediate, ($Tp^{tBu,Me}$)Mg(LA*-OBn) (**11**), containing the first ring-opened lactide inserting into the metal-alkoxy bond was observed in the ROP experiment of **10**. However, the unexpected non-opened LA intermediate, ($Tp^{tBu,Me}$)Mg(LA-H) (**12**), was obtained when using the tetrahydroborate **2** catalysed ROP. Variable temperature ^{1}H, ^{13}C{^{1}H} and ^{11}B NMR spectroscopy were utilised in the investigation of the ROP initiation using **2**. It was found that the liberated borane, produced after first hydride insertion of tetrahydroborate initiator, participating in an exchange reaction with the alkoxide

(LA-H) moiety on the active metal centre to produce $B(LA\text{-}H)_3$. The trialkyl borate ester acts as a chain-transfer agent altering the single-site metal catalysed ROP into an immortal ROP (see Chapter Four). These findings agree well to the polymerisation results, therefore an alternative mechanism to the ROP of *rac*-LA using **2** was proposed.

$(Tp^{tBu,Me})Ca(BH_4)(THF)$ (**1**) and $(Tp^{tBu,Me})Sr(BH_4)(THF)_2$ (**4**) are very active catalysts for ROP of *rac*-LA in THF at room temperature, giving higher M_n polymers than expected with moderate PDIs. Both compounds exhibit stereoselectivity over the *rac*-LA monomer yielding heterotactic PLA with P_r of 0.80 for **1** and 0.67 for **4**. However, mechanisms of ROP of *rac*-LA catalysed by the compounds containing larger metal centres (i.e. **1** and **4**) cannot be elucidated in these studies using identical methods applied in the case of **2**.

The newly proposed mechanism in the *rac*-LA ROP using **2** encourages the idea of alkoxy (LA-H) ester end-capped PLA. This polymer functionality cannot be distinguished from the accustomed aldehyde end group by MALDI-ToF mass spectrometry. The extensive spectroscopic studies in *rac*-LA ROP using and **1** and **2** including deuterium-labelling experiment of $(Tp^{tBu,Me})Ca(BD_4)(THF)$ (**1-*d*$_4$**) eventually pinpointed the existence of the novel alkoxy (LA-H) ester end capped PLA, in conjunction with the expected α,ω-telechelic dihydroxy PLA.

3.7 References for Chapter Three

1. H. D. Dyer, S. Huijser, N. Susperregui, F. Bonnet, A. D. Schwarz, R. Duchateau, L. Maron and P. Mountford, *Organometallics*, 2010, **29**, 3602.
2. T. V. Mahrova, G. K. Fukin, A. V. Cherkasov, A. A. Trifonov, N. Ajellal and J.-F. Carpentier, *Inorg. Chem.*, 2009, **48**, 4258.
3. G. G. Skvortsov, M. V. Yakovenko, P. M. Castro, G. K. Fukin, A. V. Cherkasov, J.-F. Carpentier and A. A. Trifonov, *Eur. J. Inorg. Chem.*, 2007, 3260.
4. Y. Nakayama, S. Okuda, H. Yasuda and T. Shiono, *React. Func. Polym.*, 2007, **67**, 798.
5. R. A. Collins, J. Unruangsri and P. Mountford, *Dalton Trans.*, 2013, **42**, 759.
6. M. G. Cushion and P. Mountford, *Chem. Commun.*, 2011, **47**, 2276.
7. F. Bonnet, A. R. Cowley and P. Mountford, *Inorg. Chem.*, 2005, **44**, 9046.

8. R. Han and G. Parkin, *Organometallics*, 1991, **10**, 1010.
9. R. Han and G. Parkin, *J. Am. Chem. Soc.*, 1990, **112**, 3662.
10. R. Han, M. Bachrach and G. Parkin, *Polyhedron*, 1990, **9**, 1775.
11. H. Ma, T. P. Spaniol and J. Okuda, *Angew. Chem. Int. Ed.*, 2006, **45**, 7818.
12. E. Grunova, E. Kirillov, T. Roisnel and J.-F. Carpentier, *Organometallics*, 2008, **27**, 5691.
13. J. S. Klitzke, T. Roisnel, E. Kirillov, O. d. L. Casagrande and J.-F. Carpentier, *Organometallics*, 2014, **33**, 309.
14. B. M. Chamberlain, M. Cheng, D. R. Moore, T. M. Ovitt, E. Lobkovsky and G. W. Coates, *J. Am. Chem. Soc.*, 2001, **123**, 3229.
15. C. A. Wheaton and P. G. Hayes, *J. Organomet. Chem.*, 2012, **704**, 65.
16. P. Horeglad, P. Kruk and J. Pécaut, *Organometallics*, 2010, **29**, 3729.
17. P. Horeglad, G. Szczepaniak, M. Dranka and J. Zachara, *Chem. Commun.*, 2012, **48**, 1171.
18. A. P. Dove, V. C. Gibson, E. L. Marshall, H. S. Rzepa, A. J. P. White and D. J. Williams, *J. Am. Chem. Soc.*, 2006, **128**, 9834.
19. L. Wang, C. E. Kefalidis, S. Sinbandhit, V. Dorcet, J.-F. Carpentier, L. Maron and Y. Sarazin, *Chem. –Eur. J.*, 2013, **19**, 13463.
20. N. Nomura, R. Ishii, Y. Yamamoto and T. Kondo, *Chem. –Eur. J.*, 2007, **13**, 4433.
21. S. Dagorne, F. Le Bideau, R. Welter, S. Bellemin-Laponnaz and A. Maisse-François, *Chem. –Eur. J.*, 2007, **13**, 3202.
22. M. Normand, V. Dorcet, E. Kirillov and J.-F. Carpentier, *Organometallics*, 2013, **32**, 1694.
23. J. S. Klitzke, T. Roisnel, E. Kirillov, O. d. L. Casagrande, Jr. and J.-F. Carpentier, *Organometallics*, 2014, ASAP.
24. J. J. Li, *Name Reactions*, 4th edition, Springer, 2009.
25. M. H. Chisholm, K. Choojun, J. C. Gallucci and P. M. Wambua, *Chem. Sci.*, 2012, **3**, 3445.
26. M. H. Chisholm, N. W. Eilerts, J. C. Huffman, S. S. Iyer, M. Pacold and K. Phomphrai, *J. Am. Chem. Soc.*, 2000, **122**, 11845.
27. R. Han and G. Parkin, *J. Am. Chem. Soc.*, 1992, **114**, 748.
28. M. H. Chisholm and N. W. Eilerts, *Chem. Commun.*, 1996, 853.
29. M. Karplus, *J. Chem. Phys.*, 1959, **30**, 11.

30. M. Karplus, *J. Am. Chem. Soc.*, 1963, **85**, 2870.
31. M. J. Minch, *Concept. Magnetic Res.*, 1994, **6**, 41.
32. H. Nöth and B. Wrackmeyer, *Nuclear Magnetic Resonance Spectroscopy of Boron Compounds*, 1st edition, Springer-Verlag, Berlin, Heidelberg Germany, 1978.
33. D. J. Pasto, V. Balasubramaniyan and P. W. Wojtkowski, *Inorg. Chem.*, 1969, **8**, 594.
34. A. Lang, H. Nöth and M. Thomann-Albach, *Chem. Ber.*, 1997, **130**, 363.
35. M. Bremer, H. Nöth, M. Thomann and M. Schmidt, *Chem. Ber.*, 1995, **128**, 455.
36. E. Zange, *Chem. Ber.*, 1960, **93**, 652.
37. J. Zhang, D. A. Kissounko, S. E. Lee, S. H. Gellman and S. S. Stahl, *J. Am. Chem. Soc.*, 2009, **131**, 1589.
38. R. Graf, G. Lohaus, K. Börner, E. Schmidt and H. Bestian, *Angew. Chem. Int. Ed.*, 1962, **1**, 481.
39. K. Hashimoto, *Prog. Polym. Sci.*, 2000, **25**, 1411.
40. M. G. Cushion, D.Phil Thesis, University of Oxford, 2011.
41. T. Kemmitt and G. J. Gainsford, *Int. J. Hydrogen Energ.*, 2009, **34**, 5726.
42. J. H. Golden, C. Schreier, B. Singaram and S. M. Williamson, *Inorg. Chem.*, 1992, **31**, 1533.
43. J. Knizek, H. Noeth and M. Warchhold, *Z. Naturforsch., B: Chem. Sci.*, 2006, **61**, 1079.

Chapter Four

Trialkyl borate ester and borane derivatives as a new class of chain-transfer agents in the iROP of ε-CL and *rac*-LA

4.1 Overview

This Chapter will describe the pioneering work concerning the new roles of trialkyl borate esters ($B(OR)_3$, R = alkyl group) and borane derivatives (HBPin, BPin = $BO_2(CMe)_2$) as effective chain-transfer agents (CTAs) in immortal ROP (iROP) of ε-CL and *rac*-LA. The *in situ* generated alkaline earth alkoxide catalysts, supported by $Tp^{tBu,Me}$, along with trialkyl borate esters in both separate and adduct ($\{B(OR)_4\}^-$, R = alkyl group) formations have been synthesised and assessed for iROP of ε-CL and *rac*-LA. Their behaviour in solution including the related thermodynamic parameters of dissociation and the intramolecular exchange processes have also been investigated. Comparison of the catalytic activities between the *in situ* generated initiator bearing a smaller metal centre (i.e. magnesium) and those possessing larger metal centres (i.e. calcium and strontium) will be made. Moreover, possible iROP pathways using $B(OR)_3$ and HBPin as CTAs will be proposed. Five new alkaline earth complexes are presented, along with two X-Ray crystallographic structures.

4.2 Introduction

Boron-based compounds have been utilised as versatile reagents in a variety of organic syntheses;[1-5] for example, cross-coupling reactions,[6-8] Diels-Alder reactions[5, 9] and hydroboration.[10] In addition, borane reagents have also been used in the field of organometallic catalysis.[10-15] Recent years have witnessed the widespread applications of the boron-containing compounds, including small molecule activation,[16-19] sensors,[20-22] supramolecular materials[23-27] and medication.[28, 29]

Pentafluorophenyl-substituted boranes and borates were introduced independently in 1990s by Ewen[30] and Marks[31] as co-catalysts in the Group 4 metallocene alkyls-based polymerisation of olefins. $B(C_6F_5)_3$ served as a powerful Lewis acid capable of undergoing alkyl abstraction from the metal catalyst, resulting in an active cationic initiating species facilitating olefin polymerisation.[32] In addition, the potential of $B(C_6F_5)_3$ as a co-catalyst in norbornene polymerisation using a Ni(0)-containing catalyst was also reported by Jang *et. al.*[33] The catalytic polymerisation yielded high molecular weight polynorbornene, even in the absence of MAO or trialkyl aluminium. Besides the co-catalyst role in polymerisation, Aoshima and co-workers recently demonstrated the successful copolymerisation of alkyl vinyl ethers and isobutylene oxide through cationic vinyl addition and ring opening using $B(C_6F_5)_3$ as a catalyst.

The superior catalytic activity of $B(C_6F_5)_3$ compared to other Lewis acidic catalysts ($BF_3{\cdot}OEt_2$ or $GaCl_3$) enabled the efficient cross-over reactions between the different growing polymer chains, yielding desirable multipleblock copolymer.[34]

Another class of neutral organoboranes, such as organoborane hydrides and trialkyl boranes, were employed by Chung and co-workers as facile CTAs in metallocene-mediated olefin polymerisation. It is noteworthy that the borane became incooperated at the polyolefin chain end, forming an active end group, which could subsequently be functionalised.[35-42] Metallocene-based catalysts employed in these works included $[(\eta^5\text{-}C_9H_7)_2ZrMe][MeB(C_6F_5)_3]$, $[(C_5Me_5)_2ZrMe][MeB(C_6F_5)_3]$ and $[C_5Me_4(SiMe_2N^tBu)TiMe][MeB(C_6F_5)_3]$, in conjunction with effective chain-transfer agents, namely organoborane hydrides (Figure 4.1) and trialkyl boranes.[39, 41, 42]

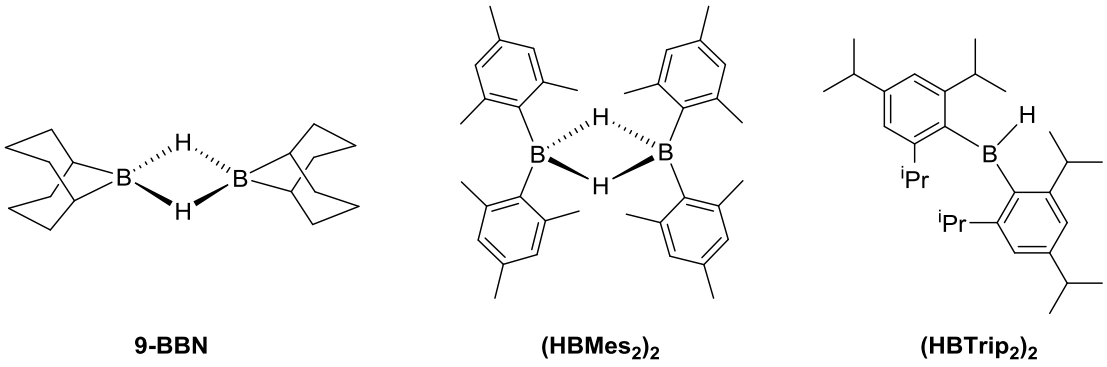

Figure 4.1. Borane derivatives as effective chain-transfer agents in metallocene-mediated olefin polymerisation.[39, 42]

The polymerisation pathway of the metallocene-mediated olefin polymerisation using borane derivatives as CTAs is illustrated in Scheme 4.1. The efficiency of this catalytic route of the functionalised polyolefins depended largely on the exchange between the propagating polyolefin chain and the B-H or B-R bond of the CTAs, facilitated by an acid-base interaction. The exchange reaction between the growing polyolefin coordinating to the metal centre and the borane chain-transfer agent proceeded through a 4-membered B-H/M-C transition state (Scheme 4.1), which is reminiscent of the precedent transition state in the catalytic hydroboration pathway.[42-45]

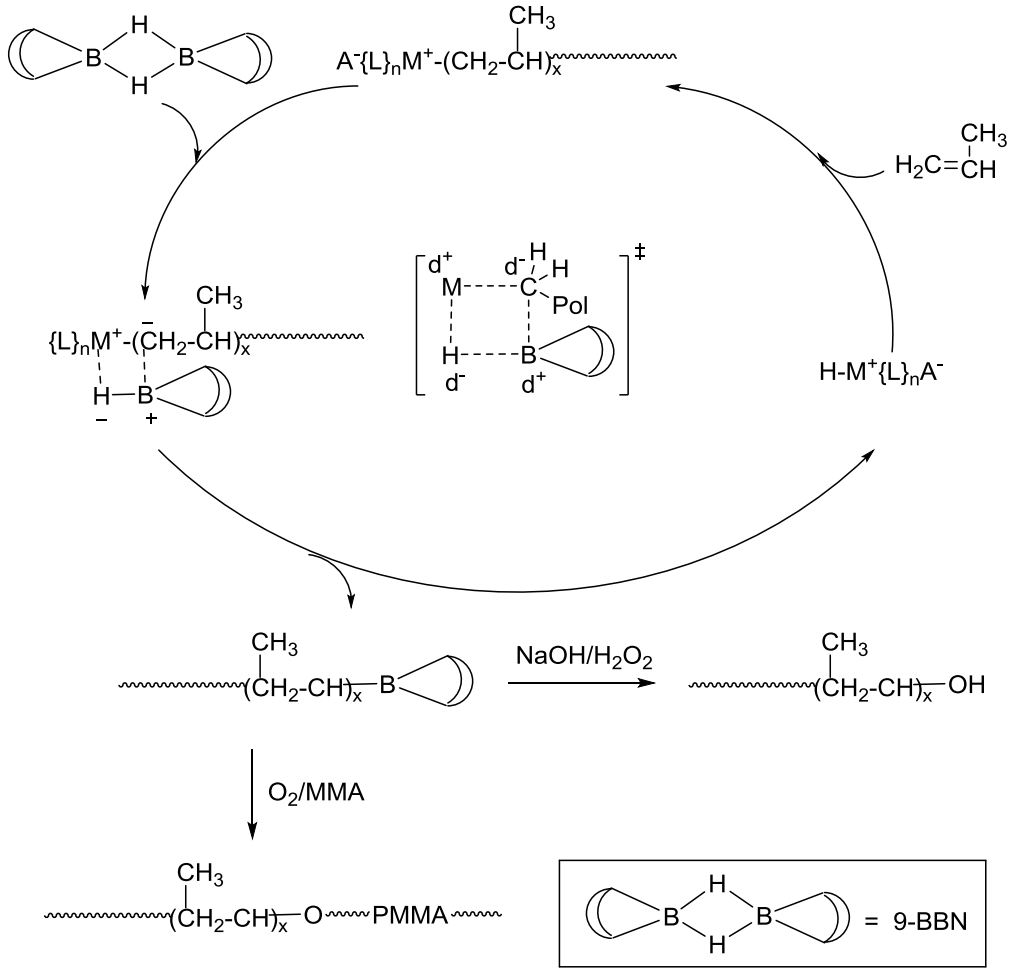

Scheme 4.1. Proposed pathway of a metallocene-based olefin polymerisation using a borane derivative (9-BBN) as a chain-transfer agent.[36]

The molecular weight of the borane-terminated polyolefin was proportional to the ratio of [monomer] to [CTA]. As mentioned previously, the borane-based temini can be converted to various functional groups or oxidised to yield stable polymeric radicals. These radicals could then participate in further radical copolymerisations with other functional monomers (Scheme 4.1).[36]

The appropriate choices of Lewis acidic boranes, metallocene catalysts and reaction conditions are essential to attain a functionalised polyolefin with good molecular weight control. This catalytic polymerisation is applicable to wide range of homo- and co-polyolefins, including polyethylene, polypropylene, syndiotactic polystyrene, poly(ethylene-*co*-styrene), poly(ethylene-*co*-propylene) and poly(ethylene-*co*-1-octene).[35-42]

So far, the use of boron-containing reagents as CTAs in iROP of cyclic esters has been unexplored. In this Chapter, a successful preliminary work on this area using $B(OR)_3$ and HBPin is reported.

4.3 *In situ* generated catalysts

Using a one pot or *in situ* synthetic strategy is well established in organic and polymer syntheses.[46-49] For example, *in situ* generated initiators in the ROP of ε-CL derived from the reactions between lanthanide tetrahydroborates and aldehyde/ketone derivatives were reported by Sun *et al*. in 2008.[50] The resultant alkoxide initiators provided efficient alternatives to the syntheses of alkoxy ester end-capped PCL. Interestingly, the by-products (trialkyl borate esters) were claimed to be innocent in the polymerisation.

In light of Sun's work, the same methodology was applied to the alkaline earth tetrahydroborate complexes, namely ($Tp^{tBu,Me}$)$Mg(BH_4)$ (**2**), ($Tp^{tBu,Me}$)$Ca(BH_4)(THF)$ (**1**) and ($Tp^{tBu,Me}$)$Sr(BH_4)(THF)_2$ (**4**). Four equivs of benzaldehyde was added into a C_6D_6 solution of **2** or **1** or **4**, on the NMR tube scale, instantaneously giving the corresponding benzyloxide species along with tribenzyl borate ester ($B(OBn)_3$) in either separate (for Mg (**10**) and Ca (**13a**), Equation 4.1) or adduct formation (for Ca (**13b**) and Sr (**14**), Equation 4.1). The different coordination of the *in situ* generated compounds, which could be conveniently identified using ^1H and ^{11}B NMR analyses, is dependent on the sizes of the metal centres. For instance, the smallest congener of the series only formed a mixture of the separate species ($Tp^{tBu,Me}$)Mg(OBn) (**10**) and $B(OBn)_3$. The mixture could be obtained in multi-gram scale in a scale-up reaction. The ^{11}B NMR analysis of the product showed a doublet and a singlet at δ = -9.4 and +18.6 ppm, corresponding to $Tp^{tBu,Me}$(B-H) and $B(OBn)_3$, respectively.

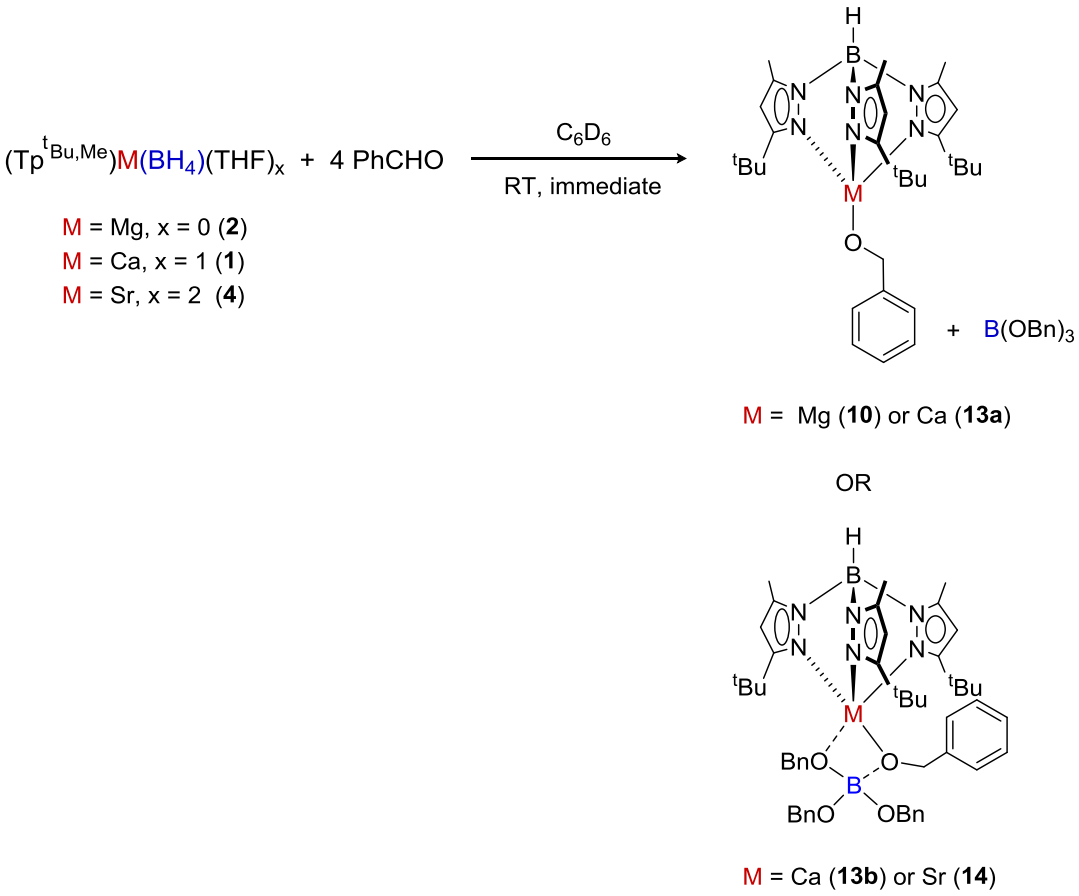

Equation 4.1

On the other hand, the *in situ* generated strontium compound existed solely as an adduct, $(Tp^{tBu,Me})Sr\{B(OBn)_4\}$ (**14**). The ^1H NMR spectrum featured a single set of resonances correlating to the ligand and the benzyl protons. Concurrently, the ^{11}B NMR analysis strongly supported the formation of a tetra-coordinated borate species with a corresponding singlet resonance at *ca*. δ = 4.0 ppm. This chemical shift is consistent with a range of other compounds featuring tetra-coordinate borates.[51] Compound **14** was synthesised in a multi-gram scale, isolated and fully characterised by NMR and IR spectroscopy, as well as elemental analysis.

As expected, the compound bearing calcium, with an ionic radius between that of Mg and Sr, existed in both separated (**13a** and $B(OBn)_3$, minor product) and adduct complexes (**13b**, major product) in solution. Their existence was also identified by ^{11}B NMR analysis, whereby two singlets are present at δ 18.6 and 4.3 ppm, in conjunction with singlet corresponding to $Tp^{tBu,Me}$(B-H) at δ -7.7 ppm. Interestingly, ^1H and $^{13}C\{^1H\}$ NMR analyses showed solely an average signal of ligand and benzyl resonances. The spectra were similar to that obtained in the strontium analogue **14**.

The removal of all volatiles followed by redissolving in C_6D_6 resulted in the loss of free THF generated in the reactions between **1** or **4** with 4 equivs. of PhCHO. This suggested that compounds **13b** and **14** contained strongly coordinated tetra-benzyloxy borates. The equilibria between the separated alkoxy compounds and $B(OR)_3$ and their corresponding adducts are dependent on the sizes of the metal centres and the solution temperature (*vide infra*) but independent of the type of solvent, as no significant change was observed in the ^{11}B NMR analysis of the calcium compounds (**13a** and **13b**) in THF-d_8.

The products from the reduction of benzaldehyde using **1** and **2** were stable in C_6D_6 solution for days. However, the formation of a trace amount of the homoleptic strontium compound (**6**) developed in C_6D_6 solution of compound **14** after 16 h.

4.3.1 Isolation of ($Tp^{tBu,Me}$)Mg(OBn) (10)

Attempts to isolate ($Tp^{tBu,Me}$)Mg(OBn) (**10**) from $B(OBn)_3$ produced in the benzaldehyde reduction using **2** were carried out. Washing with hydrocarbon solvents (i.e. pentane or hexane) was unsuccessful due to the comparable solubility of **10** and $B(OBn)_3$ in the hydrocarbon solvents. Another purification technique exploited was crystallisation in benzene at 4 °C or toluene at -30 °C. This led to the removal of $B(OBn)_3$. However, this also resulted in the formation of a new species (**10***) alongside compound **10**, and the amount of **10*** varied in each attempt of crystallisation. Moreover, no interconversion was observed between compounds **10** and **10*** on heating.

Although the tris-(pyrazolyl) borate has been widely used in organometallic research as an inert face-capping ligand, several examples in literature illustrate the possibility of ligand transformation, including the 1,2-boratropic rearrangement. An asymmetrical tris-(pyrazolyl) borate ligand bearing bulky substituents, such as *tert*-butyl in this case, may undergo a rearrangement which involves ligand reorganising without any loss of the pyrazolyl moiety as shown here. The process is driven by ultimately reducing the unfavourable steric interaction between the bulky substituent of the ligand and the sterically demanding co-ligand.[52-60]

^1H, $^{13}C\{^1H\}$ NMR and their two-dimentional NMR spectroscopic techniques were utilised in characterisation of **10***. ^1H and $^{13}C\{^1H\}$ NMR spectra of the co-crystallised product clearly show two distinct sets of resonances for the $Tp^{tBu,Me}$ ligand

substituents and benzyl groups, Figure 4.2. The ratio of the integration of the protons corresponding to the $Tp^{tBu,Me}$ ligand and the benzyl group in the co-crystallised product remained unchanged, when compared to that of compound **10**. This signifies no degradation of the $Tp^{tBu,Me}$ ligand, but more likely a change in the conformation.

Similar solution behaviour of substituted tris-(pyrozolyl) hydroborate supported compounds is well-established in the literature involving a 1,2-sigmatropic rearrangement of the ligand.[52-60] By comparison, **10*** could therefore be assigned as {HB(^{t}Bu,Me-pz)$_2$(Me,^{t}Bu-pz)}Mg(OBn) (**10***).

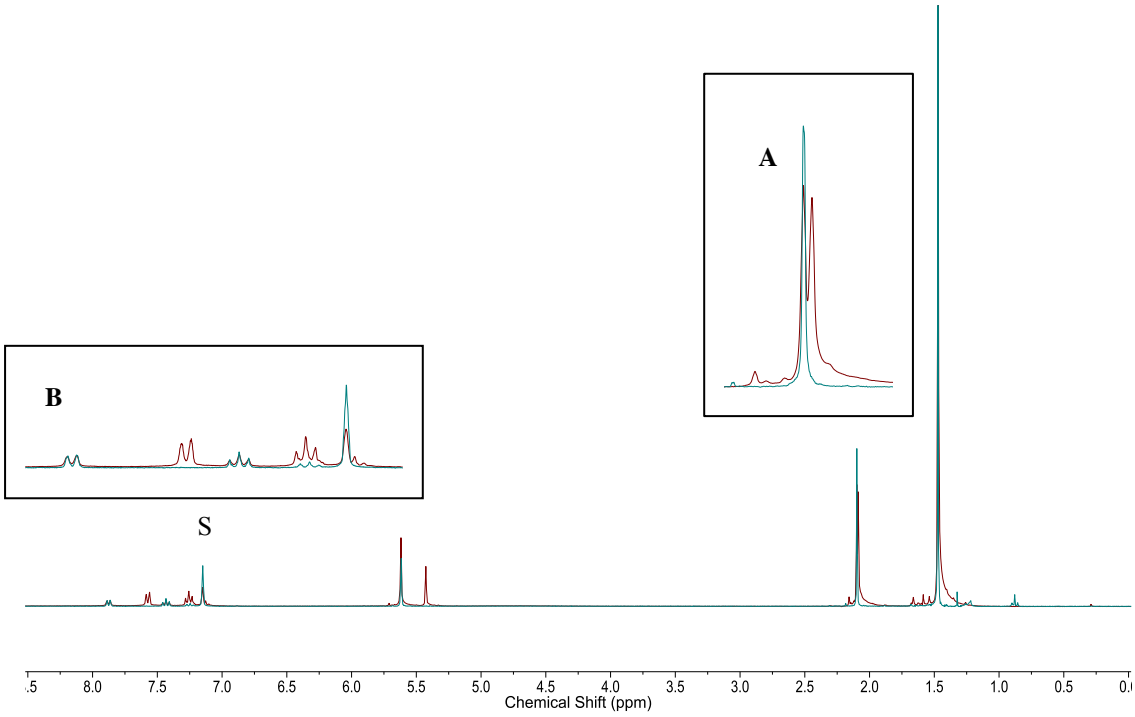

Figure 4.2. Superimposed ^{1}H NMR (299.9 MHz, C_6D_6) spectra of ($Tp^{tBu,Me}$)Mg(OBn) (**10**) (Cyan) and the co-crystallised product from the solution mixture of **10** and B(OBn)$_3$. 'S' denotes residue protio solvent. Inset '**A**' and '**B**' show the expanded regions at δ = 7.0-8.0 and 1.9-2.2 ppm, respectively.

Further ROESY analysis showed an NOE (nuclear Overhauser effect) between the *tert*-butyl substituents of the ligands and *o*-phenyl protons in both compound **10** and **10***, Figure 4.3. Unfortunately, an expected NOE effect between the methyl substituent of the {HB(^{t}Bu,Me-pz)$_2$(Me,^{t}Bu-pz)} ligand and *o*-phenyl proton of **10*** was not observed.

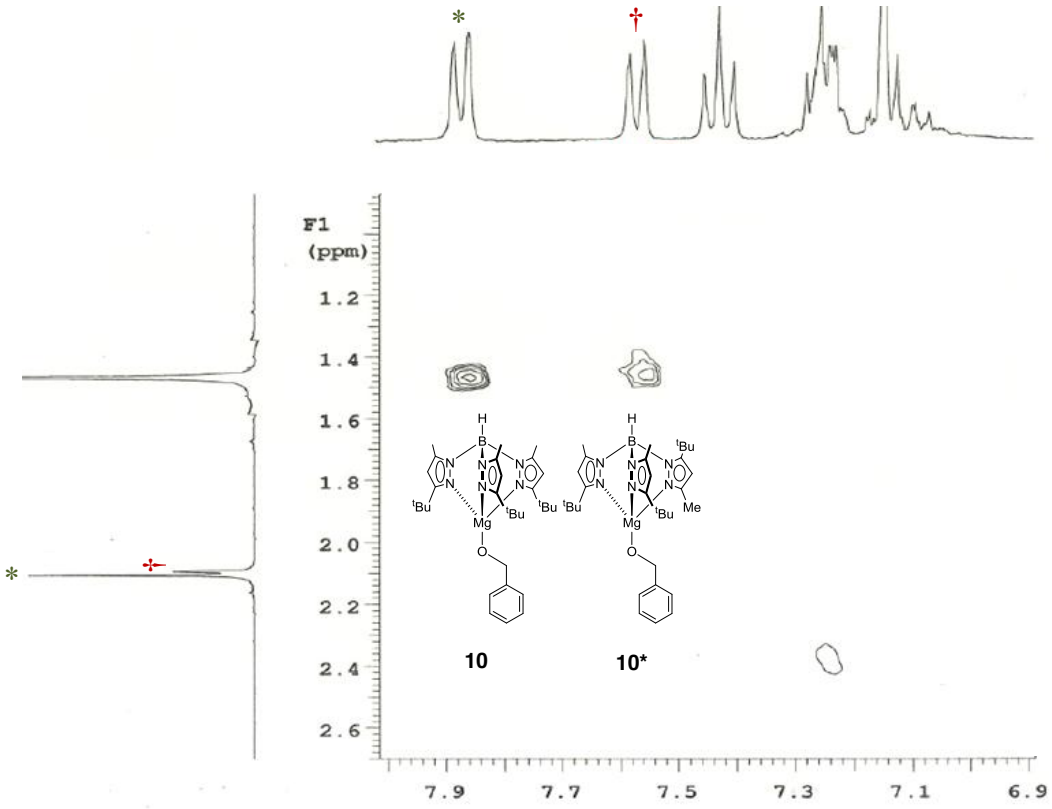

Figure 4.3. ROESY (299.9 MHz, C_6D_6) analysis of the solution mixture containing ($Tp^{tBu,Me}$)Mg(OBn) (**10**) and {HB(^{t}Bu,Me-pz)$_2$(Me,^{t}Bu-pz)}Mg(OBn) (**10***). Green asterisk and red dagger represents the resonances corresponding to compound **10** and **10***, respectively.

Since **10*** forms only in the presence of $B(OBn)_3$, it is proposed that an adduct of the type ($Tp^{tBu,Me}$)Mg{$B(OBn)_4$} may precede the 1,2-boratropic shift. Such an intermediate adduct is not directly observed in the case of **10**, but has been crystallographically characterised (see Section 4.3.3 below) in the case of the methoxy analogue ($Tp^{tBu,Me}$)Mg{$B(OMe)_4$} (**16**) which almost fully dissociates to $B(OMe)_3$ and ($Tp^{tBu,Me}$)Mg(OMe) (**15**) in solution at room temperature. The more sterically crowded (*cf* **16**) adduct, ($Tp^{tBu,Me}$)Mg{$B(OBn)_4$}, contains a tetra(benzyloxy) borate group, forming extensive steric hindrance around the small magnesium centre. A 1,2-boratropic shift of the pyrazolyl moiety *trans* to an adjacent benzyloxy group takes place, in order to minimise the steric interaction between the benzyloxy group and the bulky *tert*-butyl substituent of the $Tp^{tBu,Me}$ ligand and hence stabilise the compound. As expected, subsequent removal of $B(OBn)_3$ results in the formation of {HB(^{t}Bu,Me-pz)$_2$(Me,^{t}Bu-pz)}Mg(OBn) (**10***), Scheme 4.2.

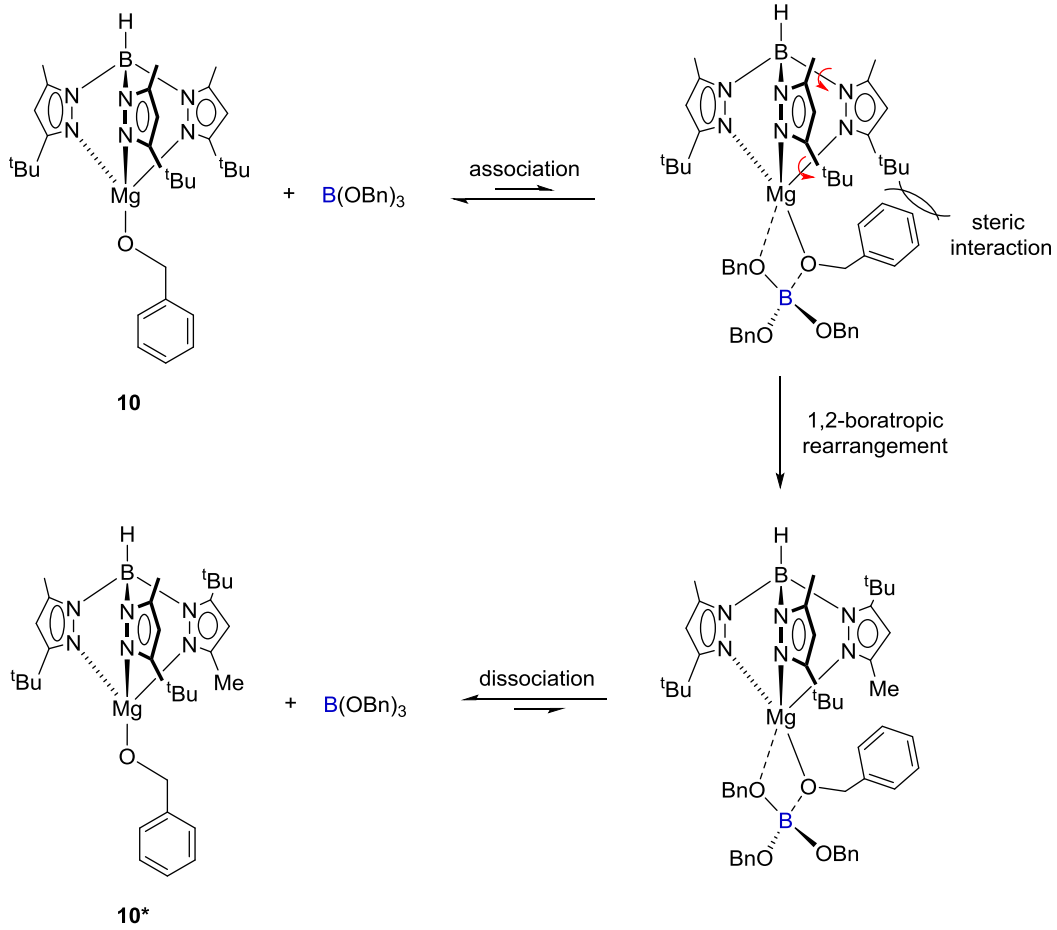

Scheme 4.2. Possible pathway to the 1,2-boratropic rearrangement product, {HB(pz^{tBu,Me})$_2$(pz^{Me,tBu})}Mg(OBn) (**10***).

To avoid the formation of **10*** following crystallisation, Lewis bases 4-methylaminopyridine (DMAP) and pyridine were added (in separate experiments) into the solution mixture of **10** and B(OBn)$_3$, in order to form DMAP·B(OBn)$_3$ or py·B(OBn)$_3$ adducts prior to crystallisation. Nevertheless the attempt was fruitless as no adduct was formed over the course of 16 h. The inaccessible formation of the B-N adduct is due to the lower Lewis acidity of B(OBn)$_3$, when compared to B(OPh)$_3$ which successful formed a known literature adduct py·B(OPh)$_3$. The overlap between the *p*-orbitals on O and B atom accounts for the reduced Lewis acidity in this trialkyl borate, whereas the delocalisation between the lone pair on the O atom and phenyl ring in triaryl borates induces less *p*-orbital overlap between the O and B atoms hence increasing the Lewis acidicity in B(OPh)$_3$.[5, 61-63]

4.3.2 The dissociation of $B(OBn)_3$ from $(Tp^{tBu,Me})Sr\{B(OBn)_4\}$ (14)

The adduct $(Tp^{tBu,Me})M\{B(OBn)_4\}$ is the predominant form obtained for heavier alkaline earth metals (Ca (**13b**) and Sr (**14**)). An equivalent of commercially available $B(OBn)_3$ was added into a C_6D_6 solution of **14**, giving rise to a new set of benzyl proton resonances in an ^1H NMR analysis. A subsequent spin-saturation transfer experiment showed exchange on the NMR timescale between the methylene protons of the benzyl groups of bound $\{B(OBn)_4\}^-$ and free $B(OBn)_3$. This exchange implies **14** undergoes a rapid dissociation/association process in solution at room temperature (Equation 4.2).

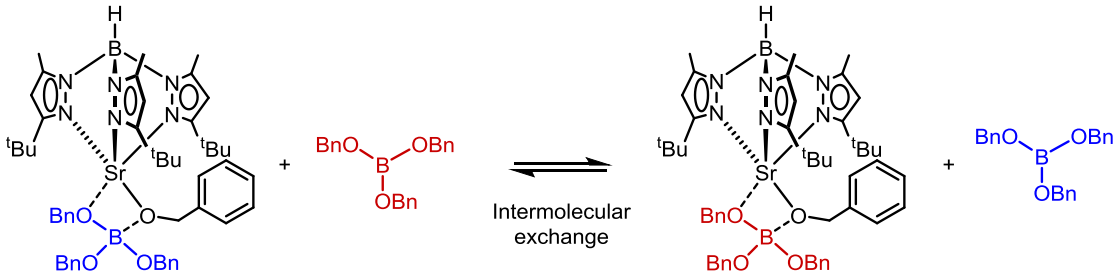

Equation 4.2

Detailed kinetic studies into the dissociation process of compound **14** were carried out. Variable-temperature ^1H NMR spectra were recorded between 20 and 68 °C (Figure 4.4). The line broadening of the resonances corresponding to the methylene protons of the benzyl groups of bound $\{B(OBn)_4\}^-$ and free $B(OBn)_3$ was measured at appropriate temperature increments. The rate constants of the dissociation reaction could then be determined from the relationship; $k = (\Delta\nu_{1/2} - \Delta\nu_{1/2\ ref})\pi$, where $\Delta\nu_{1/2}$ is the line width.[64] In turn, activation parameters associated with the dissociation process of **14** could be obtained from the Eyring plot of $\ln(k/T)$ *vs.* $1/T$ as shown in Figure 4.5.

The enthalpy and entropy of activation for the exchange process was calculated to be $\Delta H^{\ddagger} = +100(2)$ kJ mol^{-1} and $\Delta S^{\ddagger} = +67(5)$ J K^{-1} mol^{-1}, respectively. The positive value of $\Delta S^{\ddagger}$ is consistent with a dissociative exchange mechanism proceeding *via* separated $(Tp^{tBu,Me})Sr(OBn)$ and free $B(OBn)_3$.

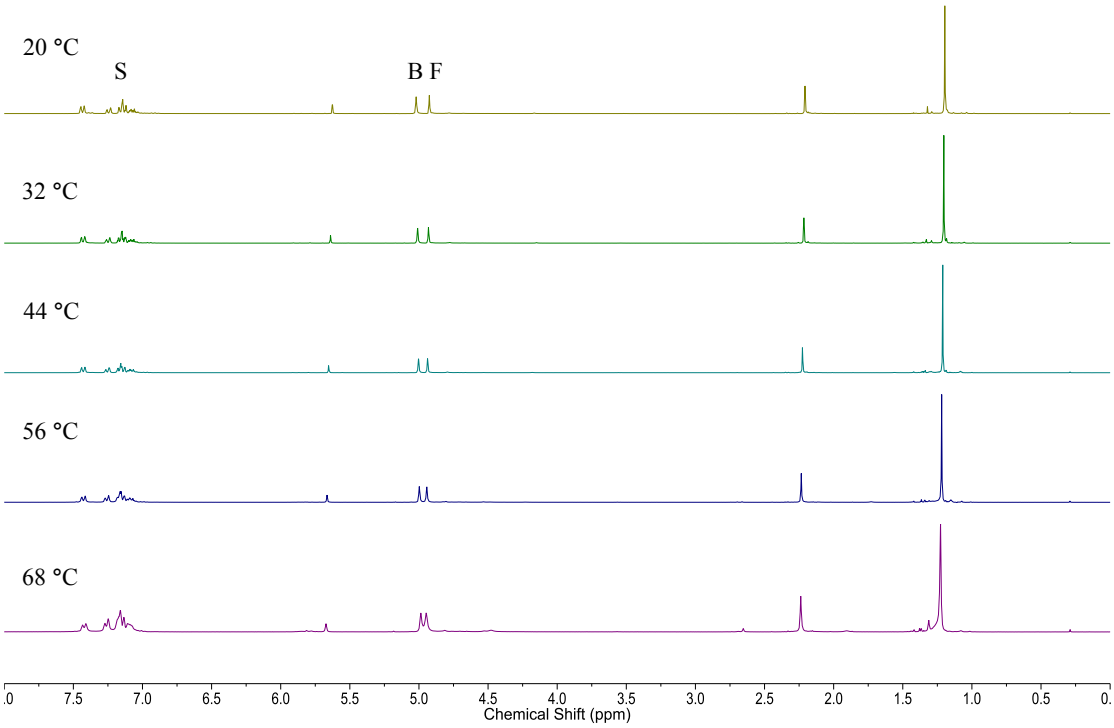

Figure 4.4. Variable temperature ^{1}H NMR (299.9 MHz, C_6D_6) spectra of a mixture of *in-situ* generated ($Tp^{tBu,Me}$)Sr{$B(OBn)_4$} (**14**) and $B(OBn)_3$. 'B', 'F' and 'S' denotes bound $B(OBn)_4$, $B(OBn)_3$ and residue protio solvent, respectively.

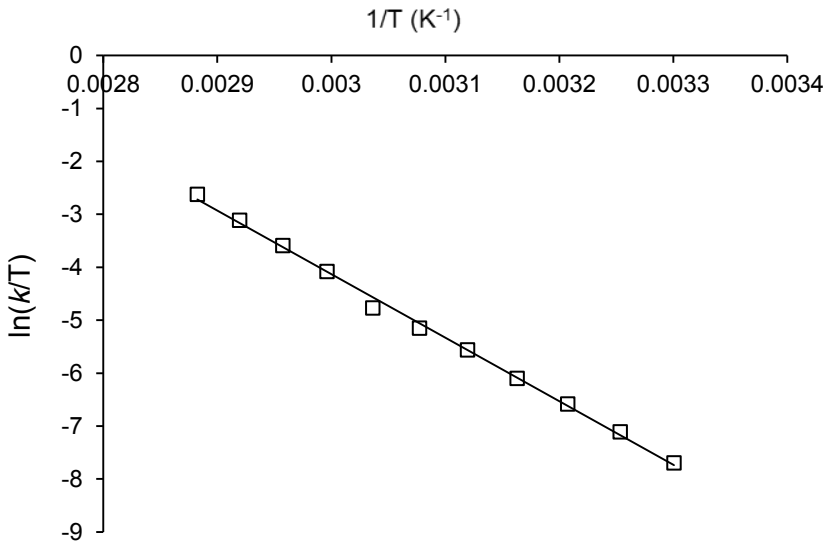

Figure 4.5. Erying Plot of ln(*k*/T) *vs*. 1/T (R^2 = 0.998): $\Delta H^{\ddagger}$ = +100(2) kJ mol^{-1} and $\Delta S^{\ddagger}$ = +67(5) J K^{-1} mol^{-1}.

4.3.3 Intramolecular exchange and its thermodynamic parameters

In addition to the dissociation of **14** described previously, other dynamic processes taking place in solution include the intramolecular exchange between the bridging and terminal benzyloxy groups of the tetra(alkoxy) borate. In order to gain some insight into this process, low temperature ^{1}H NMR analyses of **14** in toluene-d_8 were undertaken. However, only broad, undefined resonances were observed even at -90 °C. As ($Tp^{tBu,Me}$)M{$B(OBn)_4$} (M = Ca or Sr) complexes were incompetent as models for the investigation of intramolecular exchange, the synthesis of a new model ($Tp^{tBu,Me}$)Mg{$B(OMe)_4$} (**16**) was attempted.

Prior to the synthesis of ($Tp^{tBu,Me}$)Mg{$B(OMe)_4$}(**16**), a precursor ($Tp^{tBu,Me}$)Mg(OMe) (**15**) was made. By analogy to the synthesis of ($Tp^{tBu,Me}$)Mg(OBn) (**10**), a protonolysis reaction between ($Tp^{tBu,Me}$)Mg(^{n}Bu) (**8**) and methanol in C_6H_6 yielded **15** in 85 % yield. Diffraction-quality crystals were grown from a saturated *n*-hexanes solution at -20 °C. The solid state structure and its selected bond lengths and angles are shown in Figure 4.6 (top) and Table 4.1, respectively.

Partial formation of compound **16** was obtained from the reaction between compound **15** and an equivalent of $B(OMe)_3$ at room temperature (*vide infra*). Single crystals suitable for X-ray analysis of compound **16** were grown from a neat solution of compound **15** in $B(OMe)_3$ at -30 °C. The solid state structure and its selected bond lengths and angles are also shown in Figure 4.6 (bottom) and Table 4.1, respectively.

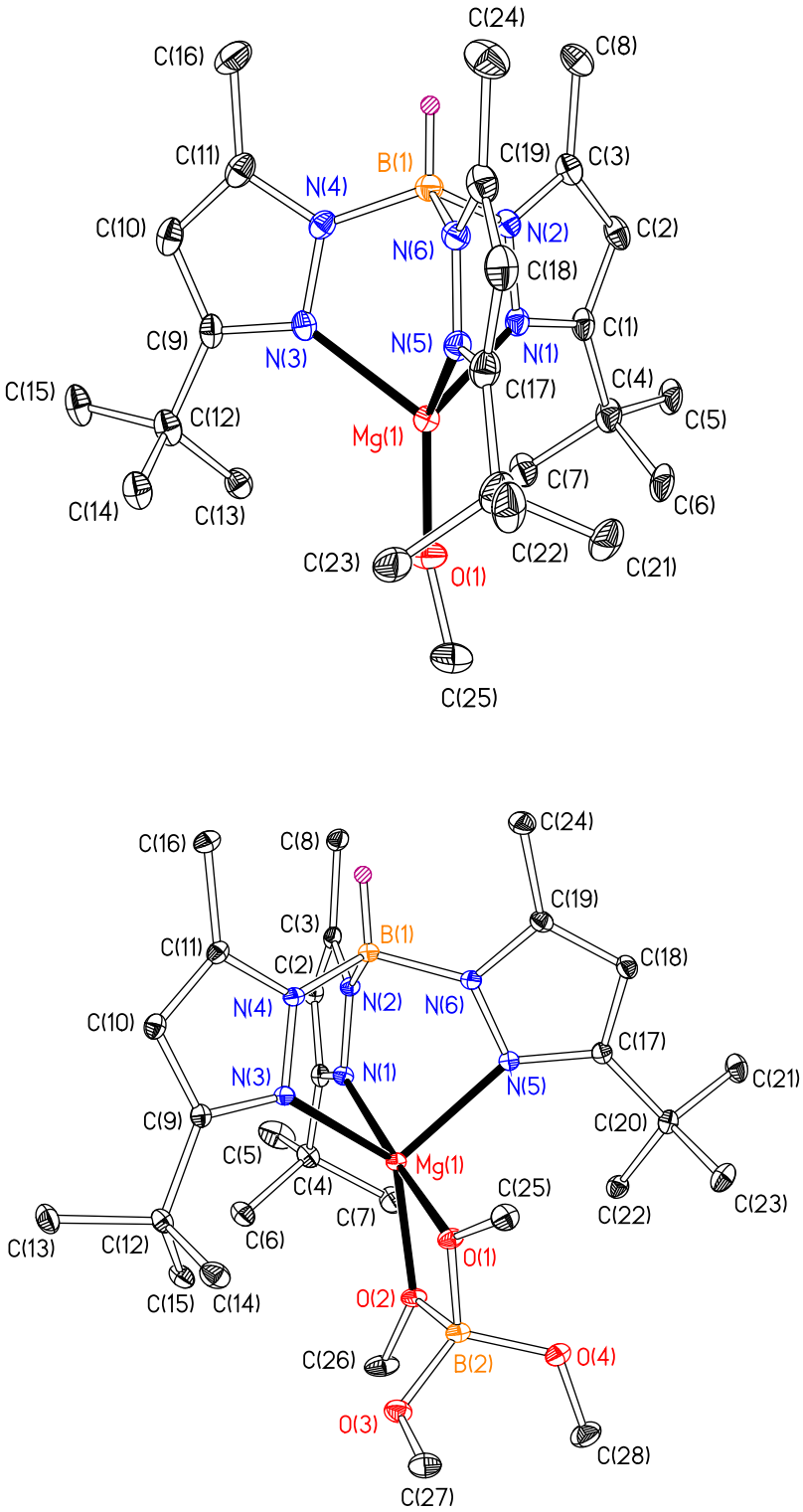

Figure 4.6. Displacement ellipsoid plot (20% probability level) of ($Tp^{tBu,Me}$)Mg(OMe) (**15**) (top) and ($Tp^{tBu,Me}$)Mg{$B(OMe)_4$} (**16**) (bottom). C- bound H atoms are omitted for clarity.

Table 4.1. Selected bond lengths (Å) and angles (°) for ($Tp^{tBu,Me}$)Mg(OMe) (**15**) and ($Tp^{tBu,Me}$)Mg{$B(OMe)_4$} (**16**).

Parameters	**15**	**16**
Mg(1)-N(1)	2.081(3)	2.2076(8)
Mg(1)-N(3)	2.089(3)	2.1763(8)
Mg(1)-N(5)	2.085(3)	2.1515(8)
Mg(1)-O(1)	1.801(2)	2.0294(7)
Mg(1)-O(2)	-	2.0391(7)
B(2)-O(1)	-	1.4858(11)
B(2)-O(2)	-	1.5276(11)
B(2)-O(3)	-	1.4366(12)
B(2)-O(4)	-	1.4342(12)
N(1)-Mg(1)-N(3)	89.76(10)	83.43(3)
N(1)-Mg(1)-N(5)	93.11(10)	83.99(3)
N(3)-Mg(1)-N(5)	92.44(11)	103.97(3)
N(1)-Mg(1)-O(1)	125.24(13)	175.05(3)
N(3)-Mg(1)-O(1)	125.65(12)	93.50(3)
N(5)-Mg(1)-O(1)	121.15(12)	93.02(3)
N(1)-Mg(1)-O(2)	-	118.00(3)
N(3)-Mg(1)-O(2)	-	128.04(3)
N(5)-Mg(1)-O(2)	-	123.78(3)
Mg(1)-O(1)-C(25)	163.7(5)	135.50(6)
Mg(1)-O(1)-C(26)	-	143.25(6)
O(1)-Mg(1)-O(2)	-	66.95(3)
Mg(1)-N(1)-N(2)-B(1)	3.41	14.01
Mg(1)-N(3)-N(4)-B(1)	2.89	8.68
Mg(1)-N(5)-N(6)-B(1)	2.09	38.79

($Tp^{tBu,Me}$)Mg(OMe) (**15**) is a four-coordinate complex with Mg(1) coordinated to the three N donors of the $Tp^{tBu,Me}$ ligand and the O(1) of the methoxy ligand. The geometry around Mg(1) is best described as tetrahedral with local C_3 symmetry. This results in the similar Mg-N bond distances (2.081(3)-2.089(3) Å), N-Mg-N' angles (89.76(10)-93.11(10) °) and Mg-N-N'-B dihedral angles (2.09-3.41 °). All bond lengths and angles associated with Mg(1) are consistent with those of ($Tp^{tBu,Me}$)Mg(OBn) (**10**) and ($Tp^{tBu,Me}$)Mg(Cl) (**3**).

The incorporation of $B(OMe)_3$ to compound **15** leads to the formation of ($Tp^{tBu,Me}$)Mg{$B(OMe)_4$} (**16**), which adopts a *pseudo* trigonal bipyramidal structure in the solid state. Mg(1) lies 0.25 Å above the least-square plane defined by N(3), N(5) and O(2), whilst N(1) and O(1) occupy the axial positions with an N(1)-Mg(1)-O(1) angle of 175.05(3)°. The significant deviation from 90° of the N(1)-Mg(1)-O(2) (118.00(3)°) and O(1)-Mg(1)-O(2) (66.95(3)°) angles cause the distortion in this molecule. The bridging B-O bond lengths (1.4858(11) and 1.5276(11) Å) in tetramethoxy borate are longer than those found for the the terminal groups (1.4366(12) and 1.4342(12) Å). This is a common feature found in bridging ligands.

The increased coordination number of O(1) and O(2) results in smaller Mg(1)-O(1)-C(25/26) (135.50(6) and 143.25(6)°) angles in comparison to that of compound **15** (163.7(5)°). The increased coordination number at magnesium also results in longer Mg-O bond lengths (2.0294(7) and 2.0391(7) Å) than the Mg(1)-O(1) bond length in **15** (1.801(2) Å), as well as a significant deviation of the pyrazolyl components from the C_3 axis defined by the $Tp^{tBu,Me}$ ligand (Mg-N-N'-B dihedral angles of 8.68-38.79°). It could be viewed that the considerable deviation of the N(5)-pyrazolyl moiety adjacent to the tetramethoxy borate is *en route* to the 1,2-boratropic rearrangement found in the more sterically hindered benzyloxy counterpart.

Closely related literature compounds to **16** are [(Tp)Ca$(HOMe)_2$(μ_4-$B(OMe)_4$)Ca$(HOMe)_2$Tp][$B(OMe)_4$] (**4.1**) and [CH{C(Me)NAr}$_2$Mg{$(Ph_2HCO)_2$Bpin}] (Ar = 2,6-$C_6H_3{}^iPr_2$, **4.2**) proposed by Winter[65] and Hill *et al.*,[11] respectively. Compound **4.1** was synthesised by protonolysis of TpCa(BH_4)(THF) and methanol, followed by crystallisation in a warm methanol solution, whilst compound **4.2** was the product of a reduction reaction between [CH{C(Me)NAr}$_2$Mg(μ-H)$_2$] and benzophenone in the presence of HBPin.

The ^{11}B NMR (CD_3OD) analysis of compound **4.1** showed a singlet with δ 5.1 ppm corresponding to the tetramethoxy borate species. On the other hand, compound **4.2** dissociated in solution giving rise to a singlet at δ 15.9 ppm corresponding to the three-coordinate boron species, $Ph_2CHOBPin$ according to the ^{11}B NMR analysis. For compound **4.1**, the C-O (*ca*. 1.414(6)-1.431(6) Å) and B-O bond lengths (1.444(6)-1.463(6) Å) associated with μ_4-$B(OMe)_4$ and methanol ligands are similar, within error, to those of compound **16**. Although compound **16** and **4.2** possess different coordination numbers and borate substituents, the Mg-O (1.9789(16) and 2.0194(16) Å) and B-O bond lengths (*ca*. 1.424(3)-1.606(3) Å) of **4.2** are similar, within error, to those of **16**.

As mentioned previously, the addition of an equivalent of $B(OMe)_3$ to a C_6D_6 solution of ($Tp^{tBu,Me}$)Mg(OMe) (**15**) resulted in partial formation of the adduct **16** at room temperature. As the adduct **16** was produced in only a small quantity at room temperature, no obvious formation of new resonances were observed in the ^1H NMR spectrum. However, the presence of the adduct **16** species can be confirmed by a small singlet at δ 3.3 ppm in the $^{11}B\{^1H\}$ analysis. The observed resonance fits in the expected region (*ca*. δ = 2-6 ppm) for tetra-alkoxy borate containing species.[51] A spin-saturation transfer experiment was also applied to the solution mixture at room temperature. The analysis showed intermolecular exchange between the methoxy group of compound **15** and $B(OMe)_3$ on the NMR timescale. The intermolecular exchange between **15** together with $B(OMe)_3$ and **16** was expected to occur concurrently with the intramolecular exchange as shown in Scheme 4.3.

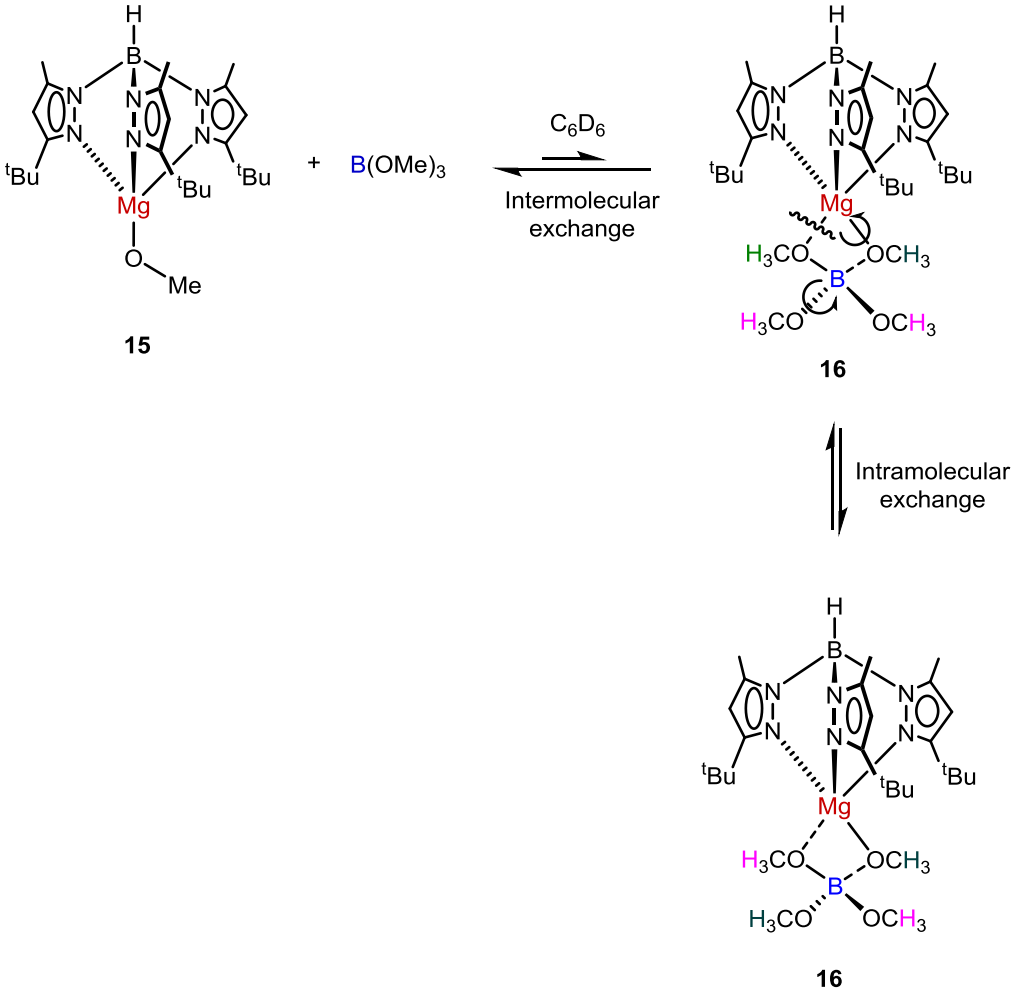

Scheme 4.3. Intermolecular exchange between ($Tp^{tBu,Me}$)Mg(OMe) (**15**) and ($Tp^{tBu,Me}$)Mg{$B(OMe)_4$} (**16**) and intramolecular exchange between terminal and bridging methoxides.

Variable temperature ^{1}H NMR studies of compound **15** and an equivalent of $B(OMe)_3$ in toluene-d_8 were carried out at -40 to -72 ºC (Figure 4.7). The equilibrium favours the formation of the adduct **16** at low temperature, consistent with the presence of a new set of signals in the ^{1}H NMR spectra. The characteristic resonances of compound **16** at δ 3.4 and 3.8 ppm correspond to the methyl protons of the bridging and terminal methoxy substituents of the borate ligand. However, a subsequent ROESY experiment failed to assign the two resonances to either the bridging or terminal methoxy groups in the ^{1}H NMR analysis. These two methyl resonances become sharper as the solution temperature was lowered, however, no change in the chemical shift and line-width of the methyl signal corresponding to free $B(OMe)_3$ was observed. Therefore, the change in the line broadening of the resonances

corresponding to the methyl protons of the bridging and terminal methoxy substituents of compound **16** solely correlates to intramolecular exchange which suggests a much slower rate of intramolecular exchange compared to intermolecular exchange under the experimental conditions.

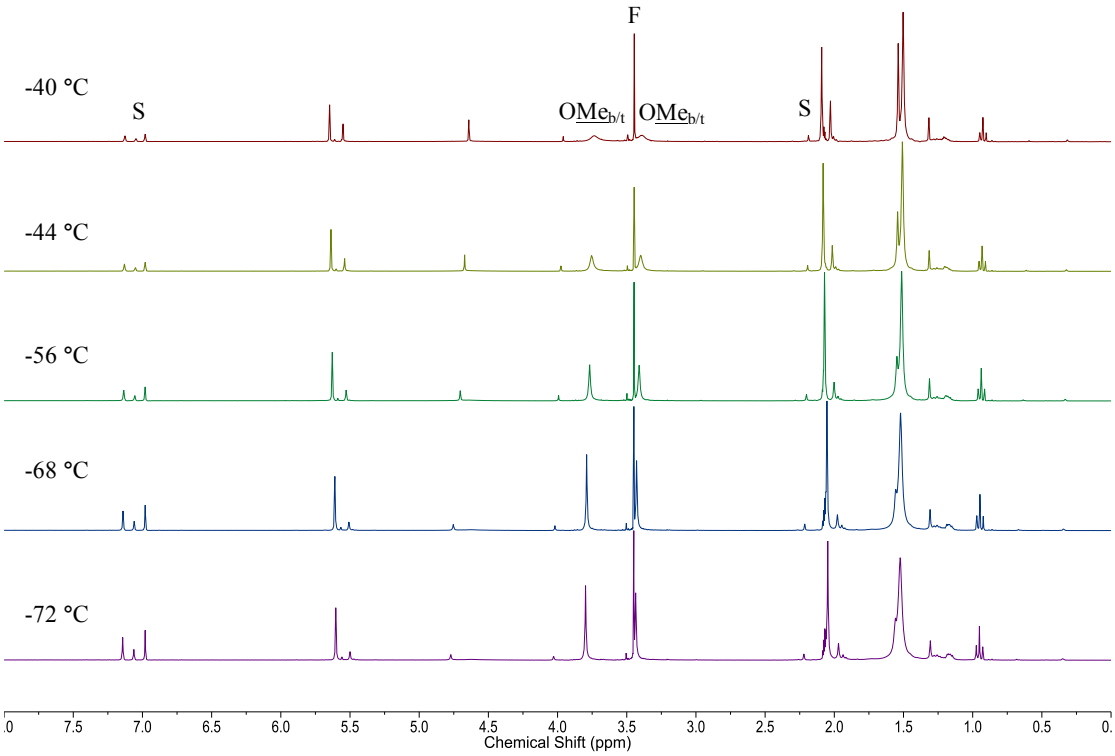

Figure 4.7. Variable temperature ^{1}H NMR (299.9 MHz, toluene-d_8) spectra of the formation of (Tp^{tBu,Me})Mg{B(OMe)$_4$} (**16**) from a 1:1 mixture of (Tp^{tBu,Me})Mg(OMe) (**15**) and B(OMe)$_3$. 'F' and 'S' denote free B(OMe)$_3$ and residue protio solvent, respectively. OMe$_{b/t}$ indicates the methyl protons of the bridging and terminal methoxy groups.

The line broadening of the resonances at δ 3.4 and 3.8 ppm was measured at appropriate temperature increments. The rate constants of the intramolecular exchange reaction could then determine from the relationship; $k = (\Delta\nu_{1/2} - \Delta\nu_{1/2\ ref})\pi$.[64] The thermodynamic parameters associated with this intramolecular exchange could then be obtained from a Eyring plot, ln(k/T) *vs*. 1/T, as shown in Figure 4.8.

The activation parameters for intramolecular exchange were found to be $\Delta H^{\ddagger}$ = +47(1) kJ mol^{-1} and $\Delta S^{\ddagger}$ = -3(3) J K^{-1} mol^{-1}, respectively. The near-zero value for $\Delta S^{\ddagger}$ is consistent with a non-dissociative exchange process.

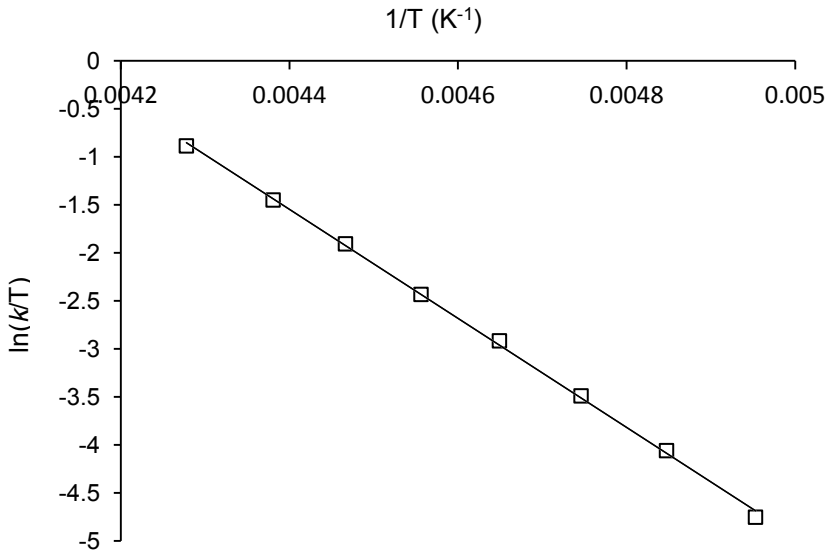

Figure 4.8. Erying Plot of ln(*k*/T) *vs*. 1/T (R^2 = 0.999): $\Delta H^{\ddagger}$ = +47(1) kJ mol^{-1} and $\Delta S^{\ddagger}$ = -3(3) J K^{-1} mol^{-1}.

4.3.4 Exchange reaction

As mentioned previously in Section 1.5, the fast and reversible chain transfer reaction between a chain transfer agent and a growing polymer chain on a metal complex is a crucial key in achieving immortal ROP. Several exchange reactions involving $B(OR)_3$ and various initiators were investigated, Figure 4.9.

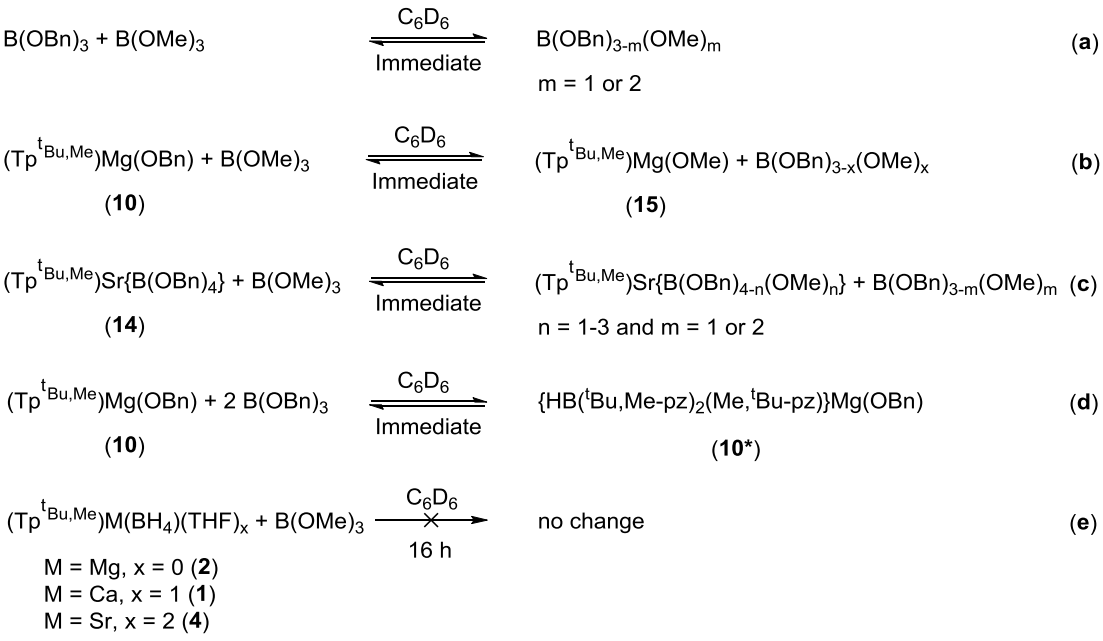

Figure 4.9 (a)-(e). Exchange reactions of $B(OR)_3$ and various initiators.

There is precedent in the literature for exchange reactions between halide and perfluoroalkyl substituted boranes and other Lewis acidic reagents or transition metal complexes.[66-69] The reaction between $B(OMe)_3$ and $B(OBn)_3$ in C_6D_6 immediately led to formation of the exchanged products $B(OBn)_{3-n}(OMe)_n$ (n = 1 or 2, Figure 4.9(a)). The ^1H NMR analysis showed distributions of the exchanged products along with the starting materials in the ratio of $B(OBn)_3$:$B(OMe)_3$:$B(OBn)_2(OMe)$:$B(OBn)(OMe)_2$ = 1:1:3:3, according to examination of the respective integrals. As expected, this ratio was disturbed when the volatiles were partially removed. This is due to the different volatility and boiling points of the various borate esters.

The exchange reaction between trialkoxy borate esters and metal alkoxide complexes was also facile. Addition of an equivalent of $B(OMe)_3$ to a C_6D_6 solution of $(Tp^{tBu,Me})Mg(OBn)$ (**10**) led to immediate formation of $B(OBn)_{3-n}(OMe)_n$ (n = 1 or 2) species, in conjunction with the minor product $(Tp^{tBu,Me})Mg(OMe)$ (**15**) (Figure 4.9(b)). This observation implies that the reaction proceeds *via* a tetra(alkoxy) borate adduct.

A similar observation was made with compound **14**, whereby an NMR tube scale reaction between **14** and $B(OMe)_3$ showed immediate exchange, producing multiple resonances corresponding to the methyl and methylene protons of the methoxy and benzyloxy substituents. This suggested the formation of $(Tp^{tBu,Me})Sr\{B(OBn)_{4-n}(OMe)_n\}$ (n = 0-4) and $B(OBn)_{3-m}(OMe)_m$ (m = 0-3) due to the dissociation and the intramolecular exchange of the adduct species (Figure 4.9(c)). The approximate distribution of the $(Tp^{tBu,Me})Sr\{B(OBn)_{4-n}(OMe)_n\}$ (n = 0-4) species can be estimated from the proton integrations of the known species. The ^1H NMR spectrum of the product mixture confirmed the presence of free $B(OBn)_3$ ($\delta_{(-OCH_2Ph)}$ = 4.92 ppm), a large decrease in the integration of methylene protons in the region found in **14** ($\delta_{(-OCH_2Ph)}$ = 5.02 ppm) and the absence of $B(OMe)_3$ ($\delta_{(-OMe)}$ = 3.43 ppm). This suggests the formation of the borate adducts containing smaller substituents (i.e. methoxy group) is more favourable to the analogues containing larger substituents (i.e. benzyloxy group).

The addition of the bulkier $B(OBn)_3$ reagent into a C_6D_6 solution of **10** instantaneously resulted in the minor formation of 1,2-boratropic shift product **10***

(Figure 4.9(d)). In contrast to the reaction (b) and (c), no reactions were observed between $B(OMe)_3$ and tetrahydroborate complexes **2**, **1** or **4** over 16 h (Figure 4.9(e)).

4.4 Immortal ROP of ε-CL and *rac*-LA using alkaline earth initiators

The principal objective of this work was to preliminarily investigate the potential of $B(OR)_3$ and HBPin as CTAs in iROP of ε-CL and *rac*-LA using alkaline earth initiators. The non-initiating ability of $B(OR)_3$ and HBPin in polymerising ε-CL and *rac*-LA was confirmed by control polymerisation experiments over the course of 12 h. The $B(OR)_3$ as CTAs used in the iROP experiments were either generated *in situ* along with the alkoxide initiators or added as a reagent into the polymerisation solution. HBPin was only added into the solution as a reagent. The iROP experiments were performed in both THF and toluene at room temperature for ε-CL, and only in THF at room temperature in the case of *rac*-LA.

The *in situ* generated catalysts and CTAs were produced under polymerisation conditions using the alkaline earth tetrahydroborate complexes **1**, **2** or **4** and 5 equivs. of benzaldehyde. The solution was stirred at room temperature for 5 mins prior to the addition of other CTAs or monomers. The excess benzaldehyde and prolonged reaction time were undertaken in the polymerisation-scale preparation to ensure the complete conversion from a tetrahydroborate to an alkoxide initiator. The polymerisation was followed by regular aliquots taken and subsequently quenched with wet THF. The polymer samples were characterised by ^{1}H NMR spectroscopy, MALDI-ToF mass spectrometry and gel permeation chromatography (GPC). It is worth noting that polycaprolactone was isolated from the polymerisation solution by precipitation with hexanes.

The possibility of side reactions associated with the excess equivalent of benzaldehyde in the presence of alkaline earth alkoxide initiator and $B(OBn)_3$ was noted. The competing side reaction, namely the Tishchenko reaction,[70-74] was observed in the *in situ* generated calcium benzyloxide (**13a**) and $B(OBn)_3$/calcium tetrabenzyloxy borate initiator (**13b**) at room temperature, but only after 16 h. The dimerisation of the excess benzaldehyde to form benzyl benzoate was catalysed by the calcium complexes. On the other hand, the Tishchenko reaction was not observed in the analogous magnesium and strontium systems. The rate of the Tishchenko

reaction is influenced by the steric and electronic factors contributed by the metal catalysts.[70, 75, 76]

Moreover, the exchange reactions between benzaldehyde and ($Tp^{tBu,Me}$)Mg(OBn) (**10**) or $B(OR)_3$ (R = Me or Bn) were also considered. The reduction of aldehydes and ketones using trialkyl borate esters is established in the literature. The reactions proceed *via* a six-membered ring transition state, which is comparable to that of the Meerwein-Ponndorf-Verley reaction. However, the reactions are only feasible at high temperature (*ca*. 110-175 ºC).[77, 78] Accordingly, a control reaction between $B(OMe)_3$ and PhCHO at room temperature showed no change over 6 h. Finally, the possibility of an exchange reaction between **10** and PhCHO was also examined through a model reaction between **10** and 4-*tert*-butylbenzaldehyde. However, no change was observed over a period of 6 h at room temperature. Overall, it can be concluded that no exchange or other reactions were observed with an excess of benzaldehyde, and hence no effect on iROP was expected.

4.4.1 Immortal ROP of ε-CL using magnesium initiators

The *in situ* generated initiator (**10**) and $B(OBn)_3$, formed from a reaction between compound **2** and 5 equivs of PhCHO, showed high activities towards iROP of ε-CL. Well-controlled iROP was obtained in THF as shown by a linear evolution of M_n (GPC) with % conversion and moderate PDIs (1.43-1.52). The gradient of the linear plot between M_n (GPC) and % conversion of 56(2) g mol^{-1} (% conversion)$^{-1}$ (R^2 = 0.995, the expected value is 57.1 g mol^{-1} (% conversion)$^{-1}$) suggests four chains of PCL produced per metal centre (red diamonds, Figure 4.10). When an equivalent of $B(OMe)_3$ was added into the solution of the *in situ* generated initiator, a well-behaved polymerisation was also obtained with a linear plot observed between M_n (GPC) and % conversion. The gradient of the plot is 28(1) g mol^{-1} (% conversion)$^{-1}$ (blue diamonds, R^2 = 0.997), whilst the expected value is 32.6 g mol^{-1} (% conversion)$^{-1}$. This implies that seven PCL chains were produced per metal centre. The molecular weight distributions of the PCL obtained were broad with PDIs (1.37-1.56).

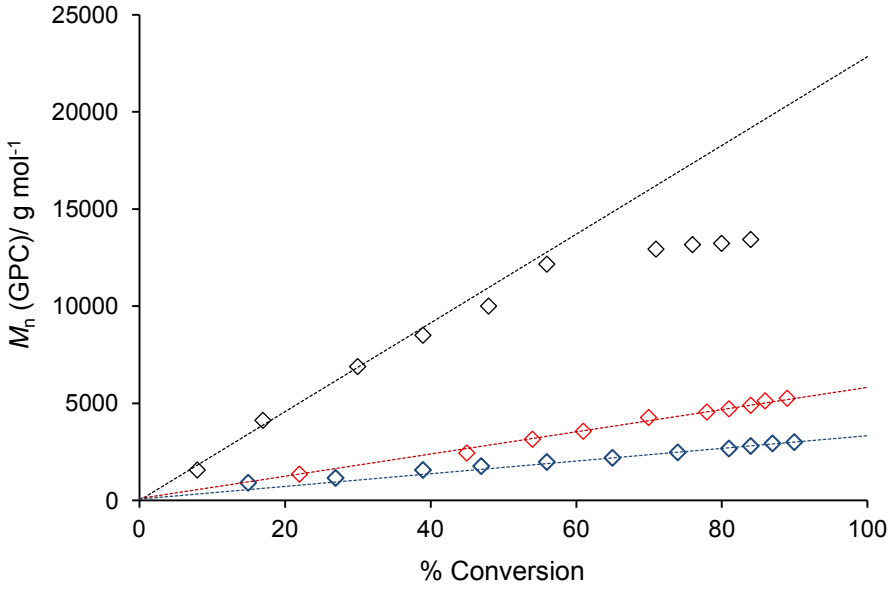

Figure 4.10. Data for iROP of ε-CL using ($Tp^{tBu,Me}$)Mg(BH_4) (**2**) and various additives. M_n (GPC) vs. Conversion plot. The black, red and blue dotted lines are that expected for one, four and seven PLA chains per metal centre, respectively. Conditions: 3.4 mL THF, 23 °C, $[\varepsilon\text{-CL}]_0$ = 1 M, $[\varepsilon\text{-CL}]_0$:[**2**]$_0$ = 200:1 and PDIs = 1.12-1.33 (black diamonds), $[\varepsilon\text{-CL}]_0$:[**2**]$_0$:[PhCHO] = 200:1:5 and PDIs = 1.43-1.52 (red diamonds), $[\varepsilon\text{-CL}]_0$:[**2**]$_0$:[PhCHO]:[$B(OMe)_3$] = 200:1:5:1 and PDIs = 1.37-1.56 (blue diamonds).

First order polymerisation kinetics were obtained with the apparent rate constants, k_{app} = 0.021(1) min^{-1} (R^2 = 0.991) and k_{app} = 0.022(1) min^{-1} (R^2 = 0.991) for the iROP of $[\varepsilon\text{-CL}]_0$:[**2**]$_0$:[PhCHO] = 200:1:5 and $[\varepsilon\text{-CL}]_0$:[**2**]$_0$:[PhCHO]:[$B(OMe)_3$] = 200:1:5:1, respectively (Figure 4.11). The propagation rates of the two iROP systems are similar to each other and to the living ε-CL ROP catalysed by catalyst **2**, within error. This indicates much faster rates of chain transfer compared to propagation in iROP using trialkyl borates. Moreover the rate of iROP is independent of the alkyl substituent under these polymerisation conditions. In an effective iROP experiment using $B(OR)_3$ reagents as chain transfer agents, the number of polymer chains produced per metal centre is 3n+1, where n is the number of equivalents of $B(OR)_3$ in solution. ^{1}H NMR spectroscopic and MALDI-ToF MS analyses of the polymer formed from the iROP of ε-CL using the *in situ* generated magnesium initiator with $[\varepsilon\text{-CL}]_0$:[**2**]$_0$:[PhCHO]:[$B(OMe)_3$] = 200:1:5:1, showed a mixture of benzyloxy ester and methoxy ester end-capped PCL (Figure 4.12).

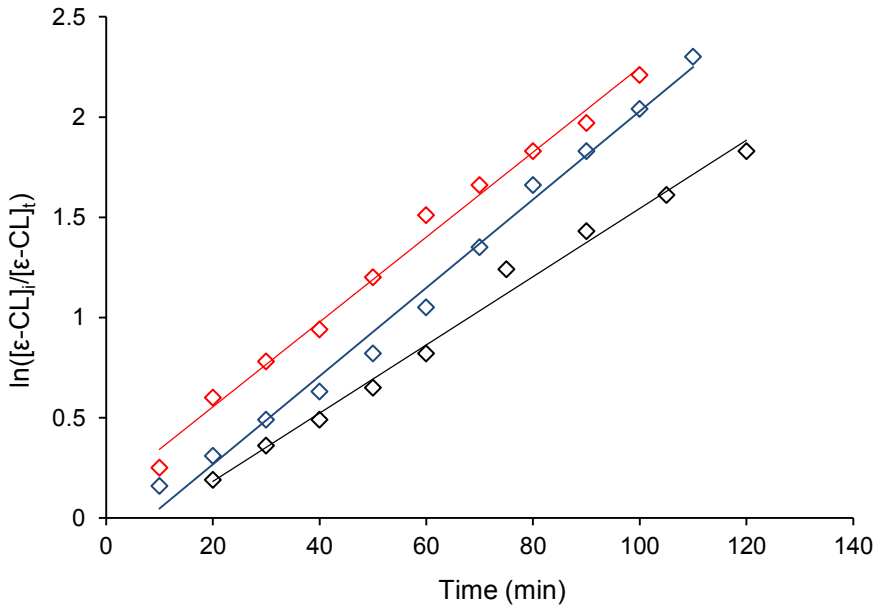

Figure 4.11. First order plot of $\ln([\varepsilon\text{-CL}]_i/[\varepsilon\text{-CL}]_t)$ *vs*. time for the iROP of ε-CL using ($Tp^{tBu,Me}$)Mg(BH_4) (**2**) and various additives. Rate constants: k_{app} = 0.017(1) min^{-1} (R^2 = 0.991, $[\varepsilon\text{-CL}]_0$:[**2**]$_0$ = 200:1, black diamonds), k_{app} = 0.021(1) min^{-1} (R^2 = 0.991, $[\varepsilon\text{-CL}]_0$:[**2**]$_0$:[PhCHO] = 200:1:5, red diamonds) and k_{app} = 0.022(1) min^{-1} (R^2 = 0.991, $[\varepsilon\text{-CL}]_0$:[**2**]$_0$:[PhCHO]:[$B(OMe)_3$] = 200:1:5:1, blue diamonds).

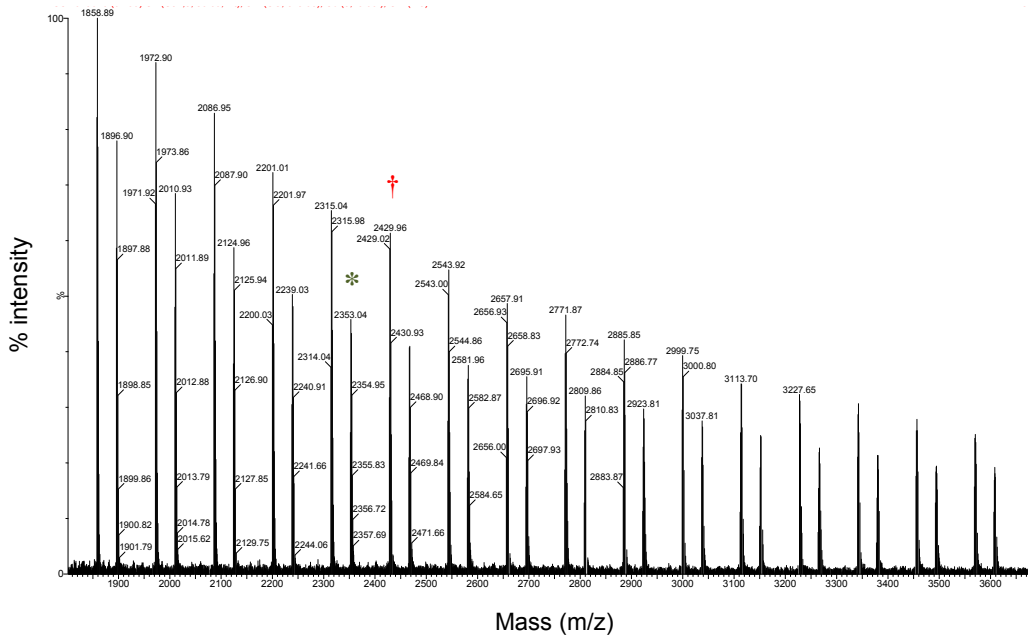

Figure 4.12. MALDI-ToF MS of a mixture of benzyloxy ester (green asterisk) and methoxy ester (red dagger) end-capped PCL obtained from the iROP of [ε-CL]:[**2**]:[PhCHO]:[$B(OMe)_3$] = 200:1:5:1 in THF at 23 °C. M_n by GPC analysis was 1,570 g mol^{-1}. K^+ dopant, Δ(m/z) = 114.1 g mol^{-1}.

$B(OMe)_3$ and HBPin were also employed as CTAs by addition into a THF solution of $(Tp^{tBu,Me})Mg(BH_4)$ (**2**) prior to polymerisation. As described previously, the exchange reactions between the tetrahydroborate group and $B(OMe)_3$ or HBPin were not observed under these conditions. The iROP catalysed by catalyst **2** in the presence of $B(OBn)_3$ or HBPin proceeded *in a* controlled manner as shown by linear plots between M_n (GPC) and % conversion (Figure 4.13). Higher than expected molecular weight PCL was obtained using catalyst **2** in the presence of 3 equivs. of HBPin. The gradient of the M_n (GPC) *vs*. % conversion plot is 88(4) g mol^{-1} (% conversion)$^{-1}$, R^2 = 0.987 (the expected M_n for four chains PCL produced per metal centre is 57.1 g mol^{-1} (% conversion)$^{-1}$). PCL with M_n closer to the expected value (40(2) g mol^{-1} (% conversion)$^{-1}$, R^2 = 0.988) was obtained when six equivs. of HBPin were added into a solution of catalyst **2** prior to polymerisation (Figure 4.14) - the expected M_n for seven chains PCL produced per metal centre is 32.6 g mol^{-1} (% conversion)$^{-1}$. In both cases, the molecular weight distributions of the resultant PCL are moderate; PDIs = 1.19-1.40 and 1.25-1.59 for iROP using 3 and 6 equivs. of HBPin, respectively.

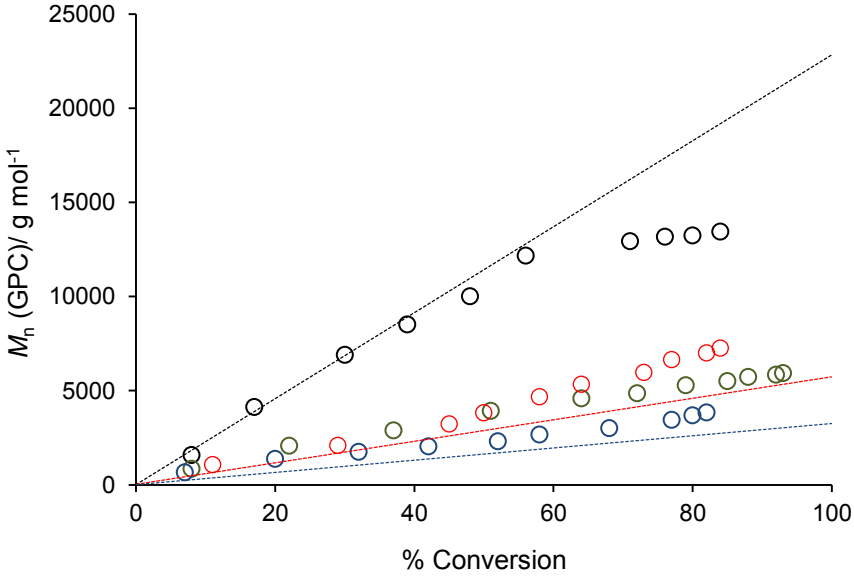

Figure 4.13. Data for iROP of ε-CL using $(Tp^{tBu,Me})Mg(BH_4)$ (**2**) and various additives. M_n (GPC) vs. Conversion plot. The black, red and blue dotted lines are that expected for one, four and seven PLA chains per metal centre, respectively. Conditions: 3.4 mL THF, 23 °C, $[\varepsilon\text{-CL}]_0$ = 1 M, $[\varepsilon\text{-CL}]_0$:[**2**]$_0$ = 200:1 and PDIs = 1.12-1.33 (black circles), $[\varepsilon\text{-CL}]_0$:[**2**]$_0$:[HBPin] = 200:1:3 and PDIs = 1.19-1.40 (red circles), $[\varepsilon\text{-CL}]_0$:[**2**]$_0$:[HBPin] = 200:1:6 and PDIs = 1.25-1.59 (blue circles), $[\varepsilon\text{-CL}]_0$:[**2**]$_0$:[$B(OMe)_3$] = 200:1:1 and PDIs = 1.24-1.58 (green circles).

The use of $B(OMe)_3$ as a CTA in the iROP of ε-CL using catalyst **2** produced PCL with M_n in much better agreement to that expected than that obtained from the equivalent experiment using HBPin as a CTA. The gradient of the M_n vs. % conversion plot is 57(2) g mol^{-1} (% conversion)$^{-1}$ (Figure 4.13). Moderate PDI values of 1.24-1.58 were also obtained. Owing to the striking performance of $B(OMe)_3$ as a CTA, the iROP was extended to cover a range of equivalents of ε-CL (200-400 equivs.) and $B(OMe)_3$ (1-4 equivs.). The linear plot between M_n *vs*. the ratio of concentration of ε-CL to the number of chains of PCL produced was obtained with a gradient of 110(3) g mol^{-1}. This is identical within error to the expected value of 114.3 g mol^{-1} (Figure 4.14).

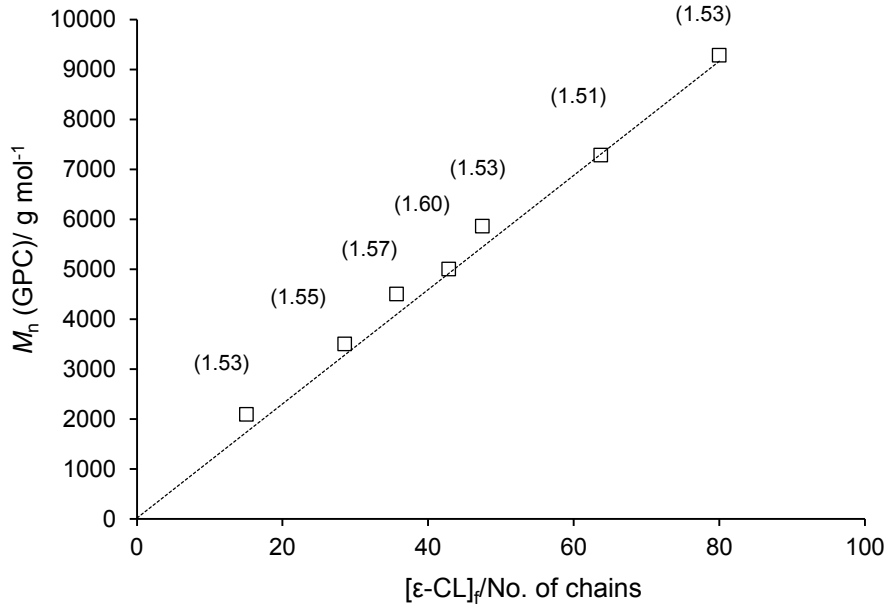

Figure 4.14. Data for iROP of ε-CL using ($Tp^{tBu,Me}$)$Mg(BH_4)$ (**2**) and various equivalents of $B(OMe)_3$. M_n (GPC) vs. [ε-CL]$_f$/No. of chains plot. The dotted line is that expected for M_n at 100% monomer conversion at each [ε-CL]$_f$/No. of chains. Conditions: 3.4 mL THF, 23 °C, [ε-CL]$_0$:[**2**]$_0$:[$B(OMe)_3$] = 200-400:1:1-4. PDI values are given in parentheses.

The benchmarking iROP of ε-CL using compound **2** with various equivalents of HBPin as a CTA showed first order consumption of ε-CL with comparable, within error, apparent rate constants; k_{app} = 0.019(1) min^{-1} (R^2 = 0.994) for [ε-CL]$_0$:[**2**]$_0$:[HBPin] = 200:1:3 and k_{app} = 0.019(1) min^{-1} (R^2 = 0.988) for [ε-CL]$_0$:[**2**]$_0$:[HBPin] = 200:1:6. These apparent rate constants of iROP using HBPin as a CTA are similar to the ROP of ε-CL using solely **2** (k_{app} = 0.017(1) min^{-1} (R^2 = 0.991)

for $[\varepsilon\text{-CL}]_0$:[**2**]$_0$ = 200:1), and marginally slower than that of the related iROP experiment using $B(OMe)_3$ as a CTA (k_{app} = 0.027(1) min^{-1} (R^2 = 0.995) for $[\varepsilon\text{-CL}]_0$:[**2**]$_0$:$[B(OMe)_3]$ = 200:1:1) (Figure 4.16). Moreover, it is worth noting that short induction periods were common among these iROP experiments.

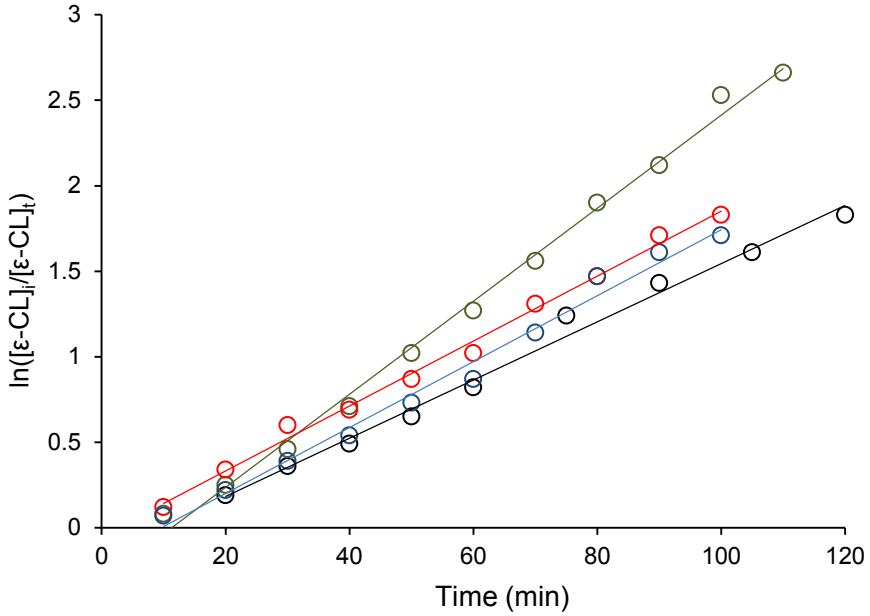

Figure 4.15. First order plot of $\ln([\varepsilon\text{-CL}]_i/[\varepsilon\text{-CL}]_t)$ *vs*. time for the iROP of ε-CL using ($Tp^{tBu,Me}$)$Mg(BH_4)$ (**2**) and various additives. Rate constants: k_{app} = 0.017(1) min^{-1} (R^2 = 0.991, $[\varepsilon\text{-CL}]_0$:[**2**]$_0$ = 200:1, black circles), k_{app} = 0.019(1) min^{-1} (R^2 = 0.994, $[\varepsilon\text{-CL}]_0$:[**2**]$_0$:[HBPin] = 200:1:3, red circles), k_{app} = 0.019(1) min^{-1} (R^2 = 0.988, $[\varepsilon\text{-CL}]_0$:[**2**]$_0$:[HBPin] = 200:1:6, blue circles) and k_{app} = 0.027(1) min^{-1} (R^2= 0.995, $[\varepsilon\text{-CL}]_0$:[**2**]$_0$:$[B(OMe)_3]$ = 200:1:1, green circles).

^{1}H NMR spectroscopic and MALDI-ToF MS analyses of the polymer formed from the iROP of ε-CL using compound **2** with $[\varepsilon\text{-CL}]_0$:[**2**]$_0$:[HBPin] = 200:1:3 or 6 showed a mixture of aldehyde end-capped and α,ω-dihydroxy telechelic PCL (Figure 4.16, top). Whilst a mixture of methoxy ester end-capped and α,ω-dihydroxy telechelic PCL was obtained through ε-CL iROP with $[\varepsilon\text{-CL}]_0$:[**2**]$_0$:$[B(OMe)_3]$ = 200:1:1 (Figure 4.16, bottom).

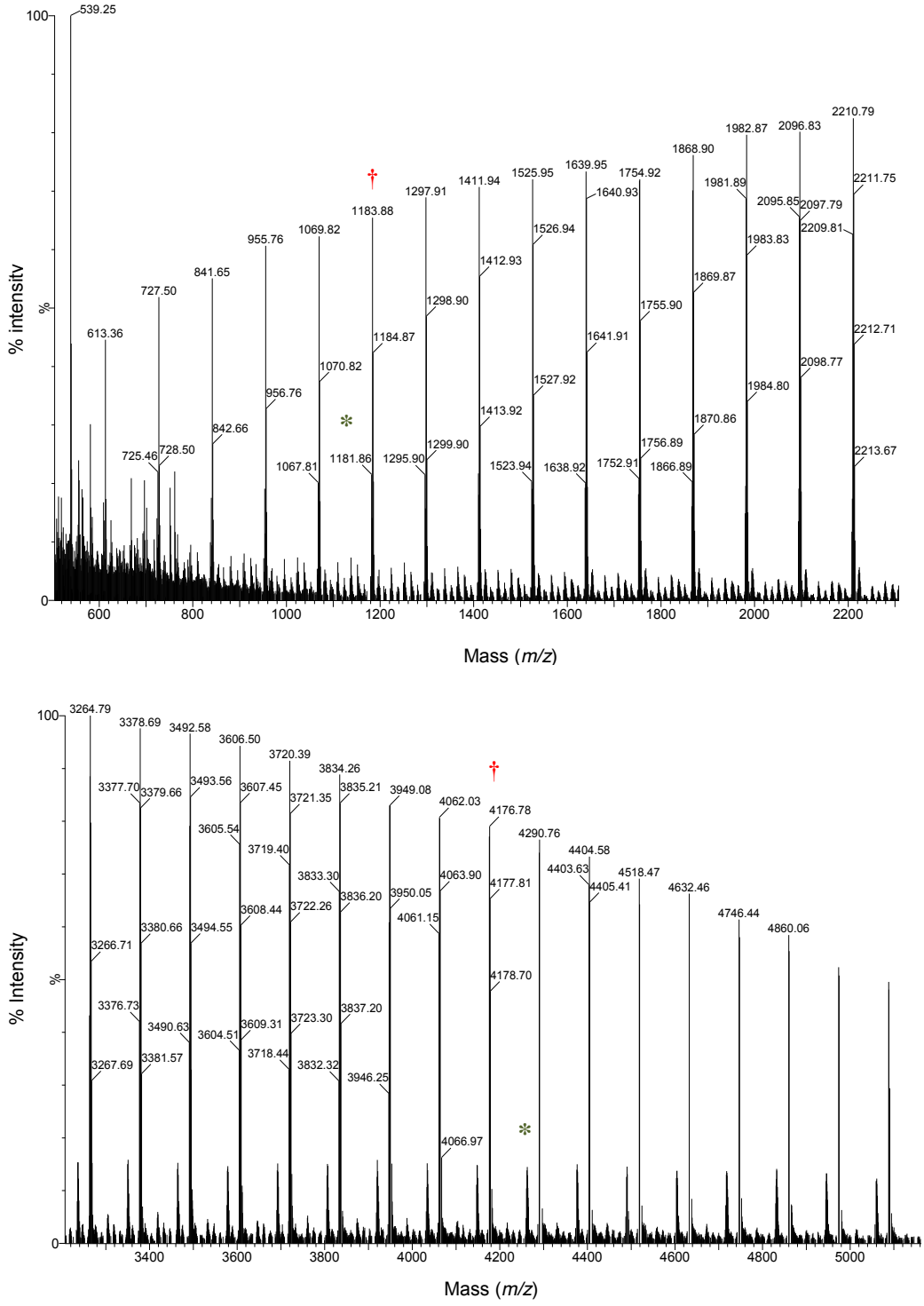

Figure 4.16. MALDI-ToF MS of a mixture of aldehyde end-capped PCL (green asterisk) and α,ω-dihydroxy telechelic PCL (red dagger) synthesised using [ε-CL]:[**2**]$_0$:[HBPin] = 200:1:3 polymerisation at 23 °C. M_n by GPC analysis was 2,090 g mol^{-1} (top). MALDI-ToF MS of a mixture of methoxy ester end-capped PCL (red dagger) and α,ω-dihydroxy telechelic PCL (green asterisk) synthesised using [ε-CL]:[**2**]$_0$:[B(OMe)$_3$] = 200:1:1 polymerisation at 23 °C. M_n by GPC analysis was 2,070 g mol^{-1}. K^+ dopant, Δ(m/z) = 114.1 g mol^{-1} (bottom).

The results obtained from the ε-CL iROP experiments in both THF and toluene using **2** with various additives are summarised in Table 4.2. The equivalent iROP experiments, using either *in situ* generated or isolated magnesium initiators with $B(OR)_3$ and HBPin as CTAs, were also carried out in toluene. The PCL obtained from these iROP experiments gave close to expected M_n and broad PDIs. Linear evolution of M_n with % conversion plots were obtained in all cases (Appendix, Figure A4.1 and A4.2). The polymer properties were analogous to those obtained from the related iROP experiments in THF.

All iROP experiments in toluene gave first order consumption of ε-CL (Appendix, Figure A4.3 and A4.4). The apparent rate constants were measured from gradients of the plots of $\ln([\varepsilon\text{-CL}]_i/[\varepsilon\text{-CL}]_t)$ *vs*. time and are summarised in Entries 8-13, Table 4.3. In general, the rates of propagation in toluene are faster than the comparable experiments in THF which is accounted for by the competition for the coordination between a donor solvent such as THF and monomer. The apparent rate constants drawn from these ε-CL iROPs in toluene are fairly similar to each other within experimental error and therefore do not indicate a change in mechanism.

Table 4.2. Immortal ring-opening polymerisation of ε-CL using ($Tp^{tBu,Me}$)$Mg(BH_4)$ (**2**) with various additives.

Entry	Catalyst	Equivs. of additive			Time (min)	Conversion (%)[c]	Yield (%)[d]	M_n (GPC)[e]	M_n (Calcd)[f]	PDI[g]	k_{app} (min^{-1})[h]	R^{2h}
		PhCHO	$B(OMe)_3$	HBPin								
1	**2**[a]				60	56	-	12,160	12,780	1.17	-	-
2	**2**[a]				120	84	79	13,440	19,180	1.33	0.017(1)	0.991
3	**2**[a]	5			100	86	64	5,270	5,020	1.48	0.021(1)	0.991
4	**2**[a]	5	1		110	90	44	3,010	3,010	1.53	0.022(1)	0.991
5	**2**[a]		1		110	93	63	5,930	5,340	1.57	0.027(1)	0.995
6	**2**[a]			3	100	84	72	7,260	4,800	1.26	0.019(1)	0.994
7	**2**[a]			6	100	82	68	3,850	2,680	1.27	0.019(1)	0.988
8	**2**[b]				80	95	83	20,690	21,690	1.18	0.045(1)	0.992
9	**2**[b]	5			90	91	49	6,650	5,300	1.55	0.026(1)	0.994
10	**2**[b]	5	1		90	96	60	3,930	3,210	1.65	0.037(1)	0.993
11	**2**[b]		1		100	100	85	5,680	5,710	1.64	0.058(1)	0.997
12	**2**[b]			3	90	99	81	8,060	5,650	1.30	0.056(1)	0.995
13	**2**[b]			6	90	98	69	5,000	3,200	1.32	0.049(1)	0.996

[a] Conditions : [ε-CL]$_0$:[**2**]$_0$:[additive] = 200:1:as stated, 3.4 mL of THF at 23 ºC, [ε-CL]$_0$ = 1.0 M. [b] Conditions : [ε-CL]$_0$:[**2**]$_0$:[additive] = 200:1:as stated, 3.4 mL of toluene at 23 ºC, [ε-CL]$_0$ = 1.0 M. [c] Measured by ^{1}H NMR ($CDCl_3$) analyses. [d] Isolated yield at 100% conversion. [e] Molecular weights (g mol^{-1}) determined by GPC in THF at 30 ºC using the appropriate Mark-Houwink corrections. [f] Expected M_n (g mol^{-1}) for stated number of chains per metal centre at the stated % conversion; M_n (Calcd for entries 1, 2 and 8) = conversion (%) × 200 × 144.1 + 4, M_n (Calcd for entries 3 and 9) = 1/4 × (conversion (%) × 200 × 144.1) + 108.1, M_n (Calcd for entries 4 and 10) = 1/7 × (conversion (%) × 200× 144.1) + 75.5, M_n (Calcd for entries 5 and 11) = 1/4 × (conversion (%) × 200 × 144.1) + 32.0, M_n (Calcd for entries 6 and 12) = 1/4 × (conversion (%) × 200× 144.1) + 2.5 and M_n (Calcd for entries 7 and 13) = 1/7 × (conversion (%) × 200 × 144.1) + 2.3. [g] PDI = M_w/M_n. [h] Apparent first-order rate constants for consumption of ε-CL with standard error and R^2 determined by linear regression analysis.

4.4.2 Proposed mechanism for the iROP of ε-CL using magnesium initiators

So far, the studies have established a new class of chain-transfer agents ($B(OR)_3$ and HBPin) in the iROP of ε-CL using $Tp^{tBu,Me}$ supported magnesium initiators. To provide further insight into the iROP process, an NMR tube scale reaction of the *in situ* generated catalyst **10** and $B(OBn)_3$, from the mixture of [**2**]:[PhCHO] in a 1:4 ratio, and 10 equivs. of ε-CL was carried out at 298 K. The reaction was monitored by ^1H and ^{11}B NMR analyses (Figure 4.17).

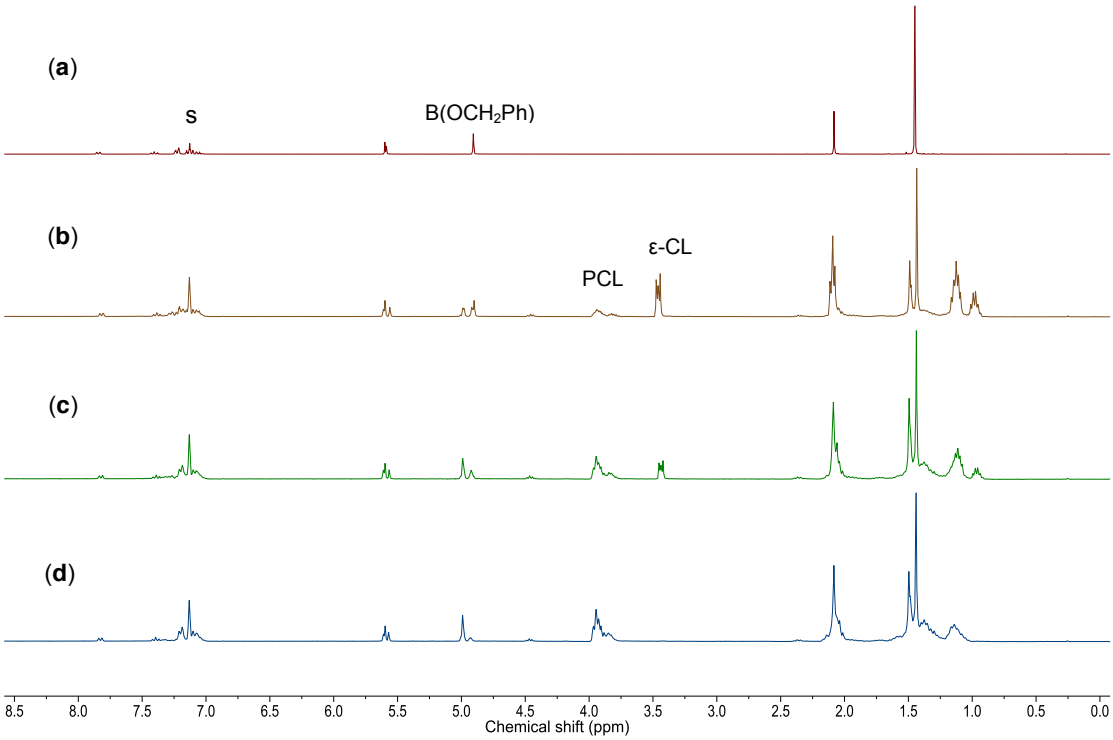

Figure 4.17. ^1H NMR spectra (299.9 MHz, C_6D_6, 298 K) of the PCL formed from the NMR tube scale *in situ* generated iROP between the *in situ* generated catalyst **10** and $B(OBn)_3$, from a mixture of [**2**]:[PhCHO] in a 1:4 ratio, and 10 equivs. of ε-CL. (a) the *in situ* generated catalyst **10** and $B(OBn)_3$, (b) 30 % PCL observed, (c) 80 % PCL observed and (d) 100 % PCL observed.

Upon polymerising ε-CL, multiple resonances corresponding to the $Tp^{tBu,Me}$ ligand and the methylene protons of the benzyloxy group were observed in ^1H NMR spectra (Figure 4.18, (b), (c) and (d)). The related ^{11}B NMR spectra showed resonances at δ = -9.5 and 18.7 ppm, corresponding to the B-H of the $Tp^{tBu,Me}$ ligand and $B(OR)_3$ (R = alkyl or polymeryl) species, respectively. These spectroscopic results therefore confirm the participation of $B(OBn)_3$ in the polymerisation. This investigation, in

conjunction with the results of the corresponding iROP (Section 4.4.1) led to the proposed pathway of iROP using $Tp^{tBu,Me}$ supported magnesium alkoxide initiators with $B(OR)_3$ (Scheme 4.4).

In the presence of $B(OR)_3$, $(Tp^{tBu,Me})Mg(OBn)$ (**10**) or $(Tp^{tBu,Me})Mg(BH_4)$ (**2**) initiates iROP *via* the coordination-insertion mechanism with $k_i >> k_p$. The well-controlled iROP experiments discussed in Section 4.4.1 signify the facile, reversible chain transfer reaction between the active growing polymer chains and the dormant species $B(OR)_3$ (R = Me or Bn) with $k_{tr} >> k_p$. Owing to the existence of an equilibrium between the magnesium alkoxide compound, $B(OR)_3$ and their adduct, the chain transfer reaction is expected to proceed *via* a tetra(alkoxy) borate adduct intermediate. During formation of the tetra-alkoxy borate adduct transition state, an intramolecular exchange between the bridging and terminal alkoxide substituents allows the formation of a new magnesium (-OR) alkoxide initiator along with a $B(OR)_3$ species (R = alkyl or polymeryl) as a new dormant species. Furthermore, it is worth noting that the rates of the reversible chain transfer reactions and the intramolecular exchange may be the cause of the broadening of the molecular weight distribution in iROP using $B(OR)_3$. Finally, termination ultimately results in the formation of multiple PCL chains produced per metal centre.

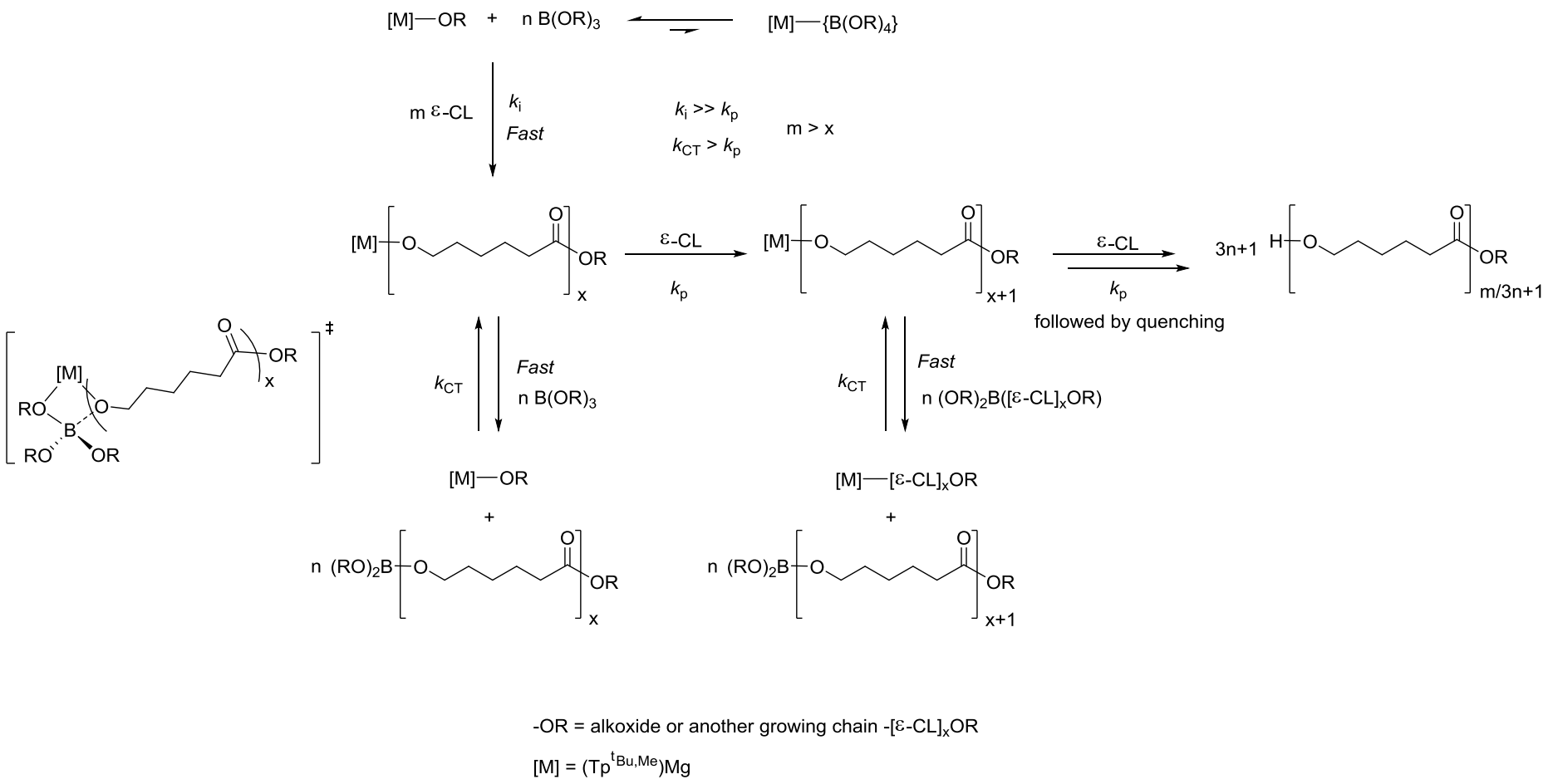

Scheme 4.4. Proposed pathway for iROP of ε-CL using $Tp^{tBu,Me}$ supported magnesium initiators and $B(OR)_3$ as CTA

iROP using ($Tp^{tBu,Me}$)$Mg(BH_4)$ (**2**) and HBPin as a CTA was expected to adopt the same pathway as previously discussed (Scheme 4.4). The chain transfer reaction between a growing polymer chain on the metal centre and HBPin, *via* a tetra-coordinate boron transition state, resulted in (OR)BPin (R = polymeryl species) and a transient magnesium hydride species (*vide infra)*. The stoichiometric ROP of ε-CL with the active magnesium hydride initiator is expected to produce aldehyde terminated PCL. Nevertheless, a side reaction could take place, whereby the excess HBPin in the presence of a magnesium alkoxide derivative could catalyse the hydroboration of aldehyde terminal PCL to –OBPin end-capped PCL and to α,ω-dihydroxy telechelic PCL after quenching (*vide infra*). The ability of HBPin to catalyse the hydroboration of a carbonyl group in the presence of metal-alkoxide compounds was also demonstrated by Clark and co-workers in 2011.[79] The presence of this side reaction is reflected in a higher molecular weight than expected PCL featuring a mixture of aldehyde and α,ω-dihydroxy end groups. The ^1H NMR ($CDCl_3$) of the isolated PCL also showed a lower than expected integration of the aldehyde proton, when calculated against the equivalents of HBPin used in the iROP experiment (Appendix, Figure A4.5)

Of special relevance to this work using HPBin as a CTA is also the work reported by Yasuda and coworkers, describing the living ROP of ε-CL using $[Cp^*Sm(\mu\text{-}H)]_2$ ($Cp^* = C_5Me_5$). The stoichiometric reaction of 0.5 equivs. of the hydride catalyst to an equivalent of ε-CL showed the formation of 1,6-hexanediol, following further aldehyde reduction by the active hydride catalyst, which was claimed as an intermediate in the polymerisation. Further aldehyde reduction by the active hydride catalyst was responsible for the observation.[80, 81]

It is also worth noting that the tetra-coordinate boron containing transition state in the chain-transfer polymerisation using HBPin as a CTA is reminiscent of the intermediate proposed in the ethylene polymerisation reported by Chung *et al*. (Scheme 4.1).[36]

4.4.3 Immortal ROP of *rac*-LA using magnesium initiators

Building on the success of iROP of ε-CL using magnesium initiators and $B(OR)_3$ or HBPin as CTAs, iROP studies with *rac*-LA were also undertaken. The detailed kinetic investigations of the iROP using either the *in situ* generated **10** and $B(OBn)_3$

or isolated **10** and various additives were carried out and directly compared. The *rac*-LA iROP results are summarised in Table 4.3.

Table 4.3. iROP of *rac*-LA using magnesium initiators and various additives

Catalyst	Additive (Equivs.)	Time (h)	Conversion (%)[b]	M_n (GPC)[c]	M_n (Calcd)[d]	PDI[e]	P_r[f]
10	-	17	86	13,540	12,500	1.10	0.61
10	$B(OBn)_3$ (1)	12	97	4,380	3,240	1.17	0.65
2	PhCHO (5)	12	93	4,420	3,460	1.15	0.67
10	BnOH (3)	4.5	95	3,820	3,530	1.11	0.66

[a] Conditions: [*rac*-LA]$_0$:[catalyst]$_0$:[additive]$_0$ = 100:1:as specified, 6.0 mL THF at 23 °C, [*rac*-LA]$_0$ = 0.5 M. [b] Determined by ^{1}H NMR integration of the OC<u>H</u>Me resonance relative intensities of the residual *rac*-LA and PLA in $CDCl_3$. [c] M_n (g mol^{-1}) determined by GPC using the appropriate Mark-Houwink corrections. [d] Expected M_n (g mol^{-1}) for 1 chain growing per metal centre at the stated conversion: M_n = conversion (%) × 100 × 144.1 + 108.1. [e] PDI = M_w/M_n. [f] Determined by analysis of the OC<u>H</u>Me resonances of selectively homonuclear decoupled ^{1}H{^{1}H} spectra.

($Tp^{tBu,Me}$)Mg(OBn) (**10**) is previously described (Chapter Three) as an efficient catalyst for the well-controlled polymerisation of *rac*-LA with one PLA chain of narrow PDI (1.06-1.13) produced per metal centre. In light of this $B(OBn)_3$ was introduced as a CTA into the system, in order to convert the traditional living ROP into iROP. The iROP using either $B(OBn)_3$ ([*rac*-LA]$_0$:[**10**]$_0$:[$B(OBn)_3$] = 100:1:1) or an *in situ* generated $B(OBn)_3$ ([*rac*-LA]$_0$:[**2**]$_0$:[PhCHO] = 100:1:5) were pursued. The investigations allowed an evaluation of $B(OBn)_3$ as a CTA in iROP of *rac*-LA.

Both iROP experiments ([*rac*-LA]$_0$:[**10**]$_0$:[$B(OBn)_3$] = 100:1:1 and [*rac*-LA]$_0$:[**2**]$_0$:[PhCHO] = 100:1:5) afforded highly controlled polymerisations, whereby a linear evolution of M_n (GPC) with % conversion was achieved with narrow PDI values (1.14-1.19 and 1.11-1.19, respectively) throughout the polymerisation (Figure 4.18). Heterotactic PLA (P_r = 0.65-0.67) featuring benzyloxy ester end-groups was obtained in both cases. The stereoselectivity in the iROP with $B(OBn)_3$ as CTA is comparable to that obtained in the *rac*-LA ROP using **10**. This suggests that the $B(OBn)_3$ has no influence over the tacticity, which is determined by the chain-end control mechanism.

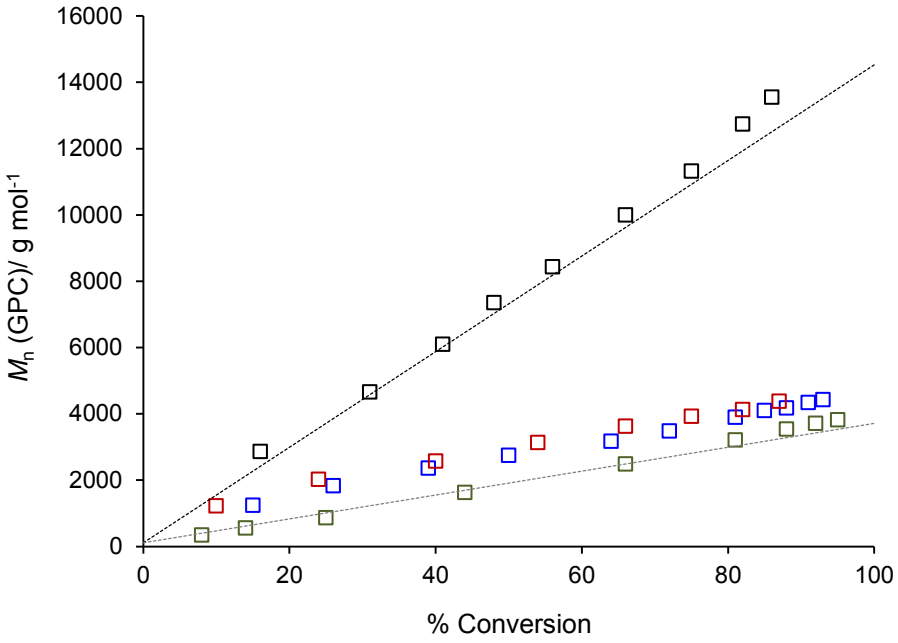

Figure 4.18. Data for the iROP of *rac*-LA using ($Tp^{tBu,Me}$)Mg(BH_4) (**2**) or ($Tp^{tBu,Me}$)Mg(OBn) (**10**) and various additives. M_n (GPC) vs. Conversion plot. The black and grey dotted lines are that expected for one and four PLA chains per metal centre, respectively. Conditions: 6.0 mL THF, 23 °C, [*rac*-LA]$_0$ = 0.5 M, [*rac*-LA]$_0$:[**10**]$_0$ = 100:1 and PDIs = 1.06-1.13 (black squares), [*rac*-LA]$_0$:[**10**]$_0$:[$B(OBn)_3$] = 100:1:1 and PDIs = 1.14-1.19 (red squares), [*rac*-LA]$_0$:[**2**]$_0$:[PhCHO] = 100:1:5 and PDIs = 1.11-1.19 (blue squares), [*rac*-LA]$_0$:[**10**]$_0$:[BnOH] = 100:1:3 and PDIs = 1.01-1.12 (green squares).

The PLA obtained from the *rac*-LA iROP, which shows good agreement to the expected M_n and narrow PDIs, reflects a high efficiency of $B(OBn)_3$ as CTA in providing a significantly higher rate of chain-transfer reaction to the rate of propagation ($k_{tr} >> k_p$). By analogy to the iROP of ε-CL, the iROP of *rac*-LA using magnesium initiator and $B(OR)_3$ as a CTA is believed to proceed *via* tetra-alkoxy borate transition state during the chain-transfer reaction (Scheme 4.4).

The apparent rates of propagation in iROP using $B(OBn)_3$ as a CTA were monitored, showing first order dependence on the *rac*-LA concentration with k_{app} = 0.188(7) h^{-1} (R^2 = 0.992) and 0.262(7) h^{-1} (R^2 = 0.993) for [*rac*-LA]$_0$:[**2**]$_0$:[$B(OBn)_3$] = 100:1:1 and [*rac*-LA]$_0$:[**2**]$_0$:[PhCHO] = 100:1:5, respectively (Figure 4.19). The apparent rate constant of the *in situ* generated iROP is marginally higher than the analogous system with the addition of $B(OBn)_3$ reagent and the *rac*-LA ROP using **10,** with short

induction periods shown in all cases. The differences in the rate constants of $B(OBn)_3$ chain-transferred iROP experiments and the ROP using **10** are not large enough, taking into account experimental error, to imply a change in mechanism. However, the small differences in the apparents constants in the presence of $B(OBn)_3$ (*in situ* generated or added) have no obvious explaination.

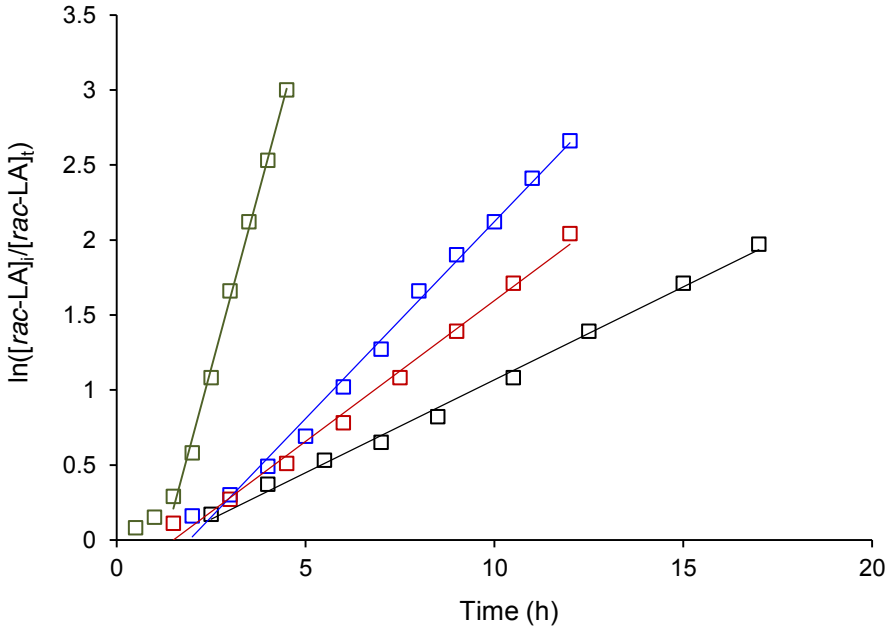

Figure 4.19. First order plot of $\ln([rac\text{-LA}]_i/[rac\text{-LA}]_t)$ *vs*. time for the iROP of *rac*-LA using ($Tp^{tBu,Me}$)$Mg(BH_4)$ (**2**) or ($Tp^{tBu,Me}$)Mg(OBn) (**10**) and various additives. Rate constants, k_{app} = 0.124(3) h^{-1} (R^2 = 0.996) for $[rac\text{-LA}]_0$:$[\mathbf{10}]_0$ = 100:1, black squares, k_{app} = 0.188(7) h^{-1} (R^2 = 0.992) for $[rac\text{-LA}]_0$:$[\mathbf{2}]_0$:$[B(OBn)_3]$ = 100:1:1, red squares, k_{app} = 0.262(7) h^{-1} (R^2 = 0.993) for $[rac\text{-LA}]_0$:$[\mathbf{2}]_0$:[PhCHO] = 100:1:5, blue squares and k_{app} = 0.93(2) h^{-1} (R^2 = 0.996) for $[rac\text{-LA}]_0$:$[\mathbf{10}]_0$:[BnOH] = 100:1:3, green squares (measured from 25 % conversion).

In contrast to the successful synthesis of **4.1**, an attempt to achieve an *in situ* generated iROP catalyst and $B(OBn)_3$ from the reaction of ($Tp^{tBu,Me}$)$Mg(BH_4)$ (**2**) and 4 equivs. of BnOH was unsuccessful. ^1H and ^{11}B NMR analyses showed the production of the desired product **10** and $B(OBn)_3$ alongside various other boron-containing species. This observation is similar to the work reported by Ephritikhine, Vigner and co-workers, whereby the alcoholysis of uranium bis(tetrahydroborate) compound resulted in the corresponding uranium alkoxide and substituted alkyl borates ($BH_{4-n}(OR)_{n-1}$, $n \leq 4$).[82]

As previously described in Section 1.5, the common chain-transfer agents used in the iROP of cyclic esters are protic species. The iROP using compound **10** and BnOH as CTA with [*rac*-LA]$_0$:[**10**]$_0$:[BnOH] = 100:1:3 was conducted under the same polymerisation conditions. This allowed a direct comparison between the protic agent and B(OBn)$_3$ as CTAs. The iROP using BnOH as a CTA illustrated a superior-controlled polymerisation, reflected by a linear increase in M_n with % conversion and narrow PDI values (1.01-1.12). The gradient of the M_n (GPC) *vs*. % conversion plot was 40.6(8) g mol^{-1} (conversion)$^{-1}$ (R^2 = 0.997), which is close to the expected value for 4 PLA chains produced per metal centre (36.0 g mol^{-1} (conversion)$^{-1}$). With close inspection, the M_n of the PLA produced in the BnOH chain-transferred iROP was closer to the expected value than those obtained in the B(OBn)$_3$ chain-transferred iROP (Figure 4.18). Furthermore, the heterotactic PLA produced (P_r = 0.66) also featured benzyloxy ester end-group.

The polymerisation kinetics was subsequently followed, showing an intriguing result. The iROP showed a significant induction period, which could involve the aggregation or coordination of the initiator **10** with BnOH, prior to rapid polymerisaiton. The apparent rate of polymerisation was first order with respect to the concentration of *rac*-LA with k_{app} = 0.93(2) h^{-1} (R^2 = 0.996), measured after 25 % monomer conversion (i.e. after the induction period). The significantly higher apparent rate constant of BnOH chain-transferred iROP than those recorded for B(OBn)$_3$ chain-transferred iROP experiments, indicates a possible change in mechanism from coordination-insertion to activated monomer mechanism. iROP proceeding through the activated monomer mechanism using alkaline earth initiators is well documented in the literature. Recent work in this area were reported by Carpentier *et al*. using [{L}M]$^+$[H$_2$N{B(C$_6$F$_5$)$_3$}$_2$]$^-$ ({L} = 2-[(1,4,7,10-tetraoxa-13-azacyclopentadecan-13-yl)methyl]-4,6-di-t*ert*-butylphenol or 2-[(1,4,7,10-tetraoxa-13-azacyclopentadecan-13-yl)methyl]-1,1,1,3,3,3-hexafluoropropan-2-ol, and M = Zn, Mg, Ca, Sr or Ba), and alcohols.[83-85]

A ^{1}H NMR (C_6D_6) analysis of an NMR tube scale reaction between (Tp^{tBu,Me})Mg(OBn) (**10**) and an equivalent of ^{i}PrOH was carried out. Neither an exchange reaction to form (Tp^{tBu,Me})Mg(O^{i}Pr) and BnOH nor a degradation of the Tp^{tBu,Me} ligand was observed in the course of 6 h at room temperature. This reinforced the possibility of activated monomer mechanism taking place when BnOH was used

as a CTA, in conjunction with compound **10**. Further in-depth NMR analyses and comparative iROP experiment are underway to explain this observation.

4.4.4 Immortal ROP of ε-CL using calcium and strontium initiators

The *in situ* generated calcium and strontium catalysts (from the reaction between **1** or **4** and 5 equivs. of PhCHO) predominantly exist as adducts, $(Tp^{tBu,Me})M\{B(OBn)_4\}$ in solution (**13b** and **14**, respectively). The *in situ* catalyst preparation and the polymerisation conditions are analogous to those stated in Section 4.4. Similar to the previous studies, the polymerisation experiments were carried out in both THF and toluene. The iROP of ε-CL using the calcium (**1**) and strontium (**4**) tetrahydroborate initiators in conjunction with various additives ($B(OR)_3$, HBPin or PhCHO) are summarised in Tables 4.4 and 4.5, respectively.

The *in situ* generated calcium catalysts **13a**/$B(OBn)_3$ and **13b** are extremely active towards the iROP of ε-CL with $B(OR)_3$ and HBPin as CTAs, over 98 % monomer conversions achieved within two mins (Entries 2, 3, 7 and 8, Table 4.4). Unfortunately, this increased rate prevents monitoring of their kinetic profiles under these conditions. Multiple PCL chains were produced per metal centre. However, the molecular weights obtained were generally higher than expected (Entries 2, 3, 7 and 8, Table 4.4). The extremely fast rate of propagation (and hence low ratio of k_{tr}/k_p) is thought to be responsible for the observations. Moderate molecular weight distribution was obtained in all cases with PDIs of 1.43-1.68. Furthermore, no kinetic difference was observed between the iROP of ε-CL in THF or toluene. This is consistent with the earlier observations stated in Section 4.3, whereby THF showed negligible effect on the association/dissociation equilibrium between the alkoxide complex and its corresponding borate adduct. The MALDI-ToF MS and ^{1}H NMR analyses showed the expected end-capped PCL: benzyloxy ester end-capped PCL (Entries 2 and 7, Table 4.4), and a mixture of benzyloxy ester and methoxy ester end-capped PCL (Entries 3 and 8, Table 4.4).

Table 4.4. Immortal ring-opening polymerisation of ε-CL using ($Tp^{tBu,Me}$)Ca(BH_4)(THF) (**1**) with various additives.

Entry	Catalyst	Equivs. of additive			Time (min)	Conversion (%)[c]	Yield (%)[d]	M_n (GPC)[e]	M_n (Calcd)[f]	PDI[g]	k_{app} (min^{-1})[h]	R^{2h}
		PhCHO	$B(OMe)_3$	HBPin								
1	**1**[a]				2	100	87	62,250	22,830	1.27	[i]	[i]
2	**1**[a]	5			1	100	83	9,410	5,730	1.68	[i]	[i]
3	**1**[a]	5	1		2	100	80	4,790	3,270	1.65	[i]	[i]
4	**1**[a]			3	5	100	82	12,360	5,710	1.44	1.20(5)	0.987
5	**1**[a]			6	7	100	67	5,950	3,260	1.48	0.84(2)	0.996
6	**1**[b]				1	100	89	55,440	22,830	1.30	[i]	[i]
7	**1**[b]	5			1	100	94	7,560	5,730	1.62	[i]	[i]
8	**1**[b]	5	1		1	98	83	3,730	3,210	1.43	[i]	[i]
9	**1**[b]			3	5	98	74	8,980	5,650	1.24	0.98(2)	0.995
10	**1**[b]			6	8	98	68	4,880	3,200	1.22	0.55(1)	0.996

[a] Conditions : $[\varepsilon\text{-CL}]_0$:[**2**]$_0$:[additive] = 200:1:as stated, 3.4 mL of THF at 23 ºC, $[\varepsilon\text{-CL}]_0$ = 1.0 M. [b] Conditions : $[\varepsilon\text{-CL}]_0$:[**2**]$_0$:[additive] = 200:1:as stated, 3.4 mL of toluene at 23 ºC, $[\varepsilon\text{-CL}]_0$ = 1.0 M. [c] Measured by ^{1}H NMR ($CDCl_3$) analyses. [d] Isolated yield at 100% conversion. [e] Molecular weights (g mol^{-1}) determined by GPC in THF at 30 ºC using the appropriate Mark-Houwink corrections. [f] Expected M_n (g mol^{-1}) for stated number of chains per metal centre at the stated % conversion; M_n (Calcd for entries 1 and 6) = conversion (%) × 200 × 144.1 + 4, M_n (Calcd for entries 2 and 7) = 1/4 × (conversion (%) × 200 × 144.1) + 108.1, M_n (Calcd for entries 3 and 8) = 1/7 × (conversion (%) × 200× 144.1) + 75.5, M_n (Calcd for entries 4 and 9) = 1/4 × (conversion (%) × 200× 144.1) + 2.5 and M_n (Calcd for entries 5 and 10) = 1/7 × (conversion (%) × 200 × 144.1) + 2.3. [g] PDI = M_w/M_n. [h] Apparent first-order rate constants for consumption of ε-CL with standard error and R^2 determined by linear regression analysis. [i] Not measured.

Table 4.5. Immortal ring-opening polymerisation of ε-CL using ($Tp^{tBu,Me}$)$Sr(BH_4)(THF)_2$ (**4**) with various additives.

Entry	Catalyst	Equivs. of additive			Time (min)	Conversion (%)[c]	Yield (%)[d]	M_n (GPC)[e]	M_n (Calcd)[f]	PDI[g]	k_{app} (min^{-1})[h]	R^{2h}
		PhCHO	$B(OMe)_3$	HBPin								
1	**4**[a]				85	97	97	30,910	22,140	1.46	[j]	[j]
2	**4**[a]	5			1	100	83	15,680	5,730	1.64	[i]	[i]
3	**4**[a]	5	1		19	98	80	5,270	3,270	1.60	[j]	[j]
4	**4**[a]			3	40	98	82	11,010	5,600	1.44	0.109(3)	0.992
5	**4**[a]			6	40	98	67	6,520	3,200	1.37	0.107(2)	0.995
6	**4**[b]				7	80	80	106,190	18,260	1.20	[i]	[i]
7	**4**[b]	5			1	100	94	16,990	5,730	1.63	[i]	[i]
8	**4**[b]	5	1		18	100	83	7,710	3,340	1.64	[j]	[j]
9	**4**[b]			3	40	95	74	10,400	5,420	1.30	0.081(2)	0.993
10	**4**[b]			6	40	99	68	4,790	3,230	1.25	[j]	[j]

[a] Conditions : $[\varepsilon\text{-CL}]_0$:[**4**]$_0$:[additive] = 200:1:as stated, 3.4 mL of THF at 23 ºC, $[\varepsilon\text{-CL}]_0$ = 1.0 M. [b] Conditions : $[\varepsilon\text{-CL}]_0$:[**4**]$_0$:[additive] = 200:1:as stated, 3.4 mL of toluene at 23 ºC, $[\varepsilon\text{-CL}]_0$ = 1.0 M. [c] Measured by ^{1}H NMR ($CDCl_3$) analyses. [d] Isolated yield at 100% conversion. [e] Molecular weights (g mol^{-1}) determined by GPC in THF at 30 ºC using the appropriate Mark-Houwink corrections. [f] Expected M_n (g mol^{-1}) for stated number of chains per metal centre at the stated % conversion; M_n (Calcd for entries 1 and 6) = conversion (%) × 200 × 144.1 + 4, M_n (Calcd for entries 2 and 7) = 1/4 × (conversion (%) × 200 × 144.1) + 108.1, M_n (Calcd for entries 3 and 8) = 1/7 × (conversion (%) × 200× 144.1) + 75.5, M_n (Calcd for entries 4 and 9) = 1/4 × (conversion (%) × 200× 144.1) + 2.5 and M_n (Calcd for entries 5 and 10) = 1/7 × (conversion (%) × 200 × 144.1) + 2.3. [g] PDI = M_w/M_n. [h] Apparent first-order rate constants for consumption of ε-CL with standard error and R^2 determined by linear regression analysis. [i] Not measured. [j] Apparent rates neither fit in first or second order plots.

HBPin also successfully acts as a CTA in the iROP of ε-CL using compound **1** (Entries 4, 5, 9 and 10, Table 4.4), giving PCL with considerably lower M_n than those obtained from the related ROP in the absence of HBPin (Entries 1 and 6, Table 4.4). However the molecular weights obtained were higher than the expected values, calculated according to the maximum number of PCL chains produced per metal centre. High k_p and hence lower than expected k_{tr}/k_p and k_i/k_p ratios could account for this observation. The PCL obtained displayed moderate molecular weight distributions with PDIs of 1.25-1.44. A mixture of aldehyde end-capped PCL and α,ω-dihydroxy telechelic PCL were also shown in the MALDI-ToF MS and ^{1}H NMR analyses.

The kinetic profiles of the iROP catalysed by **1** with HBPin as a CTA were successfully monitored. All gave first order consumption with ε-CL (Entries 4, 5, 9 and 10, Table 4.4) with similar apparent rate constants k_{app}, within error, regardless of the HBPin concentration and solvent. Polymerisation processes were controlled as evidenced by a linear increase in M_n with % monomer conversion in each case. The gradients of the M_n *vs*. % conversion plots (Appendix, Figure A4.6) were 69.5(8) (R^2 = 0.999, 3 equivs. of HBPin, THF), 43(2) (R^2 = 0.976, 6 equivs. of HBPin, THF), 83(1) (R^2 = 0.997, 3 equivs. of HBPin, toluene) and 47(1) (R^2 = 0.995, 6 equivs. of HBPin, toluene) g mol^{-1} (conversion)$^{-1}$.

The NMR tube scale reaction (C_6D_6) between compound **1** and 10 equivs. of ε-CL in the presence of 5 equivs. of HBPin showed an immediate conversion to PCL, in conjunction with multiple resonances corresponding to the Tp^{tBu,Me} ligand. The ^{11}B{^{1}H} NMR analysis showed a remaining tetrahydroborate resonance at δ = -32.5 ppm. However, the resonance at 28.5 ppm representing HBPin was no longer observed. Concurrently new singlet resonances were present at δ = 22.5 and 7.5 ppm in the ^{11}B{^{1}H} NMR spectrum corresponding to tri- and tetra-alkyl borate esters, respectively.[51] The experiment suggests that not all the catalyst was active in the initiating step. Nevertheless, the results agree with the participation of HBPin in the chain-transfer reaction or hydroboration (*vide infra*), where RO-BPin (R = alkyl or polymeryl) or (Tp^{tBu,Me})Ca{(OR)$_2$BPin} were produced.

The *in situ* generated (Tp^{tBu,Me})Sr{B(OBn)$_4$}(**14**) was also highly active towards iROP of ε-CL. Full monomer conversion was obtained within the first minute of the

polymerisation in both THF and toluene, yielding much higher than expected M_n (15,680 (THF) and 16,990 (toluene) g mol^{-1}) and moderate PDIs (1.63-1.64). The expected values were calculated based on the production of 4 PCL chains per metal centre (5,730 g mol^{-1}). However, in the presence of an equivalent of $B(OMe)_3$, a significant slower polymerisation was attained, producing a mixture between the benzyloxy ester and methoxy ester end-capped PCL with broad PDIs (1.60 and 1.64) in both THF and toluene. A higher than expected M_n was obtained in THF (5,270 g mol^{-1}, expected 3,270 g mol^{-1}) and in toluene (7,710 g mol^{-1}, expected 3,340 g mol^{-1}). The plot of % conversion *vs*. time and the first order plot showed significant induction periods (Appendix, Figure A4.7). This observation led to further investigation into the mechanistic pathway, discussed in Section 4.4.5 below. Furthermore, the apparent rates of iROP fitted neither a first or second order plot. These results strongly reflect the influence of the tetra-coordinate borate adduct as a pre-catalyst in the iROP of ε-CL with a direct comparison using the *in situ* generation of **10** and $B(OR)_3$ as CTAs.

iROP using the *in situ* generated **14** in the presence of HBPin in both THF and toluene demonstrated the chain-transfer effect with considerably lower M_n than those obtained in the absence of HBPin (Entries 4, 5, 9, and 10, Table 4.5). The PCL obtained featured broad PDIs (1.25-1.44) and a mixture of α,ω- dihydroxy telechelic and aldehyde end groups. The iROP experiments of entries 4, 5 and 9 gave first order consumption of ε-CL with similar apparent rate constants.

As previously discussed, the hydroboration of an aldehyde end-group with an excess of HBPin catalysed by metal complexes is a noted side reaction in these iROP experiments. This was confirmed by the MALDI-ToF MS of the incompletely quenched PCL formed from the iROP of **14** and HBPin (Appendix, Figure A4.8), which demonstrated a mixture of various end-capped PCL, namely HO-[PCL]-OH, HO-[PCL]-CHO, HO-[PCL]-BPin and BPin-[PCL]-BPin.

4.4.5 Mechanistic consideration of the iROP of ε-CL using ($Tp^{tBu,Me}$)Sr{$B(OBn)_4$} and various additives

Further investigations on the influence of borate adduct ($Tp^{tBu,Me}$)M{$B(OBn)_4$} as a pre-catalyst in ε-CL iROP were pursued, whereby comparative iROP experiments and spectroscopic studies of the ε-CL iROP using the *in situ* generated ($Tp^{tBu,Me}$)Sr{$B(OBn)_4$} (**14**) and various additives were carried out.

NMR tube scale iROP experiments between the *in situ* generated ($Tp^{tBu,Me}$)Sr{$B(OBn)_4$} (**14**) and 10 equivs. of ε-CL were conducted and monitored by ^1H and ^{11}B NMR analyses in both C_6D_6 and THF-d_8. In both cases, the reactions yielded PCL instantaneously after mixing. In both cases, multiple resonances corresponding to the $Tp^{tBu,Me}$ ligand and the methylene protons of the benzyl groups were observed in ^1H NMR spectra. Concurrently ^{11}B NMR spectra showed a sharp singlet and broad apparent singlets at δ = 4.3 and -7.6 ppm corresponding to tetra-alkoxy borate[51] and the $Tp^{tBu,Me}$ ligand, respectively. Although the product of the iROP was obtained as a tetra-alkoxy borate species, the nature of the initiating or propagating species remained ambiguous. Moreover these experiments confirmed the negligible effect of the donor solvent on the iROP using the borate adduct ($Tp^{tBu,Me}$)M{$B(OBn)_4$} pre-catalyst.

From Figure 4.9(c), an NMR tube scale reaction between **14** and $B(OMe)_3$ in a ratio of 1:1 was carried out, producing ($Tp^{tBu,Me}$)Sr{$B(OBn)_{4-n}(OMe)_n$} (n = 0-4) and $B(OBn)_{3-m}(OMe)_m$ (m = 0-3) with the adducts containing smaller substituted borate (i.e. methoxy group) preferentially formed in a greater quantity. The borates with methoxy substituents are believed to coordinate strongly to the metal centre forming the corresponding adducts with relative stronger Sr-O bonds than the analogues with benzyloxy substituents.

A control iROP experiment was then carried out in the presence of a significantly higher concentration of $B(OMe)_3$ (5 equivs.) in THF, whereby *in situ* generated ($Tp^{tBu,Me}$)Sr{$B(OMe)_4$} was expected to be formed in a significantly higher concentration than the other derivatives previously discussed. The subsequent iROP experiment illustrated a considerably longer induction period and polymerisation time (Entries 6 and 7, Table 4.6). A mixture of benzyloxy ester and methoxy ester end-capped PCL was obtained with slightly higher than expected M_n and moderate PDIs. On the other hand, the corresponding iROP experiment with 5 equivs. of $B(OBn)_3$ gave over 90 % monomer conversion within 10 mins. Benzyloxy ester end-capped PCL was obtained with higher than expected M_n and broad PDI (Entry 8, Table 4.6). The plot of % conversion *vs*. time and the first order plot showed a significant induction period (Appendix, Figure A4.9). Furthermore, kinetic analysis showed that the apparent rate of ε-CL was neither first nor second order.

Table 4.6. Comparative experiments on the iROP of ε-CL using ($Tp^{tBu,Me}$)$Sr(BH_4)(THF)_2$ (**4**) with various additives.[a]

Entry	Catalyst	Equivs. of additive			Time (min)	Conversion (%)[b]	Yield (%)[c]	M_n (GPC)[d]	M_n (Calcd)[e]	PDI[f]	k_{app} (min^{-1})[g]	R^{2g}
		PhCHO	$B(OMe)_3$	$B(OBn)_3$								
1	**4**				85	97	97	30,910	22,140	1.46	*i*	*i*
2	**4**		1		600	4	-	2,210	230	1.41	-	-
3	**4**		1		1,740	100	72	8,300	5,730	1.78	-	-
4	**4**	5			1	100	83	15,680	5,815	1.64	*h*	*h*
5	**4**	5	1		19	98	80	5,270	3,270	1.60	*i*	*i*
6	**4**	5	5		600	6	-	-	79	-	-	-
7	**4**	5	5		1,125	100	51	1,630	1,250	1.55	-	-
8	**4**	5		5	10	94	40	1,890	1,240	1.56	*i*	*i*

[a] Conditions : $[\varepsilon\text{-CL}]_0$:$[\mathbf{4}]_0$:[additive] = 200:1:as stated, 3.4 mL of THF at 23 ºC, $[\varepsilon\text{-CL}]_0$ = 1.0 M., $[\varepsilon\text{-CL}]_0$ = 1.0 M. [b] Measured by ^1H NMR ($CDCl_3$) analyses. [c] Isolated yield at 100% conversion. [d] Molecular weights (g mol^{-1}) determined by GPC in THF at 30 ºC using the appropriate Mark-Houwink corrections. [e] Expected M_n (g mol^{-1}) for stated number of chains per metal centre at the stated % conversion; M_n (Calcd for entries 1) = conversion (%) × 200 × 144.1 + 4, M_n (Calcd for entries 2 and 3) = 1/4 × (conversion (%) × 200 × 144.1) + 25.0, M_n (Calcd for entries 4) = 1/4 × (conversion (%) × 200× 144.1) + 108.1, M_n (Calcd for entries 5) = 1/7 × (conversion (%) × 200× 144.1) + 75.5, M_n (Calcd for entries 6 and 7) = 1/19 × (conversion (%) × 200 × 144.1) + 48.1 and M_n (Calcd for entries 8) = 1/19 × (conversion (%) × 200 × 144.1) + 108.1. [f] PDI = M_w/M_n. [g] Apparent first-order rate constants for consumption of ε-CL with standard error and R^2 determined by linear regression analysis. [h] Not measured. [i] Apparent rates neither fit in first or second order plots.

To underpin the pronounced effect of the tetra-alkoxy borate adduct produced during the experiment on the rate of polymerisation, an equivalent of $B(OMe)_3$ was added into the ROP of ε-CL using **4**. The polymerisation was significantly retarded with a very long induction period observed (4 % PCL in 600 mins, completion achieved in 1,740 mins, Entries 2 and 3, Table 4.6). A mixture of α, ω-dihydroxy telechelic PCL and methoxy ester end-capped PCL was obtained with a slightly higher than expected M_n and broad PDI. An attempt to characterise a pre-catalyst or an intermediate was unsuccessful as no change was observed by ^1H and ^{11}B NMR analyses of the solution mixture of **4**, $B(OMe)_3$ and 15 equivs. of ε-CL at 193 K. Upon monitoring the changes observed in the ^1H and ^{11}B analyses of the NMR tube scale iROP reaction at room temperature, the identification of the intermediate was also unclear.

In conclusion, the comparative iROP experiments, along with the spectroscopic studies, demonstrated a non-negligible pre-equilibrium exists between the alkoxide compound, and $B(OR)_3$, and their corresponding tetra-alkoxy borate adducts, which strongly affects the rate of ε-CL iROP. In addition, the bulkiness of the alkoxy borate substituents at the bridging positions exerts different amounts of steric hindrance and kinetic stability. $(Tp^{tBu,Me})Sr\{B(OR)_4\}$, containing smaller alkoxy substituents at the bridging positions, results in a kinetically stable product with relatively strong Sr-O bonds. These directly affect the initiation, as well as the dissociation/association and bridging-terminal exchange during the propagation. In order to underpin the mechanism regarding the iROP using $(Tp^{tBu,Me})Sr\{B(OR)_4\}$, further work including in-depth kinetic studies as well as DFT calculations are underway. However, based on the work carried out in Sections 4.4.4 and 4.4.5, possible pathways in the ε-CL iROP using $(Tp^{tBu,Me})Sr\{B(OR)_4\}$ are proposed in Scheme 4.5.

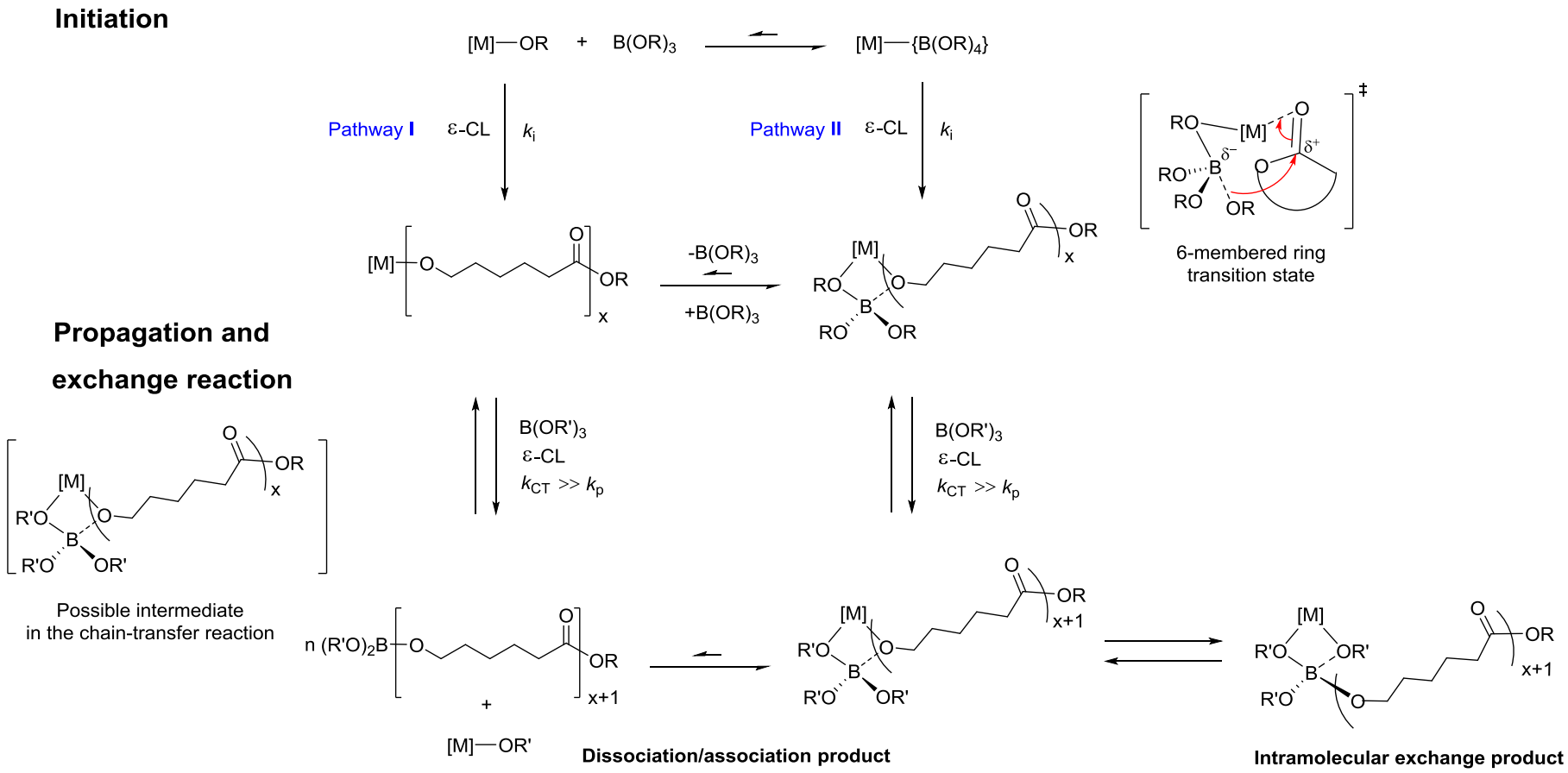

Scheme 4.5. Proposed pathways for iROP of ε-CL using ($Tp^{tBu,Me}$)Sr{$B(OBn)_4$} (**14**) and $B(OR)_3$ as CTA

4.4.6 ROP of *rac*-LA using calcium and strontium initiators

The *in situ* generated calcium catalyst **13a** along with $B(OBn)_3$ and **13b** from a reaction between **1** and 5 equivs. of PhCHO exhibits a high catalytic activity towards the ROP of 100 equivs. of *rac*-LA at room temperature, over 90 % monomer conversion was obtained in the first minute of the polymerisation. Highly heterotactic-enriched PLA (P_r = 0.81) with a moderate PDI of 1.32, as well as, a molecular weight consistent with the calculated value for one PLA chain per metal centre was attained. Building on this observation, the polymerisation was extrapolated to [*rac*-LA]$_0$:[catalyst]$_0$ = 20-300, holding the *rac*-LA concentration constant. The gradient of the plot between M_n (GPC) *vs*. equivalents of LA converted of 144(2) g mol^{-1} (equivalent)$^{-1}$ (R^2 = 0.999) agreed extremely well to the expected value of 144 g mol^{-1} (equivalent)$^{-1}$ (Figure 4.20). This suggests a superior performance of the *in situ* generated calcium catalysts in polymerising *rac*-LA at various concentrations.

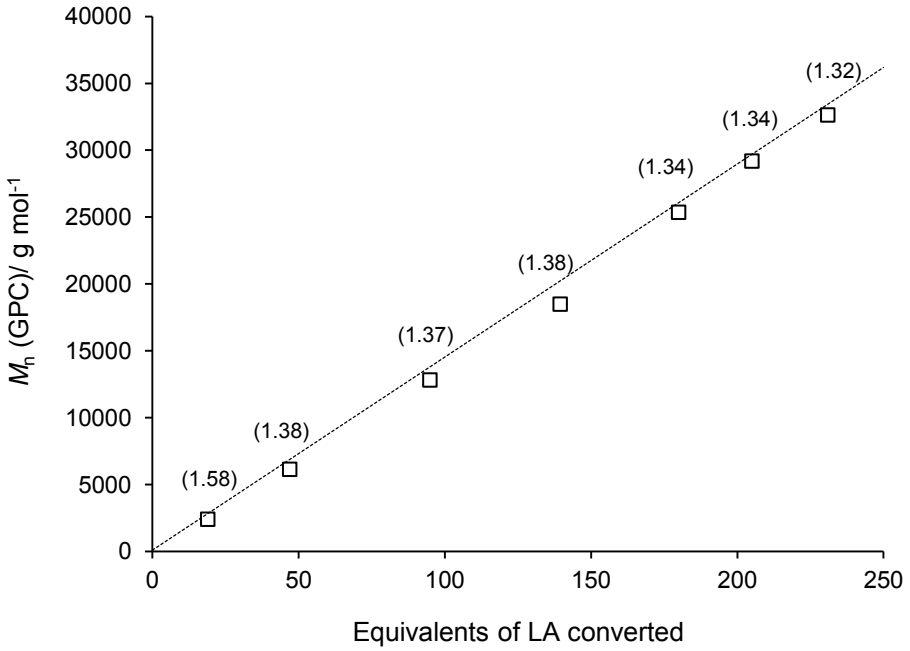

Figure 4.20. M_n (as measured by GPC) *vs*. equivalents *rac*-LA converted using ($Tp^{tBu,Me}$)Ca(BH_4)(THF) (**1**) and 5 equivs of PhCHO. The dotted line is that expected for one PLA chain per metal centre. Conditions: 6 mL THF, 23 ºC, [*rac*-LA] = 0.5 M. [*rac*-LA]$_0$:[**1**]$_0$ = 20, 50, 100, 150, 200, 250 and 300. PDI values are given in parentheses.

However, a sharp contrast was observed in the *rac*-LA ROP catalytic activity of the *in situ* generated calcium catalyst (**13a** along with $B(OBn)_3$ and **13b**) when compared to

the analogous *in situ* generated **10** and $B(OBn)_3$, which polymerised *rac*-LA in an immortal manner. The relative rates of the chain-transfer reactions compared to the rate of propagation accounts for the differences observed. The rate of propagation of the *rac*-LA ROP using the *in situ* generated calcium catalyst is considerably faster than that found using the magnesium counterpart, and in turn is faster than the rate of the chain-transfer reaction. As a consequence, the immortal behaviour of the ROP using the *in situ* generated calcium catalyst is suppressed. The ^{1}H NMR spectrum and the MALDI-ToF MS confirmed the presence of a benzyloxy ester end-capped PLA. The mass spectrum also illustrated a minor isotopic distribution of cyclic PLA with $\Delta m/z$ of 72 g mol^{-1}, reflecting the transesterification effect.

The *in situ* generated ($Tp^{tBu,Me}$)Sr{$B(OBn)_4$} (**14**) is also active towards the ROP of *rac*-LA. 49 % monomer conversion was achieved within 0.5 mins, however, only a slight increase was observed over the period of a further 2 h (77 % monomer conversion). An aggregation of the catalyst or a resting state of the catalyst with a growing polymer chain might be responsible for this observation. Similar to the observation made in the ROP using the *in situ* generated calcium catalyst, the PLA with molecular weight corresponding to the expected M_n (one chain PLA produced per metal centre) was obtained at the initial stage of polymerisation. The ROP was affected immensely by the transesterification reactions toward the higher monomer conversion, whereby an increase in PDI (from 1.29 to 1.44) and a decrease in M_n were observed (Appendix, Figure A4.10). Reminiscent of the calcium system, the MALDI-ToF MS was obtained confirming the benzyloxy ester end-group and the effect of the transesterification reaction. Finally, it is noteworthy that the immortal ROP of *rac*-LA using trialkyl borate esters was not applicable to both the *in situ* generated calcium and strontium catalysts primarily because of the relatively faster k_p than k_{tr}.

4.5 Summary and conclusions

This Chapter has developed a new class of trialkyl borate and borane derivatives as chain-transfer agents in iROP of ε-CL and *rac*-LA using alkaline earth initiators. *In situ* generation of alkaline earth initiators and trialkyl borates, either in the form of separate or adduct species, is accessible through a reaction between the corresponding tetrahydroborate compounds and four equivs. of aldehyde (PhCHO was used in this work). The reaction between **2** and 4 equivs. of PhCHO gave ($Tp^{tBu,Me}$)Mg(OBn) (**10**)

and $B(OBn)_3$. On the other hand, non-isolated $(Tp^{tBu,Me})Ca(OBn)$ (**13a**) along with $(Tp^{tBu,Me})Ca\{B(OBn)_4\}$ (**13b**) and $(Tp^{tBu,Me})Sr\{B(OBn)_4\}$ (**14**) were produced in the analogous reaction with **1** and **4**, respectively. Compound **14** was isolated in multi-gram scale and fully characterised. The forms of the products were highly influenced by the sizes of the metal centres. Attempts to isolate **10** from the solution mixture of **10** and $B(OBn)_3$ by crystallization resulted in the formation of a 1,2-boratropic shift-product, $\{HB(^tBu,Me\text{-}pz)_2(Me,^tBu\text{-}pz)\}Mg(OBn)$ (**10***).

The variable-temperature ^1H NMR analyses enabled the measurement of thermodynamic parameters of the dissociation of **14** and the intramolecular exchange between the bridging and terminal alkoxide groups of $(Tp^{tBu,Me})Mg\{B(OMe)_4\}$ (**16**). In turn, compound **16** was independently synthesised on the NMR tube scale following reaction of $(Tp^{tBu,Me})Mg(OMe)$ (**15**) with $B(OMe)_3$.

NMR tube scale reactions between various $B(OR)_3$ reagents and $B(OR)_3$ with alkaline earth alkoxide compounds (e.g. **10** and **14**) showed immediate exchange of the alkoxide substituents through the formation of tetra-alkoxy borate intermediates. These exchange reactions are key to a successful iROP experiments, leading to multi end-capped polymer chains produced per metal centre. In contrast, no exchange reactions were observed between alkaline earth tetrahydroborate compounds (**1**, **2** and **4**) with $B(OR)_3$.

$B(OR)_3$ and HBPin were efficient CTAs in the iROP of ε-CL and *rac*-LA using the *in situ* generated or isolated magnesium initiator **10**, producing the corresponding polymers with close to expected M_n and moderate PDIs for PCL or narrow PDIs for PLA. It was shown that the efficiency of $B(OR)_3$ as CTAs is independent of the alkoxy substituents. Moreover, an equivalent iROP of *rac*-LA using **10** and BnOH was pursued in order to compare the efficiency of the protic agent to $B(OR)_3$ as CTAs. The results showed a successful iROP using BnOH, however a distinctive difference in the apparent rates of propagation was observed. According to the literature and NMR spectroscopic studies, iROP using BnOH as a CTA may proceed through the activated monomer mechanism, rather than coordination-insertion, which could explain the difference in rates in this case. Further investigations regarding the change or the difference in mechanisms are underway. A mechanistic pathway of the

ε-CL iROP using magnesium alkoxide initiator **10** with $B(OR)_3$ as a CTA was also proposed and supported by the iROP results and NMR spectroscopic studies.

Chain-transfer effects in the iROP of ε-CL using larger metal catalysts (i.e. calcium and strontium) with $B(OR)_3$ and HBPin as CTAs were observed, however, giving PCL with higher than expected molecular weights. It is also found that the equilibrium between the separate alkoxide and its corresponding tetra-alkoxy borate adduct in the strontium compounds was not negligible and strongly influenced the subsequent rates of ε-CL iROP. Moreover, the comparative experiments showed that the kinetically favourable strontium adducts with smaller alkoxide substituents at the bridging positions led to the significantly reduced rate of ε-CL iROP. A possible iROP pathway using **14** was proposed, however, further works concerning DFT studies are underway.

Although the chain-transfer abilities of $B(OR)_3$ were found in the aforementioned iROP, they were not applicable to the ROP of *rac*-LA using the *in situ* generated calcium (**13a** along with $B(OBn)_3$ and **13b**) and strontium (**14**) initiators. In both cases, only one PLA chain was produced per metal centre under these polymerisation conditions. An incomplete ROP of *rac*-LA using **14** could be caused by an aggregation of the catalyst or a resting state of the catalyst with a growing polymer chain.

4.6 References

1. D. G. Hall, *Boronic acids: Preparation, Applications in Organic Synthesis and Medicine*, 2nd Edition, Wiley, Weinheim, 2011.
2. K. Ishihara and H. Yamamoto, *Eur. J. Org. Chem.*, 1999, 527.
3. A. Pelter, K. Smith and H. C. Brown, *Borane Reagents*, Academic Press, 1988.
4. W. E. Piers, *Advances in Organometallic Chemistry*, Academic Press, 2004, vol. 52, pp. 1.
5. M. Yasuda, H. Nakajima, R. Takeda, S. Yoshioka, S. Yamasaki, K. Chiba and A. Baba, *Chem. Eur. J.*, 2011, **17**, 3856.
6. N. Miyaura and A. Suzuki, *Chem. Rev.*, 1995, **95**, 2457.
7. A. Suzuki, *Angew. Chem., Int. Ed.*, 2011, **50**, 6722.
8. B. W. Glasspoole and C. M. Crudden, *Nat. Chem.*, 2011, **3**, 912.

9. M. C. Redondo, M. Veguillas, M. Ribagorda and M. C. Carreno, *Angew. Chem., Int. Ed.*, 2009, **48**, 370.
10. A. A. Oluyadi, S. Ma and C. N. Muhoro, *Organometallics*, 2013, **32**, 70.
11. M. Arrowsmith, T. J. Hadlington, M. S. Hill and G. Kociok-Koehn, *Chem. Commun.*, 2012, **48**, 4567.
12. M. Arrowsmith, M. S. Hill, T. Hadlington, G. Kociok-Köhn and C. Weetman, *Organometallics*, 2011, **30**, 5556.
13. M. D. Anker, M. Arrowsmith, P. Bellham, M. S. Hill, G. Kociok-Koehn, D. J. Liptrot, M. F. Mahon and C. Weetman, *Chem. Sci.*, 2014, **5**, 2826.
14. S. Harder and J. Spielmann, *J. Organomet. Chem.*, 2012, **698**, 7.
15. D. Mukherjee, A. Ellern and A. D. Sadow, *Chem. Sci.*, 2014, **5**, 959.
16. D. W. Stephan, *Chem. Commun.*, 2010, **46**, 8526.
17. D. W. Stephan and G. Erker, *Chem. Sci.*, 2014, **5**, 2625.
18. C. Jiang, O. Blacque, T. Fox and H. Berke, *Organometallics*, 2011, **30**, 2117.
19. K. Chernichenko, A. Madarasz, I. Papai, M. Nieger, M. Leskelae and T. Repo, *Nat. Chem.*, 2013, **5**, 718.
20. C. R. Wade, A. E. J. Broomsgrove, S. Aldridge and F. P. Gabbai, *Chem. Rev.*, 2010, **110**, 3958.
21. Z. Guo, I. Shin and J. Yoon, *Chem. Commun.*, 2012, **48**, 5956.
22. E. Galbraith and T. D. James, *Chem. Soc. Rev.*, 2010, **39**, 3831.
23. C. V. Hoven, H. Wang, M. Elbing, L. Garner, D. Winkelhaus and G. C. Bazan, *Nat. Mater.*, 2010, **9**, 249.
24. A. Caruso, Jr., M. A. Siegler and J. D. Tovar, *Angew. Chem., Int. Ed.*, 2010, **49**, 4213.
25. Z. M. Hudson and S. Wang, *Acc. Chem. Res.*, 2009, **42**, 1584.
26. D. Reitzenstein and C. Lambert, *Macromolecules*, 2009, **42**, 773.
27. E. Sheepwash, K. Zhou, R. Scopelliti and K. Severin, *Eur. J. Inorg. Chem.*, 2013, **2013**, 2558.
28. B. Rout, L. Unger, G. Armony, M. A. Iron and D. Margulies, *Angew. Chem., Int. Ed.*, 2012, **51**, 12477.
29. S. Jin, Y. Cheng, S. Reid, M. Li and B. Wang, *Med. Res. Rev.*, 2010, **30**, 171.
30. Ewen, CA-A, 1991, 2, 027; 145. *Chem. Abstr.*, 1991, 115, 136998g; 256895t..
31. X. Yang, C. L. Stern and T. J. Marks, *J. Am. Chem. Soc.*, 1991, **113**, 3623.
32. W. E. Piers and T. Chivers, *Chem. Soc. Rev.*, 1997, **26**, 345.

33. Y. Jang, H.-K. Sung, S. Lee and C. Bae, *Polymer*, 2005, **46**, 11301.
34. A. Kanazawa, S. Kanaoka and S. Aoshima, *J. Am. Chem. Soc.*, 2013, **135**, 9330.
35. T. C. M. Chung, *Macromolecules*, 2013, **46**, 6671.
36. T. C. Chung, *Prog. Polym. Sci.*, 2002, **27**, 39.
37. G. Xu and T. C. Chung, *J. Am. Chem. Soc.*, 1999, **121**, 6763.
38. G. Xu and T. C. Chung, *Macromolecules*, 1999, **32**, 8689.
39. T. C. Chung, G. Xu, Y. Lu and Y. Hu, *Macromolecules*, 2001, **34**, 8040.
40. W. Lin, J. Dong and T. C. M. Chung, *Macromolecules*, 2008, **41**, 8452.
41. W. Lin, H. Niu, T. C. M. Chung and J.-Y. Dong, *J. Polym. Sci. Part A: Polym. Chem.*, 2010, **48**, 3534.
42. S. B. Amin and T. J. Marks, *Angew. Chem., Int. Ed.*, 2008, **47**, 2006.
43. G. A. Molander and D. Pfeiffer, *Org. Lett.*, 2001, **3**, 361.
44. E. A. Bijpost, R. Duchateau and J. H. Teuben, *J. Mol. Catal. A: Chem.*, 1995, **95**, 121.
45. K. N. Harrison and T. J. Marks, *J. Am. Chem. Soc.*, 1992, **114**, 9220.
46. W. Choi, F. Sanda and T. Endo, *J. Polym. Sci. Part A: Polym. Chem.*, 1998, **36**, 1189.
47. M. Cameron, R. S. Hoerrner, J. M. McNamara, M. Figus and S. Thomas, *Org. Process Res. Dev.*, 2006, **10**, 149.
48. G. Gody, T. Maschmeyer, P. B. Zetterlund and S. Perrier, *Nat. Commun.*, 2013, **4**, 2505.
49. D. Gauthier, A. T. Lindhardt, E. P. K. Olsen, J. Overgaard and T. Skrydstrup, *J. Am. Chem. Soc.*, 2010, **132**, 7998.
50. G. Wu, W. Sun and Z. Shen, *React. Funct. Polym.*, 2008, **68**, 822.
51. H. Nöth and B. Wrackmeyer, *Nuclear Magnetic Resonance Spectroscopy of Boron Compounds*, 1st edn., Springer-Verlag, Berlin, Heidelberg Germany, 1978.
52. M. Cano, J. V. Heras, E. Santamaria, E. Pinilla, A. Monge, C. J. Jones and J. A. McCleverty, *Polyhedron*, 1993, **12**, 1711.
53. C. G. Young, L. J. Laughlin, S. Colmanet and S. D. B. Scrofani, *Inorg. Chem.*, 1996, **35**, 5368.
54. C. G. Young, M. S. Malarek, D. J. Evans, C. J. Doonan, V. W. L. Ng and J. M. White, *Inorg. Chem.*, 2009, **48**, 1960.

55. M. Cano, J. V. Heras, C. J. Jones, J. A. McCleverty and S. Trofimenko, *Polyhedron*, 1990, **9**, 619.
56. M. Cano, J. V. Heras, A. Monge, E. Pinilla, E. Santamaria, H. A. Hinton, C. J. Jones and J. A. McCleverty, *J. Chem. Soc., Dalton Trans*., 1995, 2281.
57. Y. Sun, R. McDonald, J. Takats, V. W. Day and T. A. Eberspacher, *Inorg. Chem*., 1994, **33**, 4433.
58. M. H. Chisholm, N. W. Eilerts and J. C. Huffman, *Inorg. Chem*., 1996, **35**, 445.
59. M. Silva, A. Domingos, A. Pires de Matos, N. Marques and S. Trofimenko, *J. Chem. Soc., Dalton Trans*., 2000, 4628.
60. T. Ruman, Z. Ciunik, E. Szklanny and S. Wolowiec, *Polyhedron*, 2002, **21**, 2743.
61. N. Farfan and R. Contreras, *J. Chem. Soc., Perkin Trans. 2*, 1987, 771.
62. W. Gerrard, M. F. Lappert and B. A. Mountfield, *J. Chem. Soc*., 1959, 1529.
63. M. Yasuda, S. Yoshioka, S. Yamasaki, T. Somyo, K. Chiba and A. Baba, *Org. Lett*., 2006, **8**, 761.
64. J. Sandström, *Dynamic NMR spectroscopy*, London, New York : Academic Press, London, New York, 1982.
65. M. J. Saly, J. Li, M. J. Heeg and C. H. Winter, *Inorg. Chem*., 2011, **50**, 7385.
66. R. C. Neu, G. Menard and D. W. Stephan, *Dalton Trans*., 2012, **41**, 9016.
67. T. G. Richmond and D. F. Shriver, *Organometallics*, 1984, **3**, 305.
68. A. M. Crespi and D. F. Shriver, *Organometallics*, 1985, **4**, 1830.
69. L. P. Lindeman and M. K. Wilson, *J. Chem. Phys*., 1956, **24**, 242.
70. M. R. Burgstein, H. Berberich and P. W. Roesky, *Chem. Eur. J*., 2001, **7**, 3078.
71. M.-O. Simon and S. Darses, *Adv. Synth. Catal*., 2010, **352**, 305.
72. K. A. Bernard and J. D. Atwood, *Organometallics*, 1988, **7**, 235.
73. T. Saegusa and T. Ueshima, *J. Org. Chem*., 1968, **33**, 3310.
74. F. J. Villani and F. F. Nord, *J. Am. Chem. Soc*., 1947, **69**, 2605.
75. M. R. Crimmin, A. G. M. Barrett, M. S. Hill and P. A. Procopiou, *Org. Lett*., 2007, **9**, 331.
76. H. Beberich and P. W. Roesky, *Angew. Chem., Int. Ed*., 1998, **37**, 1569.
77. H. G. Kuivila, S. C. Slack and P. K. Siiteri, *J. Am. Chem. Soc*., 1951, **73**, 123.

78. H. Iida, H. Kitamura, K. Seita and K. Yamada, *Bull. Chem. Soc. Jap.*, 1974, **47**, 1028.

79. I. P. Query, P. A. Squier, E. M. Larson, N. A. Isley and T. B. Clark, *J. Org. Chem.*, 2011, **76**, 6452.

80. M. Yamashita, Y. Takemoto, E. Ihara and H. Yasuda, *Macromolecules*, 1996, **29**, 1798.

81. N. Barros, P. Mountford, S. M. Guillaume and L. Maron, *Chem. Eur. J.*, 2008, **14**, 5507.

82. T. Arliguie, D. Baudry, M. Ephritikhine, M. Nierlich, M. Lance and J. Vigner, *J. Chem. Soc., Dalton Trans.*, 1992, 1019.

83. Y. Sarazin, B. Liu, T. Roisnel, L. Maron and J.-F. Carpentier, *J. Am. Chem. Soc.*, 2011, **133**, 9069.

84. Y. Sarazin, V. Poirier, T. Roisnel and J.-F. Carpentier, *Eur. J. Inorg. Chem.*, 2010, **2010**, 3423.

85. B. Liu, T. Roisnel and Y. Sarazin, *Inorg. Chim. Acta*, 2012, **380**, 2.

Chapter Five

New Group 2 organohydroborate complexes for the ROP of ε-CL and *rac*-LA

5.1 Overview

This Chapter will describe the synthesis and characterisation of alkaline earth organohydroborate ($HBEt_3$ and $H_2BC_8H_{14}$) complexes supported by 3-methyl, 5-*tert*-butyl tris(pyrazolyl)hydroborate ligands ($Tp^{tBu,Me}$). Their solid state structures and solution behaviours will be discussed, in conjuction with their activities towards ROP of ε-CL and *rac*-LA. Comparative studies with their analogous series of tetrahydroborate complexes in Chapter Two and other appropriate literature examples will be drawn. Moreover, the ε-CL and *rac*-LA ROP mechanistic investigations of the organohydroborate initiating groups using spectroscopic techniques will be undertaken. Five new alkaline earth organohydroborate complexes are presented, as well as, four X-Ray crystallographic structures.

5.2 Introduction

Organohydroborate (H_xBR_{4-x}, R = alkyl group and x = 1 or 2) could be viewed as an alkylborane supported hydride. By analogy, organohydroborate metal complexes are synthons for molecular metal hydrides. In many cases, stabilisation of the hydrido compounds has been achieved through the coordination of the BR_3 moieties to the hydride base.[1-3] The production of organoboranate adducts greatly enhances solubility in common organic solvents.[1, 3-7] Of the known organohydroborate metal complexes, most are lanthanide (Sm,[8] Tm,[9] Yb,[10, 11] Eu[11] and Nd[12]), transition metal (Sc,[13-15] Y,[16] Fe,[17] Zr[18, 19] and Ti[20]) and alkali (Li, Na and K)[21, 22] complexes. Intriguingly, a handful amount of non-radioactive actinide (Th[23], U[23, 24] and Np[23]) organohydroborate compounds have also been reported in the literature.

The organohydroborate complexes are conveniently prepared *via* a number of possible reactions summarised in Scheme 5.1. The most common synthetic route to organohydroborate compounds is the salt metathesis reaction between a corresponding metal halide complex and an alkali salt of the organohydroborate (Scheme 5.1 (a)). Examples of organohydroborate complexes derived from salt metathesis reactions include $[C_5H_4(CH_2)_2OMe]_2Sm(HBEt_3)$,[25, 26] $[C_5H_4(^tBu)]_2Sm(HBEt_3)(THF)_2$,[25, 26] $(Tp^{tBu,Me})Yb(HBEt_3)(THF)$[27] and $\{HC(C(Me)NAr)_2\}Sc(HBEt_3)(NHAr)$ (Ar = 2,6-$C_6H_3{}^iPr_2$).[13] Addition reaction (Scheme 5.1 (b)) between a metal hydride complex and corresponding alkylborane is widely used in the synthesis of alkali organohydroborates due to the readily accessible

starting materials.[21, 22] Moreover, this methodology is also applicable to the synthesis of the rare earth organohydroborate complexes, namely [1,2,4-(^{t}Bu)$_3$C$_5$H$_2$]$_2$Ce(HBPh$_3$)[28] and (C$_5$Me$_5$)$_2$La(HBEt$_3$)(THF).[29] Lastly, transmetalliation reaction (Scheme 5.1 (c)) was adopted by Nöth in the preparation of (ArO)$_3$Ti{(μ-H)$_2$BC$_8$H$_{14}$} (ArO = 2,6-^{i}Pr$_2$C$_6$H$_3$) from the treatment of (ArO)$_3$TiMe with (μ-H)$_2$(BC$_8$H$_{14}$)$_2$. The desired product was produced along with MeBC$_8$H$_{14}$.[30] Furthermore, the established reaction between alkali amides or alkoxides and hydridodialkylboranes to yield the corresponding alkali salt organohydroborates is well documented in literature.[31]

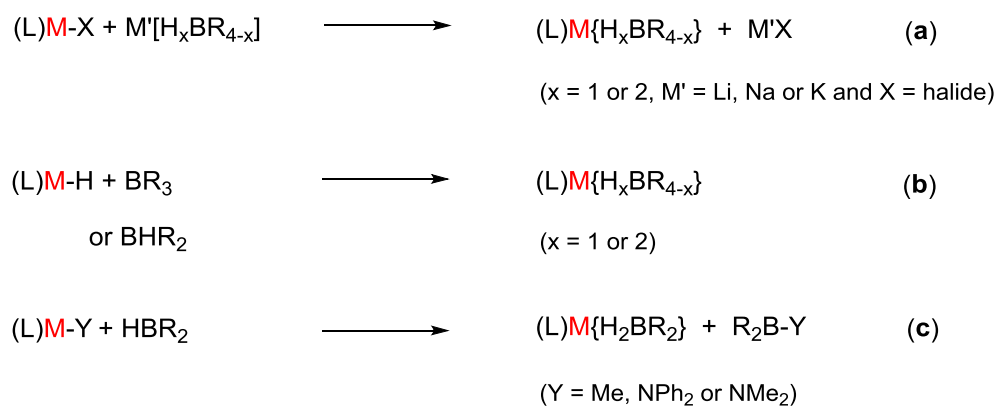

Scheme 5.1. Common synthetic routes to organohydroborate complexes; (a) salt metathesis, (b) addition and (c) transmetallation.

5.2.1 Alkaline earth organohydroborate complexes

Owing to the parallel relationships between the structures and reactivities of alkaline earth and divalent lanthanide complexes, the syntheses of well-defined alkaline earth organohydroborates as synthons for molecular main-group hydrides were undertaken. The pioneering work was carried out by Hanusa *et al*. in 2000, describing the preparation of {1,2,4-C$_5$H$_2$(SiMe$_3$)$_3$}Ca(HBEt$_3$)(THF) (**5.1**) from the salt metathesis reaction between the corresponding calcium iodide dimer and Na[HBEt$_3$] (Figure 5.1). The X-ray crystallography and spectroscopic studies of **5.1** indicate a Ca···H-BEt$_3$ interaction including the multidentate ligation of the triethylhydroborate anion to the metal centre. Accordingly, the strong coordination of organohydroborate ligand in this complex results in the difficulty in removal BEt$_3$ fragment using the competing base PMe$_3$.[1]

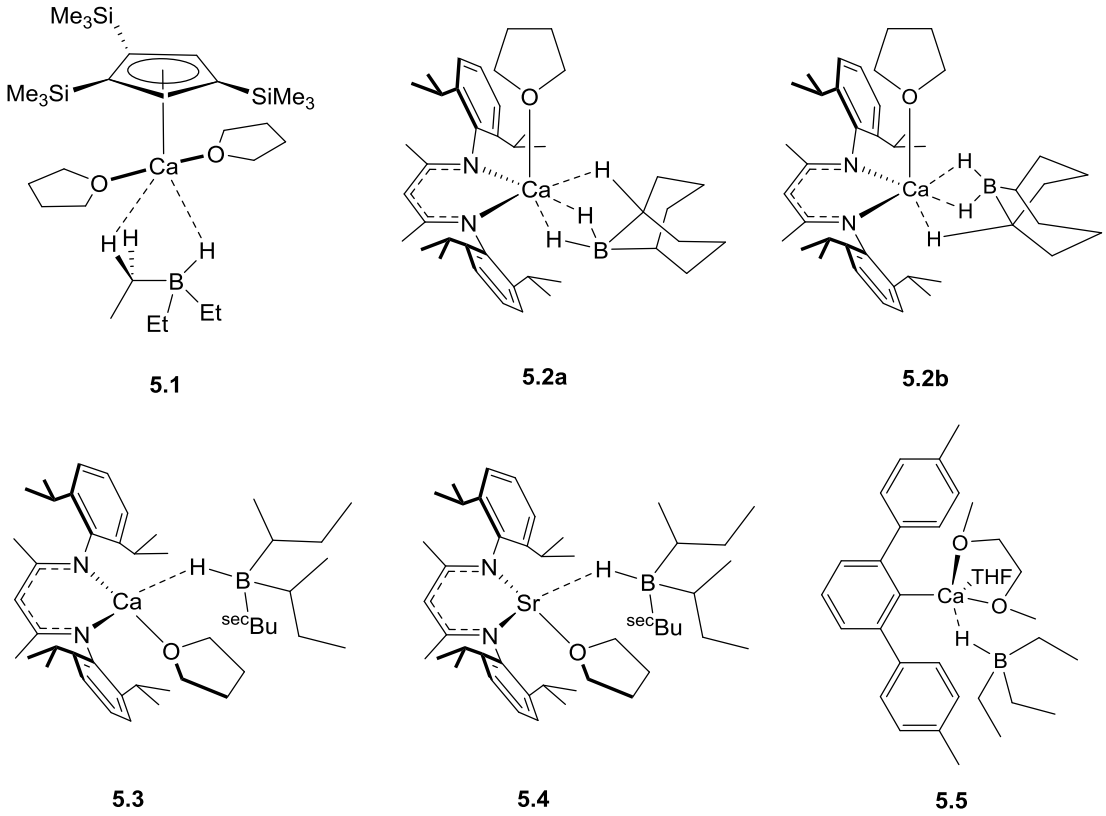

Figure 5.1. Examples of alkaline earth organohydroborate compounds.[1-3, 32]

In 2007, Barrett, Hill and their coworkers demonstrated successful σ-bond metathesis reactions between {HC(C(Me)N-2,6-$C_6H_3{}^iPr_2)_2$}Ca{$N(SiMe_3)_2$}$_3$(THF) or the related {HC(C(Me)N-2,6-$C_6H_3{}^iPr_2)_2$}Ca(NPh_2)(THF) complexes and (μ-H)$_2$(BC_8H_{14})$_2$ in toluene at 60 °C and 25 °C, respectively. These reactions produced {HC(C(Me)N-2,6-$C_6H_3{}^iPr_2)_2$}Ca{(μ-H)$_2$$BC_8H_{14}$}(THF) (**5.2**) and the corresponding aminoborane. The (μ-H)$_2$$BC_8H_{14}$ ligand normally coordinates to the metal centre through the two hydrides, as well as an apparent agostic interaction with the methine hydrogen adjacent to the boron atom. Interestingly, NMR and IR spectroscopy alongside X-ray crystallography revealed the presence of two conformers **5.2a** and **5.2b** within an asymmetric unit (Figure 5.1). The conformers differ by their coordination geometry around the metal centre.[32]

In recent years, the striking concept of heavier alkaline earth compounds stabilised by $HBEt_3$ ligands was also pursued by both Roesky[2] and Westerhausen *et al*.[3] to produce {HC(C(Me)N-2,6-$C_6H_3{}^iPr_2)_2$}M{$HB(^{sec}Bu)_3$}(THF) (M = Ca (**5.3**) or Sr (**5.4**)) and {2,6-$C_6H_3(Tol)_2$}Ca($HBEt_3$)(THF)(DME) (**5.5**), respectively (Figure 5.1). Compounds **5.3**, **5.4** and **5.5** were derived from the salt metathesis reactions between

the corresponding metal iodide complexes and alkali salts of organohydroborates. Unlike compound **5.1**, the HBR_3 ligands coordinate to the metal centres through a single M···H-BR_3 interaction.

Aside from the detailed investigations into solid state and solution behaviour of the aforementioned alkaline earth compounds, no reaction of these hydride-containing complexes is reported in the literature.

5.2.2 Reactivity of metal organohydroborate complexes

Metal organohydroborate complexes could occasionally undergo hydride abstraction. This is illustrated by the work of Chen *et al*., whereby $B(C_6F_5)_3$ removes the hydride from $Yb\{(\mu\text{-}H)_2BC_8H_{14}\}_2(THF)_4$ to form $[Yb(THF)_6][HB(C_6F_5)_3]_2$ and $(\mu\text{-}H)_2(BC_8H_{14})_2$.[11] Furthermore, metal organohydroborate compounds are widely established as nucleophilic hydride sources and reducing agents in organic, organometallic and material chemistry.[33-36] For instance, several reports have shown a significant reducing ability of organohydroborates in reduction of carbonyl groups.[12, 13] Noteworthily, reduction of carbon dioxide to formate at the atmospheric pressure using $\{2,6\text{-}C_6H_3(OP^iPr_2)_2\}Ni\{(\mu\text{-}H)_2BC_8H_{14}\}$ was reported by Guan and coworkers in 2013.[37]

As mentioned, hydride transfer and reducing potential of metal organylhydroborate complexes allows them to be suitable candidates for ε-CL and *rac*-LA ROP initiators. The studies in the previous chapters suggest that the presence of trialkyl borate esters ($B(OR)_3$), either as by-products from the exchange reaction between BH_3·THF and a metal alkoxide or as *in situ* generated products, could lead to immortal ring-opening polymerisation of ε-CL and *rac*-LA. In contradiction to the previous findings (Figure 4.9(a) and (b)), control reactions between trialkyl borane (BEt_3) and trialkyl borate ester ($B(OMe)_3$) or trialkyl borane (BEt_3) and metal alkoxide compounds ($(Tp^{tBu,Me})Mg$(S-lactate) (**9**) or $(Tp^{tBu,Me})Mg(OBn)$ (**10**)) showed no exchange between the substituents. Furthermore, it is well known in the literature that metal organylhydroborate complexes $M[H_nBR_{4-n}]$ (n = 1-3) are less prone to undergo a substituent exchange in comparison to analogous metal alkoxohydroborate complexes $M[H_nB(OR)_{4-n}]$ (n = 1-3).[38, 39] As alkyl boranes and organohydroborates are innocent in substituent exchange reactions, organohydroborates ($HBEt_3$ and $H_2BC_8H_{14}$) as

single-site initiators are expected to give living ROP with good molecular weight control and defined polylactide end-group functionality.

5.3 Synthesis and characterisation of alkaline earth triethylhydroborate complexes

Salt metathesis reactions of ($Tp^{tBu,Me}$)Ca(I)(THF) (**2.17**) or ($Tp^{tBu,Me}$)Sr(I)($THF)_2$ (**5**) with an equivalent of commercially available Na[$HBEt_3$] (1 M in toluene) in C_6H_6 at room temperature gave the corresponding ($Tp^{tBu,Me}$)Ca($HBEt_3$)(THF) (**17**) or ($Tp^{tBu,Me}$)Sr($HBEt_3$)($THF)_2$ (**18**) complexes, respectively, in 53-62% crystallised yield (Equation 5.1).

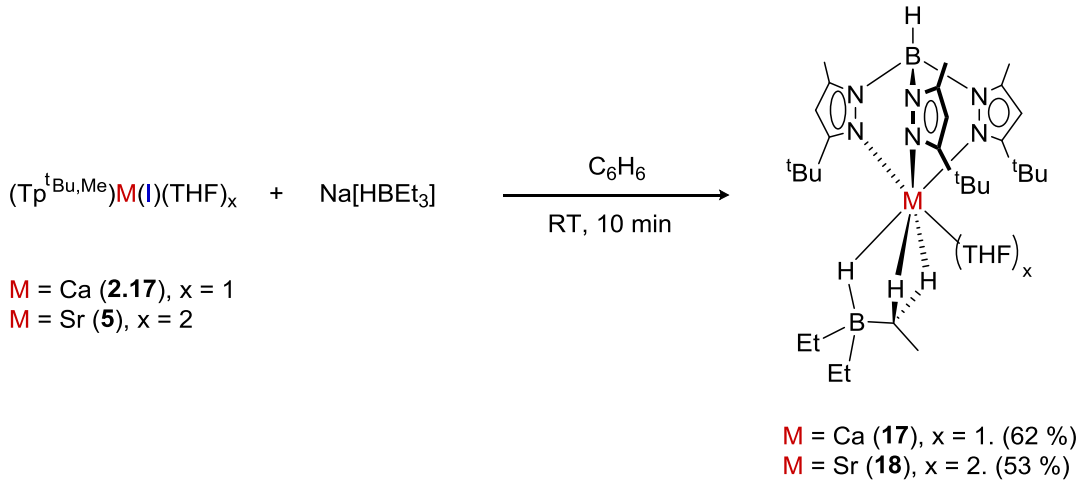

Equation 5.1

Attempts to synthesise the analogous magnesium triethylhydroborate using ($Tp^{tBu,Me}$)Mg(Cl) (**3**) and Na[$HBEt_3$] in either C_6H_6 or THF were unsuccessful due to the discrepancy between available coordination sphere around the metal centre and the steric hindrance of the $HBEt_3$ moiety. A trace amount of the new product formed during the course of several hours of reaction. The ^{1}H NMR spectrum of the solution mixture showed a new set of $Tp^{tBu,Me}$ resonances, aside from that of **3**. The corresponding ^{11}B NMR showed a doublet at δ = -8.8 ppm ($^1J_{B\text{-}H}$ = 79 Hz) of B-H($Tp^{tBu,Me}$) and a triplet at -19.3 ppm ($^1J_{B\text{-}H}$ = 59 Hz). The new product was potentially assigned to ($Tp^{tBu,Me}$)Mg(H_2BEt_2). The observation agreed with the previous reports by Fryzuk[40, 41] and Morris,[42] whereby the formation of an unexpected diethyl dihydridoborate species could be explained by the redistribution of $HBEt_3$ to H_2BEt_2 and BEt_4.

The ^{1}H NMR (C_6D_6) spectra of compounds **17** and **18** showed time averaged resonances of $HBEt_3$ at very similar chemical shifts; a triplet (δ = 1.50 (for **17**) and 1.56 (for **18**) ppm, ^{3}J = 7.5 Hz) corresponding to the methyl protons and a quartet (δ = 0.94 (for **17**) and 0.88 (for **18**) ppm, ^{3}J = 7.5 Hz) corresponding to the methylene protons of the ligand (Figure 5.2). The bridging hydride (M-H_b-B) and B-H of ($Tp^{tBu,Me}$) ligand were not detected in ^{1}H NMR spectra. One molecule of coordinated THF for **17** whereas two THF molecules for **18** was justified owing to a larger Sr^{2+} coordination sphere.

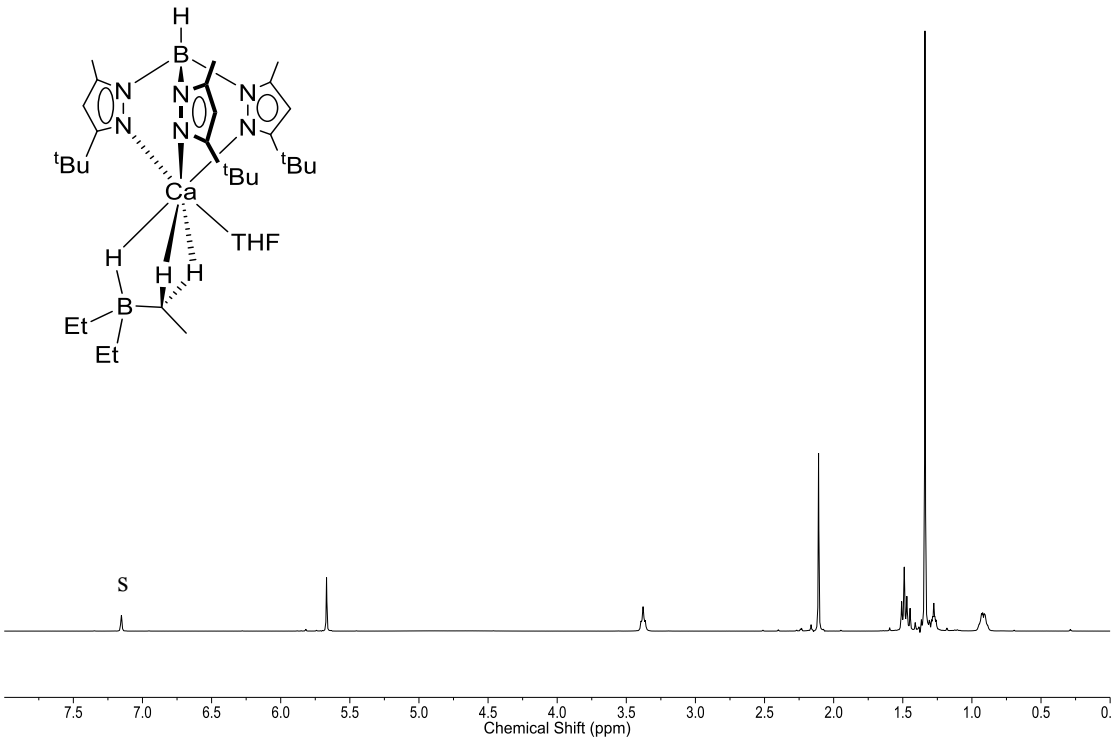

Figure 5.2. ^{1}H NMR spectrum (C_6D_6, 400 MHz, 298 K) of ($Tp^{tBu,Me}$)Ca($HBEt_3$)(THF) (**17**). "s" denotes residual protio-solevent.

As a result of a pronounced quadrupole effect, signals corresponding to the $\underline{C}H_2$ of $HBEt_3$ are not observed in the $^{13}C\{^{1}H\}$ (C_6D_6) spectra of both **17** and **18**. ^{11}B NMR resonances of $HBEt_3$ are found at δ = -10.5 ppm, $^{1}J_{B\text{-}H}$ = 46 Hz (for **17**) and δ = -11.5 ppm, $^{1}J_{B\text{-}H}$ = 54 Hz (for **18**) ppm. These are characteristic of a bridging B-H. The observed ^{11}B resonances are similar to those of **5.1** (δ = -13.3 ppm, $^{1}J_{B\text{-}H}$ = 50 Hz),[1] **5.5** (δ = -15.7 ppm), [(TMTA)K(μ-H)BEt_3]$_2$ (δ = -15.9 ppm)[3] and Na[$HBEt_3$] (δ = -12.5 ppm, $^{1}J_{B\text{-}H}$ = 50 Hz).[43] Prominent υ(B-H) stretches occur at 1889 (for **17**) and 1950 (**18**) cm^{-1} in solid state IR spectra. These B-H stretching frequencies, associated

with (μ-H)-B fragments, are in good agreement with those observed for M[HBEt$_3$] (M = Li, Na or K) (1870-1950 cm^{-1}),[44] **5.1** (1935 cm^{-1}),[1] **5.3** (1924 cm^{-1}) and **5.4** (1932 cm^{-1}).[2]

Diffraction-quality crystals of **17** were grown from a THF/pentane (1:3 v/v) mixture at -30 °C. The solid state structure and its selected bond lengths and angles are shown in Figure 5.3 and Table 5.1, respectively.

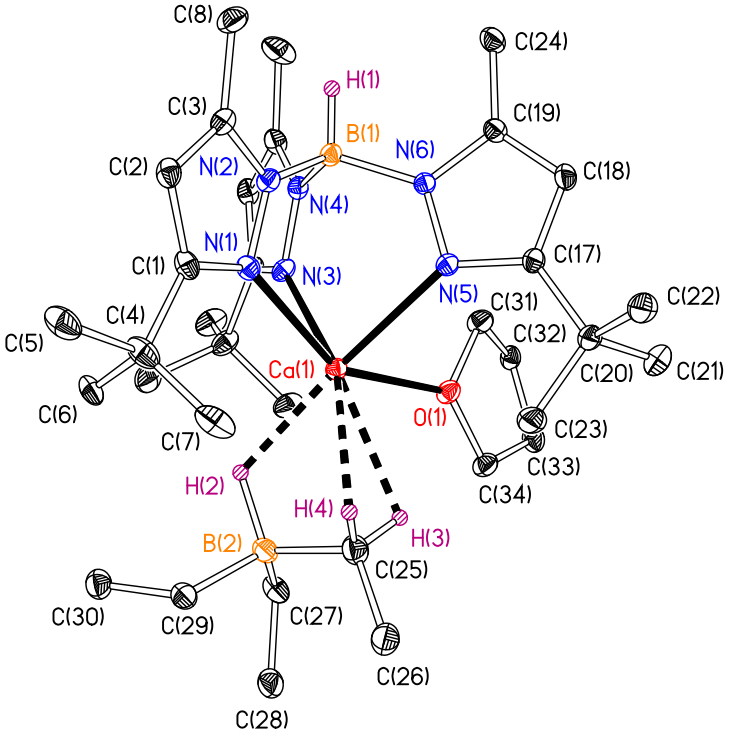

Figure 5.3. Displacement ellipsoid plot (20% probability level) of (Tp^{tBu,Me})Ca(HBEt$_3$)(THF) (**17**). C-bound H atoms (except H(3) and H(4)) omitted.

Table 5.1. Selected bond lengths (Å) and angles (°) for ($Tp^{tBu,Me}$)Ca($HBEt_3$)(THF) (**17**).

Ca(1)-N(1)	2.5064(18)	Ca(1)-H(2)	2.25(2)
Ca(1)-N(3)	2.4419(16)	Ca(1)-H(3)	2.52(3)
Ca(1)-N(5)	2.4776(18)	Ca(1)-H(4)	2.62(3)
Ca(1)-O(1)	2.4356(15)	B(2)-H(2)	1.29(3)
Ca(1)···B(2)	3.059(3)		
N(1)-Ca(1)-N(3)	79.21(6)	N(1)-Ca(1)-O(1)	150.74(5)
N(1)-Ca(1)-N(5)	76.43(5)	N(3)-Ca(1)-O(1)	86.42(6)
N(3)-Ca(1)-N(5)	92.59(6)	N(5)-Ca(1)-O(1)	78.92(6)
N(5)-Ca(1)-H(2)	168.9(7)	H(2)-Ca(1)-O(1)	106.4(6)
Ca(1)-N(1)-N(2)-B(1)	5.2	Ca(1)-N(3)-N(4)-B(1)	9.7
Ca(1)-N(5)-N(6)-B(1)	28.7		

Compound **17** is *pseudo* five-coordinate with Ca(1) coordinated to the three N donors of the $Tp^{tBu,Me}$ ligand (Ca(1)-N(1/3/5) distances of 2.5064(18), 2.4419(16) and 2.4776(18) Å, respectively), O(1) of the THF ligand (Ca(1)-O(1) distance of 2.4356(15) Å) and a κ^3-bound $HBEt_3$ ligand (Ca···B distance of 3.059(3) Å). The Ca(1)-N(1/3/5) and Ca(1)-O(1) bond lengths are similar to those of the analogous tetrahydroborate compound **1** within error (Ca(1)-N(1/3/5) distances of 2.5053(16), 2.4256(17) and 2.4307(16) Å, respectively and Ca(1)-O(1) distance of 2.4291(14) Å). Nevertheless, the Ca···B distance of **17** is longer than those of **1** (2.567(3) Å), **5.5** (2.930(5) Å), **5.3** (2.861(4) Å) and even longer than that of **5.4** with larger metal centre (3.003(3) Å).[1-3] The geometry at Ca(1) is best described as distorted octahedral with N(5) and H(2) occupying the axial positions (N(5)-Ca(1)-H(2) angle of 168.9(7) °). Ca(1) lies 0.3 Å above the least-square plane defined by N(1), N(3), H(3) and H(4).

The solid state structure confirmed the multidentate ligation of $HBEt_3$ to the metal centre through a bridging hydride and two agostic-type hydrogens of one of the ethyl substituents. The Ca(1)-H(2) bond distance of 2.25(2) Å is comparable to those of **5.1** (2.21(4) Å) and **5.3** (2.16(3) Å) but shorter than the average Ca-(μ-H) bond length of

($Tp^{tBu,Me}$)Ca(BH_4)(THF) (**1**), (2.42(11) Å). A vast number of compounds containing $HBEt_3$ or BEt_4 often exhibit agostic interactions between the metal centres and methylene hydrogens. For compound **17**, Ca(1)-H(3) and Ca(1)-H(4) bond distances of 2.52(3) and 2.62(3) Å lie within the expected range of agostic interactions previously reported.[1, 13, 29, 41, 45] Such a coordination of the $HBEt_3$ ligand results in a Ca(1)-H(2)-B(2) angle of 116.6(15) °. The Ca(1)-H(2)-B(2) angle is as expected among triethyl hydridoborate compounds with similar metal ionic radii, regardless of ligand types.[1, 3, 32] The ethyl substituents on the $HBEt_3$ ligand exert significant steric hindrance around the metal centre resulting in a noticeable deviation of one of the pyrazolyl rings from the C_3 plane of the $Tp^{tBu,Me}$ ligand (*ca*. 28.7 °).

Similar to that found in the work of Hanusa *et al*.,[1] the triethylborane in **17** or **18** cannot be removed by substitution with a strong Lewis base such as NEt_3. However, NMR tube scale reactions between **17** or **18** and BH_3·THF instantaneously yielded the tetrahydroborate analogues **1** or **4**, respectively, along with liberation of BEt_3 (confirmed by a characteristic resonance at δ = 86.4 ppm in the ^{11}B NMR spectra).[46] This observation is reminiscent of the reaction between $(C_5H_4CH_2CH_2OMe)_2Nd(HBEt_3)$ and BH_3·SMe_2.[12]

5.4 Synthesis and characterisation of alkaline earth dialkyl 9-borabicyclo [3.3.1] nonane dihydridoborate complexes

To assess a series of alkaline earth $H_2BC_8H_{14}$ complexes, salt metathesis reactions were employed. ($Tp^{tBu,Me}$)Ca(I)(THF) (**2.17**) or ($Tp^{tBu,Me}$)Sr(I)$(THF)_2$ (**5**) were treated with an equivalent of literature prepared $K[H_2BC_8H_{14}]$[21] in THF at room temperature, giving ($Tp^{tBu,Me}$)Ca{(μ-H)$_2$$BC_8H_{14}$}(THF) (**19**) or ($Tp^{tBu,Me}$)Sr{(μ-H)$_2$$BC_8H_{14}$}$(THF)_2$ (**20**) in 64 % and 59 % crystallised yield, respectively (Equation 5.2).

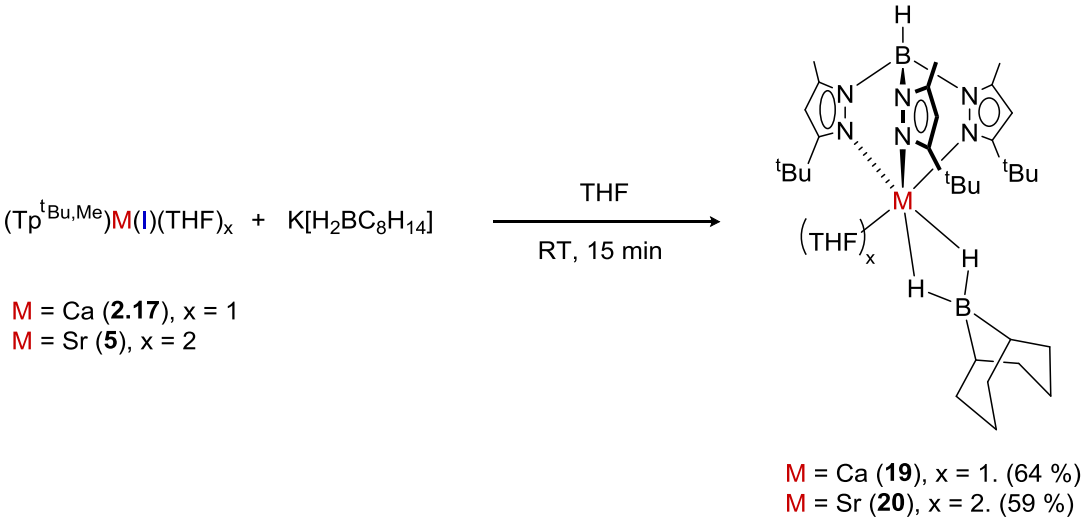

Equation 5.2

The salt metathesis method and condition cannot be directly applied to produce the analogous magnesium complex. The reaction between $(Tp^{tBu,Me})Mg(Cl)$ (**3**) and $K[H_2BC_8H_{14}]$ in THF at room temperature produced a very small amount of desired product $(Tp^{tBu,Me})Mg\{(\mu\text{-}H)_2BC_8H_{14}\}$ (**21**) in 48 h. However, a significant amount of **21** was obtained when the reaction was carried out in C_6H_6, with complete conversion achieved when heated at 50 °C for 9 h. Insolubility of the KCl by-product in C_6H_6 is postulated as the driving force in this case (Scheme 5.2(a)).

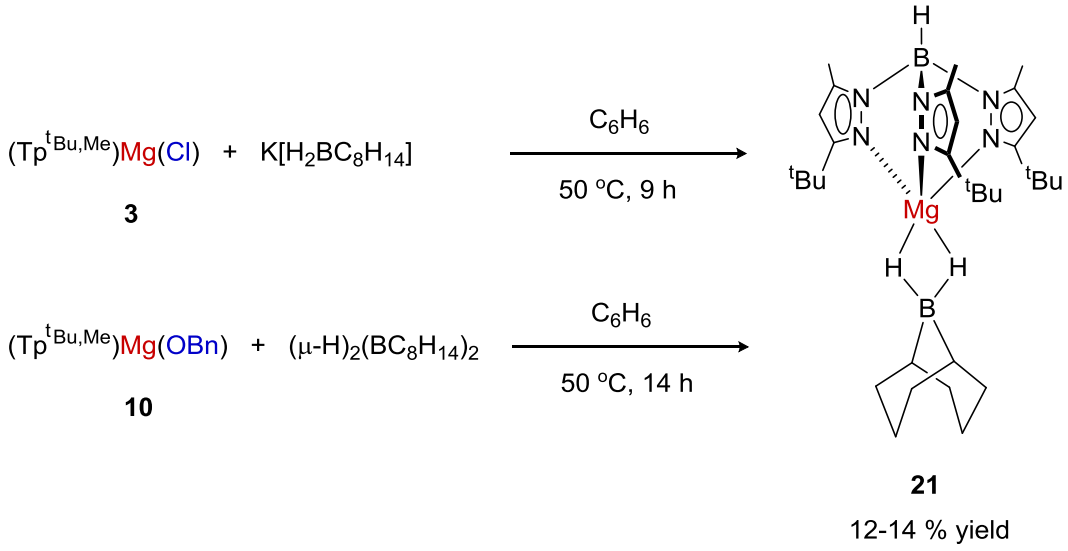

Scheme 5.2. Possible synthetic pathways to $(Tp^{tBu,Me})Mg\{(\mu\text{-}H)_2BC_8H_{14}\}$ (**21**).

Synthesis of compound **21** can also be approached through transmetallation between $(Tp^{tBu,Me})Mg(OBn)$ (**10**) and $(\mu\text{-}H)_2(BC_8H_{14})_2$ in C_6H_6 at 50 °C. Unfortunately, both

synthetic routes afforded an undesired side product. The undesired product is presumably a result of fractionalisation of the ($Tp^{tBu,Me}$) ligand due to the presence of hydride-carrying species. The observation correlates well with the literature, whereby the reaction between $(Tp^{Me2})_2Nd(Cl)$ and $K[H_2BEt_2]$ led to the formation of $(Tp^{Me2})_2Nd(pz^{Me2})$.[47] Because of the similar solubility of **21** and the competing impurity, several recrystallisation attempts in pentane or benzene at 5 °C were undertaken to isolate pure **21**. Consequently, compound **21** was obtained in a very low yield of 12-14 % (Scheme 5.2(b)).

Similar to compounds **17** and **18**, the ^1H NMR (C_6D_6) spectra of heavier alkaline earth organodihydridoborates **19** and **20** showed resonances of $(\mu\text{-}H)_2BC_8H_{14}$ at very similar chemical shifts. For example, broad multiplets at δ = 2.56, 2.41, 2.19 ppm and a broad singlet at δ = 1.61 ppm with an integral ratio of 1:4:1:1 are assigned to the γ-, β-, γ'- and α-hydrogens of the organodihydridoborate ring in **19** (Figure 5.4).

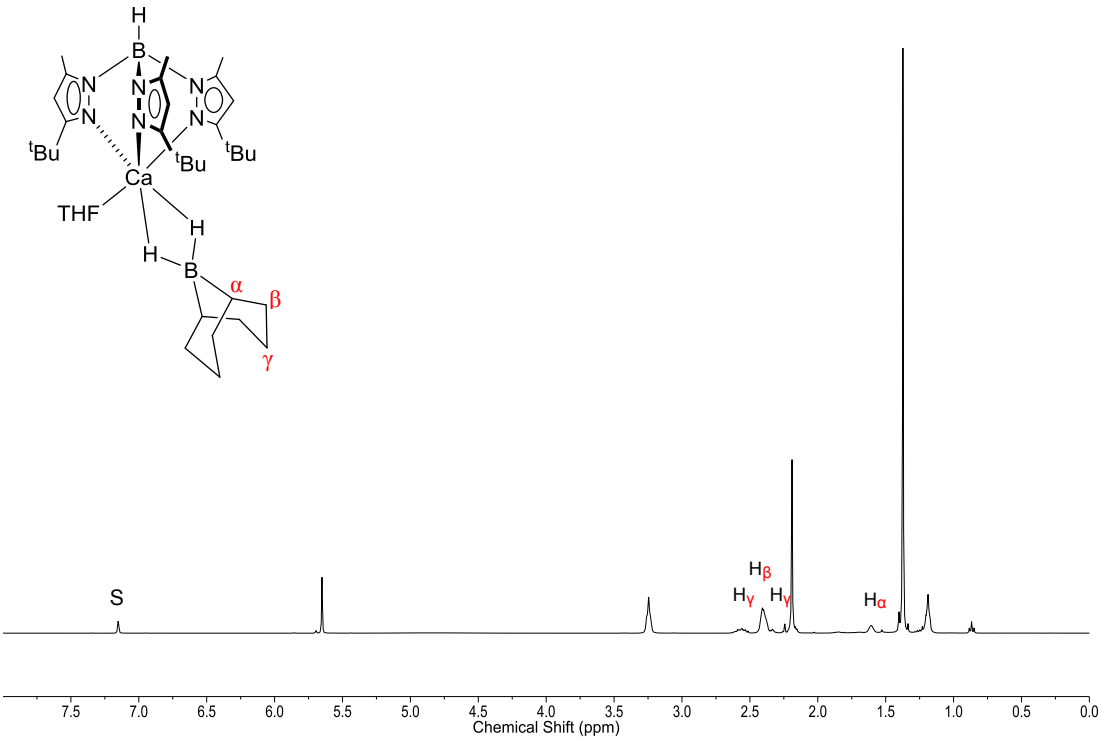

Figure 5.4. ^1H NMR spectrum (C_6D_6, 400 MHz, 298 K) of $(Tp^{tBu,Me})Ca\{(\mu\text{-}H)_2BC_8H_{14}\}(THF)$ (**19**). "s" denotes residual protio-solevent.

^1H NMR (C_6D_6) analysis of the smallest metal congener **21** illustrated a slightly different set of resonances, the β-hydrogens of $(\mu\text{-}H)_2BC_8H_{14}$ fragment became inequivalent and appeared as two broad multiplets at δ = 2.39 and 2.31 ppm with an

integral ratio of 1:1. This could be explained as the less labile $(\mu\text{-H})_2BC_8H_{14}$ moiety experiences stronger influences from the ligand substituents and metal centre in a sterically hindered compound. The bridging hydrides (M-H_b-B) and B-H of the ($Tp^{tBu,Me}$) ligand were not observed in ^1H NMR spectra, with the exception of the bridging hydrides (M-H_b-B) of **20** which appear as a 1:1:1:1 quartet at δ = 1.76 ppm with $^1J_{B\text{-}H}$ = 70 Hz. Once again, the pronounced quadrupole effect caused either the disappearance or the diminishing intensity of signals corresponding to the C_α of $(\mu\text{-H})_2BC_8H_{14}$ in the $^{13}C\{^1H\}$ NMR spectra of all three compounds. The ^{11}B NMR spectra of **19**, **20** and **21** in C_6D_6 revealed triplets at δ = -10.2 ($^1J_{B\text{-}H}$ = 70 Hz), -8.6 ($^1J_{B\text{-}H}$ = 70 Hz) and -18.2 ($^1J_{B\text{-}H}$ = 68 Hz) ppm, respectively. The relatively downfield ^{11}B shifts were observed in the compound with larger metal centres. The same observation was also made in the series of alkaline earth tetrahydroborate compounds (Chapter 2). Furthermore, the ^{11}B NMR resonances and the $^1J_{B\text{-}H}$ coupling constants of **19**, **20** and **21** are consistent with those of **5.2** (δ = -12.1 ppm, $^1J_{B\text{-}H}$ = 68 Hz)[32] and analogous alkali salts (δ = -18 to -16 ppm, $^1J_{B\text{-}H}$ = 74 Hz).[21]

Infrared spectroscopic analyses (NaCl plates, Nujol mull) show υ(B-H) stretching frequencies (symmetric and asymmetric modes) at 2092 and 2042 cm^{-1} for **19**, 2090 and 2038 cm^{-1} for **20** and 2082 and 2027 cm^{-1} for **21**. These values lie within the expected range for bridging υ(B-H) bands (1525-2150 cm^{-1}).[48, 49] Accordingly the observed B-H stretching frequencies are also similar to those of **5.2** (2023 and 2054 cm^{-1})[32], alkali salts (2080-2110 cm^{-1})[21] and lanthanide (II) dihydridoborate complexes (2118-2012 cm^{-1}).[11, 50]

Diffraction-quality crystals of **19** and **20** were grown from a THF/pentane mixture (1:3 v/v) at -30 °C, and for **21** from a saturated benzene solution at 4°C. The solid state structures of **19**, **20** and **21** and their selected bond lengths and angles are shown in Figure 5.5 and Table 5.2, respectively.

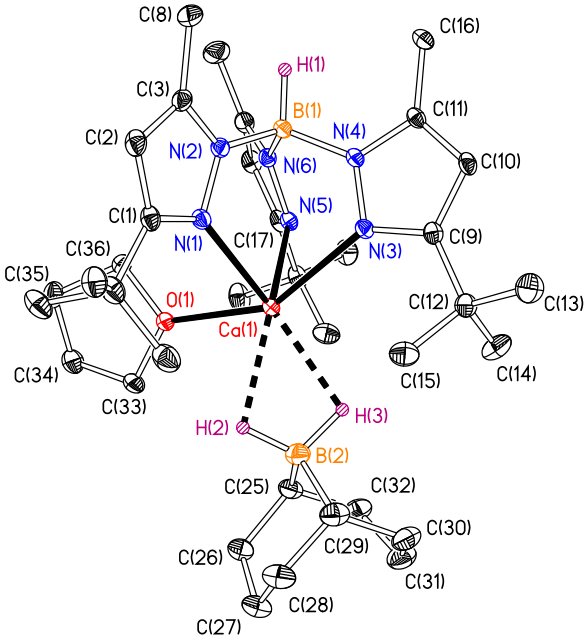

(a)

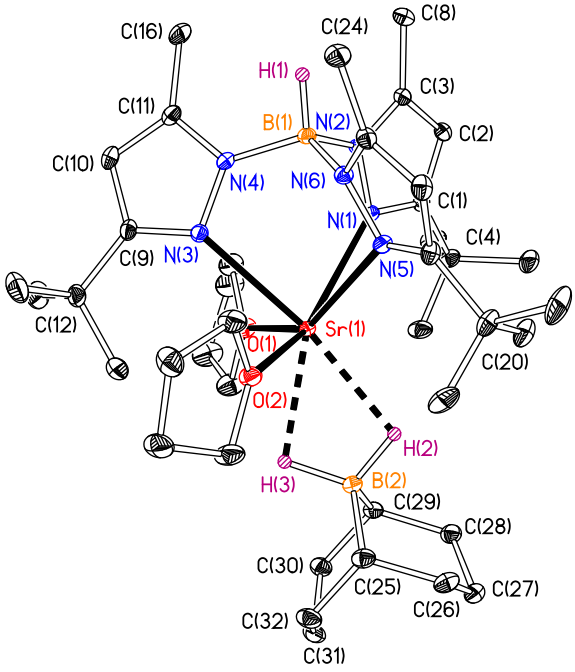

(b)

Figure 5.5. Displacement ellipsoid plots (20% probability level) of (a) ($Tp^{tBu,Me}$)Ca{(μ-H)$_2$BC$_8$H$_{14}$}(THF) (**19**), (b) ($Tp^{tBu,Me}$)Sr{(μ-H)$_2$BC$_8$H$_{14}$}(THF)$_2$ (**20**) and (c) ($Tp^{tBu,Me}$)Mg{(μ-H)$_2$BC$_8$H$_{14}$} (**21**). C-bound H atoms are omitted for clarity.

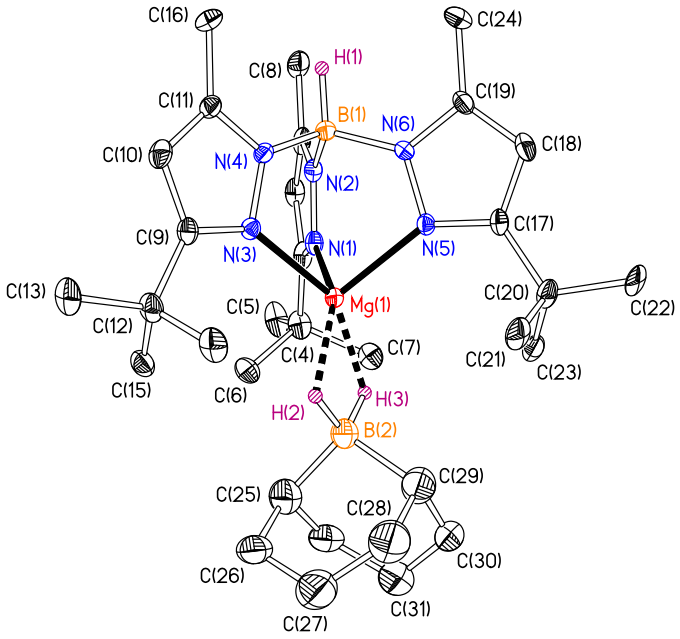

(**c**)

Figure 5.5 (continued). Displacement ellipsoid plots (20% probability level) of (a) ($Tp^{tBu,Me}$)Ca{(μ-H)$_2$BC$_8$H$_{14}$}(THF) (**19**), (b) ($Tp^{tBu,Me}$)Sr{(μ-H)$_2$BC$_8$H$_{14}$}(THF)$_2$ (**20**) and (c) ($Tp^{tBu,Me}$)Mg{(μ-H)$_2$BC$_8$H$_{14}$} (**21**). C-bound H atoms are omitted for clarity.

Table 5.2. Selected bond lengths (Å) and angles (°) for ($Tp^{tBu,Me}$)Ca{(μ-H)$_2$BC$_8$H$_{14}$}(THF) (**19**), ($Tp^{tBu,Me}$)Sr{(μ-H)$_2$BC$_8$H$_{14}$}(THF)$_2$ (**20**) and ($Tp^{tBu,Me}$)Mg{(μ-H)$_2$BC$_8$H$_{14}$} (**21**). "M" represents a metal centre in the specified compound.

Parameters	**19**	**20**	**21**
M(1)-N(1)	2.465(2)	2.7033(17)	2.140(3)
M(1)-N(3)	2.477(2)	2.6191(17)	2.136(3)
M(1)-N(5)	2.455(2)	2.6234(17)	2.125(3)
M(1)···B(2)	2.837(3)	2.975(2)	2.454(6)
M(1)-H(2)	2.327	2.471	2.140
M(1)-H(3)	2.390	2.480	1.880
M(1)···H(251) or $H_{C\alpha}$	3.725	4.215	3.707
M(1)···H(291) or $H_{C\alpha}$	4.030	3.858	3.816
B(2)-H(2)	1.200	1.266	1.203
B(2)-H(3)	1.200	1.308	1.205

Table 5.2 (continued.) Selected bond lengths (Å) and angles (°) for ($Tp^{tBu,Me}$)Ca{(μ-H)$_2$BC$_8$H$_{14}$}(THF) (**19**), ($Tp^{tBu,Me}$)Sr{(μ-H)$_2$BC$_8$H$_{14}$}(THF)$_2$ (**20**) and ($Tp^{tBu,Me}$)Mg{(μ-H)$_2$BC$_8$H$_{14}$} (**21**). "M" represents a metal centre in the specified compound.

Parameters	**19**	**20**	**21**
M(1)-O(1)	2.4106(19)	2.6301(16)	-
M(1)-O(2)	-	2.6664(15)	-
N(1)-M(1)-N(3)	75.09(7)	82.05(5)	90.50(11)
N(1)-M(1)-N(5)	91.35(8)	67.16(5)	90.76(11)
N(3)-M(1)-N(5)	78.42(7)	84.11(5)	94.86(10)
N(2)-B(1)-N(4)	110.2(2)	111.84(5)	109.9(3)
N(2)-B(1)-N(6)	111.6(2)	108.83(16)	109.6(3)
N(4)-B(1)-N(6)	111.1(2)	114.84(16)	110.5(3)
M(1)···B(2)-C(25)	120.4(2)	134.27(14)	125.8(4)
M(1)···B(2)-C(29)	132.5(3)	120.30(13)	128.7(4)
B(1)···M(1)···B(2)	165.83(10)	162.65(6)	174.12(19)
M(1)-N(1)-N(2)-B(1)	3.5	3.4	0.3
M(1)-N(3)-N(4)-B(1)	20.9	25.7	5.2
M(1)-N(5)-N(6)-B(1)	40.7	41.6	4.5

Coordination number increases from *pseudo* four-coordination in the magnesium compound **21** to five-coordination in the calcium analogue **19** and to six-coordination in the strontium congener **20**. As confirmed by ^{1}H NMR spectroscopy, solid state structures of **19** and **20** possess one and two strongly bound THF molecules, respectively. No dissociation of THF was observed in non-polar solvents. The increase in coordination number and metal centre size to charge ratio is reflected by generally longer bond distances (i.e. M-N, M-H, M-O and M···B distances) in the order of **21** < **19** < **20**.

In all cases (μ-H)$_2$BC$_8$H$_{14}$ fragments coordinate to the metal centres through two bridging hydrides. In contrast to most of the literature compounds containing (μ-H)$_2$BC$_8$H$_{14}$,[11, 20, 30, 32] there are no agostic interactions between the C$_\alpha$-H bonds and the

metal centres in **19**, **20** and **21**. The M-H_{C_α} distances (3.725 and 4.030 Å for **19**, 4.215 and 3.858 Å for **20** and 3.707 and 3.816 Å for **21**) are considerably longer than the sum of ionic radii of the metal centres and the hydrogen van der Waals radius (1.92 Å for the Mg-H, 2.20 Å for the Ca-H and 2.38 Å for the Sr-H), affirming no α-agostic interactions in these compounds.[51, 52] Reduced M-B-C_α angles to facilitate the α-agostic interactions between the metal centres and C_α-H were observed and established by Chen *et. al*.[50] This factor is used as one of the criteria to consider the existence of α-agostic interactions among the $(\mu\text{-H})_2BC_8H_{14}$ ligating compounds. For **19**, **20** and **21** with no α-agostic interactions, M-B(2)-C(25/29) angles are reasonably similar within the same compound ranging between 120.4(2)-134.27(14) °. The average M-H(2/3) bond distances of **19**, **20** and **21** are 2.359, 2.476 and 2.010 Å, respectively, and consistent with those of the tetrahydroborate counterparts (2.42(11) Å for **1**, 2.56(13) Å for **4** and 2.16(4) Å for **2**). Whilst, the M···B distances of **19**, **20** and **21** (2.837(3), 2.975(2) and 2.454(6) Å) are longer than that observed in the tetrahydroborate analogues **1**, **4** and **2** (2.567(3), 2.786(3) and 2.263(2) Å). The distinct difference could be influenced by the variation of hapticity of dialkyl dihydridoborate (κ^2) and tetrahydroborate (κ^3) ligand.

Significant steric hindrance created by the strongly bound THF molecules as well as $H_2BC_8H_{14}$ ligands was observed in **19** and **20**, by the extensive distortion of pyrazolyl rings from the C_3 planes of $Tp^{tBu,Me}$ ligands (20.9 and 40.7 ° in **19** as well as 25.7 and 41.6 ° in **20**). For **21**, only minimal distortion of the pyrazolyl rings was observed allowing the $H_2BC_8H_{14}$ ligand to align linearly to the vertical axis of the $Tp^{tBu,Me}$ ligand (B(1)···Mg(1)···B(2) = 174.12(19) °).

Reactions between **19** or **20** and BH_3·THF were also carried out and monitored using ^1H and ^{11}B NMR analyses. Unlike **17** or **18**, no immediate reactions were observed. However, the production of the corresponding tetrahydroborate analogues **1** or **4** was observed along with $(\mu\text{-H})_2(BC_8H_{14})_2$ and unreacted starting materials after 30 mins. Quantitative conversion was achieved by further addition of BH_3·THF indicating the existence of an equilibrium in these reactions. A high tendency of diorganyl dihydridoborates to undergo substituent exchange inter- or intra-molecularly is precedented in the literature.[53]

5.5 Polymerisation studies: ROP of *rac*-LA

As mentioned previously, since alkyl boranes and organohydroborates are innocent in substituent exchange reactions, organohydroborates ($HBEt_3$ and $H_2BC_8H_{14}$) as single-site initiators are expected to give living ROP with good molecular weight control and defined polylactide end-group functionality. The ROP of *rac*-LA using ($Tp^{tBu,Me}$)Mg{(μ-H)$_2$BC$_8$H$_{14}$} (**21**) was not performed owing to the low yielding synthesis of this catalyst. As a consequence, the effect of organylhydroborate towards the change in *rac*-LA ROP pathway (when compared that using ($Tp^{tBu,Me}$)Mg(BH_4) (**2**)) cannot be drawn. Nevertheless, ($Tp^{tBu,Me}$)M($HBEt_3$)(THF)$_x$ (**17**, M = Ca, x = 1, and **18**, M = Sr, x = 2) and ($Tp^{tBu,Me}$)M{(μ-H)$_2$BC$_8$H$_{14}$}(THF)$_x$ (**19**, M = Ca, x = 1 and **20,** M = Sr, x = 2) allows the systematic evaluation of the catalytic potential of organylhydroborates in initiating *rac*-LA ROP, molecular weight control and polymer functionality. Their catalytic behaviour towards ROP of *rac*-LA could be directly compared with their tetrahydroborate counterparts and between the two different organylhydroborate initiating groups. The *rac*-LA polymerisation results are summarised in Table 5.3.

Table 5.3. Polymerisation of *rac*-LA using ($Tp^{tBu,Me}$)Ca($HBEt_3$)(THF) (**17**), ($Tp^{tBu,Me}$)Sr($HBEt_3$)(THF)$_2$ (**18**), ($Tp^{tBu,Me}$)Ca{(μ-H)$_2$BC$_8$H$_{14}$}(THF) (**19**) and ($Tp^{tBu,Me}$)Sr{(μ-H)$_2$BC$_8$H$_{14}$}(THF)$_2$ (**20**) in THF.[a]

Initiator	Time (min)	Conversion (%)[b]	M_n (GPC)[c]	M_n (Calcd)[d]	PDI[e]	P_r[f]
17	1	98	4,430	14,130	4.39	0.78
18	1	95	5,390	13,700	3.48	0.67
19	1	97	14,560	13,990	1.47	0.83
20	1	95	13,620	13,700	1.77	0.66

[a] Conditions: [*rac*-LA]$_0$:[initiator] = 100:1, 6.0 mL THF at 23 °C, [*rac*-LA]$_0$ = 0.5 M. [b] Determined by ^{1}H NMR integration of the OC<u>H</u>Me resonance relative intensities of the residual *rac*-LA and PLA in $CDCl_3$. [c] M_n (g mol^{-1}) determined by GPC using the appropriate Mark-Houwink corrections. [d] Expected M_n (g mol^{-1}) for 1 chain growing per metal centre at the stated conversion; M_n (Calcd for PLA using **17** and **18**) = converstion (%) × 100 × 144.1 + 2 and M_n (Calcd for PLA using **19** and **20**) = converstion (%) × 100 × 144.1 + 4. [e] PDI = M_w/M_n. [f] Determined by analysis of the OC<u>H</u>Me resonances of selectively homonuclear decoupled ^{1}H{^{1}H} spectra.

5.5.1 ROP of *rac*-LA using ($Tp^{tBu,Me}$)Ca($HBEt_3$)(THF) (17) and ($Tp^{tBu,Me}$)Sr($HBEt_3$)$(THF)_2$ (18)

Catalysts **17** and **18** are extremely active towards the ROP of *rac*-LA, and over 95% monomer conversion was achieved within the first minute of polymerisation in both cases. However, **17** and **18** catalysed ROP in an ill-defined manner, giving much lower than expected molecular weight PLA (4,430 and 5,390 g mol^{-1}, respectively) with extremely broad PDIs of 4.39 and 3.48, respectively. Although poorly controlled ROP was observed, steresoselectivity exerted by the $Tp^{tBu,Me}$ ligand through the chain-end control mechanism was retained. Accordingly P_r values of 0.78 and 0.67 were observed in PLA produced using **17** and **18**, respectively. The degrees of heterotacticity achieved are consistent with those obtained in ROP using analogous tetrahydroborate complexes **1** (P_r = 0.80) and **4** (P_r = 0.67).

The MALDI-ToF analyses of PLA formed using **17** and **18** illustrated a predominant distribution corresponding to cyclic PLA with $\Delta m/z$ of 72 g mol^{-1} between the adjacent peak envelopes (Figure 5.6). It is therefore clear that the polymerisation reactions were significantly affected immensely by inter- and intra-molecular transesterification.

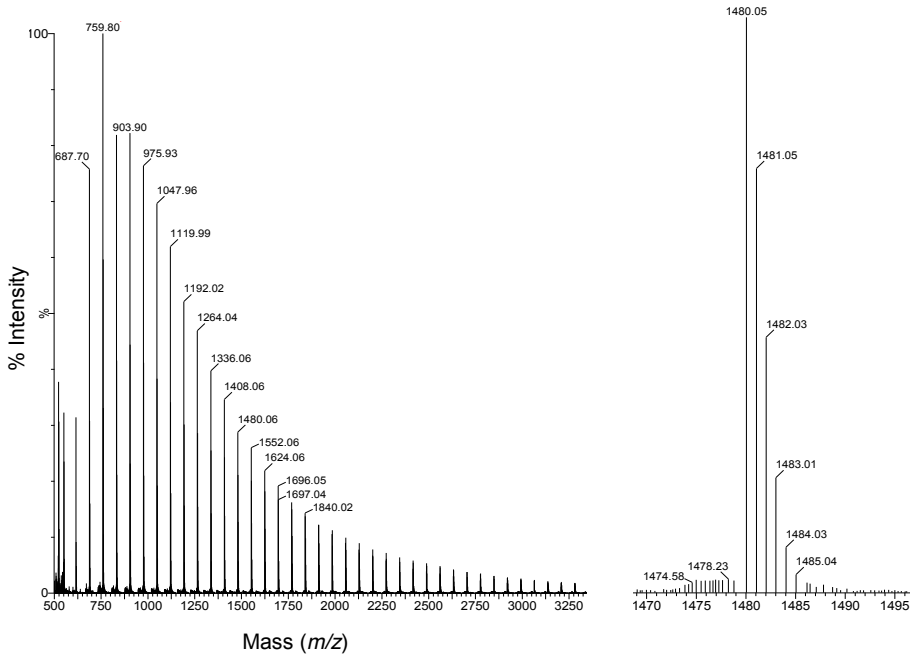

Figure 5.6. MALDI-ToF MS of PLA synthesised using ($Tp^{tBu,Me}$)Ca($HBEt_3$)(THF) (**17**). M_n by GPC analysis was 4,430 g mol^{-1} (from a [*rac*-LA]:[**17**]$_0$ = 100:1 polymerisation at RT) (left). A MALDI-ToF peak envelope of PLA with the length of 10 lactide monomer units (right). K^+ dopant.

In order to gain some insight into the behaviour of **17** and **18** towards *rac*-LA ROP, ^{1}H and ^{11}B NMR analyses of the reactions between **17** or **18** and 10 equivs. of *rac*-LA were carried out in THF-d_8. The ^{11}B NMR spectra showed the immediate disappearance of $HBEt_3$ once *rac*-LA was added, in conjunction with the formation of singlet at δ = 76.1 ppm corresponding to BEt_3.[46] The resonances corresponding to free BEt_3 appear in ^{1}H NMR analysis as a quartet and a triplet at δ = 1.00 and 0.98 ppm, respectively. However, the spectroscopic data regarding the PLA produced cannot be extracted from the ^{1}H NMR spectra due to the broadening signals corresponding to the end group functionality of the PLA in the diganostic region of δ = 4.5-5.5 ppm. These broadening resonances observed in the ^{1}H NMR analyses are similar to those of the PLA formed using tetrahydroborate counterparts. The resonances of BEt_3 observed in the NMR spectroscopic studies imply the loss of BEt_3 after the initial hydride-transfer. The growing polymer chain only coordinates to the heavier alkaline earth metal centre with a large coordination sphere. This enhances the intra-molecular back-biting of the growing polymer chains, resulting in the formation of cyclic PLA.

The results obtained enable a direct comparion between the heavier alkaline earth triethyl hydroborate and tetrahydroborate as *rac*-LA ROP initiators. The presence of multidentate boron species in the initiating or propagaing steps essentially prevents the intramolecular "back-biting" of the growing polymer chain.

5.5.2 ROP of *rac*-LA using ($Tp^{tBu,Me}$)Ca{(μ-H)$_2$BC$_8$H$_{14}$}(THF) (19) and ($Tp^{tBu,Me}$)Sr{(μ-H)$_2$BC$_8$H$_{14}$}(THF)$_2$ (20)

Compounds **19** and **20** also exhibit high catalytic activity towards the ROP of *rac*-LA at room temperature. Similar to those observed using trialkyl hydroborate counterparts, over 95% monomer conversion was obtained within the first minute of polymerisation. Benchmarking polymerisations between **19** or **20** and 100 equivs. of *rac*-LA were performed, giving heterotactic PLA with molecular weights consistent to the calculated values (Table 5.1). On the basis of **19** and **20** displaying good controlled ROP, further runs were conducted where [*rac*-LA]$_0$:[catalyst]$_0$ = 20-300, holding the *rac*-LA concentration constant. The data obtained using **19** and **20** are plotted in Figures 5.7 and 5.8, respectively.

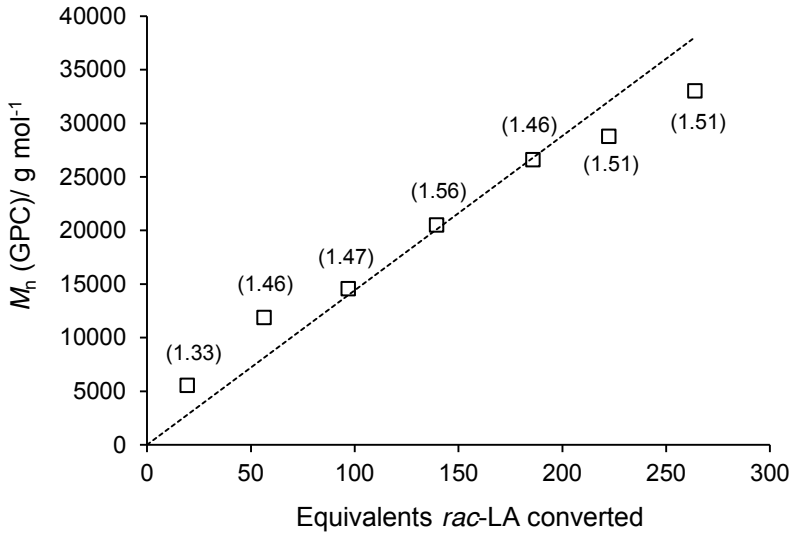

Figure 5.7. M_n (as measured by GPC) *vs*. equivalents *rac*-LA converted using ($Tp^{tBu,Me}$)Ca{(μ-H)$_2$BC$_8$H$_{14}$}(THF) (**19**). The dotted line is that expected for one PLA chain per metal centre. Conditions: 6 mL THF, 23 °C. [*rac*-LA]$_0$:[**19**]$_0$ = 20, 60, 100, 150, 200, 250 and 300. [*rac*-LA]$_0$ = 0.5 M. PDI values are given in parentheses.

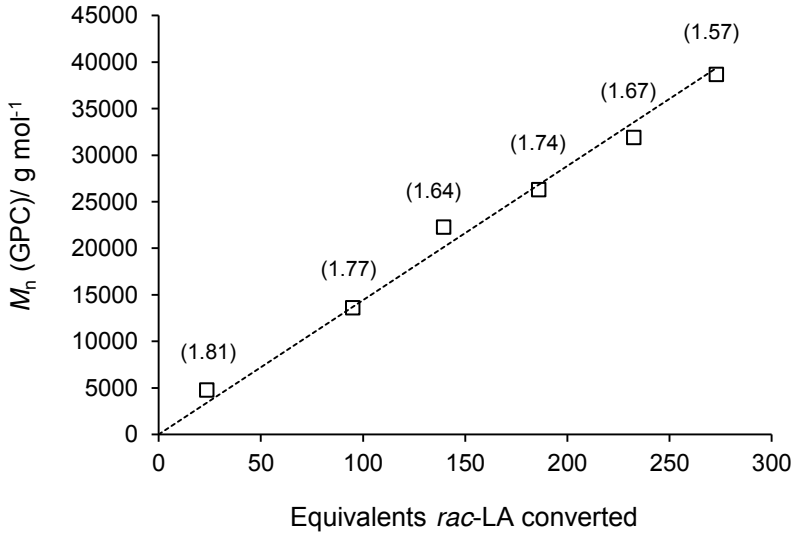

Figure 5.8. M_n (as measured by GPC) *vs*. equivalents *rac*-LA converted using ($Tp^{tBu,Me}$)Sr{(μ-H)$_2$BC$_8$H$_{14}$}(THF)$_2$ (**20**). The dotted line is that expected for one PLA chain per metal centre. Conditions: 6 mL THF, 23 °C. [*rac*-LA]$_0$:[**20**]$_0$ = 25, 100, 150, 200, 250 and 300. [*rac*-LA]$_0$ = 0.5 M. PDI values are given in parentheses.

Compounds **19** and **20** showed good promise in catalysing different loading (20-300 equivs) of *rac*-LA within 1 min. In these plots the expected line of least-squares fit

has a gradient of 144 g mol^{-1} for one chain of PLA produced per metal centre. The gradients of the least-squares fitted lines for polymerisations using **19** and **20** are 111(5) g mol^{-1} (R^2 = 0.990) and 134(6) g mol^{-1} (R^2 = 0.993), respectively. Overall, better agreement between the expected and experimental molecular weights was observed when compared to those obtained using **1** (239(7) g mol^{-1}, R^2 = 0.996)[54] and **4** (131(10) g mol^{-1}, R^2 = 0.978). Molecular weight distributions are moderate for both polymerisations, slightly broader for **20** (PDIs = 1.33-1.56 for **19** and 1.57-1.81 for **20**). The superior degree of heterotacticity was achieved in PLA formed using **19** (P_r = 0.81-0.84) than that obtained using **20** (P_r = 0.66-0.70). The levels of heterotacticity gained are similar to those obtained using analogous tetrahydroborate and triethylhydroborate initiators.

The MALDI-ToF mass spectrum of the PLA formed using **19** illustrated a major and a minor distribution with $\Delta m/z$ between the two distributions of 72 g mol^{-1}, signifying that some transesterification processes were taken place during the polymerisation. Upon closer inspection, peak envelopes consisting of isotopic distributions are consistent with the presence of cyclic PLA, alkoxy LA-H ester termini PLA and dihydroxy telechelic PLA (Figure 5.9).

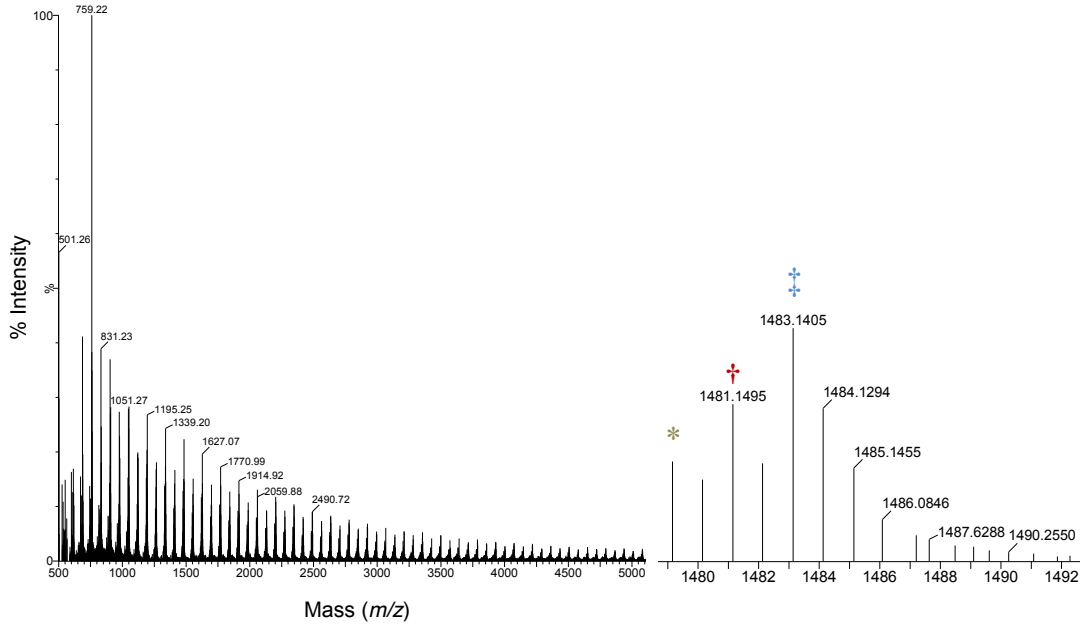

Figure 5.9. MALDI-ToF MS of PLA synthesised using ($Tp^{tBu,Me}$)Ca{(μ-H)$_2$BC$_8$H$_{14}$}(THF) (**19**), K^+ dopant. M_n by GPC analysis was 5,540 g mol^{-1} (from a [*rac*-LA]:[**19**]$_0$ = 20:1 polymerisation at RT) (left). A MALDI-ToF peak envelope of PLA with the length of 10 lactide monomer units (right). Maxima in the isotopic distributions shown are corresponding to cyclic PLA (green asterisk), -alkoxy (LA-H) ester termini (red dagger) and –CH(Me)CH$_2$OH termini (blue double dagger).

The polymer functionalities yielded using **19** are comparable to those obtained using ($Tp^{tBu,Me}$)Ca(BH$_4$)(THF) (**1**). Owing to the inapplicability of MALDI-ToF technique to quantify the exact amount of the various PLA obtained, it is impossible to manifest the ability of **19** in directing and facilitating the hydride transfers in the initiation of ROP in comparison to **1**.

As the catalyst metal centre becomes larger, the influence of alkylhydroborate initiators on polymer functionalities is overwhelmed by extensive transesterification. This is reflected in the MALDI-ToF mass spectrum obtained from the PLA formed using **20** (Figure 5.10). Like the PLA obtained using **4**, MALDI-ToF MS showed a predominant distribution consisting of peak envelopes with $\Delta m/z$ = 72 g mol^{-1} intervals. The isotopic distribution signified a large portion of cyclic PLA, in conjuction with alkoxy (LA-H) ester termini PLA and dihydroxy telechelic PLA.

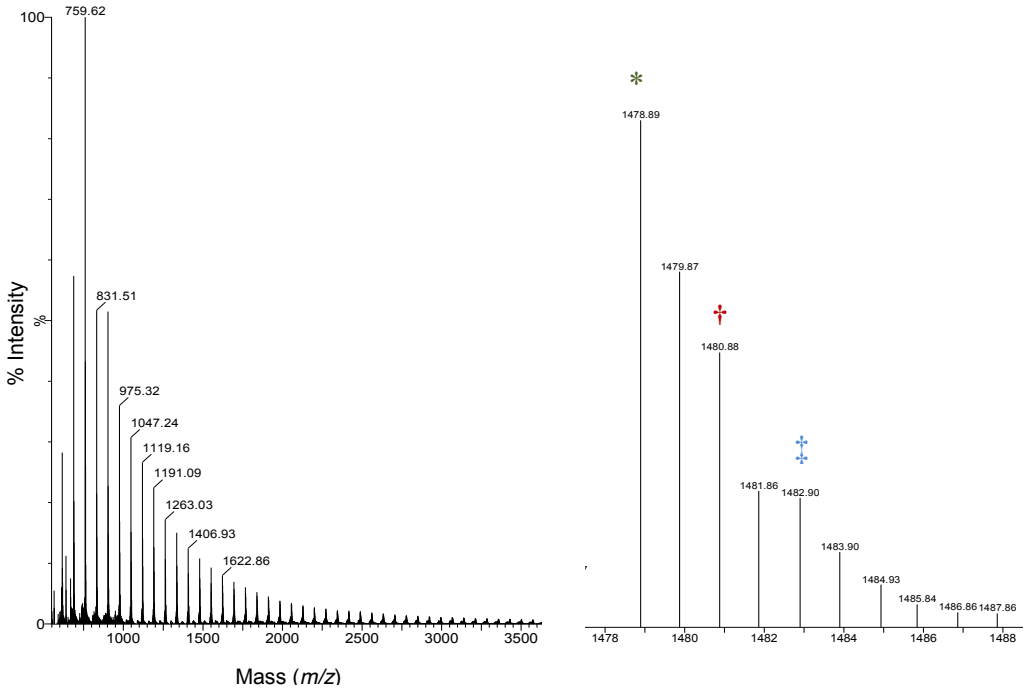

Figure 5.10. MALDI-ToF MS of PLA synthesised using ($Tp^{tBu,Me}$)Sr((μ-H)$_2$BC$_8$H$_{14}$)(THF)$_2$ (**20**), K^+ dopant. M_n by GPC analysis was 4,760 g mol^{-1} (from a [*rac*-LA]:[**20**]$_0$ = 25:1 polymerisation at RT) (left). A MALDI-ToF peak envelope of PLA with the length of 10 lactide monomer units (right). Maxima in the isotopic distributions shown are corresponding to cyclic PLA (green asterisk), -alkoxy (LA-H) ester termini (red dagger) and –CH(Me)CH$_2$OH termini (blue double dagger).

NMR tube-scale experiments were attempted to gain some insight into the *rac*-LA ROP process catalysed by ($Tp^{tBu,Me}$)M{(μ-H)$_2$BC$_8$H$_{14}$}(THF)$_x$. Resembling tetrahydroborate initiators, the initial studies showed very similar catalytic behaviour of heavier alkaline earth metal catalysts. Only the better-behaved ($Tp^{tBu,Me}$)Ca{(μ-H)$_2$BC$_8$H$_{14}$}(THF) (**19**) was studied in detail. ^{1}H and ^{11}B NMR analyses of the NMR tube-scale reaction between **19** and 5 equivs. of *rac*-LA were performed in THF-d_8. The ^{1}H NMR spectrum yielded limited information regarding the PLA and bicyclic [3.3.1] ring containing species due to broadening resonances of the end-group functionality of the PLA in the diagnostic region of δ = 4.5-5.5 ppm and the overlapping resonances of the PLA (OCHMe), ligand and (μ-H)$_2$BC$_8$H$_{14}$ containing species around δ = 1.0-2.0 ppm. Nevertheless, a more informative ^{11}B NMR analysis showed an instantaneous change after the addition of *rac*-LA from a triplet at -10.9 ppm corresponding to (μ-H)$_2$BC$_8$H$_{14}$ of **19** to a small broad singlet at δ = 57.5 ppm, a

small doublet at δ = -1.89 ppm ($^1J_{B-H}$ = 85 Hz) and a small singlet at δ = 3.7 ppm, whilst no significant change was observed for ^{11}B NMR signal of the $Tp^{tBu,Me}$ ligand. The resonance at δ = 57.5 ppm falls into a range of 52.0 to 58.1 ppm corresponding to a three-coordinate $R_2B(OR')$ species (R, R' = alkyl).[46] This implies the double hydride transfer/reduction of lactide yielding a growing chain of PLA with an alkoxy functional group coordinating to the metal centre. This species could act as a propagating intermediate (intermediate **I**) in the production of α,ω-dihydroxy telechelic PLA after quench (Scheme 5.3).

Alternatively, $(Tp^{tBu,Me})Ca\{(\mu\text{-}H)(LA\text{-}H)BC_8H_{14}\}$ formed after the first hydride transfer in the initiation, could undergo dissociation to give either the calcium hydride complex with $(LA\text{-}H)BC_8H_{14}$ or the calcium alkoxide (LA-H) complex with HBC_8H_{14}. Both the calcium hydride and alkoxide (LA-H) complexes are expected to be active ROP catalysts, giving propagating species with growing PLA chain with LA-H active end groups. The association of the metal complexes containing active growing PLA chains and the borane derivatives result in the formation of tetra-coordinate borate intermediates **II** and **III**. After hydrolytic work-up, alkoxy (LA-H) ester terminated PLA is obtained in both cases.

Although there are no other spectroscopic measurements supporting the presence of intermediate **II** and **III** in the solution mixture, the ^{11}B NMR doublet resonance at δ = -1.89 ppm ($^1J_{B-H}$ = 85 Hz) in principle corresponds to intermediate **II** containing $(\mu\text{-}H)(OR)BC_8H_{14}$ (R = PCL) moiety. This evaluation was based on the literature values of related boron-containing compounds; ^{11}B NMR resonances of -2.8 to -1.5 ppm ($^1J_{B-H}$ = 60-71 Hz) for $K[(\mu\text{-}H)(OR)BC_8H_{14}]$ (OR = O^iPr, O^nBu, $O^{sec}Bu$, 2-methyl-2-butoxy or 3-ethyl-3-penthoxy),[55] 0.6 ppm ($^1J_{B-H}$ = 80 Hz) for $Li[(\mu\text{-}H)(OMe)BC_8H_{14}]$[56] and -3.7 to -7.4 ppm ($^1J_{B-H}$ = 242-252 Hz) for $Li[HSia_2B(OR)]$ (Sia = 3-methyl-2-butyl and OR = O^iPr, O^tBu or OEt).[57] The stability of the $(\mu\text{-}H)(OR)BC_8H_{14}$ (R = alkyl) species depends largely on the steric hindrance of the alkoxy group. The unstable analogues are prone to undergo redistribution, resulting in a mixture of $H_2BC_8H_{14}$ and $(OR)_2BC_8H_{14}$.[55] The ^{11}B NMR singlet resonance at δ = 3.7 ppm, falling within the expected range for tetra(alkoxy) borates,[46] could correspond to the presence of intermediate **III** in solution.

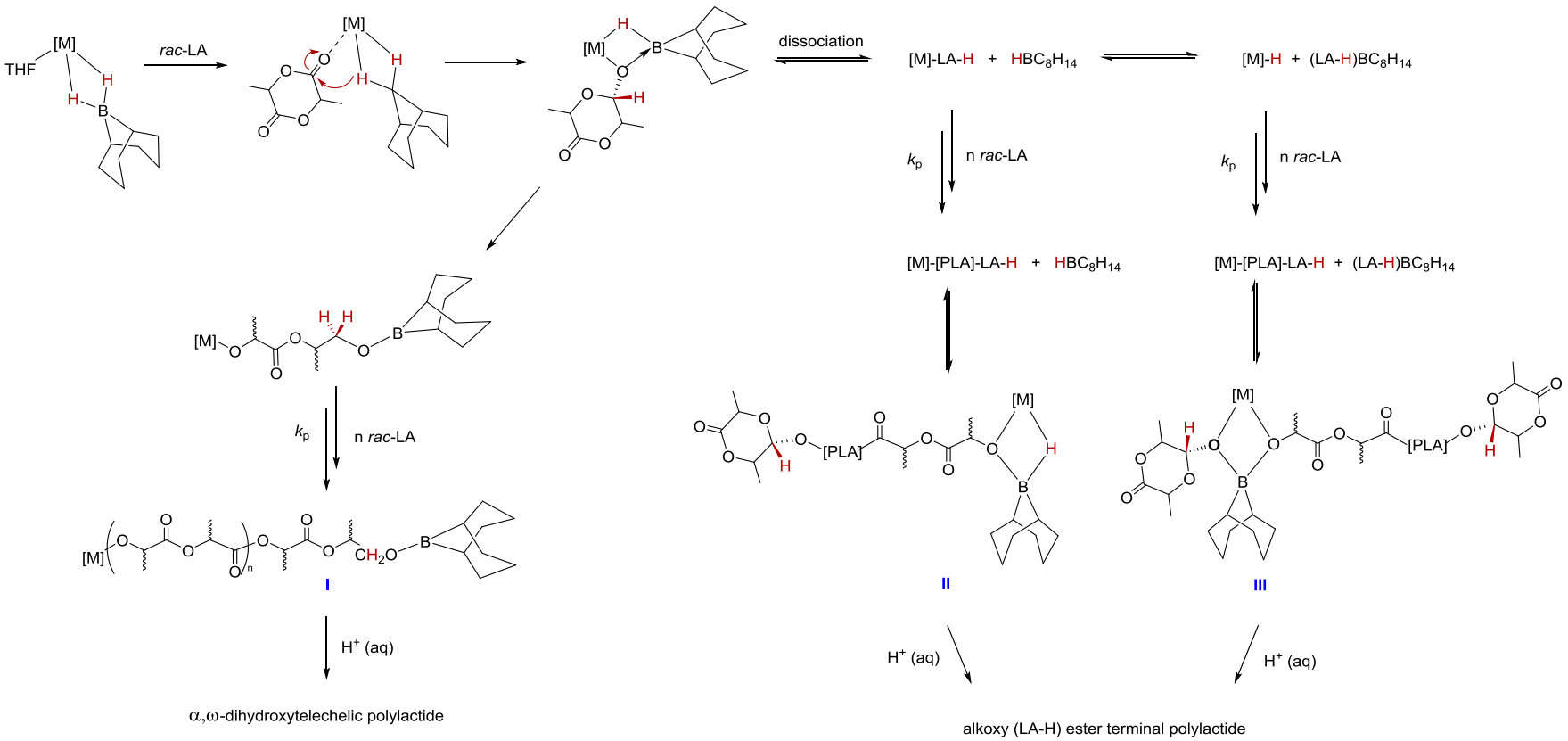

Scheme 5.3. Proposed mechanism for *rac*-LA ROP using $(Tp^{tBu,Me})Ca\{(\mu\text{-}H)_2BC_8H_{14}\}(THF)$ (**19**), [M] = $(Tp^{tBu,Me})Ca$.

5.6 Polymerisation studies: ROP of ε-CL

Owing to the ill-behaved behaviour of the $(Tp^{tBu,Me})M(HBEt_3)(THF)_x$ catalysts (**17**, M = Ca, x = 1 and **18,** M = Sr, x = 2) towards the ROP of *rac*-LA, no further experiments with ε-CL were carried out. Only $(Tp^{tBu,Me})M\{(\mu\text{-}H)_2BC_8H_{14}\}(THF)_x$ catalysts (**19**, M = Ca, x = 1 and **20**, M = Sr, x = 2) with ε-CL ROPs were therefore undertaken. The initial results showed no solvent effects on the polymerisation kinetics, and so the benchmarking ε-CL polymerisations were only performed in THF. This allows the evaluation of the catalytic potential of dialkyl dihydridoborates and their direct comparison to the analogous tetrahydroborate initiators to be determined. The results of ε-CL ROP are summarised in Table 5.4.

Table 5.4. Polymerisation of ε-CL using $(Tp^{tBu,Me})Ca\{(\mu\text{-}H)_2BC_8H_{14}\}(THF)$ (**19**) and $(Tp^{tBu,Me})Sr\{(\mu\text{-}H)_2BC_8H_{14}\}(THF)_2$ (**20**) in THF.[a]

Initiator	Time (min)	Conversion (%)[b]	M_n (GPC)[c]	M_n (Calcd)[d]	PDI[e]	Yield (%)[f]
19	1	99	25,300	22,600	1.57	59
20	1	99	22,200	22,600	1.39	61

[a] Conditions: $[\varepsilon\text{-CL}]_0 : [\text{initiator}]_0 = 200 : 1$, 3.4 mL THF at 23 °C. $[\varepsilon\text{-CL}]_0 = 1.0$ M. [b] Measured by ^1H NMR ($CDCl_3$) analyses. [c] Molecular weights (g mol^{-1}) determined from GPC using the appropriate Mark-Houwink corrections. [d] Expected M_n (g mol^{-1}) for 1 polymer chain growing per metal centre; M_n = converstion (%) × 200 × 114.1 + 4. [e] PDI = M_w/M_n. [f] PDI = M_w/M_n. [f] Isolated yield at 100% conversion.

5.6.1 ROP of ε-CL using $(Tp^{tBu,Me})Ca\{(\mu\text{-}H)_2BC_8H_{14}\}(THF)$ (19) and $(Tp^{tBu,Me})Sr\{(\mu\text{-}H)_2BC_8H_{14}\}(THF)_2$ (20)

Compounds **19** and **20** are very efficient in catalysing the ROP of ε-CL in THF at room temperature, resembling the observation made in ROP of *rac*-LA; complete conversion (*ca*. 99% monomer conversion) achieved within the first minute of polymerisation. Similar to the expected molecular weight PCL, with PDIs of 1.57 and 1.39, were also obtained using **19** and **20**, respectively. The MALDI-ToF mass spectra of PCL formed using **19** and **20** showed the expected α,ω-dihydroxy termini PCL and cyclic PCL, caused by intra-molecular transesterification (Figure 5.11).

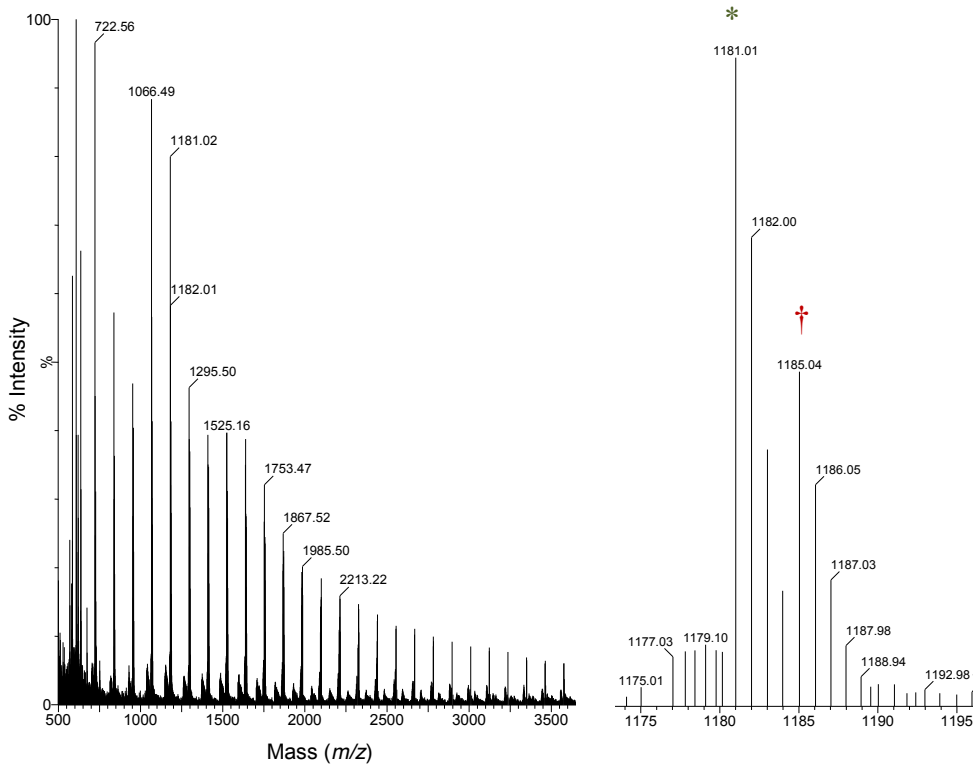

Figure 5.11. MALDI-ToF MS of PCL synthesised using $(Tp^{tBu,Me})Sr\{(\mu\text{-}H)_2BC_8H_{14}\}(THF)_2$ (**20**). K^+ dopant. M_n by GPC analysis was 2,800 g mol^{-1} (from a [ε-CL]:[**20**]$_0$ = 10:1 polymerisation at RT) (left). A MALDI-ToF peak envelope of PLA with the length of 10 caprolactone monomer units (right). Maxima in the isotopic distributions shown are corresponding to cyclic PLA (green asterisk) and hydroxide termini (red dagger).

^1H and ^{11}B NMR investigations were carried out for the reaction between **19** and **20** and 5 equivs. of ε-CL in THF-d_8. ^1H NMR analysis indicated multiple polymer species in solution. However no information regarding the bicyclic [3.3.1]-containing species was obtained due to the overlapping of the resonance with those of the polymer and the ligand.^{11}B NMR analysis showed the immediate disappearance of the resonance corresponding to the $(\mu\text{-}H)_2BC_8H_{14}$ ligand following the addition of ε-CL. Besides the unaltered signal of $Tp^{tBu,Me}$, a singlet resonance appeared at δ = 56.1 ppm. This implies that the propagating species in the ε-CL ROP are related to those observed in the comparable *rac*-LA polymerisation (intermediate **I**, Scheme 5.3).

The distribution tailing towards the low molecular weight region shown in the GPC traces are associated with the notable formation of cyclic PCL. However, no cyclic

PCL resulted from the intra-molecular transesterification was observed in the comparable ε-CL ROP using analogous tetrahydroborate complexes **1** and **4**. The explanation for this discrepancy in catalytic behaviour between catalysts **19** or **20** and **1** or **4** is currently unknown.

5.7 Summary and Conclusions

Alkaline earth organohydroborate compounds are scarce when compared with lanthanide and transition metal counterparts. Herein, a series of $(Tp^{tBu,Me})M(HBEt_3)(THF)_x$ (**17**, M = Ca, x = 1 and **18,** M = Sr, x = 2) and $(Tp^{tBu,Me})M\{(\mu\text{-}H)_2BC_8H_{14}\}(THF)_x$ (**19**, M = Ca, x = 1 and **20,** M = Sr, x = 2) were prepared in good yields *via* salt metathesis reactions between iodide analogues (**2.15** or **5**) and $Na[HBEt_3]$ or $K[H_2BC_8H_{14}]$. Compounds **17**, **19** and **20** were crystallographically characterised. The attempt to synthesise thermodynamically unfavourable $(Tp^{tBu,Me})Mg(HBEt_3)$ following reaction of chloride analogue **3** and $NaHBEt_3$ in both THF and benzene was unsuccessful. An unexpected product, $(Tp^{tBu,Me})Mg(H_2BEt_2)$, was observed during the course of reaction as a result of disproportionation of $NaHBEt_3$. $(Tp^{tBu,Me})Mg\{(\mu\text{-}H)_2BC_8H_{14}\}$ (**21**) was synthesised through either a salt metathesis reaction between **3** and $K[H_2BC_8H_{14}]$ or a transmetallation reaction between $(Tp^{tBu,Me})Mg(OBn)$ (**10**) and $(\mu\text{-}H)_2(BC_8H_{14})_2$. Both of these approaches produced the same impurity which formed from the fractionalisation of the $Tp^{tBu,Me}$ ligand in the presence of the hydride-carrying reagent. Several attempts of fractional crystallisation in pentane or benzene resulted in limited success; an extremely low yield was obtained. Nevertheless, compound **21** was crystallographically characterised. The molecular structure **17** showed the coordination of $HBEt_3$ through a bridging hydride, in conjunction with the agostic interactions between the metal centre and the methylene hydrogens of the ethyl substituents. Whilst the molecular structure of **19**, **20** and **21** confirm the κ^2-hydride bridging of $(\mu\text{-}H)_2BC_8H_{14}$ moieties to the metal centres, no C-H···M agostic interactions were observed among these compounds.

Compounds **17**, **18**, **19** and **20** were used as catalysts for ROP of *rac*-LA. $(Tp^{tBu,Me})M(HBEt_3)(THF)_x$ catalysed *rac*-LA ROP in an extremely ill-defined manner. This is due to the loss of BEt_3 after the first hydride transfer apparently resulting in an

open coordination sphere of which facilitates the intramolecular transesterification of the growing PLA chains. On the other hand, $(Tp^{tBu,Me})M\{(\mu\text{-}H)_2BC_8H_{14}\}(THF)_x$ provided better molecular weight control PLA to their tetrahydroborate counterparts in catalysing *rac*-LA ROP, whilst stereoselectivity remained unchanged. Cyclic PLA, alkoxy (LA-H) ester termini PLA and dihydroxy telechelic PLA were obtained using **19** and **20**. Spectroscopic investigations were performed to understand the initial mechanism of the dihydridoborate initiators in the ROP of *rac*-LA. Only ^{11}B NMR analysis was informative leading to a tentative mechanism. However, further isotope labelling and other studies are required to confirm the proposed mechanism.

Owing to the inefficiency of **17** and **18** in polymerising *rac*-LA, only benchmarking ε-CL ROP experiments in THF were carried out using **19** and **20**. Good agreement with expected molecular weight α,ω-dihydroxy telechelic PCL was produced along with cyclic PCL in both systems. Tentative ^1H and ^{11}B NMR analyses indicate reactive double hydride transfer in the initiating step, producing a growing PCL chain with $-OBC_8H_{14}$ end group.

The strong reducing nature of $(Tp^{tBu,Me})M\{(\mu\text{-}H)_2BC_8H_{14}\}(THF)_x$ (**19** and **20**) in ROP of cyclic esters is consistent with the literature associated with reduction using $Li[H_2BC_8H_{14}]$, reported by Rousseau *et al*.[56] The work in this Chapter illustrates the catalytic potential of organohydroborates in ROP. Further modification to the supporting ligand or organohydroborate substituents could tune ROP activity and reduce the deteriorating transesterification effect.

5.8 References

1. M. J. Harvey, T. P. Hanusa and M. Pink, *Chem*. *Commun*., 2000, 489.
2. S. Pillai Sarish, A. Jana, H. W. Roesky, T. Schulz, M. John and D. Stalke, *Inorg*. *Chem*., 2010, **49**, 3816.
3. S. Krieck, H. Görls and M. Westerhausen, *Inorg*. *Chem*. *Commun*., 2010, **13**, 1466.
4. J. Langer, K. Wimmer, H. Gorls and M. Westerhausen, *Dalton Trans*., 2009, 2951.
5. L. Orzechowski, G. Jansen, M. Lutz and S. Harder, *Dalton Trans*., 2009, 2958.

6. K. Izod, C. Wills, W. Clegg and R. W. Harrington, *Inorg*. *Chem*., 2007, **46**, 4320.
7. L. Deng, H.-S. Chan and Z. Xie, *J*. *Am*. *Chem*. *Soc*., 2006, **128**, 5219.
8. C. Cui, A. Shafir, J. A. R. Schmidt, A. G. Oliver and J. Arnold, *Dalton Trans*., 2005, 1387.
9. J. Cheng, J. Takats, M. J. Ferguson and R. McDonald, *J*. *Am*. *Chem*. *Soc*., 2008, **130**, 1544.
10. G. M. Ferrence and J. Takats, *J*. *Organomet*. *Chem*., 2002, **647**, 84.
11. X. Chen, S. Lim, C. E. Plečnik, S. Liu, B. Du, E. A. Meyers and S. G. Shore, *Inorg*. *Chem*., 2004, **43**, 692.
12. M. Visseaux, D. Baudry, A. Dormond and C. Qian, *J*. *Organomet*. *Chem*., 1999, **574**, 213.
13. F. Basuli, J. Tomaszewski, J. C. Huffman and D. J. Mindiola, *Organometallics*, 2003, **22**, 4705.
14. S. Demir, N. A. Siladke, J. W. Ziller and W. J. Evans, *Dalton Trans*., 2012, **41**, 9659.
15. M. F. Lappert, A. Singh, J. L. Atwood and W. E. Hunter, *J*. *Chem*. *Soc*., *Chem*. *Commun*., 1983, 206.
16. D. M. Lyubov, G. K. Fukin and A. A. Trifonov, *Inorg*. *Chem*., 2007, **46**, 11450.
17. Y. Yu, W. W. Brennessel and P. L. Holland, *Organometallics*, 2007, **26**, 3217.
18. X. Chen, F.-C. Liu, C. E. Plečnik, S. Liu, B. Du, E. A. Meyers and S. G. Shore, *Organometallics*, 2004, **23**, 2100.
19. Jordan, F.-C. Liu and S. G. Shore, *Inorg*. *Chem*., 1997, **36**, 5597.
20. E. J. M. Hamilton, J. S. Park, X. Chen, S. Liu, M. R. Sturgeon, E. A. Meyers and S. G. Shore, *Organometallics*, 2009, **28**, 3973.
21. R. Köster, G. Seidel, J. E. McGuire and S. G. Shore, *Inorg*. *Syn*., John Wiley & Sons, Inc., 1983, 198.
22. H. C. Brown, B. Singaram and C. P. Mathew, *J*. *Org*. *Chem*., 1981, **46**, 2712.
23. R. Shinomoto, E. Gamp, N. M. Edelstein, D. H. Templeton and A. Zalkin, *Inorg*. *Chem*., 1983, **22**, 2351.
24. P. Zanella, F. Ossola, M. Porchia, G. Rossetto, A. Chiesi Villa and C. Guastini, *J*. *Organomet*. *Chem*., 1987, **323**, 295.

25. D. Barbier-Baudry, A. Dormond and M. Visseaux, *J. Organomet. Chem.*, 2000, **609**, 21.
26. D. Baudry, A. Dormond, B. Lachot, M. Visseaux and G. Zucchi, *J. Organomet. Chem.*, 1997, **547**, 157.
27. L. Hasinoff, J. Takats, X. W. Zhang, A. H. Bond and R. D. Rogers, *J. Am. Chem. Soc.*, 1994, **116**, 8833.
28. E. L. Werkema, R. A. Andersen, A. Yahia, L. Maron and O. Eisenstein, *Organometallics*, 2009, **28**, 3173.
29. W. J. Evans, J. M. Perotti and J. W. Ziller, *Inorg. Chem.*, 2005, **44**, 5820.
30. J. Knizek and H. Nöth, *Eur. J. Inorg. Chem.*, 2011, **2011**, 1888.
31. B. Singaram, T. C. Jackson and J. Harrison, *Synlett*, 1996, 383.
32. A. G. M. Barrett, M. R. Crimmin, M. S. Hill, P. B. Hitchcock and P. A. Procopiou, *Organometallics*, 2007, **26**, 4076.
33. J. A. Gladysz, *Aldrichim. Acta*, 1979, **12**, 13.
34. T. D. Xiao, S. Torban, P. R. Strutt and B. H. Kear, *Nanostruc. Mater.*, 1996, **7**, 857.
35. C. K. Yee, R. Jordan, A. Ulman, H. White, A. King, M. Rafailovich and J. Sokolov, *Langmuir*, 1999, **15**, 3486.
36. H. Boennemann, W. Brijoux, R. Brinkmann, R. Fretzen, T. Joussen, R. Koeppler, B. Korall, P. Neiteler and J. Richter, *J. Mol. Catal.*, 1994, **86**, 129.
37. S. Chakraborty, J. Zhang, Y. J. Patel, J. A. Krause and H. Guan, *Inorg. Chem.*, 2013, **52**, 37.
38. J. Knizek, H. Noeth and M. Warchhold, *Z. Naturforsch., B: Chem. Sci.*, 2006, **61**, 1079.
39. Gmelin, *Handbook of Inorganic Chemistry*, 8th Edition, Springer-Verlag, Heidelberg, Germany, 1976.
40. M. D. Fryzuk, B. R. Lloyd, G. K. B. Clentsmith and S. J. Rettig, *J. Am. Chem. Soc.*, 1991, **113**, 4332.
41. M. D. Fryzuk, B. R. Lloyd, G. K. B. Clentsmith and S. J. Rettig, *J. Am. Chem. Soc.*, 1994, **116**, 3804.
42. G. Jia, A. J. Lough and R. H. Morris, *J. Organomet. Chem.*, 1993, **461**, 147.
43. J. L. Hubbard, *Journal of the Chemical Society, Chem. Commun.*, 1989, 1639.
44. P. Binger, G. Benedikt, G. W. Rotermund and R. Köster, *Justus Liebigs Annalen der Chemie*, 1968, **717**, 21.

45. D. M. Dawson, A. Meetsma, J. B. Roedelof and J. H. Teuben, *Inorg. Chim. Acta*, 1997, **259**, 237-239.
46. H. Nöth and B. Wrackmeyer, *Nuclear Magnetic Resonance Spectroscopy of Boron Compounds*, 1st Edition, Springer-Verlag, Berlin, Heidelberg Germany, 1978.
47. J. L. Galler, S. Goodchild, J. Gould, R. McDonald and A. Sella, *Polyhedron*, 2004, **23**, 253.
48. T. J. Marks and J. R. Kolb, *Chem. Rev*., 1977, **77**, 263.
49. K. Nakamoto, *Infrared and Raman Spectra of Inorganic and Coordination Compounds*, 6th Edition, John Wiley & Sons, Inc., Hoboken, New Jersey, 2009.
50. X. Chen, S. Lim, C. E. Plečnik, S. Liu, B. Du, E. A. Meyers and S. G. Shore, *Inorg. Chem*., 2005, **44**, 6052.
51. R. D. Shannon, *Acta Crystallogr. A*, 1976, **32**, 751.
52. R. S. Rowland and R. Taylor, *J. Phys. Chem*., 1996, **100**, 7384.
53. J. Knizek and H. Nöth, *J. Organomet. Chem*., 2000, **614–615**, 168.
54. M. G. Cushion, D.Phil Thesis, University of Oxford, 2011.
55. H. C. Brown, J. S. Cha, B. Nazer and C. A. Brown, *J. Org. Chem*., 1985, **50**, 549.
56. C. Rasset and B. Rousseau, *J. Labelled Comp. Rad*., 1994, **34**, 523.
57. S. D. Cho, H. J. Lim, H. J. Kim and J. S. Cha, *Bull. Korean Chem. Soc*., 2002, **23**, 1695.

Chapter Six

Experimental details and characterising data

6.1 General methods and instrumentation

All air and moisture sensitive manipulations were carried out using standard Schlenk line or dry-box techniques under an atmosphere of argon or dinitrogen. Toluene, THF and diethyl ether (Et_2O) were pre-dried over activated 4 Å molecular sieves prior to reflux over sodium (toluene), potassium (THF) or Na/K alloy (Et_2O) under dinitrogen atmosphere and distilled. Pentane, hexanes and benzene were degassed by sparging with dinitrogen and dried by passing through a column of the appropriate drying agent.[1] Deuterated solvents were dried over sodium (C_6D_6 and toluene-d_8), potassium (THF-d_8) and P_2O_5 ($CDCl_3$) at reflux then distilled under reduced pressure and stored under argon in Teflon valve ampoules. $CDCl_3$ was used as received for non-sensitive polymer samples.

Solution NMR samples were prepared in a dry-box in 5 mm Wilmad 507-PP tubes fitted with J. Young Teflon valves. ^{1}H, ^{2}H, $^{13}C\{^{1}H\}$, $^{11}B\{^{1}H\}$ and ^{11}B spectra were recorded on Varian Mercury-VX 300, Varian Unity Plus 500, Bruker Avance III 500 or Bruker Avance III 400 spectrometers at ambient temperature unless stated otherwise. ^{1}H and $^{13}C\{^{1}H\}$ spectra were referenced internally to residual protio-solvent (^{1}H) or solvent (^{13}C) resonances, and are reported relative to tetramethylsilane (δ = 0 ppm). ^{11}B and $^{11}B\{^{1}H\}$ spectra were referenced externally to $Et_2O{\cdot}BF_3$. Assignments were confirmed using two dimensional ^{1}H-^{1}H and ^{13}C-^{1}H NMR correlation experiments. Methanol and ethylene glycol were used as standard samples for NMR temperature calibration. IR spectra were recorded on a Perkin Elmer Paragon 1000 FTIR, a Nicolet Magna 560 E.S.P. FTIR or a Thermo Scientific Nicolet iS5 FTIR spectrometer. Samples prepared in a dry-box as Nujol mulls between NaCl plates or as solution samples (10 mg per 0.5 mL in THF). IR data are reported in wavenumber within the range 4000-400 cm^{-1}. Mass spectra were recorded by the departmental service of University of Oxford. Elemental analyses were carried out by Elemental Microanalysis Ltd. at Devon or by the Elemental Analysis Service at the London Metropolitan University.

MALDI-ToF MS analysis was performed on a Waters MALDI micro equipped with a 337 nm nitrogen laser and an accelerating voltage of 25 kV was applied. The polymer samples were dissolved in THF at a concentration of 1.0 mg mL^{-1}. The cationisation agent used was potassium trifluoroacetate (Fluka, > 99%) dissolved in THF at

concentration of 5.0 mg mL^{-1}. The matrix used was trans-2-[3-(4-tert-butylphenyl)-2-methyl-2-propenylidene]malononitrile (DCTB) (Fluka) and was dissolved in THF at a concentration of 40.0 mg mL^{-1}. Solutions of matrix, salt and polymer were mixed in a volume ratio of 4:1:4, respectively. The mixed solution was hand-spotted on a stainless steel MALDI target and left to dry. The spectra were recorded in the reflectron mode.

Polymer molecular weights (M_W, M_n and PDI) were determined by GPC using a Polymer Laboratories PL-GPC50 Plus equipped with a Polymer Laboratories Plgel Mixed-D column (7.5 mm diameter and 300 mm length) and a refractive index (RI) detector. Samples were dissolved in THF (Fisher, HPLC grade, stabilised with BHT, 2.5 ppm) at a concentration of 2.0 mg mL^{-1} and filtered before injection. The Fisher THF, with stabiliser, was also used as the eluent with a flow rate of 1.0 mL min^{-1} at 30 ºC. Linear polystyrenes (Polymer Laboratories) were used as the primary calibration standards and the appropriate Mark-Houwink corrections for poly(*rac*-LA) and poly(ε-CL) in THF at 30 ºC were applied to calculate the experimental molecular weights.[2-4]

6.2 Literature preparations and reagent purification

(3-^{t}Bu, 5-Me-pz),[5] K($Tp^{tBu,Me}$),[6] Tl($Tp^{tBu,Me}$),[6, 7] $Sr(BH_4)_2(THF)_2$[8], $K[H_2BC_8H_{14}]$[9] and ($Tp^{tBu,Me}$)Ca(I)(THF)[10] were prepared according to or adapted from literature procedures. ($Tp^{tBu,Me}$)$Ca(BD_4)$(THF) was kindly provided by Dr. Michael G. Cushion.[10] ε-CL was dried over fine CaH_2 powder for 5 days and distilled under reduced pressure. The purified liquid monomer was stored under argon in a glass ampoule fitted with a J. Young Teflon stopper. *Rac*-LA was recrystallised twice from hot toluene solutions and dried *in vacuo*. The recrystallised material was then sublimed twice under reduced pressure. The purified *rac*-LA was stored in a dry-box and used within a month of being sublimed. BnOH (anhydrous, Sigma Aldrich), PhCHO (purified by redistilled, Sigma Aldrich) and (−)-Methyl L-lactate were degassed prior to use. $B(OMe)_3$ was dried over sodium at reflux overnight then distilled under reduced pressure. The purified liquid reagents were stored under argon in glass ampoules fitted with J. Young Teflon stopper. Other commerially available reagents were used as received.

6.3 Experimental details and characterising data for Chapter Two

($Tp^{tBu,Me}$)Ca(BH_4)(THF) (1). A suspension of K($Tp^{tBu,Me}$) (1.08 g, 2.33 mmol) in THF (20 mL) was added to a solution of $Ca(BH_4)_2(THF)_2$ (0.60 g, 2.79 mmol) in THF (20 mL) at RT. The resulting suspension was stirred for 3 h. The suspension was filtered and the volatiles removed under reduced pressure, leaving a white residue. This was extracted into benzene (3 × 10 mL) and the volatiles removed under reduced pressure to give a spongy white solid. This was recrystallised from THF:hexanes (1:3 v/v) solution at -30 °C to give **1** as a colorless microcrystalline solid. Yield: 1.08 g (84 %). Diffraction-quality crystals were grown from a THF:hexanes (1:3 v/v) solution at -30 °C. ^{1}H NMR (C_6D_6, 299.9 MHz, 293 K): 5.68 (3 H, s, $N_2C_3{}^t$BuMe<u>H</u>), 3.26 (4 H, m, OC<u>H</u>$_2$CH$_2$), 2.19 (9 H, s, $N_2C_3{}^t$Bu<u>Me</u>H), 1.42 (27 H, s, $N_2C_3{}^t$<u>Bu</u>MeH), 1.17 (4 H, m, OCH$_2$C<u>H</u>$_2$) ppm, B-<u>H</u> of $Tp^{tBu,Me}$ and B<u>H</u>$_4$ not observed. ^{13}C{^{1}H} NMR (C_6D_6, 75.5 MHz, 293 K): 163.4 (3-N$_2$<u>C</u>$_3{}^t$BuMeH), 145.3 (5-N$_2$<u>C</u>$_3{}^t$BuMeH), 103.1 (4-N$_2$<u>C</u>$_3{}^t$BuMeH), 68.6 (O<u>C</u>H$_2$CH$_2$), 32.2 (N$_2$C$_3$<u>C</u>(Me$_3$)MeH), 31.5 (N$_2$C$_3$C(<u>Me</u>$_3$)MeH), 25.5 (OCH$_2$<u>C</u>H$_2$), 13.5 (N$_2$C$_3{}^t$Bu<u>Me</u>H) ppm. ^{11}B NMR (C_6D_6, 96.2 MHz, 293 K): -7.9 (br d, <u>B</u>-H of $Tp^{tBu,Me}$), -32.1 (quintet, $^1J_{B\text{-}H}$ = 84.2 Hz, <u>B</u>H$_4$) ppm. IR (NaCl plates, Nujol mull, cm^{-1}): 2558 (s), 2396(s), 2255(m), 2214(s), 1541(s), 1334(s), 1240(s), 1199(s), 1178(s), 1068(s), 1027(s), 705(s). IR (NaCl cell, THF), υ(B-H), cm^{-1}): 2562 (s, B-H of $Tp^{tBu,Me}$), 2416 (s, B-H$_t$ of BH_4), 2223 and 2174 (s, B-H$_b$ of BH_4 ; 49 cm^{-1} splitting). EI-MS: *m*/*z* = 478 (80 %), [<u>*M*</u>-THF]$^+$. Anal. found (calcd. for $C_{28}H_{52}B_2CaON_6$): C, 60.67 (61.10); H, 9.35 (9.52); N, 14.56 (15.27) %

($Tp^{tBu,Me}$)Mg(BH_4) (2). To a solid mixture of K$Tp^{tBu,Me}$ (0.82 g, 1.77 mmol) and $Mg(BH_4)_2$ (0.13 g, 2.48 mmol) was added THF (20 mL) at RT. The resulting suspension was stirred for 24 h, and the volatiles were removed under reduced pressure, leaving a white residue. This was extracted into benzene (3 x 10 mL), the solution was concentrated and cooled to 4 °C, yielding **2** as a colourless microcrystalline solid. Yield: 0.59 g (72 %). Diffraction-quality crystals were grown from a saturated benzene solution at 4 °C. ^{1}H NMR (C_6D_6, 299.9 MHz, 293 K): 5.62 (3 H, s, $N_2C_3{}^t$BuMe<u>H</u>), 2.04 (9 H, s, $N_2C_3{}^t$Bu<u>Me</u>H), 1.51 (4 H, q, B<u>H</u>$_4$, $^1J_{BH}$ = 83.4 Hz), 1.45 (27 H, s, $N_2C_3{}^t$<u>Bu</u>MeH) ppm, B-<u>H</u> of $Tp^{tBu,Me}$ not observed. ^{13}C{^{1}H} NMR (C_6D_6, 75.5 MHz, 293 K): 165.3 (3-N$_2$<u>C</u>$_3{}^t$BuMeH), 145.0 (5-N$_2$<u>C</u>$_3{}^t$BuMeH), 104.1 (4-N$_2$<u>C</u>$_3{}^t$BuMeH), 32.1 (N$_2$C$_3$<u>C</u>(Me$_3$)MeH), 31.2 (N$_2$C$_3$C(<u>Me</u>$_3$)MeH), 13.0

($N_2C_3{}^tBuMeH$) ppm. ^{11}B NMR (C_6D_6, 96.2 MHz, 293 K): -8.9 (br d, B-H of $Tp^{tBu,Me}$), -37.6 (quintet, $^1J_{B-H}$ = 68.7 Hz, BH_4) ppm. IR (NaCl plates, Nujol mull, cm^{-1}): 2558 (s), 2445(s), 2227(m), 2166(s), 1543(s), 1363(m), 1333(m), 1239(m), 1186(s), 1129(m), 1065(s), 1021(s), 863(w), 802(s), 766(s), 648(s). IR (NaCl cell, THF), ν(B-H), cm^{-1}): 2564 (s, B-H of $Tp^{tBu,Me}$), 2439 (s, B-H_t of BH_4), 2229 and 2174 (s, B-H_b of BH_4; 55 cm^{-1} splitting). EI-MS: *m/z* = 461 (5 %), $[M]^+$. Anal. found (calcd. for $C_{24}H_{44}B_2MgN_6$): C, 62.41 (62.32); H, 9.68 (9.59); N, 18.03 (18.17) %.

($Tp^{tBu,Me}$)Mg(Cl) (3). A solution of $Tl(Tp^{tBu,Me})$ (2.46 g, 3.92 mmol) in THF (20 mL) was added into a suspension of anhydrous $MgCl_2$ (0.45 g, 4.70 mmol) in THF (20 mL) at RT. The reaction mixture was stirred for 24 h, during which time a white precipitate of TlCl was formed. The white precipitate was filtered and the volatiles were removed under reduced pressure leaving a white residue. This was extracted into hexanes (3 × 15 mL), a solution was concentrated to about 15 mL and placed at -30 °C, giving a product as a white microcrystalline powder. Yield: 1.21 g (64 %). Diffraction-quality crystals were grown from a saturated Et_2O solution at 4 °C. ^1H NMR ($CDCl_3$, 400.0 MHz, 293 K): 5.83 (3 H, s, $N_2C_3{}^tBuMeH$), 2.41 (9 H, s, $N_2C_3{}^tBuMeH$), 1.42 (27 H, s, $N_2C_3{}^tBuMeH$), B-H of $Tp^{tBu,Me}$ not observed. $^{13}C\{^1H\}$ NMR ($CDCl_3$, 100.6 MHz, 293 K): 164.9 (3-$N_2C_3{}^tBuMeH$), 145.2 (5-$N_2C_3{}^tBuMeH$), 103.2 (4-$N_2C_3{}^tBuMeH$), 31.9 ($N_2C_3C(Me_3)MeH$), 31.1 ($N_2C_3C(Me_3)MeH$), 13.2 ($N_2C_3{}^tBuMeH$) ppm. ^{11}B NMR ($CDCl_3$, 128.4 MHz, 293 K): -9.4 (br d, B-H of $Tp^{tBu,Me}$) ppm. IR (NaCl plates, Nujol mull, cm^{-1}): 2576(m), 1537(s), 1364(s), 1241(m), 1198(s), 1178(s), 1068(s), 1030(m), 982(w), 840(s), 793(s), 650(s). EI-MS: *m/z* = 482 (10 %), $[M]^+$. Anal. found (calcd. for $C_{24}H_{40}B_1MgN_6Cl_1$): C, 59.47 (59.66); H, 8.51 (8.34); N, 17.26 (17.39) %.

($Tp^{tBu,Me}$)Sr(BH_4)($THF)_2$ (4). A suspension of $K(Tp^{tBu,Me})$ (1.00 g, 2.16 mmol) in THF (20 mL) was added dropwise to a solution of $Sr(BH_4)_2(THF)_2$ (0.68 g, 2.59 mmol) in THF (15 mL), all at -78 °C. The suspension was stirred at this temperature for 2 h, and then allowed to warm to RT for a further hour. After which time, the white suspension was filtered and the volatiles were removed under reduced pressure leaving a white residue. This was extracted into benzene (3 × 10 mL) and the volatiles were removed under reduced pressure to give a white powder. This was recrystallised from THF:hexanes (1:2 v/v) solution at -30 °C to give a product as a colourless

microcrystalline solid. Yield: 0.93 g (65 %). Diffraction-quality crystals were grown in a hexanes-layered THF at -30 °C. ^{1}H NMR (C_6D_6, 299.9 MHz, 293 K): 5.69 (3 H, s, $N_2C_3{}^{t}$BuMeH), 3.33 (8 H, m, OCH_2CH_2), 2.21 (9 H, s, $N_2C_3{}^{t}$BuMeH), 1.36 (27 H, s, $N_2C_3{}^{t}$BuMeH), 1.24 (8 H, m, OCH_2CH_2) ppm, B-H of $Tp^{tBu,Me}$ and BH_4 not observed. $^{13}C\{^{1}H\}$ NMR (C_6D_6, 75.5 MHz, 293 K): 162.6 (3-$N_2C_3{}^{t}$BuMeH), 145.2 (5-$N_2C_3{}^{t}$BuMeH), 102.4 (4-$N_2C_3{}^{t}$BuMeH), 67.9 (OCH_2CH_2), 31.9 ($N_2C_3C(Me_3)$MeH), 31.2 ($N_2C_3C(Me_3)$MeH), 25.2 (OCH_2CH_2), 13.2 ($N_2C_3{}^{t}$BuMeH) ppm. ^{11}B NMR (C_6D_6, 96.2 MHz, 293 K): -7.5 (br d, B-H of $Tp^{tBu,Me}$), -31.6 (quintet, $^{1}J_{B\text{-}H}$ = 84.5 Hz, BH_4) ppm. IR (NaCl plates, Nujol mull, cm^{-1}): 2558(m), 2398(m), 2245(m), 2202(m), 1540(s), 1427(s), 1334(s), 1175(s), 1143(w), 1069(s), 1029(w), 984(w), 785(m), 647(m). IR (NaCl cell, THF, ν(B-H), cm^{-1}): 2551 (s, B-H of $Tp^{tBu,Me}$), 2364 (s, B-H_t of BH_4), 2246 and 2203 (s, B-H_b of BH_4; 43 cm^{-1} splitting). EI-MS: *m*/*z* = 525 (20 %), [*M*-2THF]$^{+}$. Anal. Found (calcd. for $C_{32}H_{60}B_2N_6O_2Sr_1$): C, 57.50 (57.36); H, 9.12 (9.02); N, 12.70 (12.54) %.

($Tp^{tBu,Me}$)Sr(I)(THF)$_2$ (5). A suspension of K($Tp^{tBu,Me}$) (1.74 g, 3.77 mmol) in THF (20 mL) was added dropwise to a solution of SrI_2 (1.29 g, 3.77 mmol) in THF (15 mL), all at -78 °C. The suspension was stirred at this temperature for 2 h, and then allowed to warm to RT for a further hour. After which time, the white suspension was filtered and the volatiles were removed under reduced pressure leaving a white residue. This was extracted into benzene (3 × 10 mL) and the volatiles were removed under reduced pressure to give a white powder. This was recrystallised from THF:hexanes (1:2 v/v) solution at -30 °C to give a product as a colourless microcrystalline solid. Yield: 2.17 g (74 %). Diffraction-quality crystals were grown in a hexanes-layered THF at -30 °C. ^{1}H NMR (C_6D_6, 299.9 MHz, 293 K): 5.65 (3 H, s, $N_2C_3{}^{t}$BuMeH), 3.40 (8 H, m, OCH_2CH_2), 2.20 (9 H, s, $N_2C_3{}^{t}$BuMeH), 1.36 (27 H, s, $N_2C_3{}^{t}$BuMeH), 1.22 (8 H, m, OCH_2CH_2) ppm, B-H of $Tp^{tBu,Me}$ not observed. $^{13}C\{^{1}H\}$ NMR (C_6D_6, 75.5 MHz, 293 K): 163.0 (3-$N_2C_3{}^{t}$BuMeH), 145.7 (5-$N_2C_3{}^{t}$BuMeH), 102.7 (4-$N_2C_3{}^{t}$BuMeH), 68.6 (OCH_2CH_2), 32.7 ($N_2C_3C(Me_3)$MeH), 31.9 ($N_2C_3C(Me_3)$MeH), 25.6 (OCH_2CH_2), 13.6 ($N_2C_3{}^{t}$BuMeH) ppm. ^{11}B NMR (C_6D_6, 96.2 MHz, 293 K): -7.9 (br d, B-H of $Tp^{tBu,Me}$) ppm. IR (NaCl plates, Nujol mull, cm^{-1}): 2550(m), 1541(s), 1354(s), 1334(m), 1241(m), 1180(s), 1077 (s), 1036(w), 1021(w), 980 (w), 780(m), 645(s). EI-MS: *m*/*z* = 639 ([*M*-2THF]$^{+}$). Anal.

Found (calcd. for $C_{24}H_{41}BIN_6Sr{\cdot}1.5C_4H_8O$): C, 48.23 (48.58); H, 7.15 (7.16); N, 11.25 (11.26) %.

(κ^2,κ^3-Tp^{tBu,Me})$_2$Sr (6). To a solid mixture of K(Tp^{tBu,Me}) (1.04 g, 2.25 mmol) and SrI_2 (0.39 g, 1.13 mmol) was added THF (30 mL). The resulting suspension was stirred for 20 h. After which time, the white suspension was filtered and the volatiles were removed under reduced pressure leaving a white residue. This was extracted into benzene (3 × 10 mL) and the volatiles were removed under reduced pressure to give a white powder. This was recrystallised from hot pentane at room temperature to give a product as a white microcrystalline powder. Yield: 0.56 g (53 %). Diffraction-quality crystals were grown in a saturated benzene solution at 4 °C. ^{1}H NMR (C_6D_6, 299.9 MHz, 293 K): 5.87 (3 H, s, $N_2C_3{}^t$BuMeH), 5.75 (3 H, s, $N_2C_3{}^t$BuMeH), 2.21 (9 H, s, $N_2C_3{}^t$BuMeH), 2.18 (9 H, s, $N_2C_3{}^t$BuMeH), 1.25 (27 H, s, $N_2C_3{}^t$BuMeH), 1.15 (27 H, s, $N_2C_3{}^t$BuMeH) ppm, B-H of Tp^{tBu,Me} not observed. ^{13}C{^{1}H} NMR (C_6D_6, 75.5 MHz, 293 K): 163.1 (3-$N_2C_3{}^t$BuMeH), 162.7 (3-$N_2C_3{}^t$BuMeH), 146.7 (5-$N_2C_3{}^t$BuMeH), 145.9 (5-$N_2C_3{}^t$BuMeH), 103.9 (4-$N_2C_3{}^t$BuMeH), 103.2 (4-$N_2C_3{}^t$BuMeH), 32.4 ($N_2C_3C(Me_3)$MeH), 32.2 ($N_2C_3C(Me_3)$MeH), 31.1 ($N_2C_3C(Me_3)$MeH), 30.8 ($N_2C_3C(Me_3)$MeH), 13.7 ($N_2C_3{}^t$BuMeH), 12.2 ($N_2C_3{}^t$BuMeH) ppm. ^{11}B NMR (C_6D_6, 96.2 MHz, 293 K): -2.3 and -6.6 (br d, B-H of Tp^{tBu,Me}) ppm. IR (NaCl plates, Nujol mull, cm^{-1}): 2520(m), 2361(m), 1543(s), 1361(s), 1332(s), 1260(m), 1207(m), 1172(s), 1069(m), 1010(m), 981(m), 782(s), 649(m). EI-MS: *m*/*z* = 934 ([*M*]$^+$). Anal. Found (calcd. for $C_{48}H_{82}B_2N_{12}Sr$): C, 61.56 (61.45); H, 8.83 (8.76); N, 17.95 (17.82) %.

NMR tube scale synthesis of (Tp^{tBu,Me})Mg{(O(CH$_2$)$_5$C(O))$_{13}$O(CH$_2$)$_6$O)B(O$_2$C$_6$H$_{12}$)} (7). To clarify the chemical shift assignments of this macromolecule **7**, a diagram showing a concise atom labeling scheme of the polymeryl ligand is accompanied.

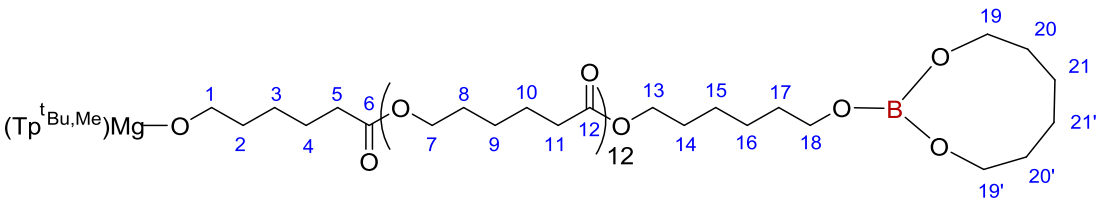

In the glovebox, a J. Young NMR tube was charged with ($Tp^{tBu,Me}$)Mg(BH_4) (**2**, 6.8 mg, 0.015 mmol) in THF-d_8 (0.5 mL) and ε-CL (8.1 μL, 0.074 mmol) at RT. After 5 h ^{1}H NMR spectroscopy showed effectively quantitative conversion to **7**. ^{1}H NMR (THF-d_8, 499.9 MHz, 298 K): 5.80 (3 H, s, $N_2C_3{}^t$BuMe<u>H</u>), 4.07 (2 H, t, ^3J = 6.8 Hz, H_1), 4.02 (26 H, t, ^3J = 6.5 Hz, $H_{7 \text{ and } 13}$), 3.76 (6 H, m, $H_{18, 19 \text{ and } 19'}$), 2.39 (9 H, s, $N_2C_3{}^t$Bu<u>Me</u>H), 2.27 (26 H, t, ^3J = 7.0 Hz, $H_{5 \text{ and } 11}$), 1.62 (54 H, m, $H_{2, 4, 8, 10 \text{ and } 14}$), 1.54 (6 H, m, $H_{17, 20 \text{ and } 20'}$), 1.46 (2 H, m, H_3), 1.42-1.40 (59 H, m, overlapping $N_2C_3{}^t$<u>Bu</u>MeH, $H_{9, 15, 16, 21 \text{ and } 21'}$) ppm, B-<u>H</u> of $Tp^{tBu,Me}$ not observed. ^{13}C{^{1}H} NMR (THF-d_8, 125.7 MHz, 298 K): 173.4 (C_6), 173.3 (C_{12}), 164.6 (3-N_2<u>C</u>$_3{}^t$BuMeH), 145.5 (5-N_2<u>C</u>$_3{}^t$BuMeH), 103.3 (4-N_2<u>C</u>$_3{}^t$BuMeH), 65.0 (C_1), 64.7-64.6 (overlapping $C_{7, 13 \text{ and } 18}$), 63.9 ($C_{19 \text{ and } 19'}$), 37.9 ($C_2$), 34.8-34.7 ($C_{5 \text{ and } 11}$) 32.6 ($C_{17, 20 \text{ and } 20'}$), 32.3 ($N_2C_3$<u>C</u>($Me_3$)MeH), 31.2 ($N_2C_3$C(<u>Me</u>$_3$)MeH), 29.8-29.5 ($C_{4 \text{ and } 10}$), 27.5 ($C_3$), 26.7-26.6 (overlapping $C_{9, 15, 16, 21 \text{ and } 21'}$), 25.8-25.7 (overlapping $C_{8 \text{ and } 14}$) 13.1 ($N_2C_3{}^t$Bu<u>Me</u>H). ^{11}B{^{1}H} NMR (THF-d_8, 160.4 MHz, 298 K): -9.5 (<u>B</u>-H of $Tp^{tBu,Me}$) and 18.3 (<u>B</u>$(OR)_3$, R = alkyl) ppm.

6.4 Experimental details and characterising data for Chapter Three

($Tp^{tBu,Me}$)Mg(^{n}Bu) (8). A solution of (^{n}Bu)$_2$Mg (1.5 mL of 1 M in heptane, 1.50 mmol) was added dropwise to a suspension of K($Tp^{tBu,Me}$) (0.68 g, 1.47 mmol) in THF (15 mL) at RT. The resulting suspension was stirred for 16 h, after which time a clear solution was obtained. The solution was filtered and all volatiles were removed under reduced pressure leaving a white residue. This was extracted into hexanes (3 × 5 mL) and the volatiles were removed under reduced pressure to give **8** as an off-white powder. Yield: 0.45 g (61 %). Diffraction-quality crystals were grown in a saturated hexanes solution at -20 °C. ^{1}H NMR (C_6D_6, 299.9 MHz, 293 K): 5.65 (3 H, s, $N_2C_3{}^t$BuMe<u>H</u>), 2.23 (2 H, m, MgCH_2C<u>H</u>$_2$CH_2CH_3), 2.13 (9 H, s, $N_2C_3{}^t$Bu<u>Me</u>H), 1.98 (2 H, m, MgCH_2CH_2C<u>H</u>$_2$CH_3), 1.44 (27 H, s, $N_2C_3{}^t$<u>Bu</u>MeH), 1.39 (3 H, t, ^3J = 7.3 Hz, MgCH_2CH_2CH_2C<u>H</u>$_3$), 0.61 (2 H, m, MgC<u>H</u>$_2$CH_2CH_2CH_3) ppm, B-<u>H</u> of $Tp^{tBu,Me}$ not observed. ^{13}C{^{1}H} NMR (C_6D_6, 75.5 MHz, 293 K): 164.4 (3-N_2<u>C</u>$_3{}^t$BuMeH), 144.3 (5-N_2<u>C</u>$_3{}^t$BuMeH), 103.2 (4-N_2<u>C</u>$_3{}^t$BuMeH), 33.3 (MgCH_2(<u>C</u>H_2)$_2$CH_3), 32.8 (MgCH_2(<u>C</u>H_2)$_2$CH_3), 31.9 (N_2C_3<u>C</u>(Me_3)MeH), 31.2 (N_2C_3C(<u>Me</u>$_3$)MeH), 15.8 (Mg<u>C</u>H_2(CH_2)$_2$CH_3), 14.6 (MgCH_2(CH_2)$_2$<u>C</u>H_3), 13.0 ($N_2C_3{}^t$Bu<u>Me</u>H) ppm. ^{11}B NMR (C_6D_6, 96.2 MHz, 293 K): -9.3 (br d, <u>B</u>-H of $Tp^{tBu,Me}$)

ppm. IR (NaCl plates, Nujol mull, cm^{-1}): 2551 (s), 1542 (s), 1434 (s), 1340 (m), 1244 (m), 1191 (s), 1068 (s), 985 (w), 853 (w), 786 (s), 650 (s). EI-MS: *m/z* = 503 (5 %), $[\underline{M}]^+$. Anal. Found (calcd. for $C_{28}H_{49}B_1N_6Mg_1$): C, 66.82 (66.61); H, 10.01 (9.78); N, 16.50 (16.65) %.

($Tp^{tBu,Me}$)Mg(S-lactate) (9). A solution of ($Tp^{tBu,Me}$)Mg(^{n}Bu) (**8**, 0.69 g, 1.37 mmol) in diethyl ether (15 mL) was treated with (−)-Methyl L-lactate (130 μL, 1.44 mmol), all at -78 °C. The immediate decolourisation was observed and the solution was allowed to warm to RT, after which time, all the volatiles were removed under *vacuo* leaving a white residue. This was extracted into pentane (3 × 5 mL), the solution was concentrated to 2 mL and placed at 4 °C giving a product as a colourless microcrystalline solid. Yield: 0.35 g (47 %). Diffraction-quality crystals were grown in a concentrated pentane solution at 4 °C. ^{1}H NMR (C_6D_6, 299.9 MHz, 293 K): 5.75 (3 H, s, $N_2C_3{}^t$BuMeH), 5.12 (1 H, q, ^3J = 7.0 Hz, OCH(Me)CO_2Me), 3.20 (3 H, s, OCH(Me)CO_2Me), 2.15 (9 H, s, $N_2C_3{}^t$BuMeH), 1.82 (3 H, d, ^3J = 7.0 Hz, OCH(Me)CO_2Me), 1.50 (27 H, s, $N_2C_3{}^t$BuMeH) ppm, B-H of $Tp^{tBu,Me}$ not observed. $^{13}C\{^1H\}$ NMR (C_6D_6, 75.5 MHz, 293 K): 191.8 (OCH(Me)CO_2Me), 163.7 (3-$N_2C_3{}^t$BuMeH), 144.4 (5-$N_2C_3{}^t$BuMeH), 103.3 (4-$N_2C_3{}^t$BuMeH), 70.7 (OCH(Me)CO_2Me), 52.8 (OCH(Me)CO_2Me), 32.1 ($N_2C_3C(Me_3)$MeH), 31.0 ($N_2C_3C(Me_3)$MeH), 23.3 (OCH(Me)CO_2Me), 13.0 ($N_2C_3{}^t$BuMeH) ppm. ^{11}B NMR (C_6D_6, 96.2 MHz, 293 K): -9.3 (br d, B-H of $Tp^{tBu,Me}$) ppm. IR (NaCl plates, Nujol mull, cm^{-1}): 2546(m), 1673(s), 1544(s), 1363(s), 1340(m), 1303(w), 1249(m), 1191(s), 1020(w), 984(w), 788(s), 644(m). EI-MS: *m/z* = 553 (5 %), $[\underline{M}]^+$. Anal. found (calcd. for $C_{28}H_{47}B_1MgN_6O_3$): C, 60.99 (61.05); H, 8.72 (8.60); N, 15.17 (15.26) %.

($Tp^{tBu,Me}$)Mg(OBn) (10). A solution of ($Tp^{tBu,Me}$)Mg(^{n}Bu) (**8**, 0.30 g, 0.59 mmol) in benzene (15 mL) was treated with benzylalcohol (75 μL, 0.65 mmol) at RT. The solution mixture was stirred for 10 mins, after which time, all the volatiles were removed under *vacuo* leaving a white residue. This was extracted into hexanes (3 × 5 mL), a solution was concentrated to about 5 mL and placed at -30 °C, giving a product as a white microcrystalline powder. Yield: 0.21 g (64 %). Diffraction-quality crystals were grown in a saturated hexanes solution at -30 °C. ^{1}H NMR (C_6D_6, 299.9 MHz, 293 K): 7.86 (2 H, d, ^3J = 7.5 Hz, *o*-C_6H_5), 7.43 (2 H, t, ^3J = 7.5 Hz, *m*-C_6H_5), 7.24 (1 H, t, ^3J = 7.5 Hz, *p*-C_6H_5), 5.62 (5 H, s, overlapping $N_2C_3{}^t$BuMeH and

OC$\underline{H}_2$Ph), 2.10 (9 H, s, $N_2C_3{}^t$Bu$\underline{Me}$H), 1.47 (27 H, s, $N_2C_3{}^t\underline{Bu}$MeH) ppm, B-$\underline{H}$ of $Tp^{tBu,Me}$ not observed. $^{13}C\{^1H\}$ NMR (C_6D_6, 75.5 MHz, 293 K): 164.3 (5-$N_2\underline{C}_3{}^t$BuMeH), 144.5 (3-$N_2\underline{C}_3{}^t$BuMeH), 128.2 (*i*-$\underline{C}_6H_5$), 127.9 (*o*-$\underline{C}_6H_5$), 127.8 (*m*-$\underline{C}_6H_5$), 125.8 (*p*-$\underline{C}_6H_5$), 103.0 (4-$N_2\underline{C}_3{}^t$BuMeH), 68.2 (O$\underline{C}H_2$Ph), 32.0 ($N_2C_3\underline{C}(Me_3)$MeH), 30.7 ($N_2C_3C(\underline{Me}_3)$MeH), 12.8 ($N_2C_3{}^tBu\underline{Me}$H) ppm. ^{11}B NMR (C_6D_6, 96.2 MHz, 293 K): -9.4 (br d, $\underline{B}$-H of $Tp^{tBu,Me}$) ppm. IR (NaCl plates, Nujol mull, cm^{-1}): 2546(m), 1538(s), 1365(s), 1244(w), 1183(s), 1066(s), 1030(m), 984(w), 854(w), 787(s), 679(w). EI-MS: *m/z* = 553 (5 %), $[\underline{M}]^+$. Anal. found (calcd. for $C_{31}H_{47}B_1MgN_6O_1$): C, 66.97 (67.10); H, 8.64 (8.54); N, 15.10 (15.15) %.

Alternative synthesis of ($Tp^{tBu,Me}$)Mg(OBn) (10). A solution of ($Tp^{tBu,Me}$)Mg(^{n}Bu) (**8**, 0.93 g, 1.85 mmol) in benzene (20 mL) was treated with benzaldehyde (207 µL, 0.65 mmol) at RT. The solution mixture was stirred for 4 h. After which time, all the volatiles were removed under *vacuo* leaving a white residue. This was extracted into hexanes (3 × 5 mL), a solution was concentrated to about 10 mL and placed at -30 °C, giving a product as a white microcrystalline powder. Yield: 0.71 g (69 %).

NMR tube scale synthesis of the first *rac*-LA insertion product ($Tp^{tBu,Me}$)Mg(LA*OBn) (11). To clarify the chemical shift assignments of compound **11**, a diagram showing a concise atom labelling scheme of the LA*OBn ligand is accompanied.

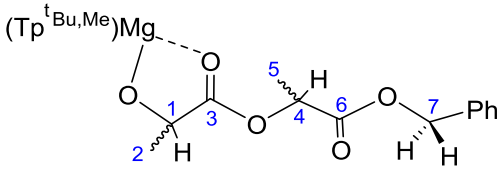

In the glovebox, a J. Young NMR tube was charged with ($Tp^{tBu,Me}$)Mg(OBn) (**10**, 22.4 mg, 0.040 mmol) and *rac*-LA (5.8 mg, 0.040 mmol) in THF-d_8 (0.5 mL) at RT. After 3 h, ^1H NMR spectroscopy showed effectively quantitative conversion to **11**. ^1H NMR (THF-d_8, 400.0 MHz, 293 K): 7.33-7.28 (5 H, m, $C_6\underline{H}_5$), 5.79 (3 H, s, $N_2C_3{}^t$BuMe$\underline{H}$), 5.38 (1 H, q, ^3J = 7.0 Hz, H_4), 5.15 (1 H, d, ^2J = 12.2 Hz, H_7), 5.08 (1 H, s, ^2J = 12.2 Hz, $H_{7'}$), 4.78 (1 H, q, ^3J = 7.0 Hz, H_1), 2.38 (9 H, s, $N_2C_3{}^t$Bu$\underline{Me}$H), 1.51 (3 H, d, ^3J = 7.0 Hz, H_2), 1.43 (3 H, d, ^3J = 7.0 Hz, H_5), 1.31 (27 H, s, $N_2C_3{}^t\underline{Bu}$MeH), B-$\underline{H}$ of $Tp^{tBu,Me}$ not observed. $^{13}C\{^1H\}$ NMR (THF-d_8, 100.6 MHz, 293 K): 188.6 (C_3), 170.4 (C_6), 164.5 (3-$N_2\underline{C}_3{}^t$BuMeH), 145.2 (5-$N_2\underline{C}_3{}^t$BuMeH),

137.0 (C_7), 129.4-129.2 ($\underline{C}_6H_5$), 103.6 (4-$N_2\underline{C}_3{}^t$BuMeH), 70.9 (C_1), 70.0 (C_4), 32.6 ($N_2C_3\underline{C}(Me_3)$MeH), 31.4 ($N_2C_3C(\underline{Me}_3)$MeH), 23.9 ($C_2$), 17.7 ($C_5$), 13.1 ($N_2C_3{}^tBu\underline{Me}$H) ppm. ^{11}B NMR (THF-$d_8$, 128.4 MHz, 293 K): -9.3 (br d, $\underline{B}$-H of Tp^{tBu,Me}) ppm.

NMR tube scale generation of the intermediate (Tp^{tBu,Me})Mg(LA-H) (12). To clarify the chemical shift assignments of compound **12**, a diagram showing a concise atom labelling scheme of the LA-H ligand is accompanied.

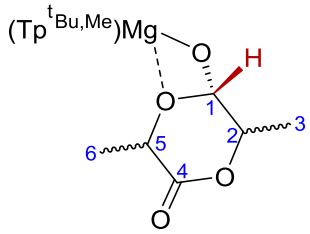

In a glove box, (Tp^{tBu,Me})Mg(BH_4) (**2**, 16.7 mg, 0.036 mmol) was weighed into a vial and dissolved in THF-d_8 (0.3 mL) and cooled to 238 K. In a separate vial, *rac*-LA (10.4 mg, 0.072 mmol) was weighed and dissolved in THF-d_8 (0.3 mL) and also cooled to 238 K. The two vials were placed on a pre-cooled tile and the solutions were combined using a pre-cooled pipette and transferred to a pre-cooled J. Young NMR tube. The sample was maintained at the preparative temperature using a dry ice/acetone bath. The NMR probe was cooled to 258 K and a blank THF-d_8 sample added before being locked and shimmed. The experimental sample then replaced the blank sample and allow to thermally equilibrated. After 10 mins at 258 K, ^{1}H and ^{11}B NMR spectra showed effectively quantitative conversion to **12**. The species was then stabilised at 228 K and fully chracterised. ^{1}H NMR (THF-d_8, 499.9 MHz, 228 K): 5.85 (3 H, s, $N_2C_3{}^t$BuMe$\underline{H}$), 5.71 (1 H, d, ^3J = 2.3 Hz, H_1), 4.42 (1 H, dq, ^3J = 2.3 and 6.6 Hz, H_2), 4.34 (1 H, q, ^3J = 6.9 Hz, H_5), 2.40 (9 H, s, $N_2C_3{}^t$Bu$\underline{Me}$H), 1.50 (3 H, d, ^3J = 6.6 Hz, H_3), 1.41 (3 H, d, ^3J = 6.9 Hz, H_6), 1.38 (27 H, s, $N_2C_3{}^t\underline{Bu}$MeH) ppm, B-$\underline{H}$ of Tp^{tBu,Me} not observed. ^{13}C{^{1}H} NMR (THF-d_8, 125.7 MHz, 228 K): 170.9 (C_4), 164.4 (3-$N_2\underline{C}_3{}^t$BuMeH), 145.9 (5-$N_2\underline{C}_3{}^t$BuMeH), 103.6 (4-$N_2\underline{C}_3{}^t$BuMeH), 96.4 (C_1), 81.2 (C_2), 71.6 (C_5), 32.5 ($N_2C_3\underline{C}(Me_3)$MeH), 31.2 ($N_2C_3C(\underline{Me}_3)$MeH), 19.3 ($C_3$), 15.7 ($C_6$) ppm. ^{11}B NMR (THF-$d_8$, 160.4 MHz, 228 K): -9.3 (app. s, $\underline{B}$-H of Tp^{tBu,Me}) ppm.

6.5 Experimental details and characterising data for Chapter Four

NMR tube scale reaction of ($Tp^{tBu,Me}$)Mg(BH_4) (2) with PhCHO (1:4 ratio). To a solution of ($Tp^{tBu,Me}$)Mg(BH_4) (**2**, 15.2 mg, 0.033 mmol) in THF-d_8. (0.5 mL) in an NMR tube equipped with a J. Young Teflon valve was added PhCHO (13.3 μL, 0.13 mmol), at RT. The ^{1}H and ^{11}B NMR spectra recorded immediately after mixing showed quantitative conversion to ($Tp^{tBu,Me}$)Mg(OBn) (**10**) and B(OBn)$_3$.

NMR tube scale synthesis of ($Tp^{tBu,Me}$)Ca(OBn) (13a)/B(OBn)$_3$ and ($Tp^{tBu,Me}$)Ca{B(OBn)$_4$} (13b). A solution of ($Tp^{tBu,Me}$)Ca(BH_4)(THF) (**1**, 19.3 mg, 0.035 mmol) in C_6D_6 (0.5 mL) was treated with benzaldehyde (14 μL, 0.140 mmol) at RT. The volatiles were removed under *vacuo* leaving a very sticky white solid, which was then redissolved in C_6D_6 (0.5 mL). ^{1}H NMR spectroscopy showed a mixture of **13a/B(OBn)$_3$** and **13b**. ^{1}H NMR (C_6D_6, 299.9 MHz, 293 K): 7.39 (8 H, d, ^3J = 7.5 Hz, *o*-$C_6\underline{H}_5$), 7.16 (8 H, t, ^3J = 7.5 Hz, *m*-$C_6\underline{H}_5$), 7.10 (4 H, t, ^3J = 7.5 Hz, *p*-$C_6\underline{H}_5$), 5.57 (3 H, s, $N_2C_3{}^t$BuMe$\underline{H}$), 4.96 (8 H, s, OC$\underline{H}_2$Ph), 2.17 (9 H, s, $N_2C_3{}^t$Bu$\underline{Me}$H), 1.27 (27 H, s, $N_2C_3{}^t\underline{Bu}$MeH) ppm, B-$\underline{H}$ of $Tp^{tBu,Me}$ not observed. ^{13}C{^{1}H} NMR (C_6D_6, 75.5 MHz, 293 K): 162.7 (3-$N_2\underline{C}_3{}^t$BuMeH), 145.0 (5-$N_2\underline{C}_3{}^t$BuMeH), 143.1 (*i*-$\underline{C}_6H_5$), 128.2 (*m*-$\underline{C}_6H_5$), 127.7 (*o*-$\underline{C}_6H_5$), 126.6 (*p*-$\underline{C}_6H_5$), 102.7 (4-$N_2\underline{C}_3{}^t$BuMeH), 65.4 (O$\underline{C}H_2$Ph), 32.2 ($N_2C_3\underline{C}(Me_3)$MeH), 31.3 ($N_2C_3C(\underline{Me}_3)$MeH), 13.5 ($N_2C_3{}^tBu\underline{Me}$H) ppm. ^{11}B NMR ($C_6D_6$, 96.2 MHz, 293 K): -7.7 (app. d, $\underline{B}$-H of $Tp^{tBu,Me}$), 4.3 (s, $\underline{B}(OBn)_4$, major) and 18.6 (s, $\underline{B}(OBn)_3$, minor) ppm. EI-MS: *m*/*z* = 570 (10 %), [$\underline{M}$]$^+$.

($Tp^{tBu,Me}$)Sr{B(OBn)$_4$} (14). A solution of ($Tp^{tBu,Me}$)Sr(BH_4)(THF)$_2$ (**4**, 0.26 g, 0.39 mmol) in benzene (15 mL) was treated with benzaldehyde (200 μL, 1.95 mmol) at RT. The solution mixture was stirred for 10 mins, after which time, all the volatiles were removed under *vacuo* leaving a very sticky white solid. This was extracted into pentane (3 × 5 mL), a solution was triturated at -78 °C, giving a product as a white powder. Crude yield: 0.24 g (65 %). ^{1}H NMR (C_6D_6, 299.9 MHz, 293 K): 7.44 (8 H, d, ^3J = 7.5 Hz, *o*-$C_6\underline{H}_5$), 7.14 (8 H, t, ^3J = 7.5 Hz, *m*-$C_6\underline{H}_5$), 7.08 (4 H, t, ^3J = 7.5 Hz, *p*-$C_6\underline{H}_5$), 5.60 (3 H, s, $N_2C_3{}^t$BuMe$\underline{H}$), 5.02 (8 H, s, OC$\underline{H}_2$Ph), 2.21 (9 H, s, $N_2C_3{}^t$Bu$\underline{Me}$H), 1.19 (27 H, s, $N_2C_3{}^t\underline{Bu}$MeH) ppm, B-$\underline{H}$ of $Tp^{tBu,Me}$ not observed. ^{13}C{^{1}H} NMR (C_6D_6, 75.5 MHz, 293 K): 162.6 (3-$N_2\underline{C}_3{}^t$BuMeH), 146.1 (5-$N_2\underline{C}_3{}^t$BuMeH), 143.6 (*i*-$\underline{C}_6H_5$), 128.4 (*m*-$\underline{C}_6H_5$), 127.5 (*o*-$\underline{C}_6H_5$), 126.7 (*p*-$\underline{C}_6H_5$), 102.7 (4-$N_2\underline{C}_3{}^t$BuMeH), 65.2 (O$\underline{C}H_2$Ph), 32.7 ($N_2C_3\underline{C}(Me_3)$MeH), 31.4

($N_2C_3C(\underline{Me}_3)MeH$), 13.6 ($N_2C_3{}^tBu\underline{Me}H$) ppm. ^{11}B NMR (C_6D_6, 96.2 MHz, 293 K): -7.7 (app. s, $\underline{B}$-H of $Tp^{tBu,Me}$) and 4.0 (s, $\underline{B}(OBn)_4$) ppm. IR (NaCl plates, Nujol mull, cm^{-1}): 2518(m), 1945(m), 1683(s), 1599(m), 1544(s), 1362(m), 1179(m), 1021(m), 914(m), 782(m), 697(m), 647(m). EI-MS: *m/z* = 952 (5 %), $[\underline{M}]^+$. Anal. found (calcd. for $C_{52}H_{68}B_2SrN_6O_4$): C, 65.83 (65.72); H, 7.32 (7.21); N, 8.77 (8.84) %.

($Tp^{tBu,Me}$)Mg(OMe) (15). A solution of ($Tp^{tBu,Me}$)Mg(^{n}Bu) (**8**, 0.30 g, 0.59 mmol) in benzene (15 mL) was treated with methanol (37 μL, 0.89 mmol) at RT. The solution mixture was stirred for 10 mins, after which time, all the volatiles were removed under *vacuo* leaving a white residue. This was extracted into hexanes (3 × 5 mL), a solution was concentrated to about 5 mL and placed at -15 °C, giving a product as a white microcrystalline powder. Yield: 0.24 g (85 %). Diffraction-quality crystals were grown in a saturated hexanes solution at -20 °C. ^1H NMR (C_6D_6, 299.9 MHz, 293 K): 5.63 (3 H, s, $N_2C_3{}^tBuMe\underline{H}$), 4.56 (3 H, s, $OC\underline{H}_3$), 2.11 (9 H, s, $N_2C_3{}^tBu\underline{Me}H$), 1.55 (27 H, s, $N_2C_3{}^t\underline{Bu}MeH$) ppm, B-$\underline{H}$ of $Tp^{tBu,Me}$ not observed. $^{13}C\{^1H\}$ NMR (C_6D_6, 75.5 MHz, 293 K): 164.2 (3-$N_2\underline{C}_3{}^tBuMeH$), 144.4 (5-$N_2\underline{C}_3{}^tBuMeH$), 102.9 (4-$N_2\underline{C}_3{}^tBuMeH$), 52.2 ($O\underline{C}H_3$), 32.0 ($N_2C_3\underline{C}(Me_3)MeH$), 30.7 ($N_2C_3C(\underline{Me}_3)MeH$), 12.7 ($N_2C_3{}^tBu\underline{Me}H$) ppm. ^{11}B NMR (C_6D_6, 96.2 MHz, 293 K): -9.2 (br d, $\underline{B}$-H of $Tp^{tBu,Me}$) ppm. IR (NaCl plates, Nujol mull, cm^{-1}): 2549(m), 1538(s), 1434(s), 1345(m), 1244(m), 1183(s), 1067(s), 1030(m), 984(m), 855(w), 788(s), 648(s). EI-MS: *m/z* = 478 (10 %), $[\underline{M}]^+$. Anal. found (calcd. for $C_{25}H_{43}B_1MgN_6O_1$): C, 62.81 (62.72); H, 9.01 (9.05); N, 17.44 (17.55) %.

NMR tube scale synthesis of ($Tp^{tBu,Me}$)Mg{B(OMe)$_4$} (16). To a solution of ($Tp^{tBu,Me}$)Mg(OMe) (**15**, 19.7 mg, 0.041 mmol) in toluene-d_8. (0.5 mL) in an NMR tube equipped with a J. Young Teflon valve was added $B(OMe)_3$ (4.6 μL, 0.041 mmol), at RT. The quantitative formation of **16** was observed at lower solution temperature (below 238 K) and compound **16** was fully characterised at 193 K. Diffraction-quality crystals were grown from a neat solution of **15** in $B(OMe)_3$ at -30 °C. ^1H NMR (tol-d_8, 499.9 MHz, 193 K): 5.51 (3 H, s, $N_2C_3{}^tBuMe\underline{H}$), 3.79 (6 H, s, $OC\underline{H}_3$), 3.43 (6 H, s, $OC\underline{H}_3$), 1.98 (9 H, s, $N_2C_3{}^tBu\underline{Me}H$), 1.56 (27 H, s, $N_2C_3{}^t\underline{Bu}MeH$) ppm, B-$\underline{H}$ of $Tp^{tBu,Me}$ not observed. $^{13}C\{^1H\}$ NMR (tol-d_8, 125.7 MHz, 193 K): 163.0 (3-$N_2\underline{C}_3{}^tBuMeH$), 144.4 (5-$N_2\underline{C}_3{}^tBuMeH$), 103.0 (4-$N_2\underline{C}_3{}^tBuMeH$), 50.7 ($O\underline{C}H_3$), 49.7 ($O\underline{C}H_3$), 32.0 ($N_2C_3\underline{C}(Me_3)MeH$), 30.4 ($N_2C_3C(\underline{Me}_3)MeH$), 13.0

($N_2C_3{}^tBuMeH$) ppm. ^{11}B NMR (tol-d_8, 160.4 MHz, 193 K): -10.3 (br d, B-H of $Tp^{tBu,Me}$) and 3.0 (s, {$B(OMe)_4$}) ppm.

6.6 Experimental details and characterising data for Chapter Five

($Tp^{tBu,Me}$)Ca($HBEt_3$)(THF) (17). A solution of ($Tp^{tBu,Me}$)Ca(I)(THF) (0.65 g, 0.98 mmol) in 20 mL of benzene was treated with Na[$HBEt_3$] (1 M in toluene) (0.98 mL, 0.98 mmol) at RT. A white precipitate was formed instantaneously after mixing. The suspension was stirred for 10 mins before filtration. All the volatiles were removed under *vacuo* leaving a white solid. This was recrystallised from THF:pentane (1:5 v/v) solution at -30 °C to give **17** as a colourless microcrystalline solid. Yield: 0.39 g (62 %). Diffraction-quality crystals were grown from a THF:pentane (1:5 v/v) solution at -30 °C. ^1H NMR (C_6D_6, 400.0 MHz, 293 K): 5.67 (3 H, s, $N_2C_3{}^tBuMeH$), 3.37 (4 H, m, OCH_2CH_2), 2.11 (9 H, s, $N_2C_3{}^tBuMeH$), 1.50 (9 H, t, ^3J = 7.5 Hz, $HB(CH_2CH_3)_3$), 1.34 (27 H, s, $N_2C_3{}^tBuMeH$), 1.28 (4 H, m, OCH_2CH_2), 0.94 (6 H, q, ^3J = 7.5 Hz, $HB(CH_2CH_3)_3$) ppm, $HBEt_3$ and B-H of $Tp^{tBu,Me}$ not observed. $^{13}C\{^1H\}$ NMR (C_6D_6, 100.6 MHz, 293 K): 164.4 (3-$N_2C_3{}^tBuMeH$), 146.3 (5-$N_2C_3{}^tBuMeH$), 103.6 (4-$N_2C_3{}^tBuMeH$), 68.4 (OCH_2CH_2), 32.2 ($N_2C_3C(Me_3)MeH$), 31.4 ($N_2C_3C(Me_3)MeH$), 25.6 (OCH_2CH_2), 13.4 ($N_2C_3{}^tBuMeH$), 13.2 ($HB(CH_2CH_3)_3$) ppm. No signal was observed in ^{13}C NMR spectra for $HB(CH_2CH_3)_3$. ^{11}B NMR (C_6D_6, 128.4 MHz, 293 K): -7.6 (app. s, B-H of $Tp^{tBu,Me}$), -10.5 (d, $^1J_{B\text{-}H}$ = 46.0 Hz, $HBEt_3$) ppm. IR (NaCl plates, Nujol mull, cm^{-1}): 2570(m), 1889(s), 1541(s), 1352(m), 1240(m), 1180(s), 1067(s), 1021(s), 982(w), 866(m), 790(s), 645(s). EI-MS: *m/z* = 98 (5 %), $[HBEt_3]^+$, 463 (100%), $[(Tp^{tBu,Me})Ca]^+$. Anal. found (calcd. for $C_{34}H_{64}B_2CaN_6O_1$): C, 64.24 (64.35); H, 10.25 (10.16); N, 13.34 (13.24) %.

($Tp^{tBu,Me}$)Sr($HBEt_3$)$(THF)_2$ (18). A solution of ($Tp^{tBu,Me}$)Sr(I)$(THF)_2$ (**5**, 0.55 g, 0.70 mmol) in 20 mL of benzene was treated with Na[$HBEt_3$] (1 M in toluene) (7.0 mL, 70 mmol) at RT. A white precipitate was formed instantaneously after mixing. The suspension was stirred for 10 mins before filtration. All the volatiles were removed under *vacuo* leaving a white solid. This was recrystallised from THF:pentane (1:3 v/v) solution at -30 °C to give **18** as a colorless microcrystalline solid. Yield: 0.28 g (53 %). Diffraction-quality crystals were grown from a THF:pentane (1:3 v/v) solution at -20 °C. ^1H NMR (C_6D_6, 400.0 MHz, 293 K): 5.69 (3 H, s, $N_2C_3{}^tBuMeH$), 3.32 (8 H, m, OCH_2CH_2), 2.17 (9 H, s, $N_2C_3{}^tBuMeH$), 1.56 (9 H, t, ^3J = 7.5 Hz,

HB($CH_2C\underline{H}_3$)$_3$), 1.33 (27 H, s, $N_2C_3{}^t\underline{Bu}MeH$), 1.24 (8 H, m, $OCH_2C\underline{H}_2$), 0.88 (6 H, q, ^3J = 7.5 Hz, HB($C\underline{H}_2CH_3$)$_3$) ppm, $\underline{H}BEt_3$ and B-$\underline{H}$ of $Tp^{tBu,Me}$ not observed. $^{13}C\{^1H\}$ NMR (C_6D_6, 100.6 MHz, 293 K): 163.5 (3-$N_2\underline{C}_3{}^t$BuMeH), 146.1 (5-$N_2\underline{C}_3{}^t$BuMeH), 103.2 (4-$N_2\underline{C}_3{}^t$BuMeH), 68.3 ($O\underline{C}H_2CH_2$), 32.6 ($N_2C_3\underline{C}(Me_3)MeH$), 31.5 ($N_2C_3C(\underline{Me}_3)MeH$), 25.6 ($OCH_2\underline{C}H_2$), 13.6 ($N_2C_3{}^t\underline{Bu}MeH$), 13.6 (HB($CH_2\underline{C}H_3$)$_3$) ppm. No signal was observed in ^{13}C NMR spectra for HB($\underline{C}H_2CH_3$)$_3$. ^{11}B NMR (C_6D_6, 128.4 MHz, 293 K): -7.6 (app. s, $\underline{B}$-H of $Tp^{tBu,Me}$), -11.5 (d, $^1J_{B\text{-}H}$ = 54.0 Hz, $H\underline{B}Et_3$) ppm. IR (NaCl plates, Nujol mull, cm^{-1}): 2766(m), 2570(m), 1950(s), 1541(s), 1351(s), 1240(m), 1177(s), 1069(s), 1025(s), 982(m), 868(m), 790(s), 647(s). EI-MS: *m*/*z* = 683 (5 %), [*M*-THF]$^+$. Anal. found (calcd. for $C_{38}H_{72}B_2SrN_6O_2$): C, 60.36 (60.51); H, 9.61 (9.62); N, 11.25 (11.14) %.

($Tp^{tBu,Me}$)Ca{(μ-H)$_2$BC_8H_{14}}(THF) (19). A solution of K[$H_2C_8H_{14}$] (0.13 g, 0.83 mmol) in THF (15 mL) was added into a solution of ($Tp^{tBu,Me}$)Ca(I)(THF) (0.46 g, 0.69 mmol) in THF (10 mL) at RT. A white precipitate was formed instantaneously after mixing. The suspension was stirred for 15 mins before all the volatiles were removed under *vacuo* leaving a white residue. This was extracted into benzene (3 × 5 mL) and the volatiles were removed under reduced pressure to give a white powder. This was recrystallised from THF:pentane (1:3 v/v) solution at -30 °C to give **19** as a colorless microcrystalline solid. Yield: 0.29 g (64 %). Diffraction-quality crystals were grown from a THF:pentane (1:3 v/v) solution at 4 °C. ^1H NMR (C_6D_6, 400.0 MHz, 293 K): 5.65 (3 H, s, $N_2C_3{}^t$BuMe$\underline{H}$), 3.24 (4 H, m, $OC\underline{H}_2CH_2$), 2.56 (2 H, m, γ-(μ-H)$_2$B$C_8\underline{H}_{14}$), 2.41 (8 H, m, β-(μ-H)$_2$B$C_8\underline{H}_{14}$), overlapping 2.19 (9 H, s, $N_2C_3{}^t\underline{Bu}MeH$) and 2.19 (2 H, m, γ-(μ-H)$_2$B$C_8\underline{H}_{14}$), 1.61 (2 H, br. s, α-(μ-H)$_2$B$C_8\underline{H}_{14}$), 1.37 (27 H, s, $N_2C_3{}^t\underline{Bu}MeH$), 1.19 (4 H, m, $OCH_2C\underline{H}_2$), (μ-$\underline{H}$)$_2$BC_8H_{14} and B-$\underline{H}$ of $Tp^{tBu,Me}$ not observed. $^{13}C\{^1H\}$ NMR (C_6D_6, 100.6 MHz, 293 K): 163.3 (3-$N_2\underline{C}_3{}^t$BuMeH), 145.3 (5-$N_2\underline{C}_3{}^t$BuMeH), 102.9 (4-$N_2\underline{C}_3{}^t$BuMeH), 68.4 ($O\underline{C}H_2CH_2$), 35.4 (β-(μ-H)$_2$B$\underline{C}_8H_{14}$), 32.2 ($N_2C_3\underline{C}(Me_3)MeH$), 31.4 ($N_2C_3C(\underline{Me}_3)MeH$), 26.6 (γ-(μ-H)$_2B\underline{C}_8H_{14}$), 25.6 ($OCH_2\underline{C}H_2$), 22.7 (α-(μ-H)$_2B\underline{C}_8H_{14}$), 13.5 ($N_2C_3{}^t\underline{Bu}MeH$) ppm. ^{11}B NMR (C_6D_6, 128.4 MHz, 293 K): -8.1 (app. s, $\underline{B}$-H of $Tp^{tBu,Me}$), -10.2 (t, $^1J_{B\text{-}H}$ = 70.1 Hz, (μ-H)$_2\underline{B}C_8H_{14}$) ppm. IR (NaCl plates, Nujol mull, cm^{-1}): 2854(s), 2547(m), 2092(m), 2043(m), 1541(s), 1432 (s), 1360(s), 1240(m), 1198(s), 1177(s), 1073(s), 1066(s), 1034(s), 1011(w), 985(m), 877(w), 793(s), 647(s). EI-MS: *m*/*z* = 123 (40 %),

$[(\mu\text{-H})_2BC_8H_{14}]^+$, 463 (100%), $[(Tp^{tBu,Me})Ca]^+$. Anal. found (calcd. for $C_{36}H_{64}B_2CaN_6O_1$): C, 65.51 (65.65); H, 9.90 (9.79); N, 12.64 (12.76) %.

$(Tp^{tBu,Me})Sr\{(\mu\text{-H})_2BC_8H_{14}\}(THF)_2$ (20). A solution of $K[H_2C_8H_{14}]$ (0.18 g, 1.08 mmol) in THF (15 mL) was added into a solution of $(Tp^{tBu,Me})Sr(I)(THF)_2$ (**5**, 0.71 g, 0.91 mmol) in THF (10 mL) at RT. A white precipitate was formed instantaneously after mixing. The suspension was stirred for 15 mins before all the volatiles were removed under *vacuo* leaving a white residue. This was extracted into benzene (3 × 5 mL) and the volatiles were removed under reduced pressure to give a white powder. This was recrystallised from THF:pentane (1:3 v/v) solution at -30 °C to give **20** as a colorless microcrystalline solid. Yield: 0.41 g (59 %). Diffraction-quality crystals were grown from a THF:pentane (1:3 v/v) solution at -20 °C. ^{1}H NMR (C_6D_6, 400.0 MHz, 293 K): 5.66 (3 H, s, $N_2C_3{}^t$BuMeH), 3.32 (8 H, m, OCH_2CH_2), 2.58 (2 H, m, γ-$(\mu\text{-H})_2BC_8H_{14}$), 2.41 (8 H, m, β-$(\mu\text{-H})_2BC_8H_{14}$), overlapping 2.21 (9 H, s, $N_2C_3{}^t$BuMeH) and 2.21 (2 H, m, γ-$(\mu\text{-H})_2BC_8H_{14}$), 1.76 (2 H, q, J_{HB} = 71.0 Hz, $(\mu\text{-H})_2BC_8H_{14}$), 1.57 (2 H, br. s, α-$(\mu\text{-H})_2BC_8H_{14}$), 1.32 (27 H, s, $N_2C_3{}^t$BuMeH), 1.24 (8 H, m, OCH_2CH_2), B-H of $Tp^{tBu,Me}$ not observed. $^{13}C\{^1H\}$ NMR (C_6D_6, 100.6 MHz, 293 K): 162.9 (3-$N_2C_3{}^t$BuMeH), 145.6 (5-$N_2C_3{}^t$BuMeH), 102.7 (4-$N_2C_3{}^t$BuMeH), 68.2 (OCH_2CH_2), 35.5 (β-$(\mu\text{-H})_2BC_8H_{14}$), 32.3 ($N_2C_3C(Me_3)$MeH), 31.4 ($N_2C_3C(Me_3)$MeH), 26.7 (γ-$(\mu\text{-H})_2BC_8H_{14}$), 25.3 ($OCH_2CH_2$), 13.3 ($N_2C_3{}^t$BuMeH) ppm. No signal was observed in ^{13}C NMR spectra for α-$(\mu\text{-H})_2BC_8H_{14}$. ^{11}B NMR ($C_6D_6$, 128.4 MHz, 293 K): -7.7 (app. s, B-H of $Tp^{tBu,Me}$), -8.6 (t, $^1J_{B\text{-}H}$ = 70.4 Hz, $(\mu\text{-H})_2BC_8H_{14}$) ppm. IR (NaCl plates, Nujol mull, cm^{-1}): 2855(s), 2545(m), 2090(m), 2038(m), 1541(s), 1430 (s), 1360(s), 1240(m), 1202(m), 1175(s), 1072(s), 1034(s), 1009(w), 984(m), 878(w), 789(s), 647(s). EI-MS: *m/z* = 123 (10 %), $[(\mu\text{-H})_2BC_8H_{14}]^+$, 511 (100%), $[(Tp^{tBu,Me})Sr]^+$. Anal. found (calcd. for $C_{40}H_{72}B_2SrN_6O_2$): C, 61.64 (61.73); H, 9.40 (9.32); N, 10.72 (10.80) %.

$(Tp^{tBu,Me})Mg\{(\mu\text{-H})_2BC_8H_{14}\}$ (21). To a solid mixture of $(Tp^{tBu,Me})Mg(OBn)$ (**10**, 0.18 g, 0.32 mmol) and $(\mu\text{-H})_2(BC_8H_{14})_2$ (77.0 mg, 0.34 mmol) was added benzene (20 mL) at RT. The solution was heated at 50 °C for 14 h, after which time all the volatiles were removed under reduced pressure. The resulting residue was washed with hexanes (3 × 5 mL) and dried under *vacuo*. The crude product was recrystallised from a saturated benzene solution at 4 °C to give **21** as a colourless microcrystalline

solid. Yield: 0.022 g (12 %). Diffraction-quality crystals were grown from a saturated benzene solution at 4 °C. ^{1}H NMR (C_6D_6, 400.0 MHz, 293 K): 5.63 (3 H, s, $N_2C_3{}^{t}$BuMeH), 2.51 (2 H, m, γ-(μ-H)$_2$BC$_8$H$_{14}$), 2.39 (4 H, m, β-(μ-H)$_2$BC$_8$H$_{14}$), 2.31 (4 H, br. s, β-(μ-H)$_2$BC$_8$H$_{14}$), 2.14 (2 H, m, γ-(μ-H)$_2$BC$_8$H$_{14}$), 2.06 (9 H, s, $N_2C_3{}^{t}$BuMeH), 1.78 (2 H, br. s, α-(μ-H)$_2$BC$_8$H$_{14}$), 1.43 (27 H, s, $N_2C_3{}^{t}$BuMeH), (μ-H)$_2$BC$_8$H$_{14}$ and B-H of Tp^{tBu,Me} not observed. ^{13}C{^{1}H} NMR (C_6D_6, 100.6 MHz, 293 K): 165.5 (3-$N_2C_3{}^{t}$BuMeH), 145.0 (5-$N_2C_3{}^{t}$BuMeH), 103.9 (4-$N_2C_3{}^{t}$BuMeH), 34.6 (β-(μ-H)$_2$BC$_8$H$_{14}$), 32.1 ($N_2C_3C(Me_3)$MeH), 31.2 ($N_2C_3C(Me_3)$MeH), 25.5 (γ-(μ-H)$_2$BC$_8$H$_{14}$), 13.1 ($N_2C_3{}^{t}$BuMeH) ppm. No signal was observed in ^{13}C NMR spectra for α-(μ-H)$_2$BC$_8$H$_{14}$). ^{11}B NMR (C_6D_6, 128.4 MHz, 293 K): -9.4 (app. s, B-H of Tp^{tBu,Me}), -18.2 (t, $^{1}J_{B-H}$ = 68.0 Hz, (μ-H)$_2$BC$_8$H$_{14}$) ppm. IR (NaCl plates, Nujol mull, cm^{-1}): 2564(m), 2082(m), 2027(m), 1542(s), 1365(s), 1241(m), 1193(s), 1167(s), 1019(w), 984(m), 852(w), 787(s), 650(s). EI-MS: *m/z* = 571 (5%), $[M]^+$. Anal. found (calcd. for $C_{32}H_{56}B_2MgN_6$): C, 67.12 (67.34); H, 10.13 (9.89); N, 14.56 (14.72) %.

Alternative synthesis of (Tp^{tBu,Me})Mg{(μ-H)$_2$BC$_8$H$_{14}$} (21). To a solid mixture of (Tp^{tBu,Me})Mg(Cl) (**3**, 0.15 g, 0.31 mmol) and K[H$_2$BC$_8$H$_{14}$] (50.6 mg, 0.31 mmol) was added benzene (20 mL). The suspension was heated at 50 °C for 9 h, after which time the suspension was filtered. The filtrate was reduced to 5 mL and placed at 4 °C, giving **20** as a microcrystalline solid. Yield: 0.025 g. (14 %).

6.7 Polymerisation procedures

General procedure for the polymerisation of ε-CL. In a dry-box, a solution of ε-CL (0.378 g, 3.3 mmol) in solvent (toluene or THF, 3.0 mL, at RT) was added quickly in one portion to a stirred solution of catalyst in solvent (toluene or THF, 0.4 mL, at RT). [ε-CL]$_0$:[catalyst]$_0$ is 200:1 or as specified. Aliquots (approx. 0.1 mL) were taken at the appropriate time intervals and quenched outside the dry-box with wet THF (1 mL) or inside the dry-box with degassed, wet THF (1 mL). The volatiles were removed from the aliquots by evaporation to give PCL. The monomer to polymer conversion was determined using ^{1}H NMR ($CDCl_3$) analysis, and measured by integration of the resonances of PCL and unreacted ε-CL. Aliquots were then recovered for GPC and MALDI-ToF MS analyses. Isolated yields were obtained by precipitation of PCL from the polymer solution by addition of hexaness (20 mL) with vigorous stirring. The polymer was filtered and dried in *vacuo*.

General procedure for the polymerisation of *rac*-LA. In a dry-box, a solution of *rac*-LA (0.432 g, 3.0 mmol) in solvent (THF, 4.0 mL, at 70 ºC or RT) was added quickly in one portion to a stirred solution of catalyst in solvent (THF, 2.0 mL, at 70 ºC or RT). [*rac*-LA]$_0$:[catalyst]$_0$ is 100:1 or as specified. Aliquots (approx. 0.1 mL) were taken at the appropriate time intervals and quenched outside the dry-box with wet THF (1 mL) or inside the dry-box with degassed, wet THF (1 mL). The volatiles were removed from the aliquots by evaporation to give PLA. The monomer to polymer conversion was determined using ^{1}H NMR ($CDCl_3$) analysis, and measured by integration of the C<u>H</u>(Me) resonances of PLA and unreacted *rac*-LA. Aliquots were then recovered for GPC and MALDI-ToF MS analyses.

Representative procedure for ε-CL polymerisations with various additives (Chapter Four). In a dry-box, a solution of ε-CL (0.378 g, 3.3 mmol) in solvent (toluene or THF, 0.4 mL, at RT) was added quickly in one portion to a 5 minute-stirred mixture of catalyst and additive in solvent (toluene or THF, 3.0 mL, at RT). [ε-CL]$_0$:[catalyst]$_0$:[additive]$_0$ is 200:1:1 or as specified. Aliquots (approx. 0.1 mL) were taken at the appropriate time intervals and quenched outside the dry-box with wet THF (1 mL) or inside the dry-box with degassed, wet THF (1 mL). The volatiles were removed from the aliquots by evaporation to give PCL. The monomer to polymer conversion was determined using ^{1}H NMR ($CDCl_3$) analysis, and measured by integration of the resonances of PCL and unreacted ε-CL. Aliquots were then recovered for GPC and MALDI-ToF MS analyses. Isolated yields were obtained by precipitation of PCL from the polymer solution by addition of hexanes (20 mL) with vigorous stirring. The polymer was filtered and dried in *vacuo*.

Representative procedure for *rac*-LA polymerisations with various additives (Chapter Four). In a dry-box, a solution of *rac*-LA (0.432 g, 3.0 mmol) in solvent (THF, 4.0 mL at RT) was added quickly in one portion to a 5 minute-stirred mixture of catalyst and additive in solvent (THF, 2.0 mL at RT). [*rac*-LA]$_0$:[catalyst]$_0$:[additive]$_0$ is 100:1:1 or as specified. Aliquots (approx. 0.1 mL) were taken at the appropriate time intervals and quenched outside the dry-box with wet THF (1 mL) or inside the dry-box with degassed, wet THF (1 mL). The volatiles were removed from the aliquots by evaporation to give PLA. The monomer to polymer conversion was determined using ^{1}H NMR ($CDCl_3$) analysis. Aliquots were then recovered for GPC and MALDI-ToF MS analyses.

6.8 X-Ray data collection and processing parameters

Crystal structure determinations for $(Tp^{tBu,Me})Ca(BH_4)(THF)$ (1), $(Tp^{tBu,Me})Mg(BH_4)$ (2), $(Tp^{tBu,Me})Mg(Cl)$ (3), $(Tp^{tBu,Me})Sr(BH_4)(THF)_2$ (4), $(Tp^{tBu,Me})Sr(I)(THF)_2$ (5), $(\kappa^2,\kappa^3\text{-}Tp^{tBu,Me})_2Sr$ (6), $(Tp^{tBu,Me})Mg(^nBu)$ (S8S), $(Tp^{tBu,Me})Mg$(S-lactate) (9), $(Tp^{tBu,Me})Mg(OBn)$ (10S), $(Tp^{tBu,Me})Mg(OMe)$ (15), $(Tp^{tBu,Me})Mg\{B(OMe)_4\}$ (16), $(Tp^{tBu,Me})Ca(HBEt_3)(THF)$ (17), $(Tp^{tBu,Me})Ca\{(\mu\text{-}H)_2BC_8H_{14}\}(THF)$ (19), $(Tp^{tBu,Me})Sr\{(\mu\text{-}H)_2BC_8H_{14}\}(THF)_2$ (20), and $(Tp^{tBu,Me})Mg\{(\mu\text{-}H)_2BC_8H_{14}\}$ (21). Crystal data collection and processing parameters are given in Table 6.1. Crystals were mounted on glass fibers using perfluoropolyether oil and cooled rapidly in a stream of cold dinitrogen using an Oxford Cryosystems Cryostream unit. Diffraction data were measured using either an Enraf-Nonius Kappa-CCD or Oxford Diffraction/Agilent Technologies Supernova diffractometer using Mo-K_α or Cu-K_α radiation, respectively. As appropriate, absorption and decay corrections were applied to the data and equivalent reflections merged.[11, 12] The structures were solved with SIR92[13] or Superflip,[14] and further refinements and other crystallographic calculations were performed using the CRYSTALS program suite.[15] Other details of the structure solution and refinements (CIF data) are provided in the Supporting Information (CD Appendix).

Table 6.1. X-ray data collection and processing parameters

compound	$(Tp^{tBu,Me})Ca(BH_4)(THF)$ (**1**)	$(Tp^{tBu,Me})Mg(BH_4)$ (**2**)	$(Tp^{tBu,Me})Mg(Cl)$ (**3**)
empirical formula	$C_{28}H_{52}B_2N_6O_1Ca\cdot 0.5C_5H_{12}$	$C_{24}H_{44}B_2N_6Mg$	$C_{24}H_{40}B_1N_6Cl_1Mg$
fw	586.54	462.58	483.19
temp / K	150	210	150
wavelength / Å	0.71073	0.71073	0.71073
space group	$I\,2_1/a$	$P\,2_12_12_1$	$I\,\bar{4}3d$
a / Å	20.9226(3)	9.75540(10)	22.374(3)
b / Å	16.1574(2)	17.7749(2)	22.374(3)
c / Å	21.6436(3)	18.2266(3)	22.374(3)
α / deg	90	90	90
β / deg	95.5320(8)	90	90
γ / deg	90	90	90
V / $Å^3$	7282.65(17)	3160.52(7)	11201(2)
Z	8	4	16
d (calcd) / $Mg\cdot m^{-3}$	1.070	0.972	1.146
abs coeff / mm^{-1}	0.202	0.076	0.181
R indices: R_1 =	0.0510[a]	0.0466[a]	0.0288[a]
R_w =	0.0609[a]	0.0489[a]	0.0317[a]

[a] $R_1 = \Sigma||F_o|-|F_c|| / \Sigma|F_o|$; $R_w = \sqrt{\{\Sigma w(|F_o|-|F_c|)^2 / \Sigma w|F_o|^2\}}$ for data with $I > 3\sigma(I)$.

[b] $R_1 = \Sigma||F_o|-|F_c|| / \Sigma|F_o|$; $R_w = \sqrt{\{\Sigma w(|F_o|-|F_c|)^2 / \Sigma w|F_o|^2\}}$ for data with $I > 2\sigma(I)$.

Table 6.1. X-ray data collection and processing parameters

compound	$(Tp^{tBu,Me})Sr(BH_4)(THF)_2$ (**4**)	$(Tp^{tBu,Me})Sr(I)(THF)_2$ (**5**)	$(\kappa^2,\kappa^3\text{-}Tp^{tBu,Me})_2Sr$ (**6**)
empirical formula	$C_{32}H_{60}B_2N_6O_2Sr\cdot 0.25C_6H_{14}$	$C_{32}H_{56}B_1N_6O_2Sr\cdot 1.25C_4H_8O_1$	$C_{48}H_{80}B_2N_{12}Sr\cdot C_6H_6$
fw	691.65	872.30	1012.60
temp / K	150	150	150
wavelength / Å	0.71073	0.71073	0.71073
space group	*C* $2_1/m$	*P* bca	*P* $\bar{1}$
a / Å	21.5758(3)	31.7600(3)	11.8178(2)
b / Å	12.7376(2)	12.6593(1)	11.8683(2)
c / Å	14.9913(2)	46.0197(6)	20.8614(5)
α / deg	90	90	95.7529(7)
β / deg	98.8755(6)	90	95.1637(8)
γ / deg	90	90	98.2302(9)
V / $Å^3$	4070.64(10)	18502.7(3)	2865.02(10)
Z	4	16	2
d (calcd) / $Mg\cdot m^{-3}$	1.129	1.252	1.174
abs coeff / mm^{-1}	1.358	1.870	0.986
R indices: R_1 =	0.0360[a]	0.0663[a]	0.0476[a]
R_w =	0.0400[a]	0.0580[a]	0.0454[a]

[a] $R_1 = \Sigma||F_o|-|F_c|| / \Sigma|F_o|$; $R_w = \sqrt{\{\Sigma w(|F_o|-|F_c|)^2 / \Sigma w|F_o|^2\}}$ for data with $I > 3\sigma(I)$.

[b] $R_1 = \Sigma||F_o|-|F_c|| / \Sigma|F_o|$; $R_w = \sqrt{\{\Sigma w(|F_o|-|F_c|)^2 / \Sigma w|F_o|^2\}}$ for data with $I > 2\sigma(I)$.

Table 6.1. X-ray data collection and processing parameters

compound	($Tp^{tBu,Me}$)Mg(^{n}Bu) (**8**)	($Tp^{tBu,Me}$)Mg(S-lactate) (**9**)	($Tp^{tBu,Me}$)Mg(OBn) (**10**)
empirical formula	$C_{28}H_{49}B_1N_6Mg$	$C_{28}H_{47}B_1N_6O_3Mg$	$C_{31}H_{47}B_1N_6O_1Mg$
fw	504.85	550.84	554.87
temp / K	150	150	150
wavelength / Å	1.54180	0.71073	0.71073
space group	*R3c*	*P* 1	*R3c*
a / Å	30.5774(2)	11.95180(20)	30.6018(2)
b / Å	30.5774(2)	12.55940(20)	30.6018(2)
c / Å	19.6078(2)	12.67340(20)	19.5407(2)
α / deg	90	71.0557(7)	90
β / deg	90	84.6168(7)	90
γ / deg	120	77.4892(9)	120
V / Å^3	15876.7(2)	1756.036(50)	15847.6(2)
Z	18	2	18
d (calcd) / Mg·m^{-3}	0.950	1.042	1.046
abs coeff / mm^{-1}	0.594	0.084	0.080
R indices: R_1 =	0.0578[a]	0.0467[a]	0.0860[a]
R_w =	0.0670[a]	0.0519[a]	0.0957[a]

[a] $R_1 = \Sigma||F_o|-|F_c|| / \Sigma|F_o|$; $R_w = \sqrt{\{\Sigma w(|F_o|-|F_c|)^2 / \Sigma w|F_o|^2\}}$ for data with $I > 3\sigma(I)$.

[b] $R_1 = \Sigma||F_o|-|F_c|| / \Sigma|F_o|$; $R_w = \sqrt{\{\Sigma w(|F_o|-|F_c|)^2 / \Sigma w|F_o|^2\}}$ for data with $I > 2\sigma(I)$.

Table 6.1. X-ray data collection and processing parameters

compound	($Tp^{tBu,Me}$)Mg(OMe) (**15**)	($Tp^{tBu,Me}$)Mg{ $B(OMe)_4$} (**16**)	($Tp^{tBu,Me}$)Ca($HBEt_3$)(THF) (**17**)
empirical formula	$C_{25}H_{43}B_1N_6O_1Mg$	$C_{28}H_{52}B_2N_6O_4Mg$	$C_{34}H_{64}B_2N_6O_1Ca$
fw	478.77	582.69	634.62
temp / K	150	150	150
wavelength / Å	0.71073	1.54180	0.71073
space group	*R3c*	$P\ \bar{1}$	$P\ 2_12_12_1$
a / Å	30.6704(6)	12.0396(5)	12.03670(10)
b / Å	30.6704(6)	12.1901(5)	16.94720(29)
c / Å	19.4082(4)	12.5731(8)	18.72140(29)
α / deg	90	83.932(4)	90
β / deg	90	85.207(4)	90
γ / deg	120	65.647(4)	90
V / $Å^3$	15810.8(5)	1670.04(15)	3818.948(96)
Z	18	2	4
d (calcd) / $Mg \cdot m^{-3}$	0.905	1.159	1.104
abs coeff / mm^{-1}	0.072	0.778	0.197
R indices: R_1 =	0.0665[b]	0.0327[a]	0.0415[a]
R_w =	0.0520[b]	0.0376[a]	0.0447[a]

[a] $R_1 = \Sigma||F_o|-|F_c|| / \Sigma|F_o|$; $R_w = \sqrt{\{\Sigma w(|F_o|-|F_c|)^2 / \Sigma w|F_o|^2\}}$ for data with $I > 3\sigma(I)$.

[b] $R_1 = \Sigma||F_o|-|F_c|| / \Sigma|F_o|$; $R_w = \sqrt{\{\Sigma w(|F_o|-|F_c|)^2 / \Sigma w|F_o|^2\}}$ for data with $I > 2\sigma(I)$.

Table 6.1. X-ray data collection and processing parameters

compound	$(Tp^{tBu,Me})Ca\{(\mu\text{-}H)_2BC_8H_{14}\}(THF)$ (**19**)	$(Tp^{tBu,Me})Sr\{(\mu\text{-}H)_2BC_8H_{14}\}(THF)_2$ (**20**)	$(Tp^{tBu,Me})Mg\{(\mu\text{-}H)_2BC_8H_{14}\}$ (**21**)
empirical formula	$C_{36}H_{64}B_2N_6O_1Ca$	$C_{40}H_{72}B_2N_6O_2Sr$	$C_{32}H_{56}B_2N_6Mg_1$
fw	658.65	778.29	570.76
temp / K	150	150	150
wavelength / Å	0.71073	0.71073	1.54180
space group	$P\ \bar{1}$	$P\ \bar{1}$	*R 3*
a / Å	12.9236(2)	11.95470(10)	31.117(2)
b / Å	13.0250(2)	12.4098(2)	31.117(2)
c / Å	14.1669(3)	15.5242(2)	10.0132(10)
α / deg	81.0462(7)	82.1020(6)	90
β / deg	73.8989(7)	77.4277(6)	90
γ / deg	76.0182(9)	74.8445(7)	120
V / $Å^3$	2213.22(7)	2161.76(5)	8396.5(11)
Z	2	2	9
d (calcd) / $Mg\cdot m^{-3}$	0.988	1.196	1.016
abs coeff / mm^{-1}	0.172	1.286	0.605
R indices: R_1 =	0.0866[a]	0.0392[a]	0.0991[a]
R_w =	0.0920[a]	0.0454[a]	0.1059[a]

[a] $R_1 = \Sigma||F_o|-|F_c|| / \Sigma|F_o|$; $R_w = \sqrt{\{\Sigma w(|F_o|-|F_c|)^2 / \Sigma w|F_o|^2\}}$ for data with $I > 3\sigma(I)$.

[b] $R_1 = \Sigma||F_o|-|F_c|| / \Sigma|F_o|$; $R_w = \sqrt{\{\Sigma w(|F_o|-|F_c|)^2 / \Sigma w|F_o|^2\}}$ for data with $I > 2\sigma(I)$

6.9 References

1. A. B. Pangborn, M. A. Giardello, R. H. Grubbs, R. K. Rosen and F. J. Timmers, *Organometallics*, 1996, **15**, 1518-1520.
2. A. Rudin and H. L. W. Hoegy, *J. Polym. Sci. A: Polym. Chem.*, 1972, **10**, 217.
3. I. Barakat, P. Dubois, R. Jérôme and P. Teyssié, *J. Polym. Sci. A: Polym. Chem.*, 1993, **31**, 505.
4. J. R. Dorgan, J. Janzen, D. M. Knauss, S. B. Hait, B. R. Limoges and M. H. Hutchinson, *J. Polym. Sci. B: Polym. Phys.*, 2005, **43**, 3100.
5. F. W. Swamer and C. R. Hauser, *J. Am. Chem. Soc.*, 1950, **72**, 1352.
6. S. Trofimenko, J. C. Calabrese, J. K. Kochi, S. Wolowiec, F. B. Hulsbergen and J. Reedijk, *Inorg. Chem.*, 1992, **31**, 3943.
7. R. Santi, A. M. Romano, A. Sommazzi, M. Grande, C. Bianchini and G. Mantovani, *J. Mol. Catal. A: Chem.*, 2005, **229**, 191.
8. M. Bremer, H. Nöth, M. Thomann and M. Schmidt, *Chem. Ber.*, 1995, **128**, 455.
9. R. Köster, G. Seidel, J. E. McGuire and S. G. Shore, *Inorg. Syn.*, John Wiley & Sons, Inc., 1983, 198.
10. M. G. Cushion, D.Phil Thesis, University of Oxford, 2011.
11. Z. Otwinowski and W. Minor, *Processing of X-ray Diffraction Data Collected in Oscillation Mode*, Academic Press, New York, 1997.
12. Agilent Technologies, Oxford, 2011.
13. A. Altomare, G. Cascarano, C. Giacovazzo, A. Guagliardi, M. C. Burla, G. Polidori and M. Camalli, *J. Appl. Crystallogr.*, 1994, **27**, 435.
14. L. Palatinus and G. Chapuis, *J. Appl. Crystallogr.*, 2007, **40**, 786.
15. P. W. Betteridge, J. R. Carruthers, R. I. Cooper, K. Prout and D. J. Watkin, *J. Appl. Crystallogr.*, 2003, **36**, 1487.

Appendix

A1. Characterisation of the products formed, after hydrolytic work-up, in the NMR tube scale polymerisation of ($Tp^{tBu,Me}$)$Mg(BH_4)$ (2) and 5 equivs. of ε-CL.

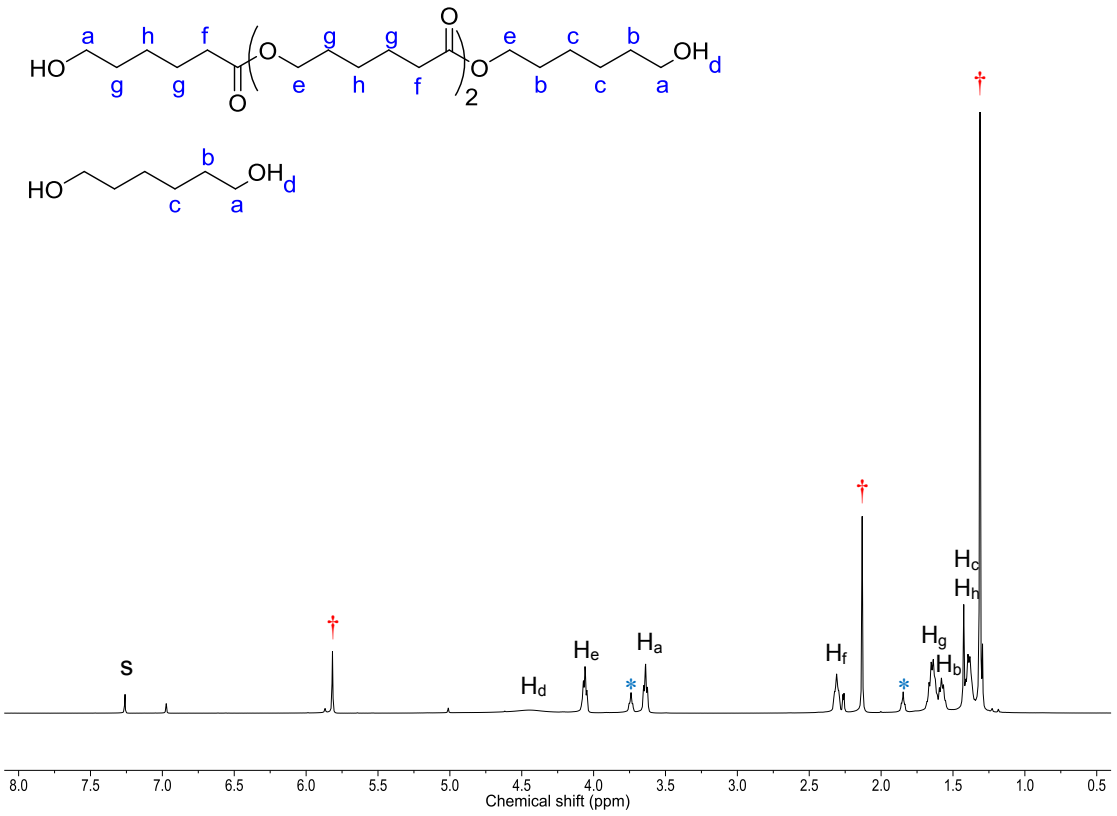

Figure A1.1. ^{1}H NMR spectrum ($CDCl_3$, 499.9 MHz, 298 K) of the mixture of PCL ($H\{O(CH_2)_5C(O)\}_4$-$O(CH2)_6OH$) and 1,6-hexanediol produced after hydrolytic work-up of the polymerisation between ($Tp^{tBu,Me}$)$Mg(BH_4)$ (**2**) and 5 equivs. of ε-CL. "s" denotes residual protio-solvent. Blue asterisks and red daggers denote residue THF and catalyst, respectively.

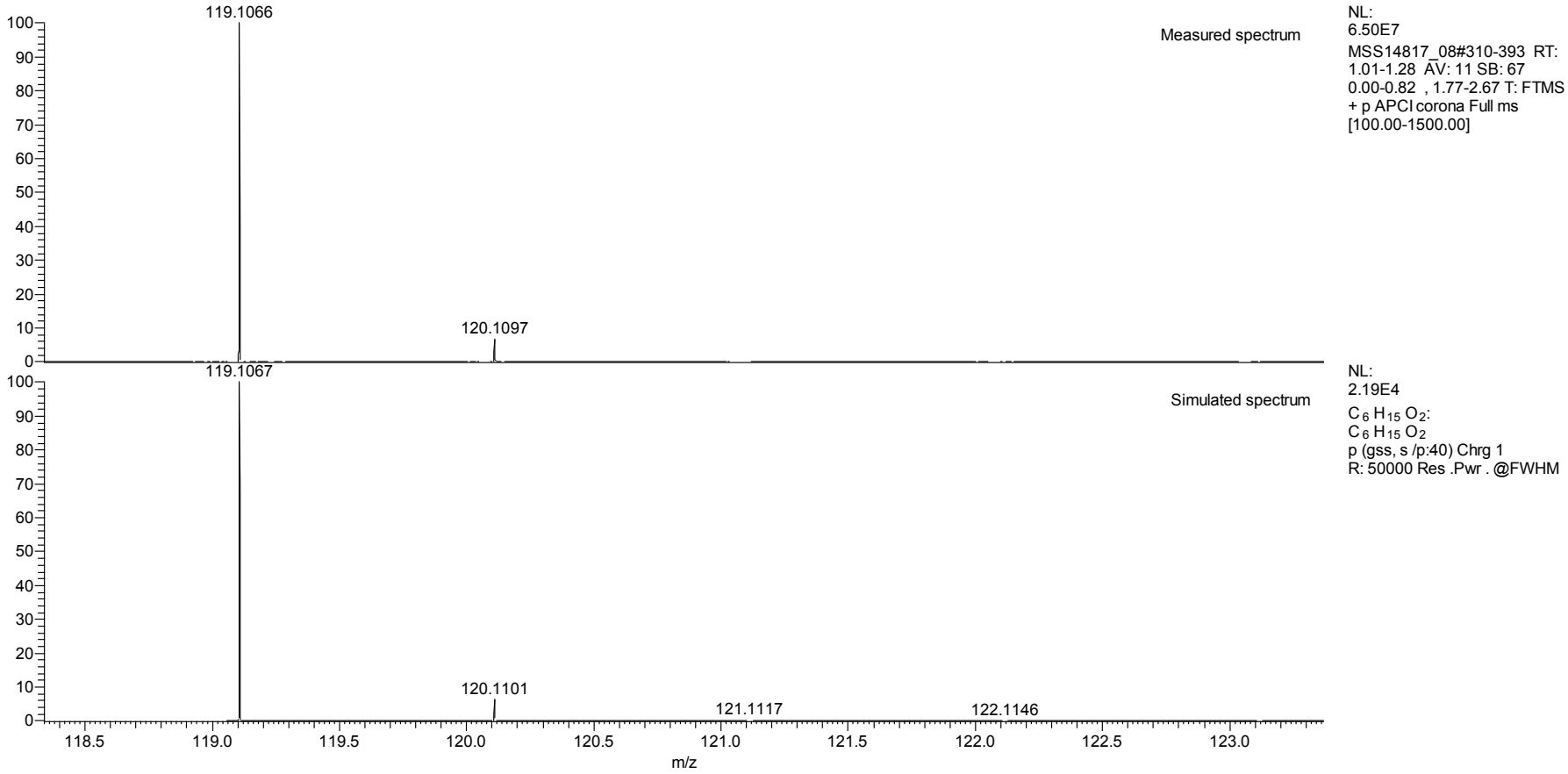

Figure A1.2. Electrospray mass spectra of the mixture of PCL ($H\{O(CH_2)_5C(O)\}_4$-$O(CH2)_6OH$) and 1,6-hexanediol produced after hydrolytic work-up of the polymerisation between ($Tp^{tBu,Me}$)$Mg(BH_4)$ (**2**) and 5 equivs. of ε-CL. The spectra confirm the presence of 1,6-hexanediol ($C_6H_{15}O_2$) and PCL ($H\{O(CH_2)_5C(O)\}_3$-$O(CH2)_6OH$, $C_{24}H_{45}O_8$).

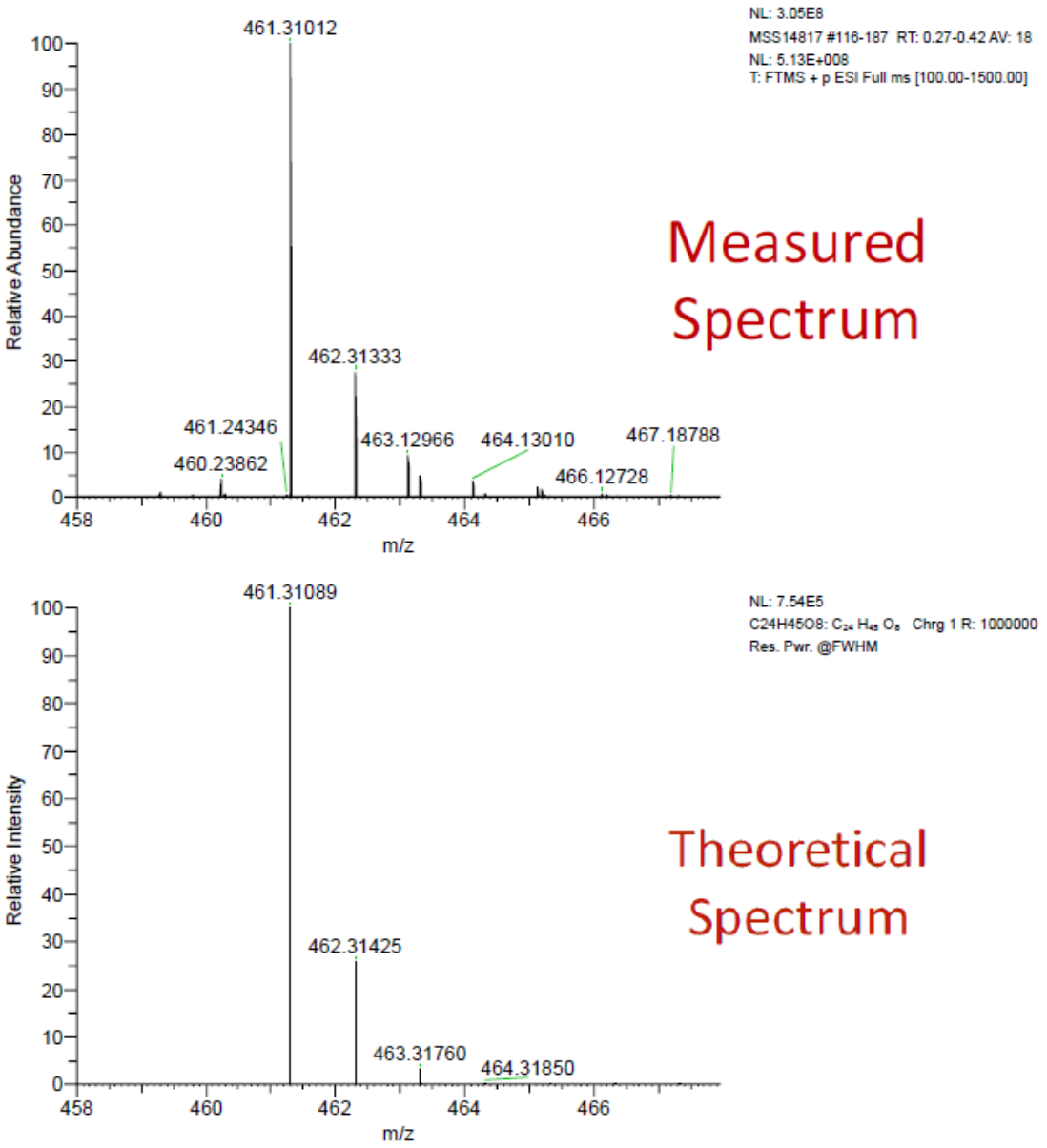

Figure A1.2 (continued). Electrospray mass spectra of the mixture of PCL ($H\{O(CH_2)_5C(O)\}_4$-$O(CH2)_6OH$) and 1,6-hexanediol produced after hydrolytic work-up of the polymerisation between ($Tp^{tBu,Me}$)$Mg(BH_4)$ (**2**) and 5 equivs. of ε-CL. The spectra confirm the presence of 1,6-hexanediol ($C_6H_{15}O_2$) and PCL ($H\{O(CH_2)_5C(O)\}_3$-$O(CH2)_6OH$, $C_{24}H_{45}O_8$).

A.3 $^{13}C\{^{1}H\}$ NMR spectroscopic characterisation of species formed during the ROP of *rac*-LA using ($Tp^{tBu,Me}$)Mg(BH_4) (2)

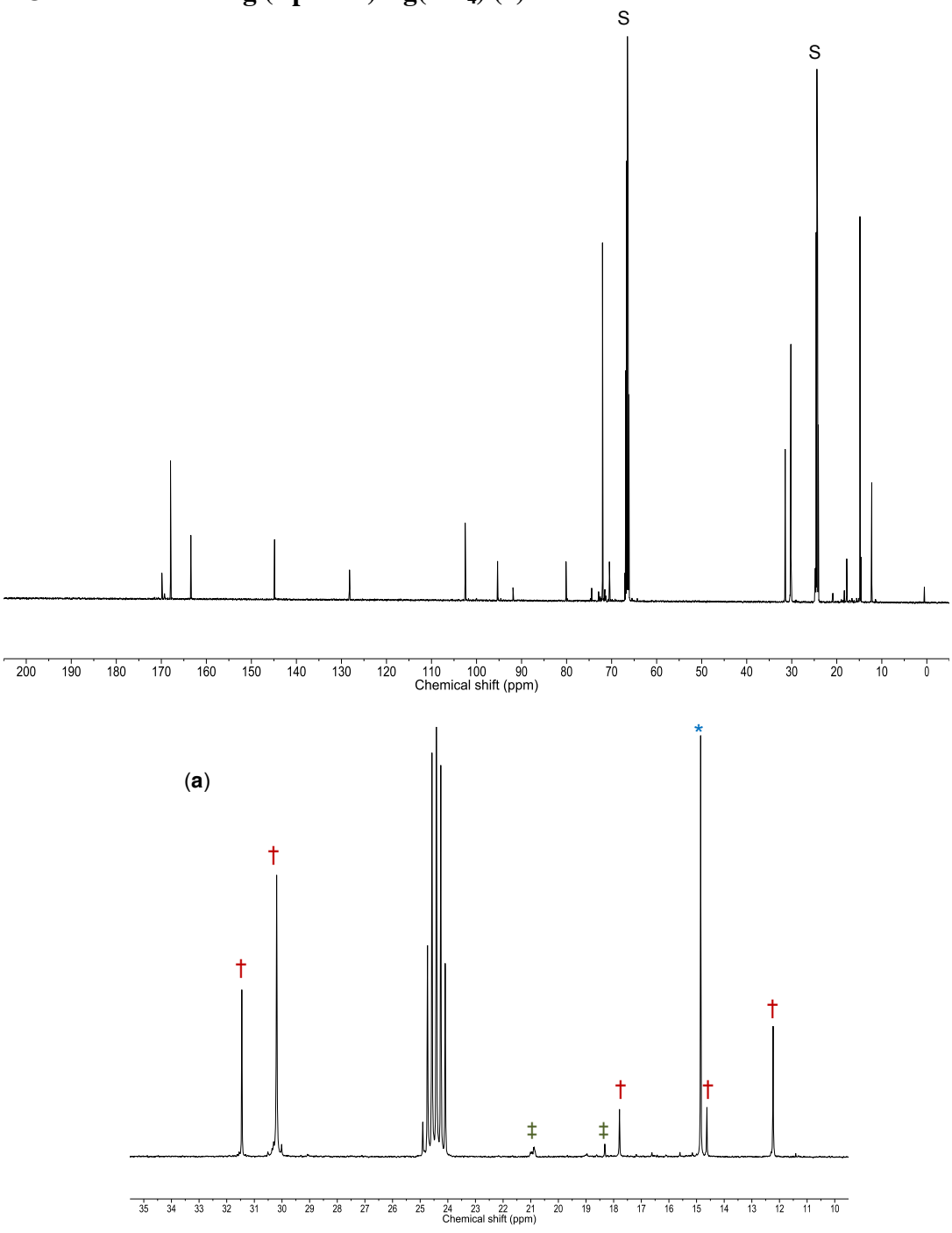

Figure A3.1. $^{13}C\{^{1}H\}$ NMR spectrum (THF-d_8, 125.7 MHz, 228 K) of species formed during the ROP of *rac*-LA using ($Tp^{tBu,Me}$)Mg(BH_4) (**2**) and 5 equivs. of *rac*-LA. (a) An expanded region of δ = 10-35 ppm. (b) An expanded region of δ = 60-85 ppm. (c) An expanded region of δ = 90-180 ppm. "s" denotes residual protio-solvent. Blue asterisks, red daggers, green double daggers and brown triangle denote unreacted *rac*-LA, compound **12**, B(LA-H)$_3$ and C_6H_6 residue, respectively.

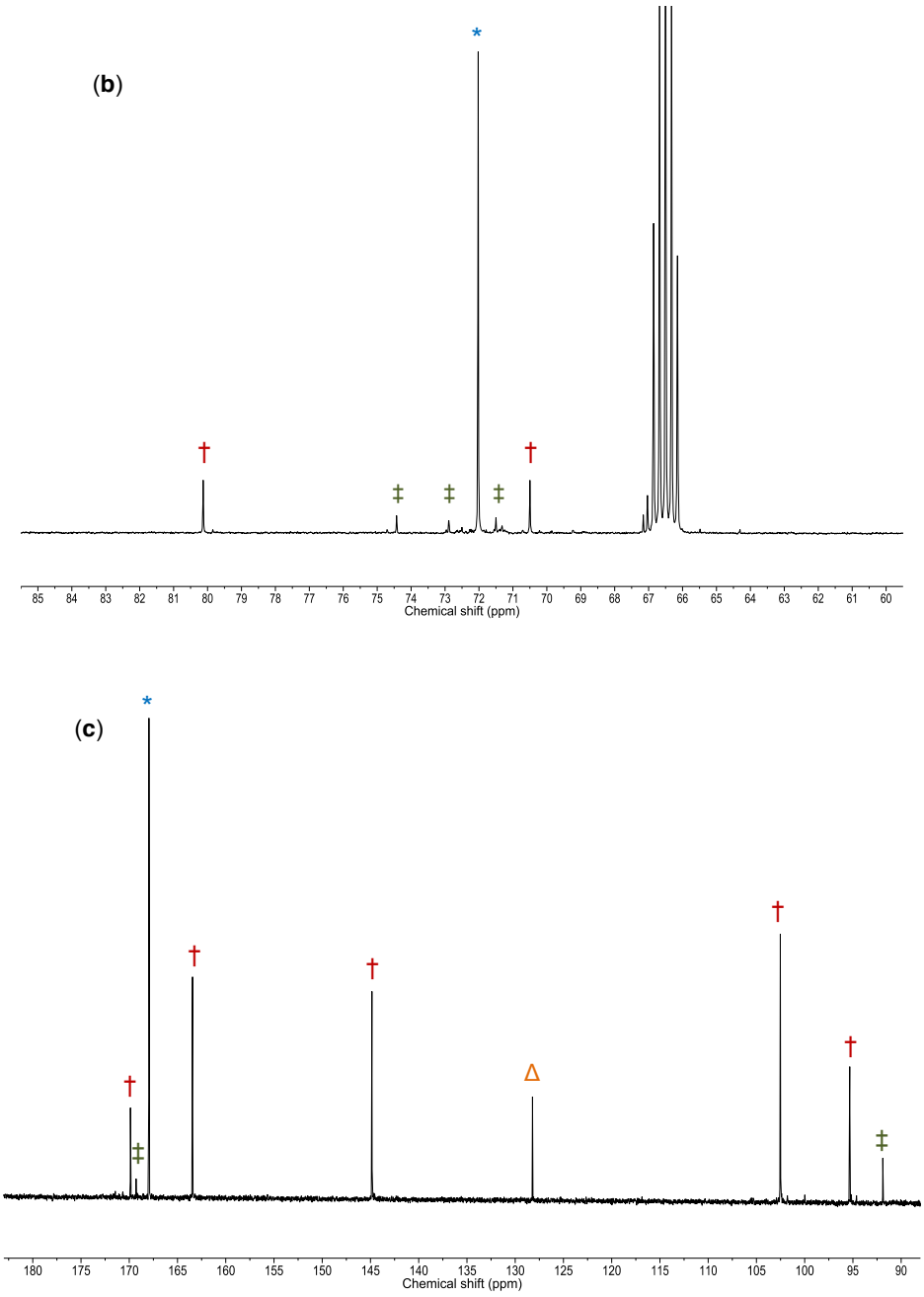

Figure A3.1 (continued). $^{13}C\{^{1}H\}$ NMR spectrum (THF-d_8, 125.7 MHz, 228 K) of species formed during the ROP of *rac*-LA using ($Tp^{tBu,Me}$)Mg(BH_4) (**2**) and 5 equivs. of *rac*-LA. (a) An expanded region of δ = 10-35 ppm. (b) An expanded region of δ = 60-85 ppm. (c) An expanded region of δ = 90-180 ppm. "s" denotes residual protio-solvent. Blue asterisks, red daggers, green double daggers and brown triangle denote unreacted *rac*-LA, compound **12**, B(LA-H)$_3$ and C_6H_6 residue, respectively.

A4. Immortal polymerisation of ε-CL and *rac*-LA using group 2 initiators

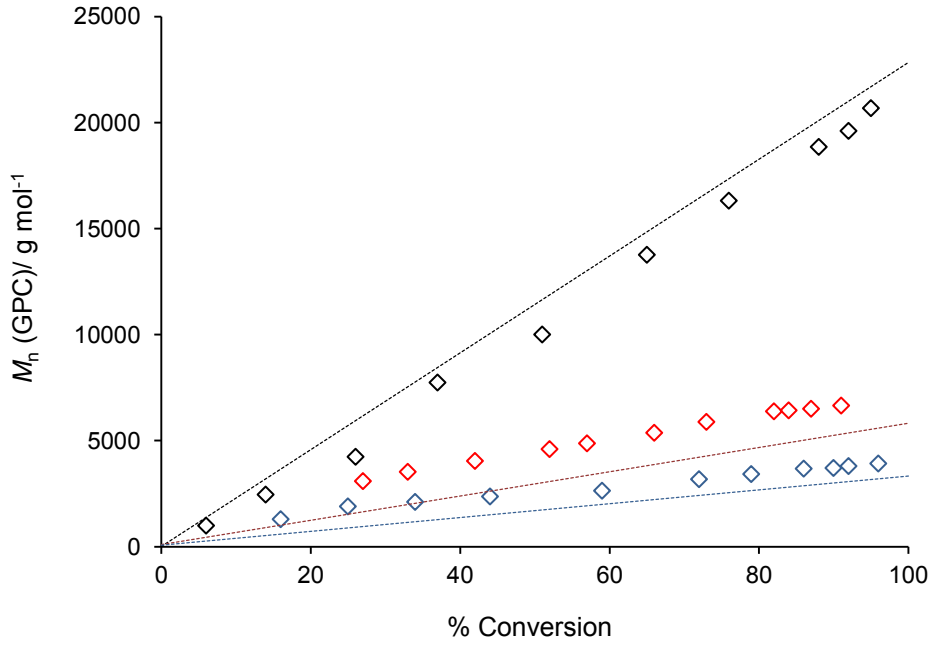

Figure A4.1. Data for iROP of ε-CL using (Tp^{tBu,Me})Mg(BH$_4$) (**2**) and various additives. M_n (GPC) vs. conversion plot. The black, red and blue dotted lines are that expected for one, four and seven PCL chains per metal centre, respectively. Conditions: 3.4 mL toluene, 23 °C, [ε-CL]$_0$ = 1 M, [ε-CL]$_0$:[**2**]$_0$ = 200:1 and PDIs = 1.11-1.20 (black diamonds), [ε-CL]$_0$:[**2**]$_0$:[PhCHO] = 200:1:5 and PDIs = 1.30-1.56 (red diamonds), [ε-CL]$_0$:[**2**]$_0$:[PhCHO]:[B(OMe)$_3$] = 200:1:5:1 and PDIs = 1.46-1.69 (blue diamonds).

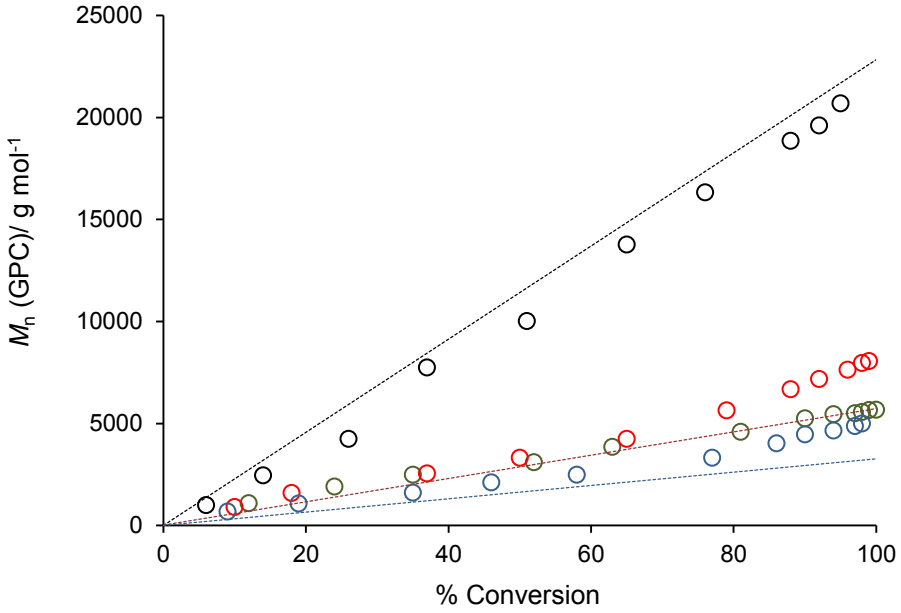

Figure A4.2. Data for iROP of ε-CL using ($Tp^{tBu,Me}$)Mg(BH_4) (**2**) and various additives. M_n (GPC) vs. conversion plot. The black, red and blue dotted lines are that expected for one, four and seven PCL chains per metal centre, respectively. Conditions: 3.4 mL toluenen, 23 °C, $[\varepsilon\text{-CL}]_0$ = 1 M, $[\varepsilon\text{-CL}]_0$:[**2**]$_0$ = 200:1 and PDIs = 1.11-1.20 (black circles), $[\varepsilon\text{-CL}]_0$:[**2**]$_0$:[HBPin] = 200:1:3 and PDIs = 1.27-1.46 (red circles), $[\varepsilon\text{-CL}]_0$:[**2**]$_0$:[HBPin] = 200:1:6 and PDIs = 1.31-1.47 (blue circles), $[\varepsilon\text{-CL}]_0$:[**2**]$_0$:[$B(OMe)_3$] = 200:1:1 and PDIs = 1.19-1.65 (green circles).

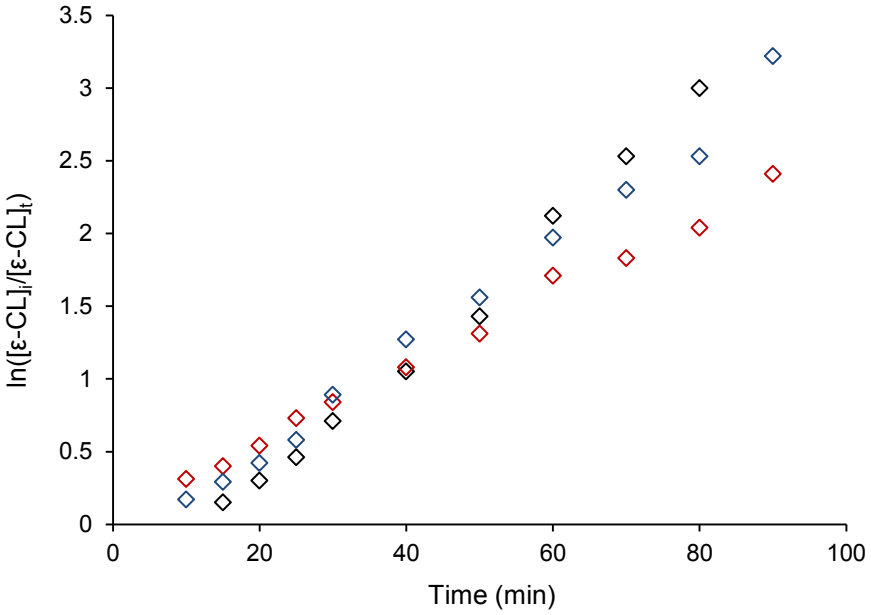

Figure A4.3. First order plot of $\ln([\varepsilon\text{-CL}]_i/[\varepsilon\text{-CL}]_t)$ *vs*. time for the iROP of ε-CL using $(Tp^{tBu,Me})Mg(BH_4)$ (**2**) and various additives in toluene. Rate constants: k_{app} = 0.045(1) min^{-1} (R^2 = 0.992, $[\varepsilon\text{-CL}]_0$:[**2**]$_0$ = 200:1, black diamonds), k_{app} = 0.026(1) min^{-1} (R^2 = 0.994, $[\varepsilon\text{-CL}]_0$:[**2**]$_0$:[HBPin] = 200:1:3, red diamonds) and k_{app} = 0.037(1) min^{-1} (R^2 = 0.993, $[\varepsilon\text{-CL}]_0$:[**2**]$_0$:[HBPin] = 200:1:6, blue diamonds).

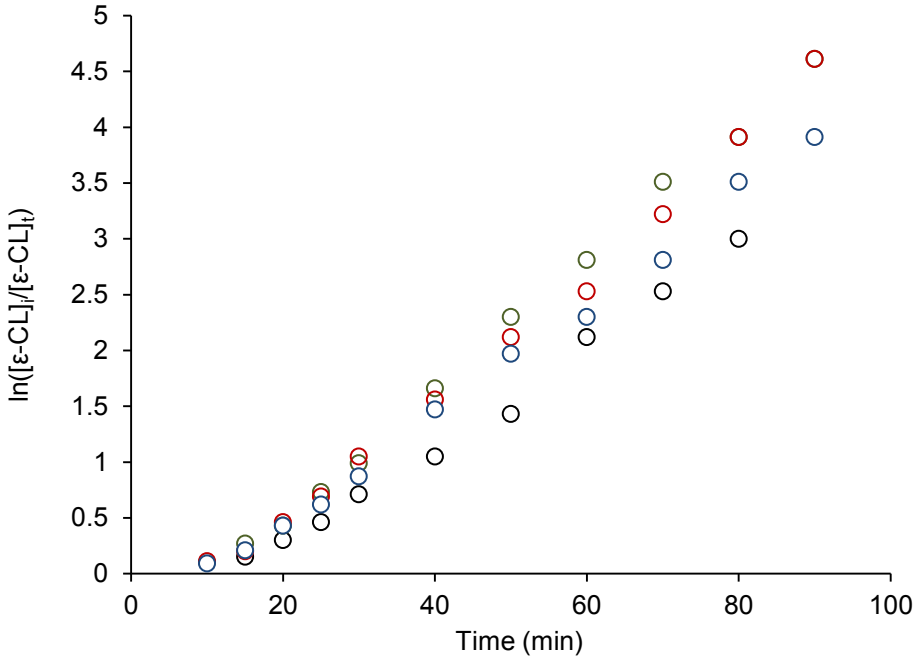

Figure A4.4. First order plot of $\ln([\varepsilon\text{-CL}]_i/[\varepsilon\text{-CL}]_t)$ *vs*. time for the iROP of ε-CL using ($Tp^{tBu,Me}$)$Mg(BH_4)$ (**2**) and various additives in toluene. Rate constants: k_{app} = 0.045(1) min^{-1} (R^2 = 0.992, $[\varepsilon\text{-CL}]_0$:[**2**]$_0$ = 200:1, black circles), k_{app} = 0.056(1) min^{-1} (R^2 = 0.995, $[\varepsilon\text{-CL}]_0$:[**2**]$_0$:[HBPin] = 200:1:3, red circles), k_{app} = 0.049(1) min^{-1} (R^2 = 0.996, $[\varepsilon\text{-CL}]_0$:[**2**]$_0$:[HBPin] = 200:1:6, blue circles) and k_{app} = 0.058(1) min^{-1} (R^2= 0.997, $[\varepsilon\text{-CL}]_0$:[**2**]$_0$:[$B(OMe)_3$] = 200:1:1, green circles).

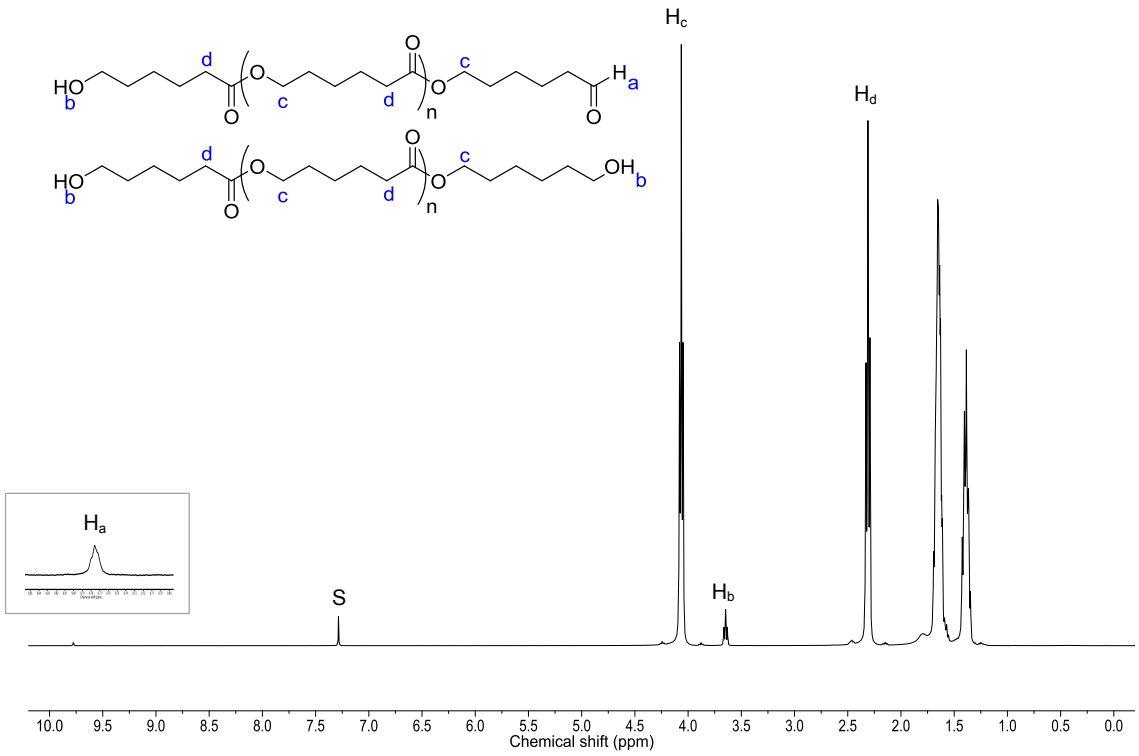

Figure A4.5. ^{1}H NMR spectrum ($CDCl_3$, 400.0 MHz, 298 K) of the isolated PCL from the iROP of ($Tp^{tBu,Me}$)Mg(BH_4) (**2**) and 200 equivs. of ε-CL, in the presence of 6 equivs. of HPin as CTA. "s" denotes residual protio-solvent. An inset shows an aldehyde resonance at δ = 9.78 ppm.

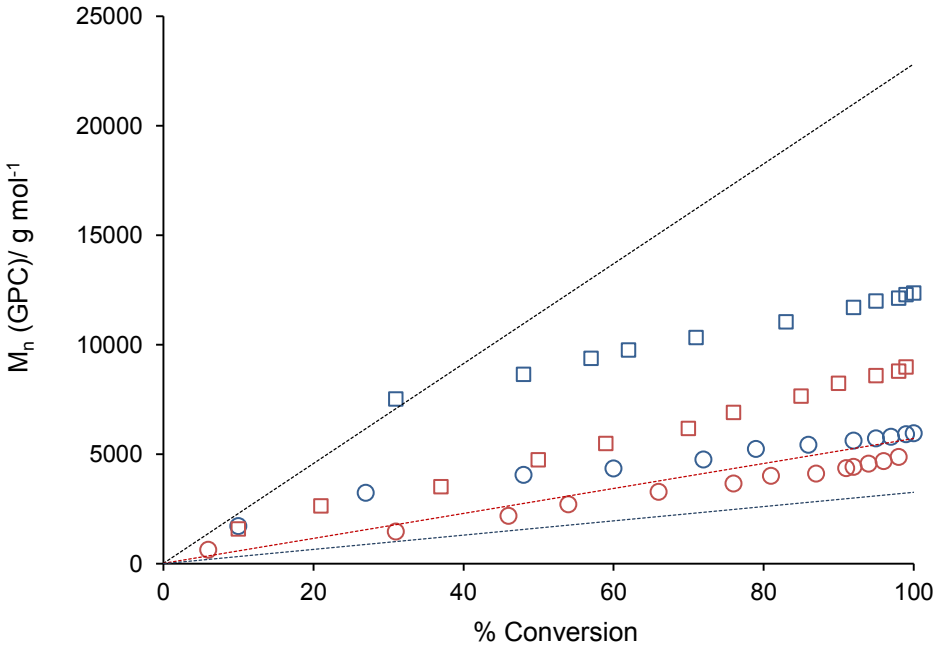

Figure A4.6. Data for iROP of ε-CL using ($Tp^{tBu,Me}$)Ca(BH_4)(THF) (**1**) and various additives. M_n (GPC) vs. conversion plot. The black, red and blue dotted lines are that expected for one, four and seven PCL chains per metal centre, respectively. Conditions: 3.4 mL THF and toluenen, 23 °C, $[\varepsilon\text{-CL}]_0$ = 1 M, $[\varepsilon\text{-CL}]_0$:[**1**]$_0$:[HBPin] = 200:1:3, PDIs = 1.44-1.64 (blue squares, THF), $[\varepsilon\text{-CL}]_0$:[**1**]$_0$:[HBPin] = 200:1:6, PDIs = 1.48-1.65 (blue circles, THF), $[\varepsilon\text{-CL}]_0$:[**1**]$_0$:[HBPin] = 200:1:3, PDIs = 1.24-1.50 (red squares, toluene) and $[\varepsilon\text{-CL}]_0$:[**1**]$_0$:[HBPin] = 200:1:6, PDIs = 1.22-1.38 (red circles, toluene).

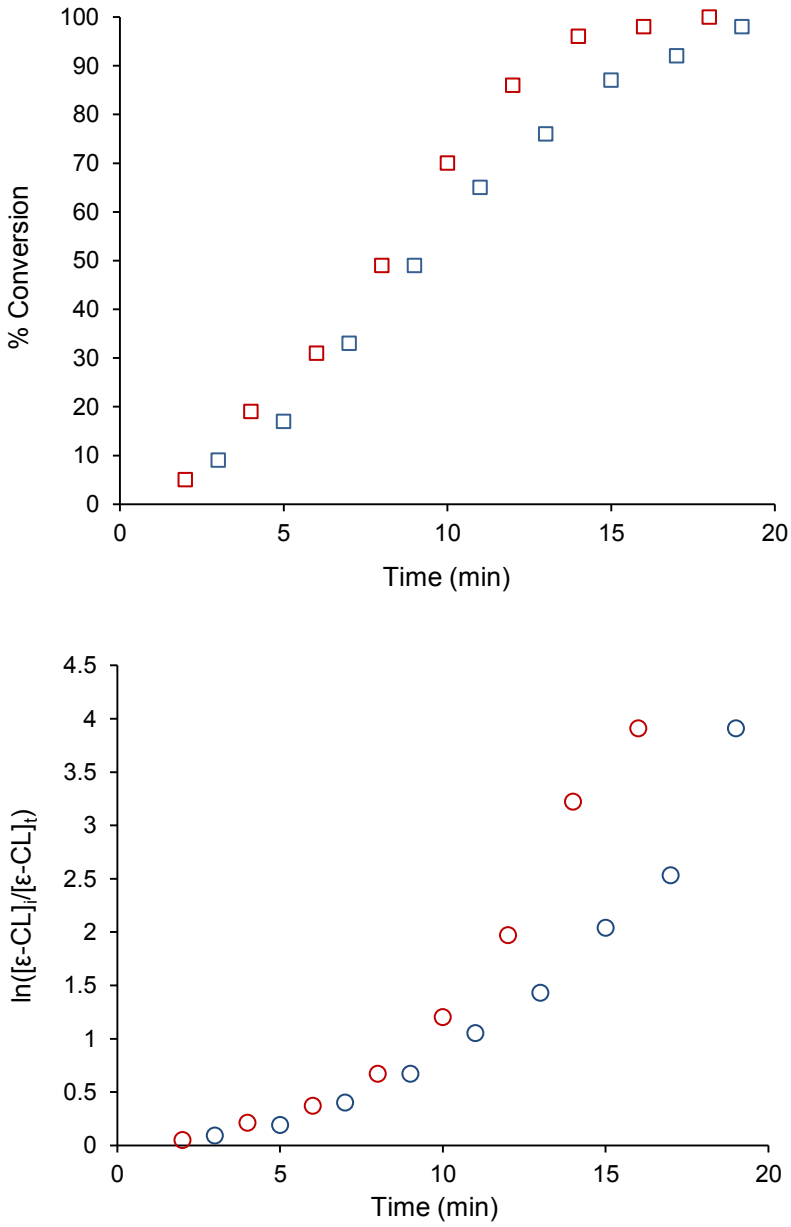

Figure A4.7. (Top) Plot of % conversion *vs*. time for the iROP of ε-CL using the *in situ* generated ($Tp^{tBu,Me}$)Sr{$B(OBn)_4$} (**14**), in the presence of $B(OMe)_3$ as a CTA. Conditions: 3.4 mL THF and toluenen, 23 °C, $[\varepsilon\text{-CL}]_0$ = 1 M, $[\varepsilon\text{-CL}]_0$:$[\mathbf{4}]_0$:[PhCHO]:$[B(OMe)_3]$ = 200:1:5:1, PDIs = 1.30-1.67 (blue squares, THF) and PDIs = 1.41-1.64 (red squares, toluene). (Bottom) Corresponding first order plot of $\ln([\varepsilon\text{-CL}]_i/[\varepsilon\text{-CL}]_t)$ *vs*. time of the iROP stated above (blue circles for the iROP in THF and red circles for the iROP in toluene).

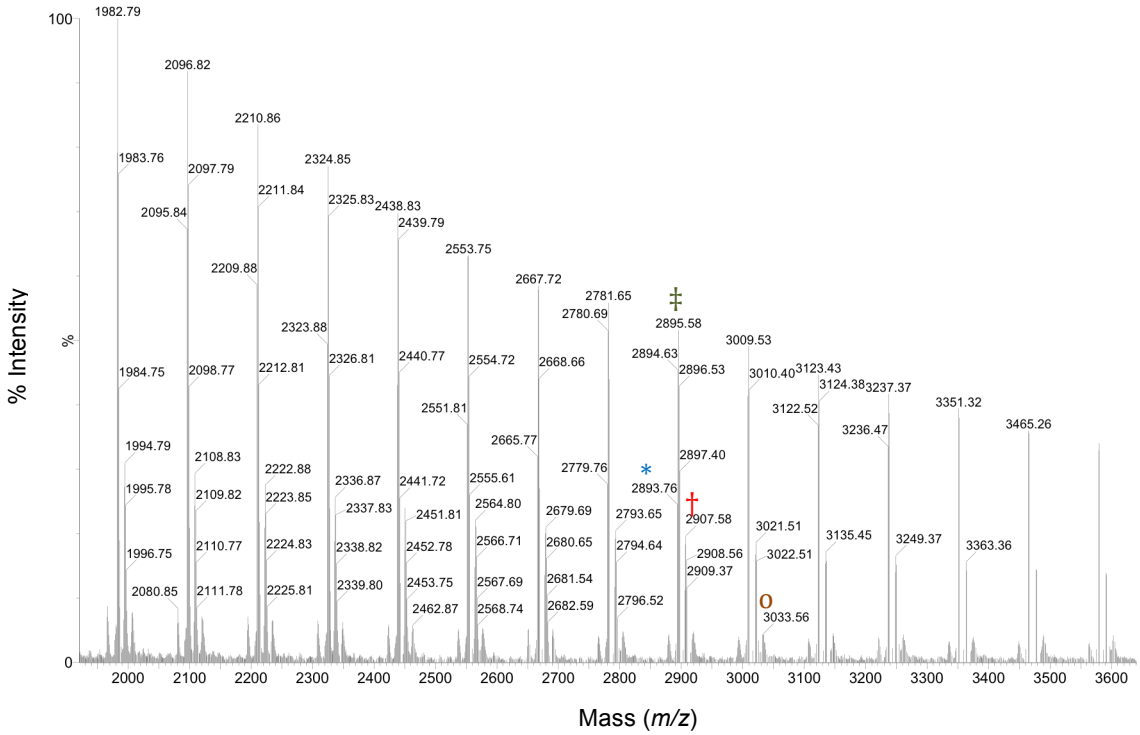

Figure A4.8. MALDI-ToF MS of a mixture of aldehyde/alcohol (blue asterisk), α,ω-dihydroxy telechelic (green double dagger), alcohol/-OBPin (red dagger) and -OBPin/-OBPin (brown circle) end-capped PCL obtained from the iROP of [ε-CL]:[**4**]:[HBPin] = 200:1:6 in THF at 23 °C. M_n by GPC analysis was 1,660 g mol^{-1}. K^+ dopant, Δ(*m/z*) = 114.1 g mol^{-1}.

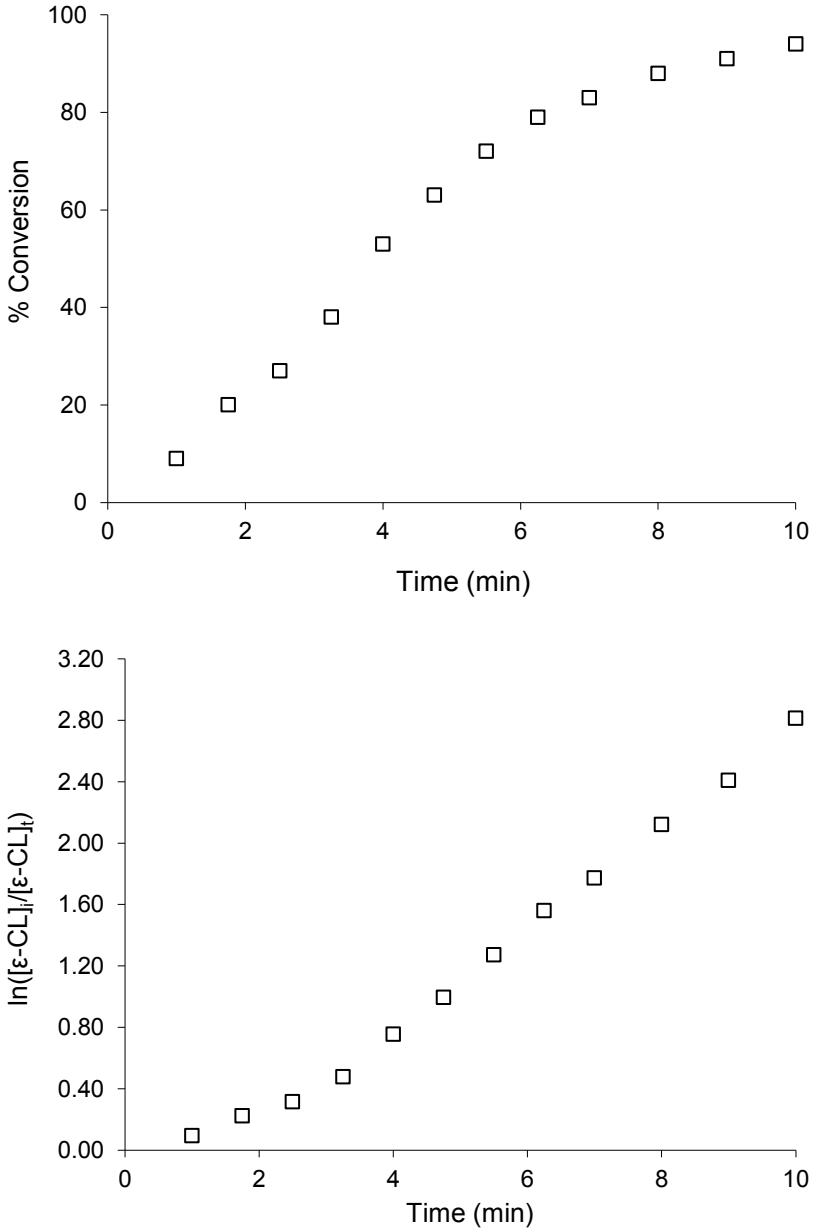

Figure A4.9. (Top) Plot of % conversion *vs*. time for the iROP of ε-CL using the *in situ* generated ($Tp^{tBu,Me}$)Sr{$B(OBn)_4$} (**14**), in the presence of $B(OBn)_3$ as a CTA. Conditions: 3.4 mL THF, 23 °C, $[\varepsilon\text{-CL}]_0$ = 1 M, $[\varepsilon\text{-CL}]_0$:[**4**]$_0$:[PhCHO]:[$B(OBn)_3$] = 200:1:5:5, PDIs = 1.29-1.57. (Bottom) Corresponding first order plot of $\ln([\varepsilon\text{-CL}]_i/[\varepsilon\text{-CL}]_t)$ *vs*. time of the iROP of ε-CL stated above.

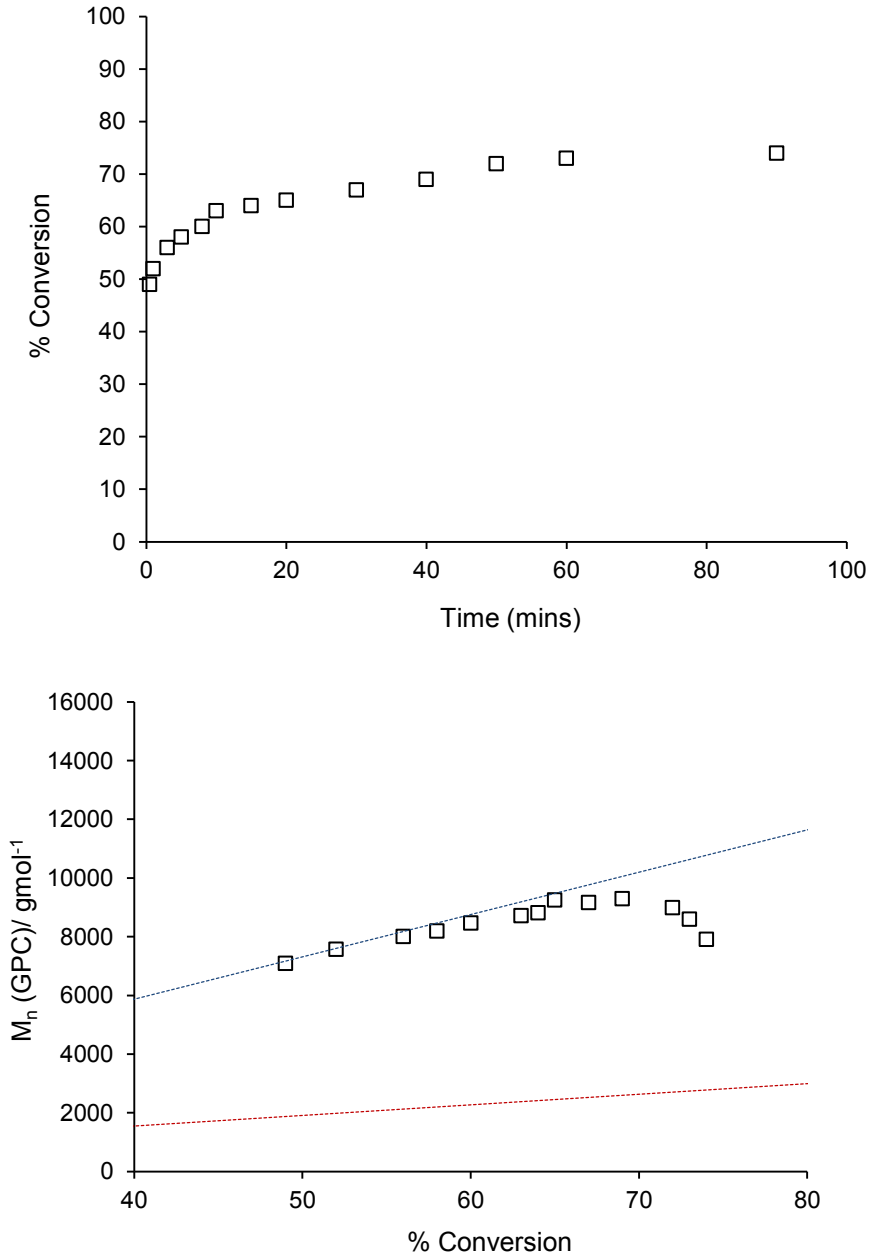

Figure A4.10. (Top) Plot of % conversion *vs*. time for the ROP of *rac*-LA using the *in situ* generated ($Tp^{tBu,Me}$)Sr{$B(OBn)_4$} (**14**). Conditions: 6 mL THF, 23 °C, [*rac*-LA]$_0$ = 0.5 M, [*rac*-LA]$_0$:[**4**]$_0$:[PhCHO] = 100:1:5, PDIs = 1.18-1.34. (Bottom) Plot of M_n (GPC) *vs*. % conversion of *rac*-LA using the *in situ* generated ($Tp^{tBu,Me}$)Sr{$B(OBn)_4$} (**14**). The blue and red dotted lines are that expected for one and four PLA chains per metal centre.